Sorption-effect chromatography

SORPTION-EFFECT CHROMATOGRAPHY

by

Robert Ian Meacham

A Doctoral Thesis

Submitted in partial fulfilment of the requirements
for the award of
Doctor of Philosophy of the Loughborough University of Technology

1990

Abstract

The objective of this work has been to develop an understanding of the changes in volumetric flow rate that occur during chromatography so that flow rate measurements can be used as the basis of an analytical method. It is suggested that the total amount of gas which adsorbs on a column equals the total amount of gas which elutes from the end of the column.

The sorption effect is the name given to changes in gas flow rate as solute adsorbs onto and desorbs from an adsorbent column. The existence of the sorption effect is verified by preliminary experiments.

The effects of atmospheric pressure fluctuations, temperature fluctuations, viscosity differences, and changes in pneumatic resistance along the flow path are eliminated by further developing a prototype chromatograph with which the sorption effect had previously been observed.

Single solute samples of hydrogen and argon, and mixtures of the two, are chromatographed to determine whether the area of the adsorption peak equals the sum of the areas of the desorption peaks.

A correction factor is derived which takes account of the fact that not all the sample gas is adsorbed. This enables the composition of the original gas mixture to be determined. The correction factor is calculated for each of the test gases and applied to the experimental analyses. The measured compositions agree with the original sample compositions to within 1%.

Acknowledgements

I would like to thank all my friends and colleagues in the Chemical Engineering Department who offered help and encouragement, especially my two Supervisors, Bryan Buffham and Geoff Mason.

CHAPTER ONE - INTRODUCTION

1.1 Introduction

"Chromatography is a physical method of separation, in which the components to be separated are distributed between two phases, one of these phases constituting a stationary bed of large surface area, the other being a fluid that percolates through the stationary bed" (Keulemans (1957)). The moving phase may be a gas or a liquid and the stationary phase may be a liquid or a solid which is capable of adsorption. The scope of the work reported in this thesis is in the field of gas-solid chromatography where the mobile phase is a gas (the carrier gas) and the stationary phase is a solid. The solid is in particulate form and is packed as uniformly as possible into a long, narrow tube or column. During operation the packed column is continually purged with carrier gas. A small quantity of adsorbable solute introduced into the carrier gas at the upstream end of the column will be distributed between the two phases according to its affinity for the stationary phase. The extent of adsorption of a solute is determined by its partition coefficient, K (Tranchant (1969)). This is the ratio of the amount of solute per unit volume of stationary phase to the amount of solute per unit volume of the mobile phase. For a given column, the capacity factor, k is given by :

$$k = K\frac{V_S}{V_G} \tag{1.1}$$

where V_S and V_G are the respective volumes of the stationary and mobile phases. The capacity factor is related to the solute retention time, t_r, by :

$$\frac{t_m}{t_r} = \frac{1}{1+k} \tag{1.2}$$

where t_m is the retention time of an unadsorbed gas, i.e. the gas hold-up time. Obviously, the higher the value of k, the more highly adsorbed the solute is.

Imagine the carrier gas to be unadsorbed (K = 0). The slug of gas containing the solute enters the column and solute is adsorbed from the front of the band. Solute which remains in the gas phase passes further into the column and is adsorbed until the entire sample slug has entered the column. Once the complete band is within the column, adsorption at the front of the band continues, but solute is desorbed at the rear of the band (Figure 1.1). In this fashion, solute molecules move through the column. The more highly adsorbed a solute species is, the longer it takes to travel through the column. Different solutes with different adsorption coefficients will therefore travel at different rates along the column and will tend to segregate into separate zones. If the experimental conditions are favourable these zones will become completely isolated from each other

during the passage through the column (Figure 1.2). Each band can then be individually detected as it leaves the column. A record of the detector response with time is known as a chromatogram, chart trace or simply, trace.

Figure 1.1 - How a Sample Band Moves Along the Column

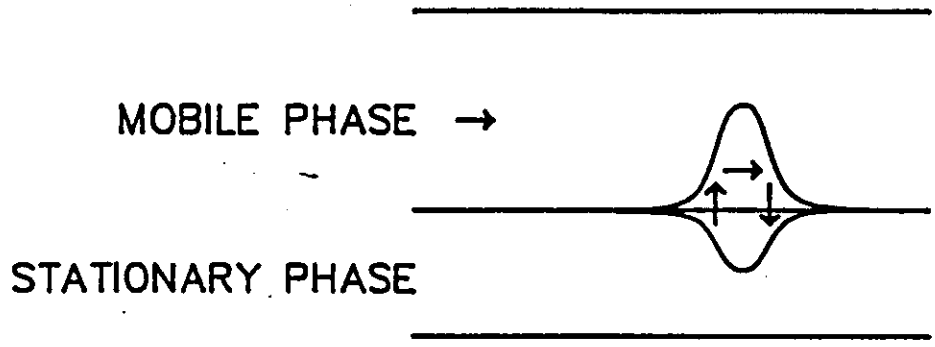

The two Gaussian-shaped peaks represent the sample concentration profile in the mobile phase and in the stationary phase. The sample gas is contained within a band whose limits are where the upstream and downstream sample concentration is zero. Adsorbed sample gas is desorbed at the rear of the sample band and moves with the mobile phase to the front of the band where it is resorbed.

The method described above is known as elution chromatography, where a multicomponent sample gas is injected into a chromatograph, separated into its different components which are conventionally then identified by monitoring some physical property which changes with changes in the composition of the gas leaving the column.

Two further techniques are frontal analysis and displacement development and these are described by Conder and Young (1979).

Frontal analysis refers to a process in which the sample is introduced continuously instead of as a discrete slug of gas. The resultant detector response will show a step change in composition when the composition front "breaks through" rather than the peak obtained in elution chromatography.

In displacement development (Purnell (1967)), a very highly-adsorbed displacing species is used to dislodge the sample solutes from the column. The sample solutes are separated in accordance with how strongly each is adsorbed, with the least strongly adsorbed emerging from the column first. This technique can be used for separating mixtures, the study of on-column reactions, and finite solute concentration work (Conder and Young (1979)).

Figure 1.2 - Separation of a Multicomponent Sample

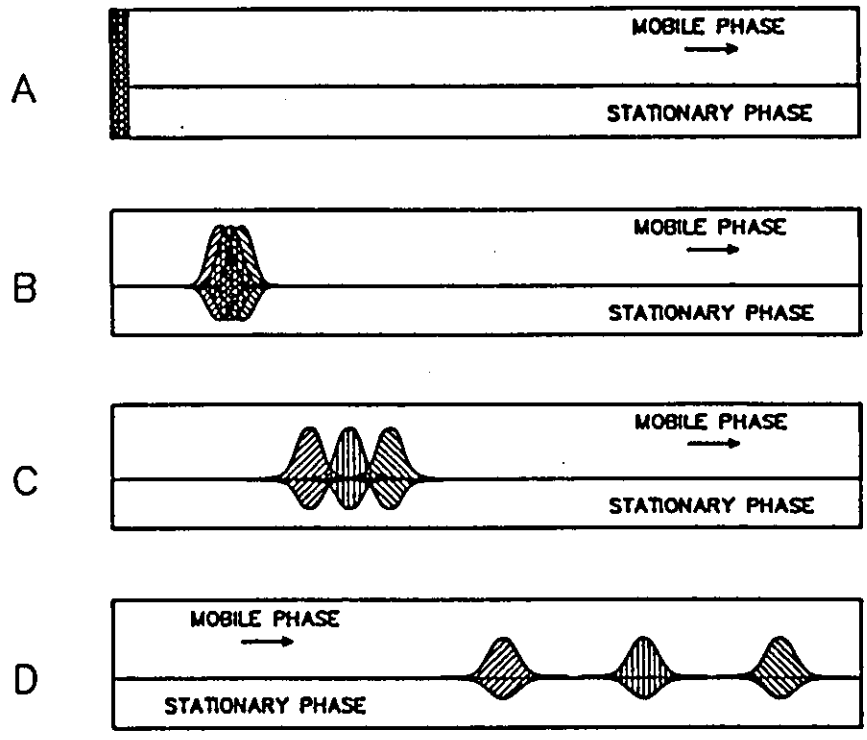

Parts A to D show schematically how the concentration profiles change as a three-component sample moves through a column. The sample band is moving left to right.

A The sample band containing three components enters the column.

B The band has begun to broaden but there is no significant separation.

C The separation of the three components is not quite complete.

D Three distinct, separate sample bands are now present in the column.

These are the different techniques available to the chromatographer, the methods are also classified by the choice of detector e.g. Flame Ionisation Detector chromatography, Thermal Conductivity Detector chromatography.

1.2 Sorption-Effect Chromatography (Buffham, Mason and Meacham (1986))

In this form of chromatography a flowmeter is used to detect the flow rate changes associated with the adsorption and desorption of gas from an adsorbent column ("the sorption effect"). The mobile phase must be gaseous for these changes to be observable. The effect is negligible in liquid-liquid chromatography because the solute has similar partial molar volumes in both phases (Conder (1974)).

1.2.1 The Sorption Effect

The sorption effect was first reported in 1957 by Bosanquet and Morgan as the changes in local velocity during gas sorption. However, prior to this, Griffiths, James and Phillips (1952) had attempted to measure composition by the pressure developed across a flow impedance. When they had appreciable dead volume between the column and the impedance, they noticed a sharp peak at the beginning of the response which was, most likely, the sorption effect. Dimbat, Porter and Stross, in 1956, reported an increase in back pressure on the column and detector as the sample components emerge. Van de Craats (1958) described how a dissolved component, upon reaching the end of the column, is transferred to the gaseous phase causing a flow increase. This results in the peak area being smaller than that corresponding to the measured flow rate. A correction factor, in terms of retention volume, is derived. Golay (1964) cited the sorption effect as the primary cause of errors in retention time measurements. Weinstein (1960) monitored changes in pressure and flow rate caused by the presence of a sample species. Practical procedures for avoiding errors from this source were recommended (Weinstein (1961)). Dyson and Littlewood (1967(I),(II)) included the sorption effect in their treatment of possible errors. Scott (1964) observed both adsorption and desorption peaks using a flame thermocouple detector as a flowmeter. The detector is sensitive to flow rate changes and changes in the calorific value of the gas but the chromatograph was configured such that the eluted solute did not enter the detector. Thus, the detector responded explicitly to changes in flow. Amy, Brand and Baitinger (1961) included alternate lengths of packing and gas mixing sections in their column. Each mixing section consisted of a teflon spacer with a hole bored through the centre. They observed a series of surges in the column outlet pressure corresponding to the number of restrictions in the column before the pressure surge caused by the main elution peak. Their explanation was that there were two effects occurring in the mixing sections: solute desorbing at the end of each packed section caused a flow increase; and second the effect on gas density of the sample passing through the orifice in the spacer. The pressure drop across an orifice (ΔP_o) is given by :

$$\Delta P_o = K_o \rho F^2 \qquad (1.3)$$

where K_o is a constant, ρ is the density of the gas in the orifice and F is the volumetric flow rate (Annino and Voyksner (1977)). In general, the density of the gas in the orifice was increased by the presence of the sample gas and consequently the flow rate decreased. The authors suggested that the size of the restriction could be adjusted so that the two effects were exactly cancelled. Sewell and Stock (1970) measured changes in flow rate at the column outlet, and, changes in the column pressure drop by monitoring the inlet

pressure. The chart recordings that they produced bear a similarity to those of Dyson and Littlewood (1967(I),(II)). Their explanation was that the sample produced a back pressure, reducing the flow rate, until it eluted from the column, when the sorption effect was observed. Van Swaay (1963) described an integral flowmeter which he theorised would show a step change in the output as sample components eluted from the column. Guiochon and Jacob (1971) surmised the pressure profile in the column as a sample band passed for the cases where a) the flow rate was constant in which case the inlet pressure must increase all the time that the peak remains in the column, and b) the column pressure drop was constant in which case the carrier gas inlet velocity must vary.

The following workers have all incorporated the sorption effect in their theoretical work. Peterson and Helfferich (1965) assumed that there was local equilibrium with no diffusional effects, that the equilibrium isotherm was linear across the concentration range encountered, that the mobile phase was an ideal gas, that there was no effect from the heat of adsorption and that the column pressure drop was negligible. They did not assume that the gas velocity remains constant throughout the region of a solute pulse. Only in the infinitely dilute concentration range can this assumption be made. Previously, formulae derived for liquid-phase chromatography had been applied to gas chromatography with the assumption that sorbed molecules do not contribute to the mobile-phase flux. They derived equations for the retention volume of :

a large sample pulse in a pure carrier gas
a concentration front in an initially solute-free column
a tracer pulse
a concentration pulse in a partially presaturated column.

Krige and Pretorius (1965(I)) derived expressions to calculate front retention times and flow rate variation with time for a single, undiluted solute and a binary, diluted solute mixture assuming sharp fronts and non-linear distribution isotherms. They (1965(II)) predicted the retention times for the frontal analysis of a methane and carbon dioxide mixture with and without taking the sorption effect into account. Good agreement was obtained with the experimental retention times for the calculations which included the sorption effect. The retention time is the time taken by a characteristic point of fixed concentration to pass from column inlet to column outlet, and is fundamentally related to the gradient of the distribution isotherm at that concentration (Conder and Young (1979)). Conder and Purnell (1968) derived an equation relating retention time to the equilibrium isotherm taking the following factors into account : nonlinearity of the isotherm, the sorption effect, gas compressibility, gas imperfection and the dependence of the isotherm on total pressure. Conder (1974) simplified the derivation by considering

an incompressible, perfect gas. Valentin and Guiochon (1976(I)) developed a model for the determination of equilibrium isotherms by injecting a pulse over a step of constant concentration. The isotherms they derived from experimental results (1976(II)) for *n*-pentane in squalene and *n*-hexane on graphitised carbon black were in excellent agreement with the corresponding isotherms calculated by static methods. Yeroshenkova *et al.* (1980) included the sorption effect and axial diffusion in their study of the shape of chromatographic elution peaks for both linear and non-linear isotherms. They derived equations for the mobile-phase velocity in terms of the mobile-phase velocity in the absence of solute, Henry's coefficients for solute and eluent and mobile-phase concentration, and for the case where the isotherm is non-linear extra factors were included to take account of the non-linearity. The authors assumed that the isotherm could be described by a quadratic equation.

1.2.2 Sorption-Effect Chromatography in Principle

Consider the case where the carrier gas flowing through the columns is unadsorbed and the effluent flow rate is being monitored (Buffham, Mason and Meacham (1986)). An adsorbable sample gas is injected into one channel. As the extra gas is introduced upstream, gas is pushed from the outlet and there is a flow surge until the pressures in the system have re-equilibrated. When the sample gas reaches the column some of it is adsorbed. Because adsorbed molecules occupy less space than those in the gas phase, there is a pause in flow as some sample gas is removed temporarily from the carrier gas stream. Once all the sample gas has entered the column it can be considered to move as a band. Sample gas is adsorbed at the front of the band and desorbed at the rear of the band as shown in Figure 1.1. Assuming that the partition coefficient does not alter along the column, the net quantity of adsorbed sample gas will remain constant whilst the sample band remains in the column so that the flow rate remains steady. When the sample reaches the end of the column, the sample gas desorbs, re-enters the mobile phase and causes a flow surge. The time integral of the flow rate is then a measure of the volume of sample gas which was adsorbed. The idealised sorption-effect chromatogram for a binary sample gas i.e. the variation of effluent flow rate with time, is shown in Figure 1.3.

If the carrier gas is adsorbed at all, then, when the sample gas is adsorbed at the front of the column, some carrier gas will desorb (because the concentration of carrier in the gas phase has dropped) and the flow perturbation is a measure of the net change in the amount of gas sorbed. As the band moves through the column, sample gas is adsorbed at the front of the band and desorbed at the rear as before, but carrier gas is

Figure 1.3 - An Idealised Sorption-Effect Chromatogram for the Separation of a Binary Mixture in a Non-Sorbed Carrier Gas

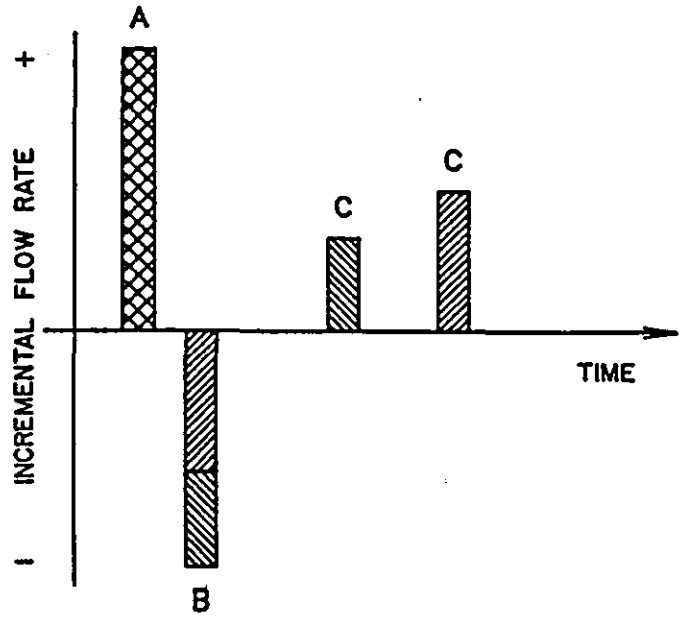

A : The pressure surge caused by sample injection
B : The flow pause caused by adsorption of the sample gases
C : The flow surge caused by the elution of the sorbed gases.

desorbed at the front of the band and resorbed at the rear of the band. As for the adsorption peak, subsequent desorption peaks will indicate the amount of sample gas desorbing less the amount of carrier gas resorbing at the end of the column.

Sorption-effect chromatography differs from conventional chromatography in that it is the flow rate that is measured and not the composition. The flowmeter responds to the sample injection and the entry of the sample gas into the column. The response of the flowmeter to the desorption of sample gas peaks resembles a conventional chromatogram but the integral of a 'flow' peak with time represents an actual gas volume.

1.3 Previous Work

Buffham, Mason and Yadav (1984) presented a theory for the determination of gas-solid equilibrium data using frontal chromatography. The basis of the theory is that the retention times, when defined in terms of arithmetic means, depend on the steady-state conditions before and after the transient and not on the mass-transfer processes (Buffham (1973, 1978)). This is a departure from the usual approach to mathematical modelling of chromatographic processes where terms representing local rates of mass transfer are

incorporated into differential mass balances. The method uses a dual-column chromatograph where pure carrier gas flows in one channel and carrier gas diluted with a small amount of a second gas flows in the other. The total flow rates are assumed to be different in each channel. From an initial steady state the flows are switched so that a composition transient and a flow transient are imposed on each column. Where the mobile phase has a constant molar density and the perturbations are small, the retention times of the composition transient and for the flow transient (τ_x, τ_n respectively) are:

$$\frac{1}{\delta X_1}\int_0^{\infty} x^* dt = \tau_x = \frac{V}{Q^0}\left[\varepsilon + (1-\varepsilon)\left(X_2^0\frac{dq_1}{dc_1} + X_1^0\frac{dq_2}{dc_2}\right)\right] \tag{1.4}$$

$$\frac{1}{N^0\delta X_1}\int_0^{\infty} n^* dt = \tau_n = (1-\varepsilon)\left(\frac{V}{Q^0}\right)\left(\frac{dq_1}{dc_1} - \frac{dq_2}{dc_2}\right) \tag{1.5}$$

where V is the volume of the column with a void fraction of ε, X_1^0 and X_2^0 are the initial steady-state mole fractions of species 1 and 2, q_1,q_2 and c_1,c_2 are the molar concentrations in the stationary and mobile phases, respectively, of the two gas species. Q^0 is the volumetric flow rate. The terms on the left-hand side of equations 1.4 and 1.5* can be evaluated from chromatograms produced by monitoring the composition and flow transients. Buffham, Mason and Yadav (1985) calculated the gradient of the equilibrium curve at infinite dilution for nitrogen and argon on 5A molecular sieve. The theory has been developed further (Mason and Buffham (1989).

The apparatus used to produce these results is shown in Figure 1.4. A high pressure drop across the needle valves was used to set constant carrier gas flow rates. A switching valve situated upstream of the columns allowed the two gas streams to be interchanged. The composition was monitored using a thermal conductivity detector. Capillary flow restrictors were fitted to the column outlets and a differential pressure transducer connected between the restrictor inlets. A change in flow rate in either capillary is indicated by a change in the differential pressure thus enabling the differential flow rate to be monitored. Several undergraduate projects have been concerned with developing the apparatus and validating the theory. The first undergraduate experimenters experienced "considerable flow instability" and constant drifting. They were adding the diluent gas into one flow channel upstream of the needle valve. To overcome these problems the valves were used in conjunction with pressure regulators with an extra needle valve upstream of each column but downstream of the switching valve. With this configuration pure argon was used to feed one column and a ready-made dilute mixture of nitrogen in argon used to feed the other. In a later project, capillary flow restrictors were used with needle valves and pressure regulators to set the flows in each channel.

* x^* and n^* are transient composition and flow perturbations produced by the composition change δX_i in the total flow N^0.

The step changes in flow and composition were introduced by switching two smaller gas streams between the carrier streams, one of the same gas as the carrier and one of a second gas. During the course of these experiments it was realised that sorption-effect chromatography could be developed as a novel analytical method. Other applications of the technique became apparent. Rathor, Buffham and Mason (1987) described how the presence and position of a void zone in a packed column can be detected using a capillary flow meter. They packed a column so that it contained a void zone. A gas sample was injected into the carrier gas stream flowing through the column containing the void. The flow was perturbed by the introduction of the sample and by the sample gas being adsorbed at the start of the column. The flow then returned to its previous rate. As the leading edge of the band of adsorbable sample gas reached the void, gas started to desorb, followed by resorption as the band left the void and re-entered the packing. Consequently there was a surge in flow followed by a pause in flow resulting in a 'doublet' on the sorption-effect chromatogram. The flow rate was constant again until the sample gas desorbed at the end of the column causing a flow surge. The ratio of the time that the doublet occurs to the time that the sample band leaves the column (as indicated by the desorption peak) gives the position of the void as a proportion of the length of the column. Rathor, Buffham and Mason (1988) derived an equation to calculate the volume of a void zone using measurements taken from the sorption-effect chromatogram produced when a sample band traverses a column containing a void.

Figure 1.4 - The Initial Experimental Apparatus

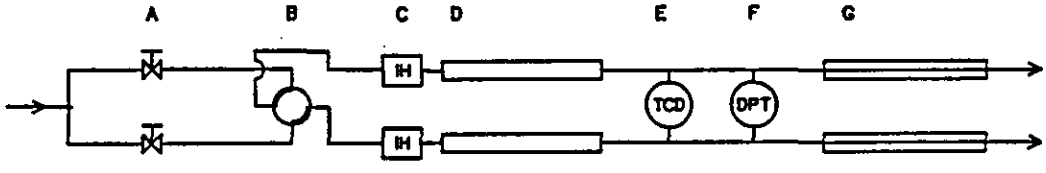

A : Needle Valve
B : Switching Valve
C : Injection Head
D : Chromatographic Column
E : Thermal Conductivity Detector
F : Differential Pressure Transducer
G : Flow-Detecting Capillary.

1.4 Preliminary Experiments

It was known from the earlier work that the injection and passage of a sample gas mixture could be detected by using the same apparatus as that used to observe composition and flow transients. The apparatus was used in a different manner in that pure carrier gas flowed in both channels of the chromatograph instead of one stream being a dilute binary mixture and also the switching valve was redundant, the sample being introduced by syringe through a septum. Figure 1.5 shows the chromatograms produced when 0.02mL of air is injected into one of the two parallel, pure helium carrier gas streams. The upper trace is the response of the TCD with time, the lower trace is the response of the differential flowmeter. A complex sequence of flow changes occurs as the sample is injected. First there is an increase in flow followed by a decrease in flow. The initial expected response as the sample is injected is a flow surge because extra gas is being pushed into the system. The secondary response is a flow pause as the sample gas is adsorbed at the start of the column. The expected separation of oxygen and nitrogen is indicated by two later peaks on both the flow chromatogram and the TCD chromatogram.

To determine how the flow response varies with the gases involved, four different gases, namely helium, hydrogen, argon and nitrogen, were each used in turn as the carrier gas. The remaining three gases were used either on their own or in combination to make up the samples to be injected.

1.4.1 Using a Helium Carrier Gas

Figure 1.6 shows the chromatograms produced by injecting a mixture of equal parts of nitrogen, argon and hydrogen into helium. Helium is only weakly adsorbed by 5A molecular sieve. The upper and lower traces are the responses of the TCD and the differential flowmeter respectively. The injection peak (Peak A on the flow trace) is of the same composite nature as in Figure 1.5, a flow surge and flow pause combined. There are three desorption peaks as confirmed by the TCD chromatogram. The earliest of these peaks (peak B) is due to the hydrogen emerging from the column. This peak appears to be a flow surge superimposed on a flow pause. Peak C is a flow surge due to the elution of the argon gas. The final peak (D) is a flow surge caused by the nitrogen eluting. These identifications are confirmed by the response to the injection of each of the sample components individually (Figures 1.7 - 1.9). Figure 1.7 shows the detector responses to the injection of a pure hydrogen sample into helium carrier gas. The flow trace shows initially a surge in flow followed immediately by a pause in flow after the sample has been injected. The elution of the hydrogen gas produces a similar peak to the peculiar,

Figure 1.5 - The Injection of Air into a Helium Carrier Gas

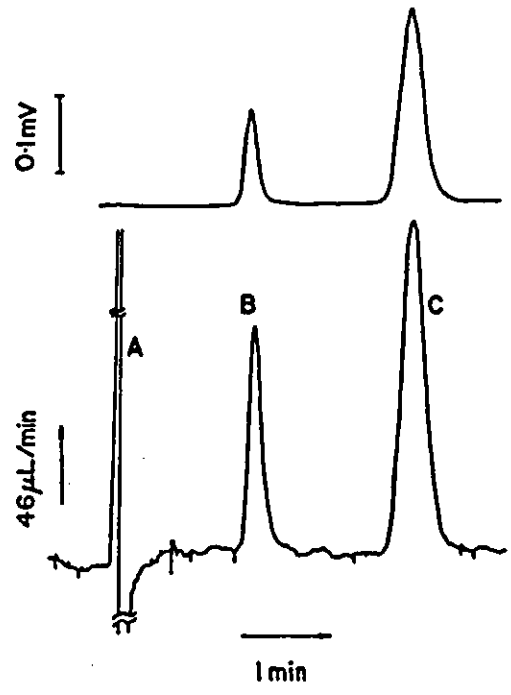

The flow trace (lower) shows :-
A : The combined effect of the sample injection and sample adsorption
B : The elution of oxygen
C : The elution of nitrogen
The composition trace (upper) shows only the elution of the sample gases.

first elution peak (B) shown on the flow trace in Figure 1.6, firstly a flow surge superimposed on a flow pause. The chart traces produced by injecting a pure argon sample into helium carrier gas is shown in Figure 1.8. The injection of the gas again causes first a surge in flow followed by a smaller pause in flow. Later there is a flow surge as the argon elutes from the column at a time corresponding to the time of the second elution peak (C) on the flow trace shown in Figure 1.6. Similarly, injection of a pure nitrogen sample into helium carrier gas causes a flow surge followed by a flow pause and the subsequent elution of the sample results in a flow surge (Figure 1.9). The time of the nitrogen elution peak corresponds to the time of the final elution peak (D) on the flow trace shown in Figure 1.6. The peaks detected by the TCD as shown on the upper traces in Figures 1.7 to 1.9 correspond to the three peaks on the upper trace in Figure 1.6.

Figure 1.6 - The Injection of a Hydrogen/Argon/Nitrogen Sample into Helium Carrier Gas

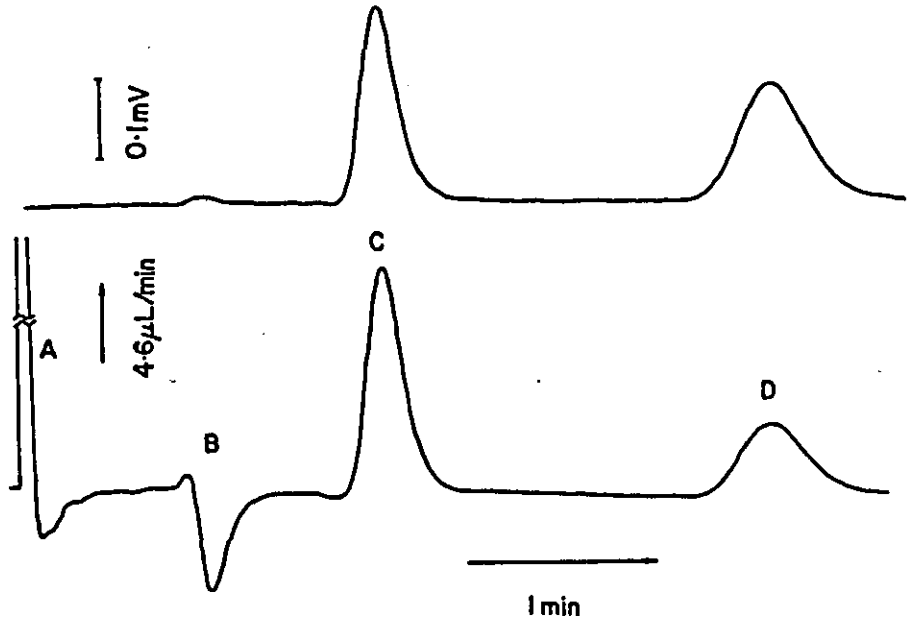

The flow trace (lower) shows
A : the combined injection and adsorption peak
B : a curious double peak caused by hydrogen elution
C : the argon elution peak
D : the nitrogen elution peak.
The composition trace (upper) shows the desorption peaks.

Figure 1.7 - The Injection of a Hydrogen Sample into Helium Carrier Gas

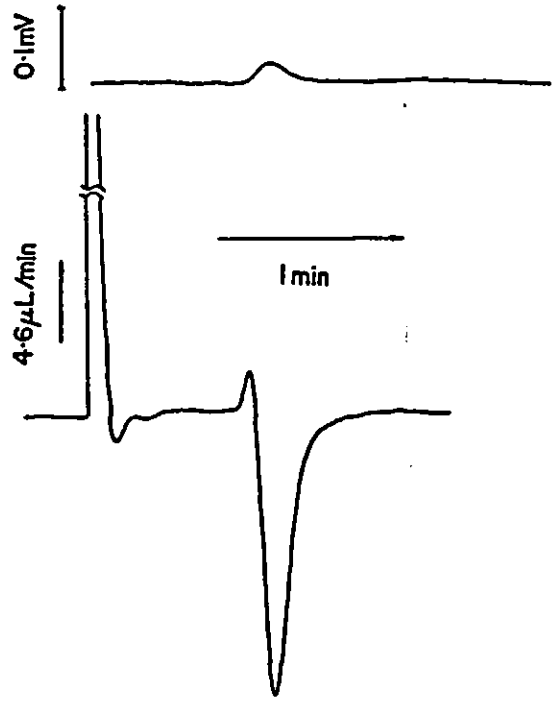

Upper trace - TCD response
Lower trace - flowmeter response

Figure 1.8 - The Injection of an Argon Sample into Helium Carrier Gas

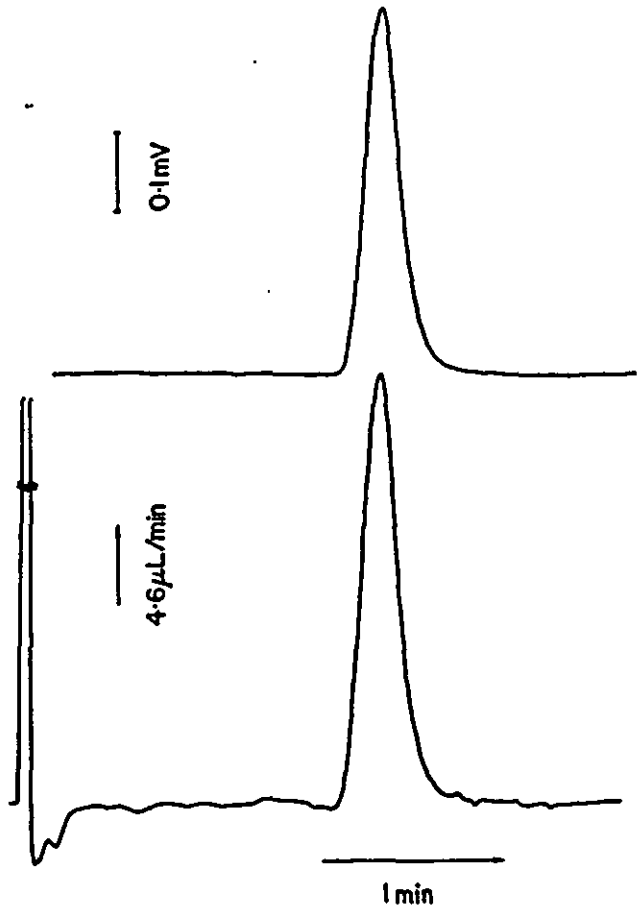

Upper trace - TCD response
Lower trace - flowmeter response

1.4.2 Using a Hydrogen Carrier Gas

The chromatograms shown in Figure 1.10 were produced using hydrogen as the carrier gas and injecting a sample mixture of equal parts of nitrogen, argon and helium. Hydrogen is only weakly adsorbed by 5A molecular sieve, if at all. The TCD trace (upper) is again as expected, showing the three desorption peaks. The flow trace (lower) has a less pronounced combination injection peak. The flow pause (combined with the flow surge), if any, is lost in the baseline ripples. The helium emerges first and gives a response similar to that of a hydrogen sample into helium. However, in this case, the first effect is a pause in flow followed by a larger surge in flow, giving a curious double peak. The elution of argon and nitrogen are as before in Figure 1.6.

Figure 1.9 - The Injection of a Nitrogen Sample into Helium Carrier Gas

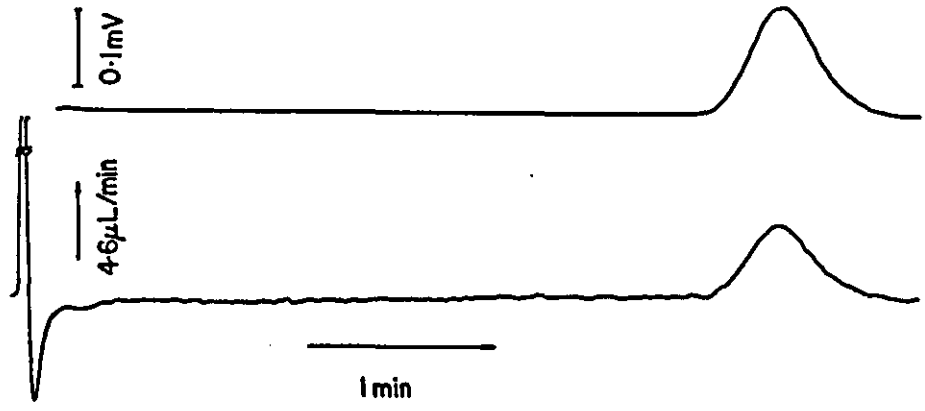

Upper trace - TCD response
Lower trace - flowmeter response

Figure 1.11 shows the chromatograms produced by the passage of a pure helium sample being injected into a hydrogen carrier gas. The injection of the sample causes a surge on the flow trace but there is no flow pause immediately following the surge unlike on the flow chromatogram in Figure 1.10. The desorption of the helium band causes a flow pause superimposed on a flow surge which occurs at a similar time to the earliest desorption peak (B) on the flow trace in Figure 1.10. The injection peak for an argon sample in the hydrogen carrier gas is of the same form as that in Figure 1.10. The peak consists of a flow surge followed immediately by a flow pause. The desorption peak corresponds to the second desorption peak (C) in Figure 1.10 and is a flow surge. The injection of nitrogen produces the 'familiar' flow surge followed immediately by a flow pause. The elution of the nitrogen causes a flow increase occurring at the same time as the third elution peak (D) in Figure 1.10. Comparison of the composition (upper) trace in Figure 1.10 with the composition traces (upper) in Figures 1.11 to 1.13 shows that each of the three peaks in Figure 1.10 are reproduced.

Figure 1.10 - The Injection of a Helium/Argon/Nitrogen Sample into Hydrogen Carrier Gas

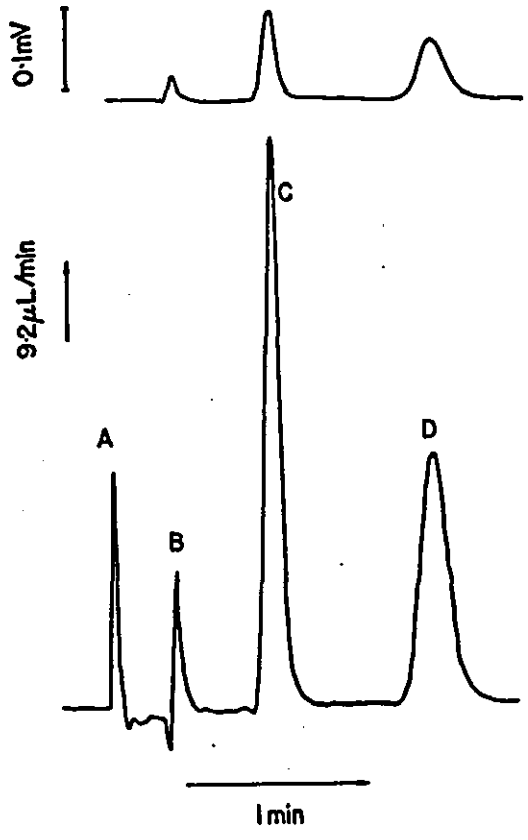

The flow trace (lower) shows

A : the injection peak combined with the adsorption peak

B : a curious double peak caused by the helium band leaving the column

C : the argon elution peak

D : the nitrogen elution peak

The TCD trace (upper) shows the three desorption peaks.

Figure 1.11 - The Injection of a Helium Sample into Hydrogen Carrier Gas

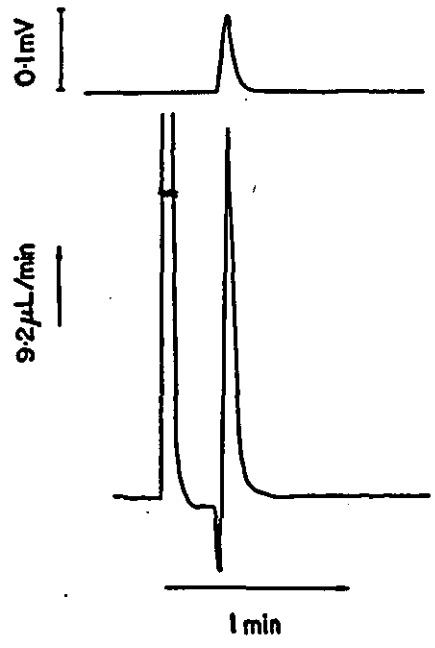

Upper trace - TCD response
Lower trace - flowmeter response

Figure 1.12 - The Injection of an Argon Sample into Hydrogen Carrier Gas

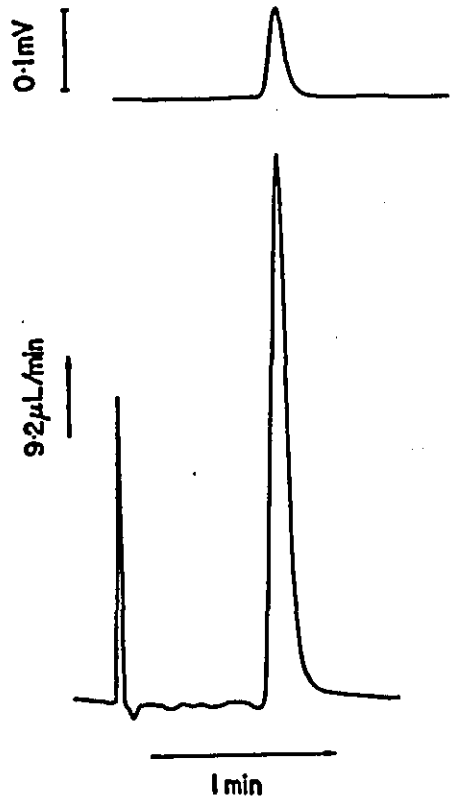

Upper trace - TCD response
Lower trace - flowmeter response

1.4.3 Using an Argon Carrier Gas

Figure 1.14 shows the response to a mixture of equal parts of hydrogen, helium and nitrogen being injected into an argon carrier gas. Argon is adsorbed by 5A molecular sieve. The injection peak is the first to appear on the flow trace (lower). There appears to be no flow pause superimposed on the injection peak. The first peak is due to the emergence of the helium gas and is a flow pause. The second peak is also a flow pause caused by the emergence of the hydrogen gas. The hydrogen and helium components are not completely resolved on the TCD trace but the flow trace appears to return almost to baseline between the two peaks. Much later, the nitrogen peak is visible as a flow surge. The TCD trace (upper) shows the three expected desorption peaks.

Figure 1.13 - The Injection of a Nitrogen Sample into Hydrogen Carrier Gas

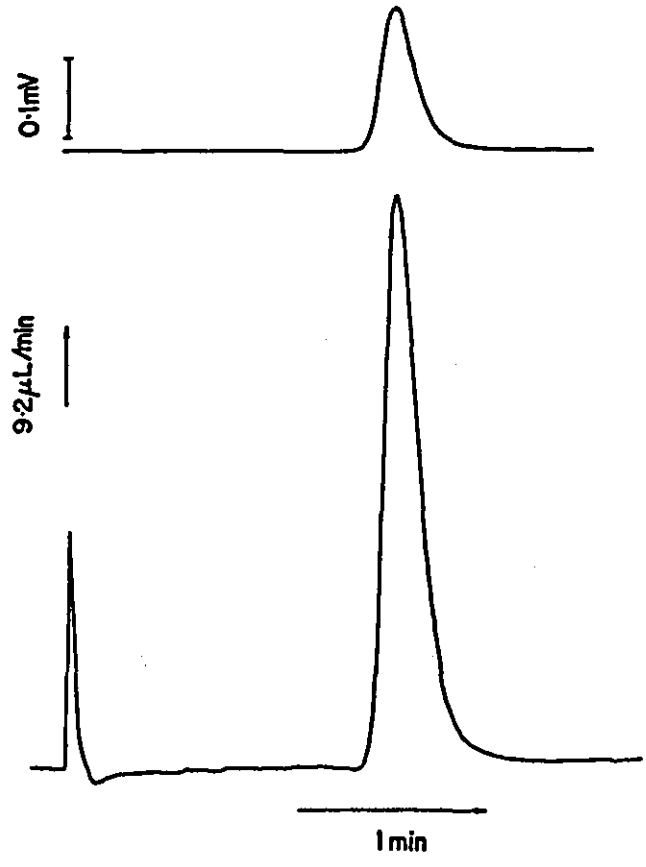

Upper trace - TCD response
Lower trace - flowmeter response

The flow response to the injection of a pure helium sample (Figure 1.15 - lower trace) into argon carrier gas is a flow surge as the sample is injected and a flow pause as the sample elutes from the column. The elution peak may be preceded by a slight flow surge. The TCD response (upper trace) shows only the helium desorption peak. Figure 1.16 shows the chromatograms produced by the injection of a pure hydrogen sample into argon. On the flow trace (lower) there is a flow surge as the sample is injected and, as with the helium sample, a flow pause as the sample is eluted. The composition trace (upper) again shows only one peak, caused by the elution of the sample. For a nitrogen sample being injected the first response is a flow surge followed immediately by a flow pause and the later response is a flow surge as the nitrogen elutes (Figure 1.17).

Figure 1.14 - The Injection of a Helium/Hydrogen/Nitrogen Sample into Argon Carrier Gas

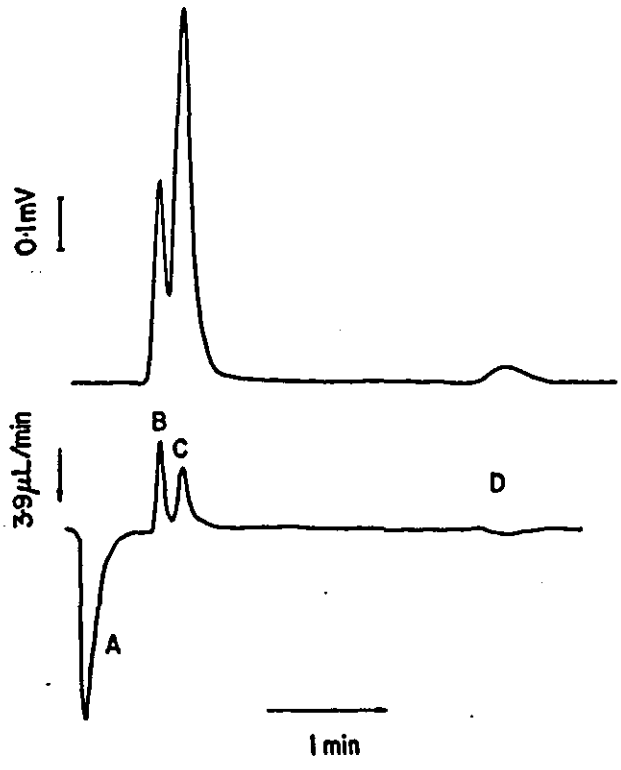

The flow trace (lower) shows

A : the injection peak

B : the peak caused by the helium leaving the column

C : the peak caused by the hydrogen leaving the column

D : a peak in the opposite sense to B and C caused by the nitrogen leaving the column.

The composition trace (upper) shows the three desorption peaks.

Figure 1.15 - The Injection of a Helium Sample into Argon Carrier Gas

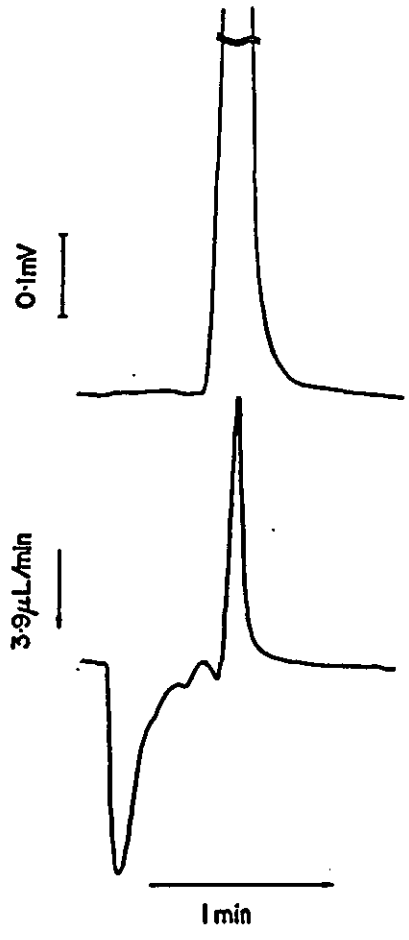

Upper trace - TCD response
Lower trace - flowmeter response

Figure 1.16 - The Injection of a Hydrogen Sample into Argon Carrier Gas

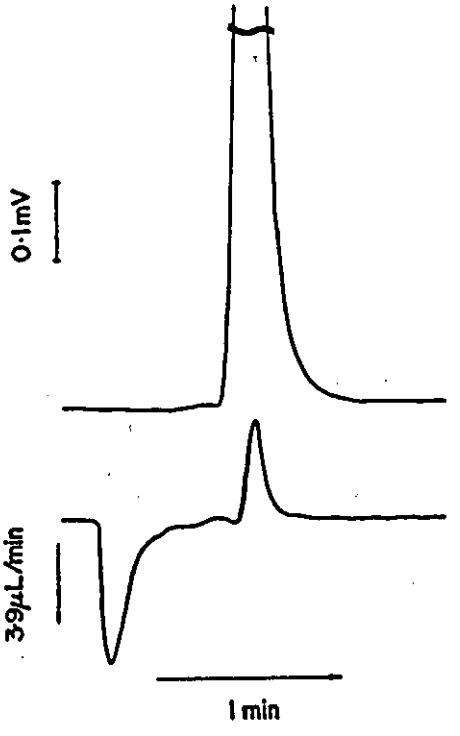

Upper trace - TCD response
Lower trace - flowmeter response

Figure 1.17 - The Injection of a Nitrogen Sample into Argon Carrier Gas

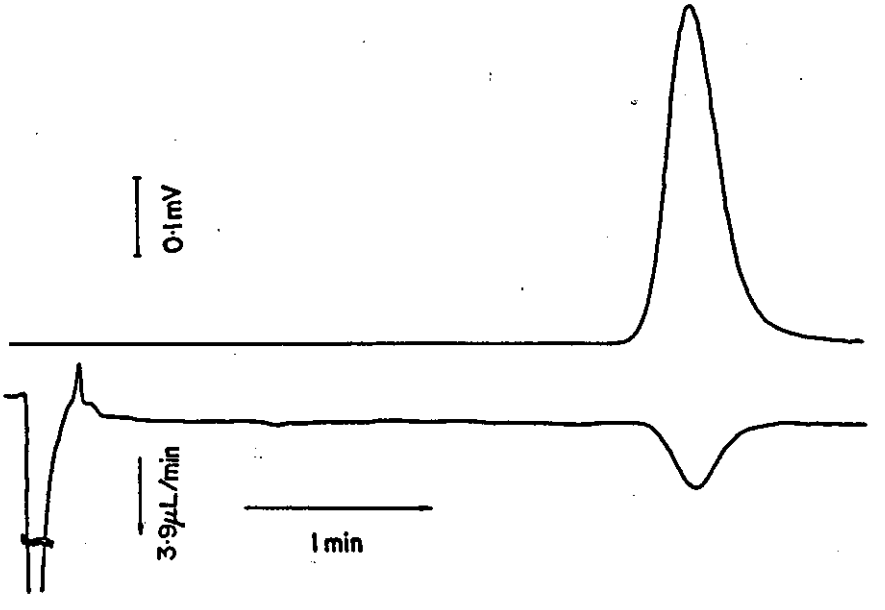

Upper trace - TCD response
Lower trace - flowmeter response

1.4.4 Using a Nitrogen Carrier Gas

Figure 1.18 shows a hydrogen, helium and argon sample being injected into nitrogen. Nitrogen is relatively strongly adsorbed on 5A molecular sieve. The TCD chromatogram is the upper trace and the flowmeter response the lower. The injection peak (Peak A on the flow trace) has a slight step after the peak maximum and there is no overshoot to the other side of the baseline. Once more the helium peak (B) and the hydrogen peak (C) show up as flow pauses. The later argon peak (D) is also a flow pause.

Figure 1.18 - The Injection of a Helium/Hydrogen/Argon Sample into Nitrogen Carrier Gas

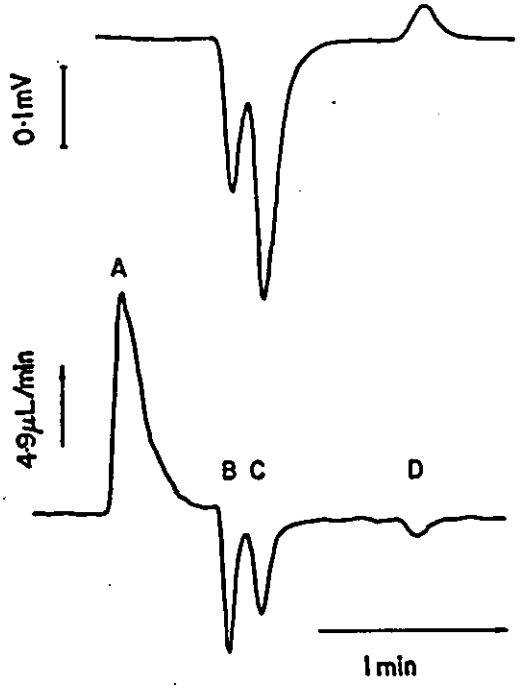

The flow trace (lower) shows
A : the combined injection and adsorption peak
B : the peak caused by helium leaving the column
C : the peak caused by hydrogen leaving the column
D : the peak, in the opposite sense to B and C, caused by argon leaving the column.
The composition trace shows the three elution peaks.

The injection and desorption peaks for separate injections of the pure sample components take the same form as those in Figure 1.18. Figure 1.19 shows the chromatograms produced by injecting helium into nitrogen carrier gas, Figure 1.20 shows those produced by injecting hydrogen into nitrogen and Figure 1.21 shows the traces for an argon sample in nitrogen carrier gas.

Figure 1.19 - The Injection of a Helium Sample into Nitrogen Carrier Gas

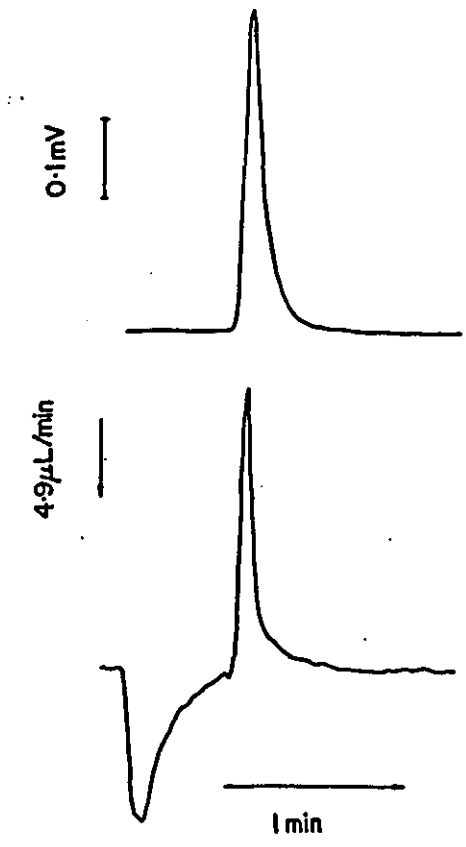

Upper trace - TCD response
Lower trace - flowmeter response

Figure 1.20 - The Injection of a Hydrogen Sample into Nitrogen Carrier Gas

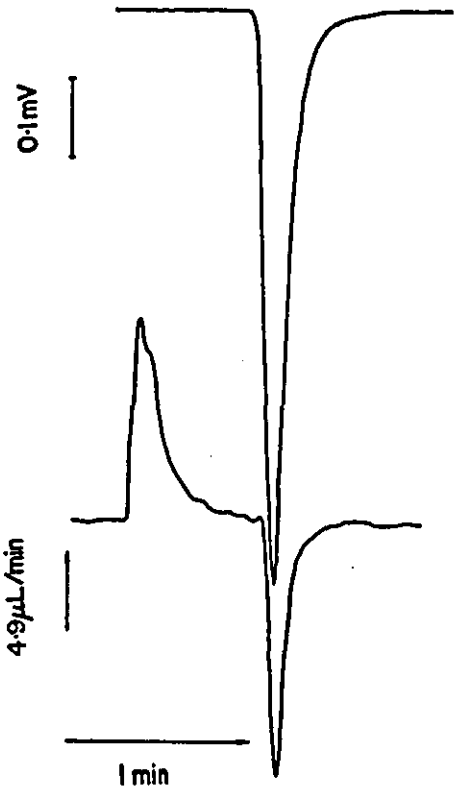

Upper trace - TCD response
Lower trace - flowmeter response

Figure 1.21 - The Injection of an Argon Sample into Nitrogen Carrier Gas

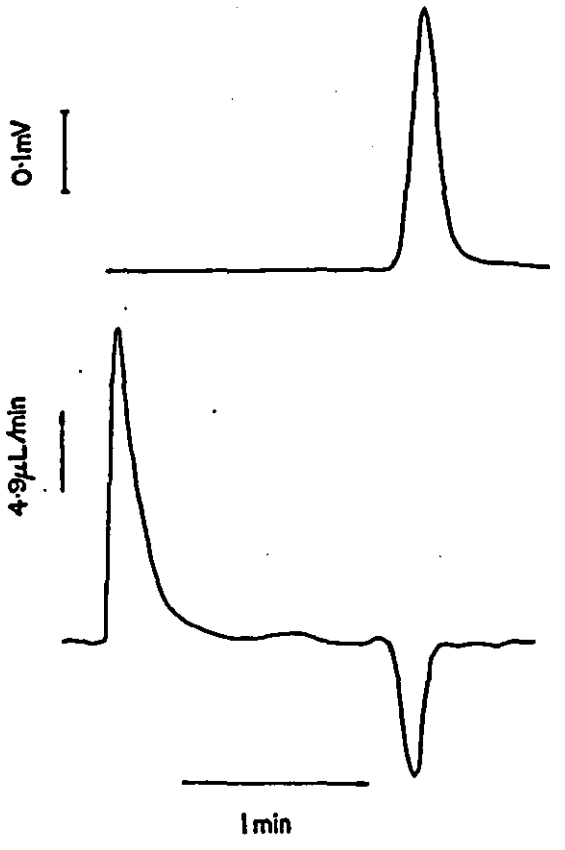

Upper trace - TCD response
Lower trace - flowmeter response

1.4.5 Summary of Preliminary Results

Carrier Gas	Form of Peak [Flow surge (+) Flow pause (-)]					Corres-ponding Figure
	Injection	He	H_2	Ar	N_2	
He	+/-	x	+/-	+	+	1.6
	+/-	x	+/-	x	x	1.7
	+/-	x	x	+	x	1.8
	+/-	x	x	x	+	1.9
H_2	+/-	-/+	x	+	+	1.10
	+	-/+	x	x	x	1.11
	+/-	x	x	+	x	1.12
	+/-	x	x	x	+	1.13
Ar	+	-	-	x	+	1.14
	+	+(?)/-	x	x	x	1.15
	+	x	-	x	x	1.16
	+/-	x	x	x	+	1.17
N_2	+	-	-	-	x	1.18
	+	-	x	x	x	1.19
	+	x	-	x	x	1.20
	+	x	x	-	x	1.21

1.5 The Work Reported in this Thesis

Although these traces confirm that the flow of gas through a chromatograph is disturbed by the introduction and subsequent passage of a sample gas, the observed flow perturbations have not been fully explained by these preliminary experiments. This phenomenon is worth investigating further because the only condition to be satisfied for flow changes to occur is that a chromatographic separation is possible. The method, unlike other methods, does not rely on changes in a physical property of the gas in order that the sample species may be detected and could be used for any combination of gases having different partition coefficients. In addition, this technique is potentially an absolute analytical method needing no calibration because the observed flow rate changes represent molar quantities. The work described in the remainder of this thesis covers:

i) the identification and elimination of random flow rate fluctuations which can be seen superimposed on the more major effects in Figure 1.5

ii) establishing why the form of the injection peak varies depending on which gases are involved and their respective roles (i.e. carrier or sample)

iii) what causes some of the peaks produced to take a peculiar form in one carrier gas only to yield an expected shape of response in a different carrier gas

iv) the reason why some elution peaks on the sorption-effect chromatogram indicate an increase in flow rate and some indicate a decrease in flow rate, and some indicate both an increase and a decrease

v) what effect changes in viscosity and density have on the sorption-effect chromatogram

vi) the significance of the relative areas of the peaks produced as the sample enters the column and those produced as the sample components elute from the column

vii) how the areas of the elution peaks can be used to determine the original sample composition.

CHAPTER TWO - THE SORPTION-EFFECT CHROMATOGRAPH

2.1 Conventional Gas Chromatography

The apparatus with which chromatography is performed is generally known as a chromatograph. Typically a gas chromatograph consists of :

a) a gas supply with a flow control system

b) a means of sample introduction

c) one or more adsorbent columns, and,

d) a detector which will differentiate between pure carrier gas and a mixture of carrier gas and the resolved sample species. This is the fundamental difference between conventional chromatography and sorption-effect chromatography where the detector is a flowmeter.

The complete apparatus is normally housed in one 'box', incorporating a thermostatted oven for the column(s) and a thermostatted chamber for the detector. In some cases the detector may be positioned within the oven. The flow controllers are usually mounted on an instrument panel together with the temperature controller and temperature indicator. A means of introducing sample gas is included upstream from the column(s) and the detector is located downstream. The detector may use the effluent from one column as a reference stream for the other, i.e. take a differential measurement, or, it may measure an absolute property of the gas eluting from the flow channel into which the sample was introduced. The output of the detector is amplified and sent to a chart recorder and/or an integrator.

2.2 The Generation of a Stable Carrier-Gas Flow Rate

As stated earlier, in order to be able to measure the various flow changes which occur as a sample band passes through a chromatograph, the carrier-gas flow rate must be highly stable. The flow rate is sensitive to various external parameters such as temperature and pressure, and the sorption effect is not the only phenomenon to produce fluctuations in the flow rate, hence, care must be taken in the construction of the more conventional parts of a sorption-effect chromatograph.

In conventional chromatography, the precision needed for carrier-gas flow-rate control varies with the chromatographer's needs (Purnell (1967)) and for routine analysis very close control is not essential. In the simplest case the cylinder pressure regulator may suffice. The inclusion of a pressure-regulating valve upstream of the column will reduce the effect of pressure changes downstream in the system provided that a very

large pressure drop is employed across it. The internal volume of the valve will change with temperature because of expansion or contraction of the valve body hence the pressure drop across the valve will change with temperature.

Lack of sensitivity of a detector to flow rate changes is often listed as one of the conditions to be met (e.g. Dimbat, Porter and Stross (1956); Boer (1957); James (1957); McWilliam (1959); Schmauch (1959)) - of course, that is not the case in sorption-effect chromatography (and some others form of chromatography). In practice this condition is not met and several attempts have been made to produce a stable carrier-gas flow rate to minimise irregularities in the detector response. Conder and Young (1979) state that if the column does not have a large pressure drop then either a flow impedance is needed upstream of the column or a precision flow controller must be used. Van de Craats (1958) found that flow changes were less pronounced when a restriction (such as a needle valve) was used upstream of the column, and, Dyson and Littlewood (1967(I),(II)) used needle valves, in conjunction with a pressure control, to keep the column upstream pressure constant. Haarhoff and van der Linde (1965) employed a differential flow controller to minimise flow velocity changes. Valentin and Guiochon (1976(II)) controlled the column inlet pressure with respect to a reference pressure (atmospheric) but, for the precision their work required, deemed it unnecessary to control the reference pressure, or the column outlet pressure. Time-dependent pressure profiles resulting from fluctuations due to inadequate pressure regulation, flow start-up and other flow rate changes were studied by Schettler and Giddings (1965). Their study was conducted on an apparatus where make-up gas was fed into the system downstream of the detector to ensure that the outlet pressure remained constant (within 'acceptable' limits). The make-up flow rate was much larger than the carrier-gas flow rate. A regulator was used by Dimbat, Porter and Stross (1956) to control the pressure at the head of the column. They assumed that small flow deviations would be smoothed out by their column acting as a buffer. A tank was used as a buffer in the reference supply to the TCD. They dismissed the use of a pressure-developed-across-a-constriction type of flowmeter because of the change in back pressure as samples emerge from a column (which was probably due to the sorption effect). Adlard, Khan and Whitham (1960) and Huber and Gerritse (1971) set the carrier-gas flow rate by developing a constant pressure head followed by a large, constant pneumatic impedance, a capillary choke. James and Phillips (1952) developed a similar but more sophisticated system in which excess carrier gas is 'blown off' through a sintered disk. Greene, Moberg and Wilson (1956) continually adjusted their pressure regulator upstream of the column to maintain the correct pressure drop.

2.3 Sample Introduction

The sample gas is usually introduced by syringe injection through an injection head containing a septum, or, by use of a gas sampling valve. The problems associated with these methods are thoroughly dealt with by Debbrecht (1985). It is necessary that the injection procedure be able to provide a sample having a composition representative of the sample mixture and of known, reproducible size.

2.3.1 Injection by Syringe

Figure 2.1 shows a cross-section of a Pye injection head. The injection head is the fitting at the head of the column. Carrier gas enters the head through the side port. The syringe needle is inserted through the rubber septum and the sample gas injected. When the needle is removed the septum should seal the hole but in practice this area is very susceptible to leaks. Leaks will not make much difference to the operation of a conventional chromatograph but are unacceptable when small flow rates are being measured. Some injection heads incorporate a heater for vaporising liquid samples.

Figure 2.1 - A Cross-Sectional View of the Pye Injection Head

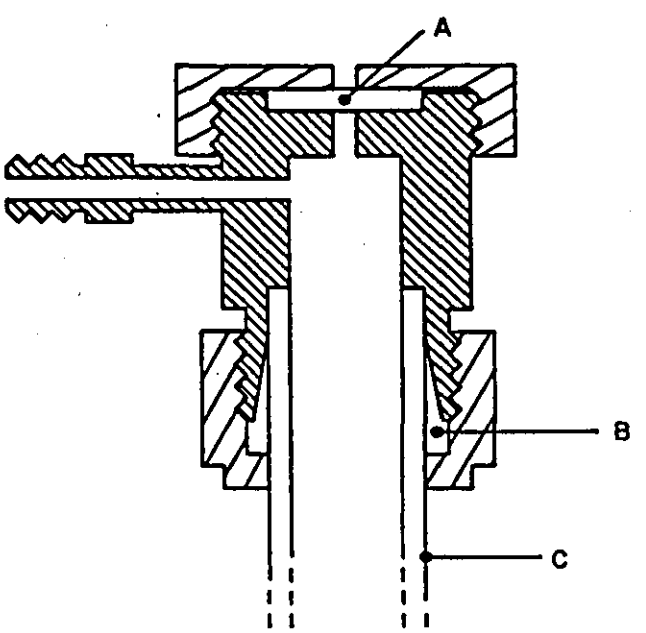

A : Rubber Septum
B : Ferrule
C : Column Wall

In Chapter 1, the 'injection' peak was shown to vary in shape and sense according to the gases present. Every injection of gas reported caused a flow surge. In some cases this flow surge was followed closely by a reduction in flow so that the two effects were partly superimposed but in other cases the flow surge was the only observed effect. Use of a syringe to inject the sample gas results in the following flow perturbations. Upon insertion of the needle through the septum, the carrier gas in the injection head and the sample gas in the syringe reach the same pressure. Invariably the pressure in the injection head is greater than that of the sample gas at atmospheric pressure so carrier gas leaves the system to raise the pressure in the syringe. A temporary reduction in flow can be observed as this occurs. This was not recorded on any of the chromatograms in Chapter 1. If no further action is taken after needle insertion, the baseline will return to its previous value. Depressing the syringe plunger reduces the volume of the flow system and gas is pushed out at the downstream end of the chromatograph. This causes a temporary increase in flow until the pressure in the system returns to its former level. This action will always cause a surge in flow rate. If the sample is injected directly into the column then the flow perturbations caused by the sample gas reaching the adsorbent will be superimposed in part onto the flow surge caused by injection.

2.3.2 Gas Sampling Valves

Gas sampling valves are more convenient and more reliable than syringes. There are many makes of valve but the principles involved are the same. Each valve has two components which are pressed together to form a gas-tight seal. When the valve is switched, one of the components will move relative to the other. The moving part of the valve may be rectangular, cylindrical or disc-shaped. The stationary component has tappings from the mating surface through to the external valve ports. Flow paths are bored into, or scored onto the moving part so that different ports of the valve can be connected together at different times. The valves shown in Figures 2.2 and 2.3 employ a plastic disc which rotates on a polished metal surface carrying access holes to each of the valve ports. One manufacturer of this type of valve is a company called Specac.

2.3.2.1 Internal Loop Sample Valves

Figure 2.2 shows a valve which is capable of delivering very small samples whose size is determined by the volume of the slot on the upper surface of the disc. There is a by-pass channel on the underside of the disc connected to the upper surface of the disc by a hole at each end. Figure 2.2 (III) represents the surface with the access holes to the valve ports. Part (I) shows the surface of the disc which seals with part (III) with the disc in the load position. The sample gas stream enters port 2, flows along the sample volume

cut into the surface of the disc, and exits via port 4. The carrier gas enters port 1, passes along the by-pass slot, and exits via port 3. When the disc is rotated to the position shown in part (II) of Figure 2.2, the sample volume is switched between ports 1 and 3 and that volume of sample is introduced into the carrier stream. The sample flow is shut off.

Figure 2.2 - Operation of a 4-Port Sample Valve

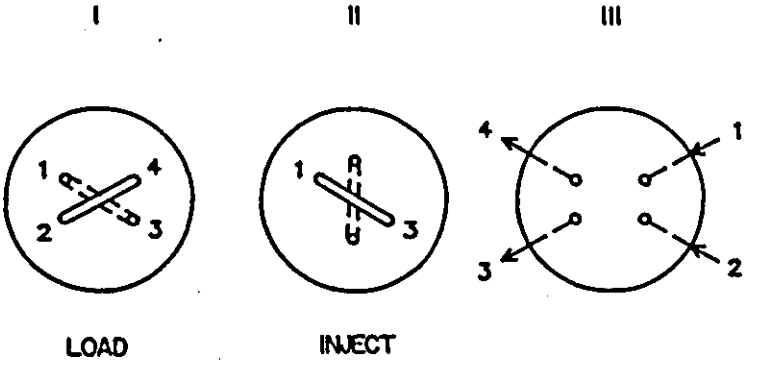

I : The disc surface shown with the valve in 'load' position
II : The disc surface shown with the valve in 'inject' position
III : The stationary surface with which the rotating disc makes a gas-tight seal

2.3.2.2 External Loop Sample Valves

Figure 2.3 shows a valve suitable for introducing relatively large samples by way of an external sample loop. The valve has six ports (Figure 2.4 (III)). The sample loop is connected between ports 1 and 4. The disc is scored with three equidistant 60° arcs so that the valve ports are connected in pairs. When the disc is in the load position (Figure 2.4(I)), the sample gas stream flows in at port 2, along one flow slot on the disc to port 1, through the sample loop to port 4, along a second flow slot to port 3 and out. Carrier gas enters port 6, flows along the remaining slot to port 5 and out. When the disc is rotated 60° (Figure 2.4(II)), port 6 is connected to port 1 and port 4 to port 5 so the sample gas contained in the sample volume is swept into the carrier stream. The sample stream flows into port 2, along the remaining slot and out of port 3.

Figure 2.3 - Operation of a 6-Port Sample Valve

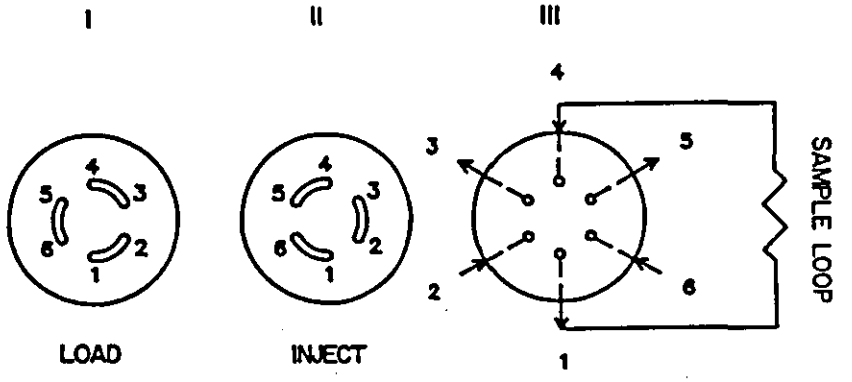

I : The disc surface shown with the valve in 'load' position
II : The disc surface shown with the valve in 'inject' position
III : The stationary surface with which the rotating disc makes a gas-tight seal

2.3.2.3 Operation

In general, the mass of sample used is similar in all variations of elution chromatography so, because liquids are more dense than gases, very small sample volumes tend to be used for liquid samples and the larger sample volumes for gas samples. The operation of sample valves for introducing gas samples will be dealt with here.

The sample gas supply is connected to the sample inlet port. This may be direct from a gas bottle regulator or via a gas mixing system (See Appendix I). There is a needle valve at the sample outlet port to limit the flow rate of the sample gas vent. The sample loop is then maintained at the supply pressure and the sample size can be varied in accordance with this pressure i.e. the sample size can be increased twofold by doubling the supply pressure (absolute). This is the case regardless of which type of sample valve, described above, is used. Carrier gas flows into and out of the sample valve via the remaining ports but, in order not to shut off the carrier flow during switching, a by-pass loop is employed (shown schematically in Figure 2.4).

Upon turning the valve to the inject position, the sample volume is switched into the carrier flow. One of three things could now happen. If the sample pressure is greater than the pressure of the carrier gas at this point in the system, the sample gas will expand into the system and cause a flow surge. If the sample pressure and the carrier gas pressure are exactly matched, the flow rate will not be perturbed at all. If the sample pressure is less than that of the carrier gas then the sample slug will be compressed by the carrier

Figure 2.4 - The Pipework Configuration to a Sample Valve Ensuring that the Carrier Gas Flow is not Interrupted

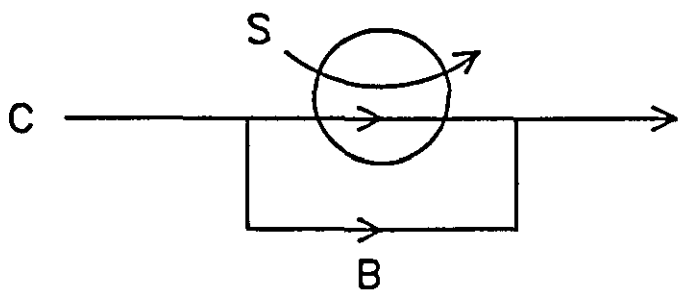

S : sample gas flow path
C : carrier gas flow path
B : by-pass loop

gas and the flow will drop as this takes place. The most common occurrence is that the sample pressure is much higher than that of the carrier gas and the 'injection' is marked by a flow surge.

2.4 The Chromatographic Columns

The column packing material must be capable of adsorption in order to effect a separation. Solute can be adsorbed by a surface in two ways (Littlewood (1970)), physical adsorption and chemisorption. The former of these is prevalent in gas chromatography. The physical bonds between the solute and the adsorbent surface are easily formed and broken whereas any chemical bonds are much stronger. Chemisorption usually occurs at temperatures above those normally used for gas chromatography. Several varieties of activated adsorbents are in general use (Purnell (1967)). The most common are carbon, alumina, silica and zeolites.

At this stage in the development of the method all that the columns were required to do was separate a mixture of permanent gases (in the first instance, air) so columns similar to those with which the earlier experiments had been performed (described in Chapter 1) were chosen.

The Pye chromatograph uses 1.5m×6mm o.d.×4mm i.d. glass columns with 1.5mm o.d. stainless steel tubing at the outlet connected via a glass to metal seal. This tubing connects the column directly to the TCD. As in the previous work the columns were packed with 22-30 mesh (710-500μm) 5A molecular sieve.

2.4.1 Zeolites (Molecular Sieves)

The word zeolite is derived from the Greek "zeo" meaning boil and "lithos" meaning stone. Zeolites (Barrer (1978)) are crystalline metal aluminosilicates with a three-dimensional interconnecting network structure of silica and alumina tetrahedra. Some occur naturally and some have only been produced synthetically. Zeolites are of interest because they have the capacity to sorb gases, vapours and liquids, to catalyse reactions, and to act as cation exchangers. The fundamental building blocks in zeolites are SiO_4 and AlO_4. Cations are required to neutralise any charge. Water molecules and cations are free to move within the crystals and so can be readily removed or exchanged respectively.

Molecular Sieve 5A is a form of zeolite A, a synthetically produced zeolite. Calcium is the cation associated with this form. (Molecular Sieves 3A and 4A are the potassium and sodium forms of zeolite A respectively). The crystals contain interconnecting cavities of uniform size, separated by narrower openings, or pores, of equal uniformity. (The type number for zeolite A is an indication of the pore diameter in angstroms.) On formation, this network is filled by water molecules which can be driven off by moderate heat without altering the crystal structure. Once the water has been removed, the crystal has an enormous surface area and pore volume available for adsorption. The regeneration process can be repeated indefinitely under the correct circumstances. Molecular Sieves are thermally stable to around 550°C but repeated heating above 320°C will shorten the useful life of the adsorbent.

5A Molecular Sieve will adsorb many different molecules. For this work its suitability is that it will adsorb gases which are readily, commercially available i.e. N_2, O_2, H_2, Ar, CO_2, CH_4, Air, etc, etc....

2.5 Chromatographic Detectors

2.5.1 Detection Principles

Boer (1957) suggested that there are three basic principles for a detecting system :

a) the change in gas flow rate due to the emergence of a component

b) the reduction in concentration of the carrier gas, and,

c) the change in some property of the gas

a) and b) involve accurate measurement of small changes in large values but could eliminate the need for calibration, however, most detecting systems are based on principle c).

Many authors have suggested which the important factors are regarding chromatographic detectors (Dimbat, Porter and Stross (1956); Boer (1957); James (1957); McWilliam (1959); Schmauch (1959)). In general there are four main considerations (McWilliam 1959) :

i) Sensitivity - the detector has a high sensitivity to all substances irrespective of their chemical nature. Sensitivity can be expressed in several different ways but the most convenient representation is that of the minimum detectable level (O'Brien (1985)). Figure 2.5 shows a typical peak with peak height, S, peak base width, W, and noise level, N. The detected level (g/sec) is the mass of the sample component divided by the width at half the peak height and this corresponds to a signal-to-noise ratio of S/N. The minimum detectable level, MDL, is that which corresponds to a signal-to-noise ratio of two (i.e. MDL = 2× the detected level/S/N).

ii) Response time - must be short enough to ensure that negligible peak distortion occurs. Long response times cause band broadening and sometimes peak asymmetry and may result in overlap between species (Schmauch (1959)).

iii) Relationship between detector output and molecular parameter - if the response is dependent on some simple law it may be possible to dispense with empirical calibration for each and every substance and conditions. Accuracy depends on linearity and reproducibility.

iv) Ease of construction and operation.

Figure 2.5 - Calculation of the Minimum Detectable Level of a Sample Species

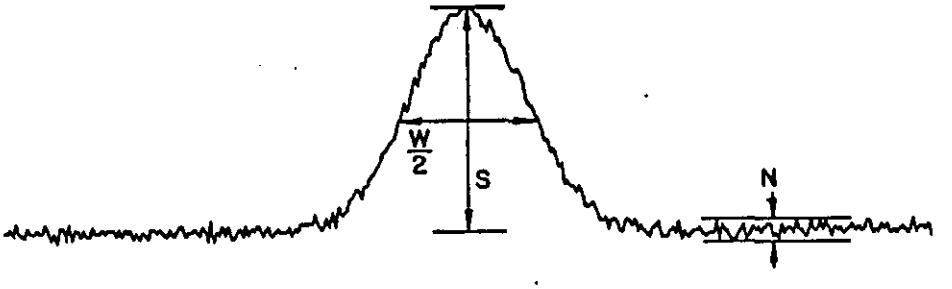

As stated by Boer (1957), the most commonly used chromatographic detectors measure some physical property of the gas passing through them. Obviously this property must vary with composition and it is unlikely that the same detector will be suitable for every gas combination.

2.5.2 Conventional Detectors

The two most commonly used detectors are the thermal conductivity detector (TCD) and the flame ionisation detector (FID).

2.5.2.1 The Thermal Conductivity Detector

The TCD uses the principle that heat loss from a filament wire in a gas stream varies with the thermal conductivity of the gas flowing over it thereby altering the filament resistance (O'Brien (1985)). The detector needs to be calibrated for the component and the concentration range in which it is being used (Keulemans, Kwantes and Rijnders (1957)). Hydrogen and helium have similar thermal conductivities so if one or the other is used as a carrier gas the sensitivity of the detector is increased but it is difficult to detect one gas in the other. Care must be taken if hydrogen is chosen as the carrier gas!
Schmauch and Dinerstein (1960) claim that the TCD output is linear up to about 8 mol per cent using a helium carrier gas.

2.5.2.2 The Flame Ionisation Detector

During the combustion of hydrogen in air, relatively few ions form within the flame, however, the presence of an organic compound produces a large increase in ion production. The FID has two electrodes with a potential difference between them to provide a means of detection via the ion current. When an organic compound enters the detector there is an increase in the number of ions produced in the flame thus the presence of the sample gas is detected. Obviously, for the sample to be detectable the sample material must be combustible (O'Brien (1985)). The FID possesses the widest linear dynamic range of any detector presently known (David (1974)).

Descriptions of a range of commonly used detectors can be found in most text books on chromatography.

2.5.3 Unconventional Detection Methods

There have been several attempts to exploit other flow-related detection principles. The gas-density meter (Martin and James (1956)) is a pneumatic analogy of the Wheatstone bridge. Effluent from a chromatograph enters the apparatus and is divided into two streams which flow along two different legs of the bridge. Reference gas enters through a second port and is divided into two streams. Each reference stream then combines with an effluent stream and is vented. The channels along which the reference streams flow are connected together via a small chamber in which a heater is situated. A thermocouple junction is positioned in each of the connecting tubes between the

detection chamber and the reference channels. When both effluent and reference gases have the same density flow rates can be adjusted so that the detection chamber and the thermocouple junctions register the same temperature. A change in density of the effluent gas causes a pressure difference and consequently gas flow across the detection chamber and thermocouple junctions. One junction then becomes hotter than the other and the thermocouple output provides a measure of the direction and rate of gas flow and thus of the density difference between effluent and reference streams. Testerman and McLeod (1964(I)) used the change in frequency of a whistle to detect the appearance of different species in the carrier gas stream. The whistle frequency varies with a number of parameters, gas velocity being amongst them so the whistle detector would respond to the sorption effect. Annino *et al.* (1976,1977,1981) and Waters (1976) were concerned with a totally pneumatic analyser comprising of a jewelled orifice and a compensating capillary tube such that the detector response be directly proportional to the composition of the gas flowing through the orifice. The pressure drop through an orifice varies with flow rate and gas density according to

$$\Delta P_o = k_o \rho F^2 \tag{2.1}$$

whereas the pressure drop through a capillary varies with flow rate and gas viscosity according to

$$\Delta P_c = K_c \eta F \tag{2.2}$$

where ΔP is the pressure drop, k is a constant, subscripts o and c refer to the orifice and the capillary respectively. F is the volumetric flow rate, ρ, the gas density and η, the gas viscosity. The change in pressure drop across the orifice for a density change (i.e. when a sample component arrives) is given by

$$\frac{\delta \Delta P_o}{\delta \rho} = k_o F^2 \tag{2.3}$$

whereas for a flow rate change

$$\frac{\delta \Delta P_o}{\delta F} = 2 k_o \rho F \tag{2.4}$$

For the capillary

$$\frac{\delta \Delta P_c}{\delta F} = k_c \eta \tag{2.5}$$

$$\frac{\delta \Delta P_c}{\delta \eta} = k_c F \tag{2.6}$$

Changes in flow rate are eliminated by amplifying the pressure signals at appropriate gains, A_o and A_c, so that

$$2A_o k_o \rho F = A_c k_c \eta \tag{2.7}$$

and the pressure variation is only due to density and viscosity changes :

$$\delta P_{out} = A_o k_o F^2 \delta\rho - A_c k_c F \delta\eta \tag{2.8}$$

Griffiths, James and Phillips (1952) used a flow-impedance method in an attempt to follow changes in gas composition but neglected to include the sorption effect. They noticed a different response when their experimental configuration included appreciable 'dead volume' between column and flow impedance and when the impedance was directly downstream of the column. Conder and Young (1979) describe the variation of flow rate with the passage of a sample band and the significance of column pressure drop and gas viscosity but only with respect to analytical errors. The combined effects of the sorption effect and viscosity changes were recorded by Dyson and Littlewood (1967(I),(II)) using a capillary viscometer. They used their measurements to examine molecular properties, but also, they highlighted the large experimental error possible during chromatography because of these effects. Giddings, Kao and Kobayashi (1966) used a capillary tube to measure viscosity over a wide range of conditions. The suggestion that viscosity measurement could be used to obtain quantitative results was made by James (1957). Van Swaay proposed that the automatic flowmeter described in 1963 could be used to detect the elution of sample components but did not report any results. Simpson (1970) claims that the only absolute detector available (that is, requiring no prior calibration) is the Brunel mass detector (Bevan, Gough and Thorburn (1969)). Here, eluted bands are adsorbed completely by an activated charcoal 'bucket', the mass of which is continuously monitored. The presence of an eluted component is indicated by a step on the chart recording of the output from the "automatically recording microbalance". Quantitative data are obtained directly from the step height measurements. Janak and Novak (1964,1965) described a pneumatic detector responding to changes in the pressure drop across a capillary (or an orifice) caused by changes in the composition of the gas.

2.6 The Sorption-Effect Chromatograph

The principal components of the sorption-effect chromatograph are not dissimilar to those of a conventional chromatograph. However, because the apparatus is required to measure the flow perturbations which occur as a sample gas adsorbs or desorbs it is important that the carrier gas flow rate is stable otherwise the sorption effect may be lost in general baseline noise, and, the detector must of course be sensitive to flow rate.

Accordingly, the basic system comprises of four main components :

i) the flow-setting system - to provide a stable carrier gas flow rate

ii) the means of sample introduction

iii) the chromatographic columns - to perform the separation, and

iv) the flowmeter - to detect the small changes in flow due to the passage of a sample species through the chromatograph.

Two parallel flow channels are used, one being the reference stream for the other.

2.6.1 The Flow-setting System

A schematic diagram of the system used to generate a stable carrier gas flow rate is shown in Figure 2.6. The flow-setting system consists of two matched, high flow resistance capillary chokes. The pressure at the upstream ends of the two chokes is maintained by a back-pressure regulator (Porter 9000 AMBF 30 or similar) which vents any excess gas to atmosphere. Provided that the BPR is always venting, this pressure will remain constant within the capabilities of the BPR. The BPR incorporates a pressure gauge to assist reproducibility of carrier gas flow rates. A mass-flow regulator (MFR) is included upstream of the BPR. The role of this MFR is merely as a flow adjuster to ensure that enough gas is supplied for the BPR to always be able to vent some gas (and thus maintain the pressure) but not to vent an excessive quantity. Gas is fed directly from the bottle regulator to the MFR. MFRs are designed to deliver a constant mass flow of pure gas and are sometimes used as the sole means of setting a constant carrier-gas flow rate but no MFR has been found that is adequate for the purposes of sorption-effect chromatography. There are two types, one for constant upstream, variable downstream pressure applications and one for constant downstream, variable upstream pressure applications. Here the MFR is not being used as a precision flow controller so it is immaterial which type is used, in fact, use of a needle valve would probably suffice. The Brooks Model 8744 MFR supplied with the Pye chromatograph was used in this work.

Because the composition of the gas in the chokes never changes, the only ways that the flow rate can change are :
if the pneumatic resistance of either choke changes with temperature,
if the pressure is disturbed upstream of the chokes.

If the pressure drop across the chokes represents the greater part of the total system pressure drop then small changes in pneumatic resistance downstream of the chokes will not significantly affect the rate at which gas is delivered to the columns.

Figure 2.6 - The Generation of a Stable Carrier Gas Flow Rate

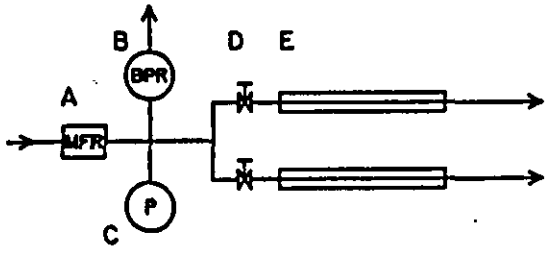

A : Mass-Flow Regulator
B : Back-Pressure Regulator
C : Pressure Gauge
D : Trimming Needle Valve
E : Flow-Setting Choke

In practice the chokes cannot be perfectly matched, so needle valves are included to provide a means of balancing the flows in each channel. The pressure drop across each needle valve must be small compared to that across each choke because the pneumatic resistance of a needle valve is much more sensitive to temperature changes than that of a choke.

Connecting pipework is either 3mm o.d.(1.5mm i.d.) or 1.5mm o.d.(1.1mm i.d or 0.8mm i.d.) connected using the appropriate Swagelok fittings. The flow-setting chokes are described in more detail later in this chapter.

2.6.2 The Sorption-Effect Detector

The capillary flow meter which is the sorption-effect detector is made up of two matched, low flow resistance capillary tubes with a differential pressure sensing device, (in this case a differential pressure transducer (DPT) - Furness FCO40 10mmH_2O/V), connected across the upstream ends of the two capillaries (Figure 2.7). It is desirable for both capillaries to have the same pneumatic resistance. The capillaries are matched by swapping them over and trimming as necessary until the DPT output remains unchanged regardless of which capillary is connected to which column outlet (with gas flowing through the system, of course). Once this has been achieved, the two carrier-gas flow rates can be equalised by adjusting the appropriate valve until the DPT output is zero.

Figure 2.7 - The Differential Flow Meter

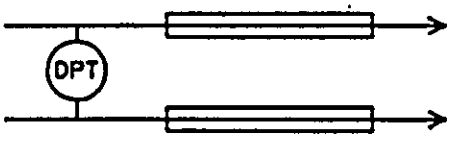

2.6.3 Flow in the Flow-Detecting Capillary Tubes

The Hagen-Poiseulle equation describes laminar flow down a capillary tube.

$$Q = \frac{\pi d^4}{128\mu}\left(-\frac{\delta P}{\delta L}\right) \tag{2.9}$$

where :

$-\frac{\delta P}{\delta L}$ is the pressure gradient

μ is the gas viscosity

Q is the volumetric flow rate

d is the pipe diameter.

For compressible flow PQ is assumed to be constant.

If pressure $P = P_0$ at a distance from the capillary inlet, $l = 0$ and $P = P_1$ at $l = L$, then

$$(PQ)_0 = (PQ)_1 = \frac{\pi d^4}{256\mu L}(P_0^2 - P_1^2) \tag{2.10}$$

If the gas density does not change by more than ten per cent, Boucher and Alves (1973) advise that the gas flow in a tube can be described as incompressible. Coulson and Richardson (1980(I)) suggest that if the total pressure drop down the pipe is a small proportion of the inlet pressure then the fluid can be treated as incompressible.

If $(P_0 - P_1)$ is small compared to the absolute pressure then the equation simplifies to give the volumetric flow at the capillary outlet :

$$Q_1 = \frac{\pi d^4}{128\mu L}(P_0 - P_1) \tag{2.11}$$

So, for a given capillary tube, the pressure drop is given by :

$$\Delta P = k\mu Q \tag{2.12}$$

where k is a constant.

2.6.4 Differential Flow Rate Measurement

If the composition of the gas flowing down a capillary is constant (and therefore the viscosity is constant) then any increase in the volumetric flow rate will cause an increase in pressure drop down the tube. If the capillary is venting at a constant pressure (e.g. atmospheric) then because of the increased pressure drop down the tube, the upstream pressure must be increased according to :

$$\Delta P = k_1 Q \tag{2.13}$$

where k_1 is a constant. Consider a capillary flow meter, such as that described earlier, positioned at the downstream end of a dual-channel chromatograph. A change in the flow rate in one channel relative to the other will cause the differential pressure between the upstream ends of the capillaries to be modified. This will be observed as a change in the transducer output on a chart recorder.

2.6.5 Composition Change Measurement

If the composition of the gas within one of the flow-detecting capillaries changes this almost inevitably means that the gas viscosity will be modified and the pressure drop down that capillary will change, in that, if the volumetric flow rate remains constant, the pressure drop is directly proportional to the gas viscosity. Once again this will alter the upstream pressure of the affected capillary because the downstream pressure is constant i.e.

$$\Delta P = k_2 \mu \tag{2.14}$$

where k_2 is a constant.

So, the capillary flowmeter, primarily intended here to detect changes in volumetric flow rate is also sensitive to changes in composition. This is the converse of some configurations of TCD which are used to detect changes in composition but which are also sensitive to changes in flow rate

2.6.6 Initial Specifications

The flow-setting chokes were chosen to be 6" lengths of 0.006" stainless steel capillary tubing (0.15m×1.6mm o.d.×0.15mm i.d.). The flow-detecting capillaries were arbitrarily required to have in the region of one-hundred-and-fifty times less pneumatic resistance.

Applying the Hagen-Poiseulle equation for one flow-setting choke and one flow-detecting capillary :

$$\frac{Q_S}{Q_D} = \frac{\Delta P_S \pi d_S^4}{128 \mu L_S} \times \frac{128 \mu L_D}{\Delta P_D \pi d_D^4} \tag{2.15}$$

For the same pressure drop and same gas :

$$\frac{Q_S}{Q_D} = \frac{d_S^4}{d_D^4} \times \frac{L_D}{L_S} \approx \frac{1}{150} \tag{2.16}$$

Selecting 0.030" i.d. tubing for the flow-detecting capillaries :

$$L_D = \frac{1}{150} \times \frac{0.030^4}{0.006^4} \times 0.15$$

$$= 0.625 \text{ m}$$

For the above calculation to be valid the flow must be incompressible and laminar. Let $\Delta P = 10^3 Nm^{-2}$ i.e. 1% of the outlet pressure (atmospheric).

$$Q_D = \frac{\Delta P_D \pi d_D^4}{128 \mu L_D} \tag{2.17}$$

Considering helium gas:

viscosity $\mu_{He} = 1.8 \times 10^{-5} \text{ Nsm}^{-2}$

density $\rho_{He} = 0.1786 \text{ kgm}^{-3}$ @ STP

$$Q_D = 7.4 \times 10^{-7} \text{ m}^3\text{s}^{-1}$$

For the flow to be laminar, Reynold's number, Re, must be less than about 2000.

$$Re = \frac{\rho v d}{\mu} = \frac{4\rho Q}{\pi \mu d} \qquad (2.18)$$

$$= \frac{4 \times 0.1786 \times 7.4 \times 10^{-7}}{\pi \times 1.8 \times 10^{-5} \times 0.762 \times 10^{-3}}$$

$$\approx 12 \quad \text{(laminar flow)}$$

The flow-detecting capillaries were specified as 0.62m×1.6mm o.d.×0.762mm i.d.

2.7 Summary of Initial Sorption-Effect Chromatograph Equipment Specifications

The sorption-effect chromatograph at this stage in the development is summarised in Figure 2.8.

Figure 2.8 - The Initial Sorption-Effect Chromatograph

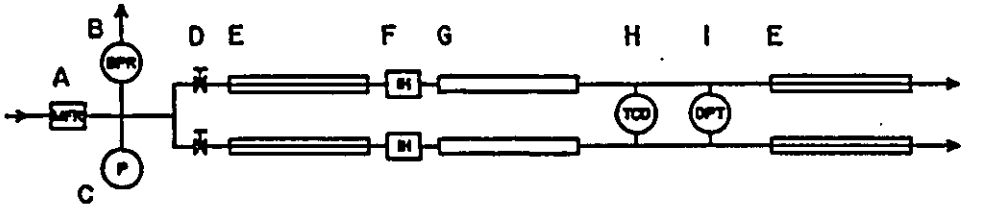

A	Brooks 8744 Mass-Flow Regulator (or similar)	
B	Porter 9000 AMBF Back-Pressure Regulator (or similar)	
C	Pressure Gauge	
D	Nupro Needle Valve (or similar)	
E	Flow Restrictor -	Upstream 15cm x 1.5mm o.d. x 0.15mm i.d. Downstream 62cm x 1.6mm o.d. x 0.762mm i.d. Stainless Steel
F	Pye Injection Head	
G	6mm o.d. x 4mm i.d. glass columns (with 1.5mm o.d. exit pipe) packed with 5A molecular sieve (500-710μm)	
H	Semi-diffusion-type Thermal Conductivity Detector as supplied with the Pye 104	
I	Differential Pressure Transducer - Furness Controls FCO 040 ±10mmH_2O/V	

CHAPTER THREE - PRESSURE NOISE

3.1 Introduction

The largest sources of random noise which affect the sorption-effect chromatograph are changes in oven temperature and atmospheric pressure. These manifest themselves as flow rate variations. The effects of temperature fluctuations are dealt with in the following chapter, along with steps taken to reduce thermal noise. This chapter is concerned with the response of the chromatograph to the sort of pressure variations experienced in the laboratory, such as, the opening of doors, gusts of wind etc., and what means have been discovered to minimise these effects.

3.2 How Pressure Fluctuations Affect the Sorption-Effect Chromatograph

Figures 3.1 and 3.2 show the baseline flow rate through a chromatograph which has no protection against atmospheric pressure surges, recorded on a relatively calm day, and on a very windy day respectively. The rapid flow rate deviations are attributable to pressure changes and these are superimposed on the thermal noise.

Figure 3.1 - Pressure Fluctuations Recorded on a Relatively Still Day

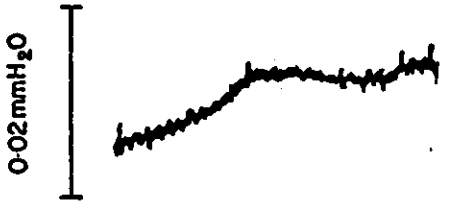

Figure 3.2 - Pressure Fluctuations Recorded on a Relatively Windy Day

An external pressure surge affects an unprotected system by entering the system where it is exposed to atmosphere. The most obvious place for this is the gas exit vent. The pressure wave then propagates up the flow-detecting chokes to the transducer and beyond. Ideally, the pneumatic resistance per unit length of system is identical in each flow channel. If this were the case, an intruding pressure wave would reach both sides of the differential pressure transducer (DPT) at the same instant and no disturbance would be recorded. In practice, imbalances could occur in almost every part of the system. An investigation was performed to see how the removal of various components altered the sensitivity to a semi-standard atmospheric pressure surge (the rapid opening of the laboratory door).

3.3 Dynamic Pressure Tests

Figures 3.3 to 3.6 show the response of the DPT in various experimental configurations when the carrier gas is flowing. All chart traces were recorded at the same sensitivity.

Figure 3.3 is the response to an external pressure surge of the complete apparatus (as shown in Figure 2.8 Chapter 2). The pressure fluctuation recorded from the top of the peak to the bottom of the trough is approximately 1mmH_2O and is slightly asymmetrical with the greater part of the response below the baseline.

Figure 3.3 - The Response of the Differential Pressure Transducer to a Surge in External Pressure

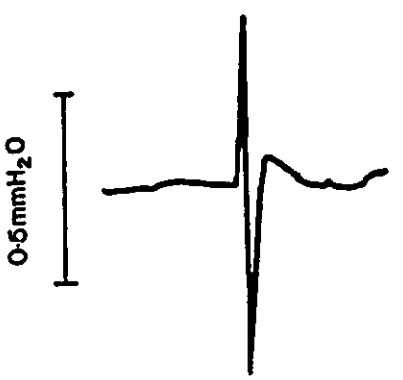

When the columns have been by-passed (Figure 3.4a) the effect of the pressure wave is shown in Figure 3.4b. The magnitude of the response is slightly less than before (about 0.75mmH_2O) and is more balanced. From this it appears that the columns do not play a very significant role in the reaction to pressure noise. This may be the case, but columns have, as a matter of policy, always been prepared as a matching pair with the same mass of adsorbent in each. This means that if the empty columns were identical, the packed columns should have the same packed length and the same pneumatic resistance. The minor contribution of these columns to the noise is probably because they are fairly well matched.

Figure 3.5b is the DPT response to a pressure surge when the columns and the TCD have been removed so the flow system is that shown in Figure 3.5a. The peak represents a pressure surge of about 0.025mmH_2O. Evidently the presence of the TCD is a major obstacle to the elimination of pressure surges. The effect could be due to

Figure 3.4 - Measuring the Sensitivity of the Apparatus to External Pressure Surges After the Removal of Various Components

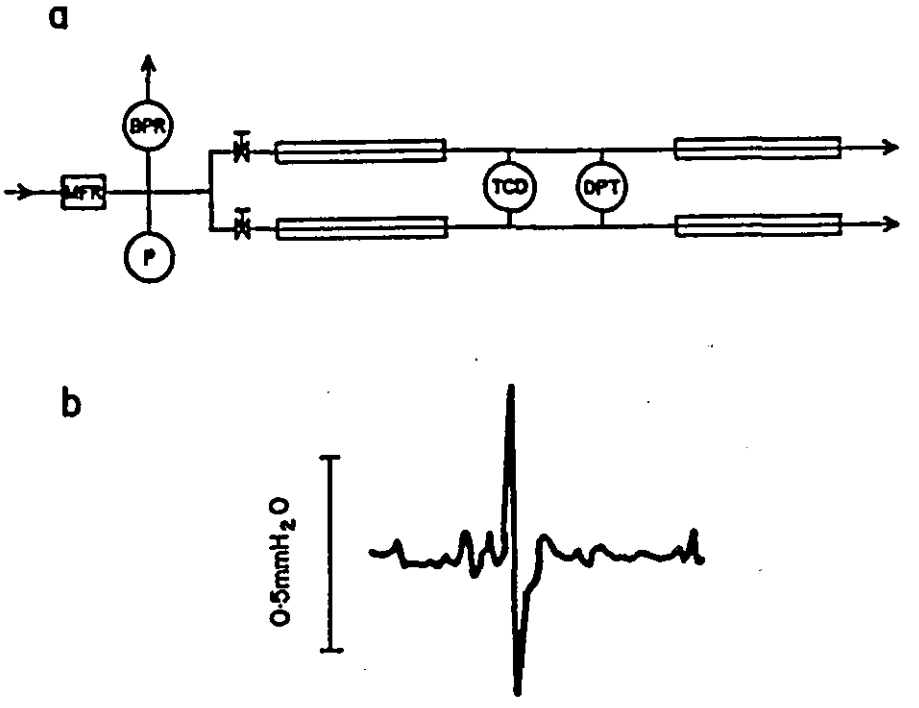

a : The experimental configuration with the columns removed
b : The response of the DPT using this configuration.

the detection chambers in each channel of the TCD having different volumes. It might be thought that only the flow-detecting capillaries would be important as far as propagating pressure pulses at equal speeds is concerned because they are the only part of the apparatus between the pressure-sensing device and the atmosphere but the parts of the chromatograph upstream (with regard to the carrier flow) of the DPT are obviously similarly significant.

Different extra volumes were added between the TCD and the DPT, in one flow channel only, to observe the change in response. Figure 3.6a shows the apparatus configuration with volume added as a side arm. Figure 3.6b is the DPT response when the extra volume is approximately 1.3cm^3 (10cm of 4mm i.d. Tubing). Figure 3.6c was recorded with 46cm of the same tubing (5.8cm^3) and Figure 3.6d with around 75cm (9.5cm^3). The larger the volume imbalance, the larger the magnitude of the pressure surge, and the longer the pressure within the system takes to re-equilibrate.

Figure 3.5 - Measuring the Sensitivity of the Apparatus to External Pressure Surges After the Removal of Various Components

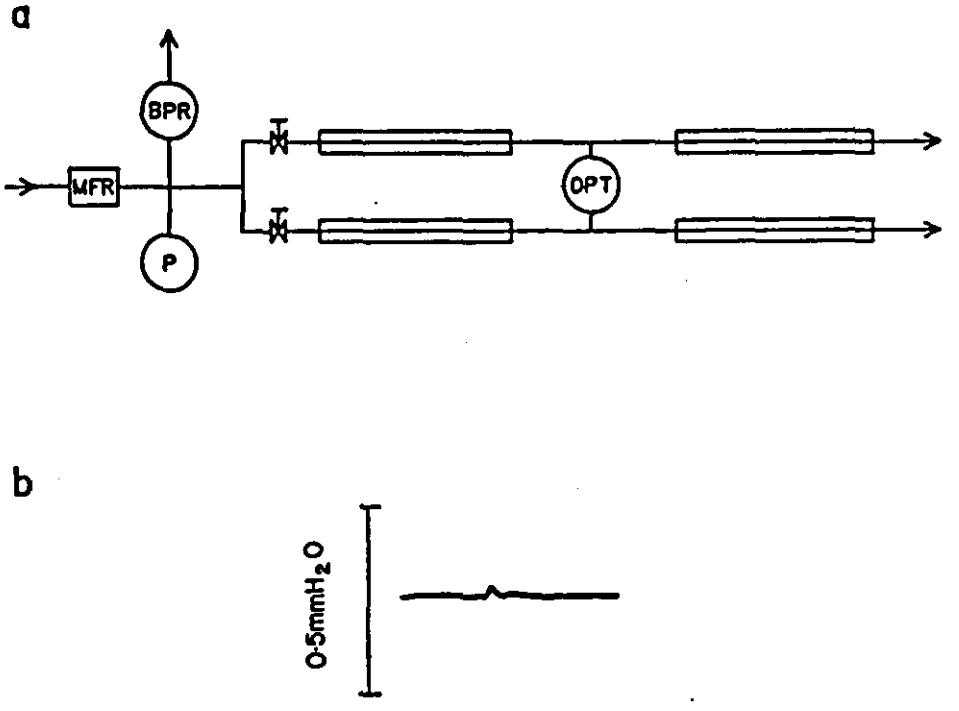

a : The experimental configuration with the columns and the TCD removed
b : The response of the DPT using this configuration.

Figure 3.6 - Measuring the Sensitivity of the Apparatus to External Pressure Surges with Added Volume in One Flow Channel

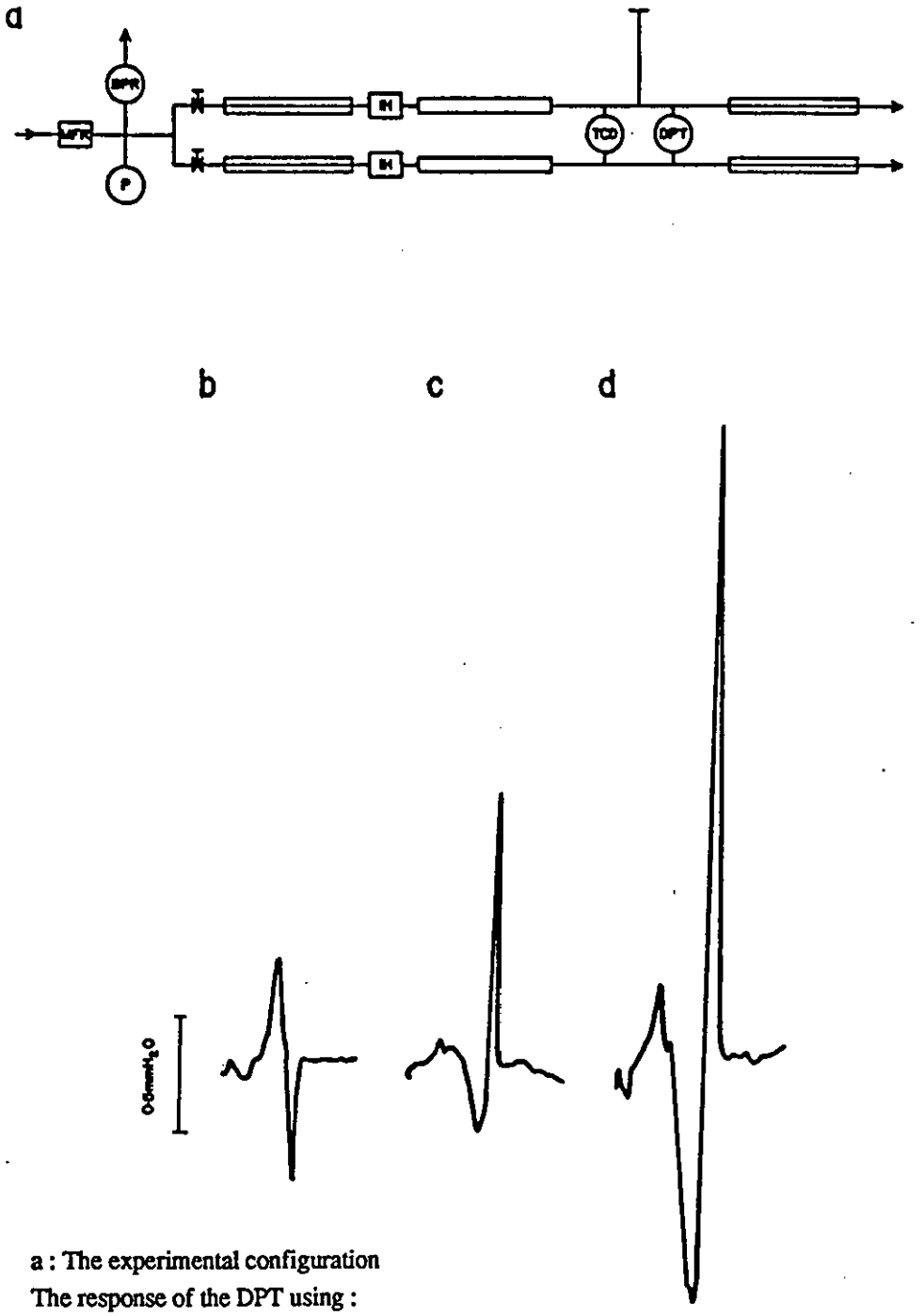

a : The experimental configuration
The response of the DPT using :
b : 1.3cm^2 added volume
c : 5.8cm^2 added volume
d : 9.5cm^2 added volume.

3.4 Static Pressure Tests

The previous experimentation was performed with carrier gas flowing through the apparatus and the results showed that the TCD was a major cause of pressure noise. Because the pressure pulse/surge enters the system at its downstream end, this part of the apparatus was isolated and gradually built up, by adding components to the upstream end, to investigate what effect each component plays.

Figure 3.7 - A Schematic Diagram of the Differential Pressure Transducer

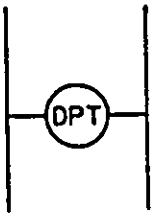

The first test was to check the reaction of the DPT on its own. The DPT consists of two inlet ports and two outlet ports. Changes in differential pressure are measured by small changes in capacitance caused by the displacement of a steel diaphragm. One side of this 'capacitor' is ported into one flow channel and the other side ported into the second channel. This is shown schematically in Figure 3.7. When the two outlet ports are capped off (Figure 3.8a) the response of the DPT to a pressure surge is shown in Figure 3.8b. The peak represents a pressure change of less than 0.025mmH_2O (the recorder sensitivity was 50mV full-scale deflection, transducer output 10mmH_2O/V). Secondly, the outlets were ported together and each inlet connected to a T-piece, the third leg of the T-piece being left open to atmosphere (Figure 3.9a). Figure 3.9b shows the response to the pressure surge for this configuration. The peak is less than 0.01mmH_2O (chart sensitivity 0.1V f.s.d.). These two tests indicate that the transducer itself is relatively immune to pressure surges.

Figure 3.8 - Measuring the Sensitivity of the Differential Pressure Transducer to External Pressure Surges

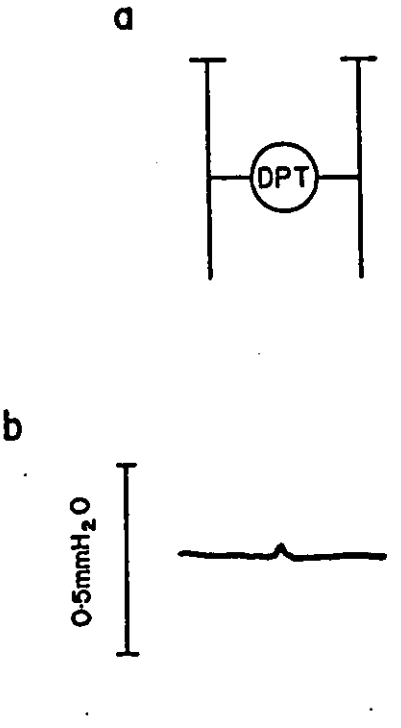

a : The DPT with the outlet ports capped off
b : The response of the DPT in this configuration.

Figure 3.9 - Measuring the Sensitivity of the Differential Pressure Transducer to External Pressure Surges

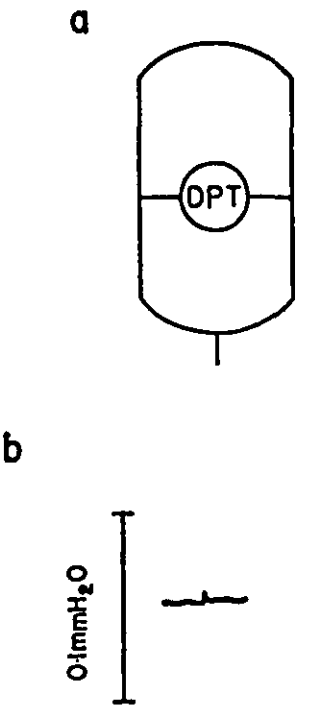

a : The DPT with the outlet ports connected to each other and the inlet ports connected to a T-piece which has its third port open to atmosphere

b : The response of the DPT in this configuration.

The next test was to check the combination of DPT and flow-detecting capillaries. The capillaries were capped off as in Figure 3.10a. Figure 3.10b records a pressure deviation of around 0.6mmH_2O. Whether the capillaries were ported together (Figure 3.11) or the DPT inlets ported together (Figure 3.12) no response to the pressure surge was identifiable on a range of 5mmH_2O f.s.d. The addition of a length of 3mm i.d. tubing on only one of the inlets, with the capillaries ported together (Figure 3.13a), did have a detrimental effect but the magnitude of the effect is still much less than that recorded with the complete chromatograph (Figure 3.13b).

Figure 3.10 - Measuring the Sensitivity of the Differential Pressure Transducer to External Pressure Surges

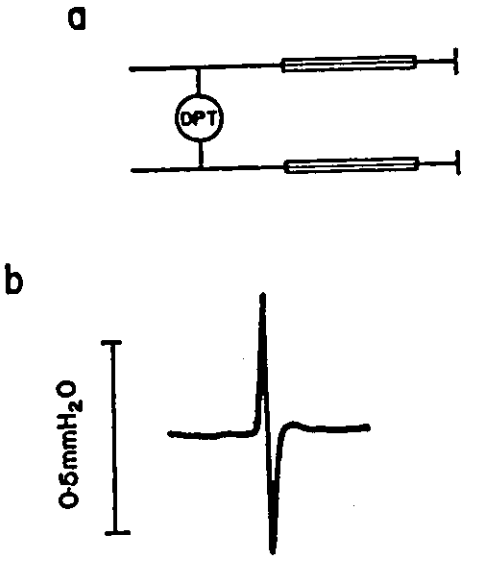

a : The flowmeter with the downstream ends of the capillaries capped off and the inlets open
b : The response of the DPT in this configuration.

Figure 3.11 - Measuring the Sensitivity of the Differential Pressure Transducer to External Pressure Surges with the Downstream Ends of the Capillaries Connected Together and the Inlets Open.

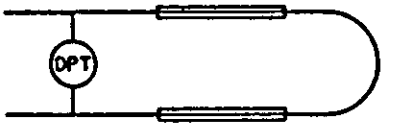

Figure 3.12 - Measuring the Sensitivity of the Differential Pressure Transducer to External Pressure Surges with the Inlets Connected Together and the Downstream Ends of the Capillaries Open

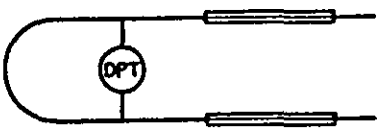

Figure 3.13 - Measuring the Sensitivity of the Differential Pressure Transducer to External Pressure Surges

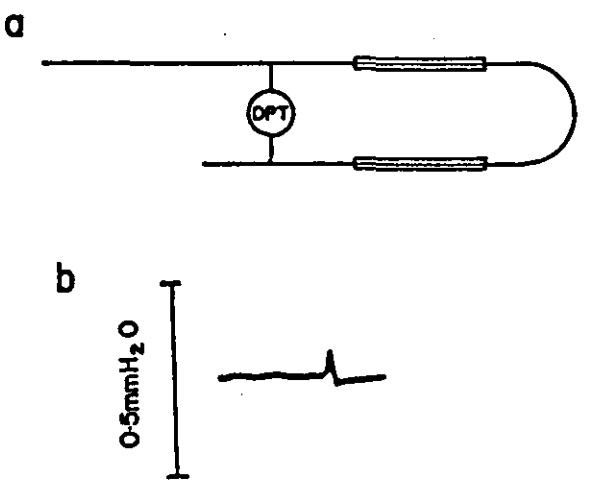

a : The flowmeter with the downstream ends of the capillaries connected together and the inlets open with added volume on one inlet

b : The DPT response in this configuration.

The dynamic pressure tests proved fairly conclusively that the component which causes the biggest pressure noise problem is the TCD. Figures 3.14b, 3.14c and 3.14d show the reaction when the TCD is included and its inlet ports connected (Figure 3.14a). From peak to trough the pressure variation is in the region of 1-2mmH_2O. The difference in amplitude illustrates that the controlled pressure surge is not exactly standard but for the purposes of the investigation it was adequate. Figure 3.15b results from using the same configuration only with extra volume in one flow channel (Figure 3.15a). The effect is reduced considerably. Having positively identified the

Figure 3.14 - Measuring the Sensitivity of the Differential Pressure Transducer and the TCD to External Pressure Surges

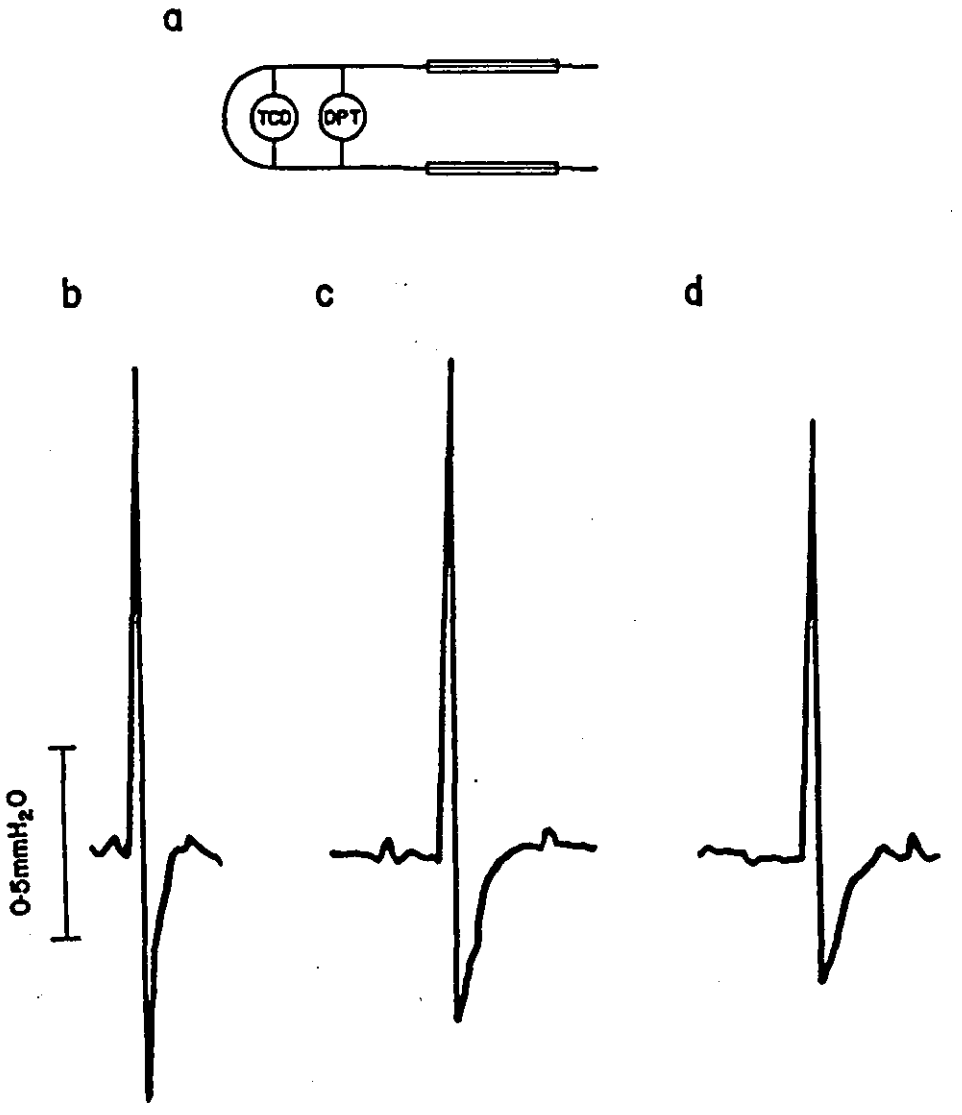

a : The detector combination with the TCD inlets ported together and the downstream ends of the capillaries open

b,c,d : The DPT response to three different, induced pressure surges.

problem with the TCD, a second TCD was tested showing better pressure insensitivity (Figures 3.16a and 3.16b). The connections to the outlet ports were switched between tests and the direction of the pressure pulse was also reversed.

Figure 3.15 - Measuring the Sensitivity of the Differential Pressure Transducer and the TCD to External Pressure Surges

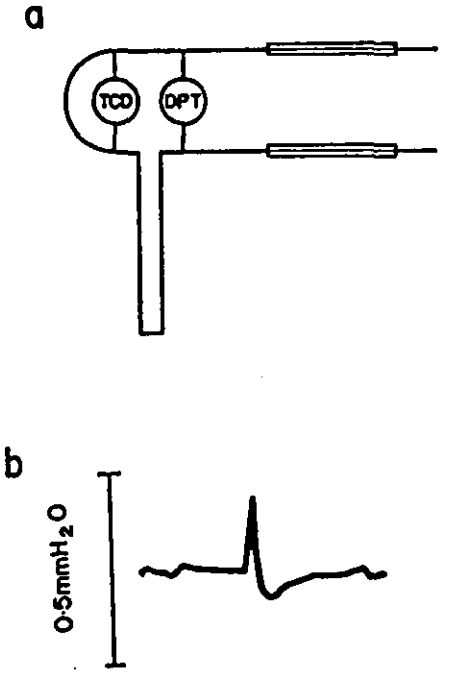

a : The detector combination with the TCD inlets ported together, with added volume between one TCD outlet and the corresponding DPT inlet, and the downstream ends of the capillaries open

b : The DPT response using this configuration.

3.5 Reducing the Sensitivity of the Apparatus to Pressure Fluctuations

Various attempts were made to buffer the system from these pressure variations using large volumes without much success. It is possible, however, to isolate the equipment from atmosphere at the carrier-gas exit by connecting the flow-detecting capillaries together and venting them through a back-pressure regulator (such as is used in the flow-setting system) set at a pressure slightly above ambient pressure. A Porter AMBF (Figure 3.17) was used here. It has three ports, inlet, gauge and outlet. The diaphragm has a valve seat which blocks the outlet when there is insufficient gas pressure to force the diaphragm away from the valve orifice. The diaphragm is loaded via a spring which is loaded in turn by a screw. The strength of spring determines the maximum back pressure attainable (Porter supply springs for two different ranges, a 15 and a 30 psi). The reference pressure, therefore, is atmospheric pressure plus the contribution of the spring. Consequently any change in atmospheric pressure will affect the back pressure at which the regulator vents.

Figure 3.16 - Measuring the Sensitivity of the Differential Pressure Transducer and a Different TCD to External Pressure Surges

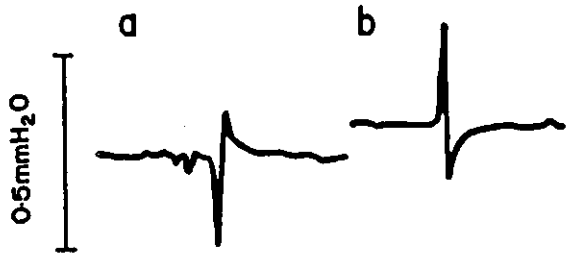

a : The DPT response using the same configuration as in Figure 3.14 but with a different TCD
b : The DPT response with the TCD outlet connections to DPT inlets reversed.

Figure 3.17 - The Porter Back-Pressure Regulator

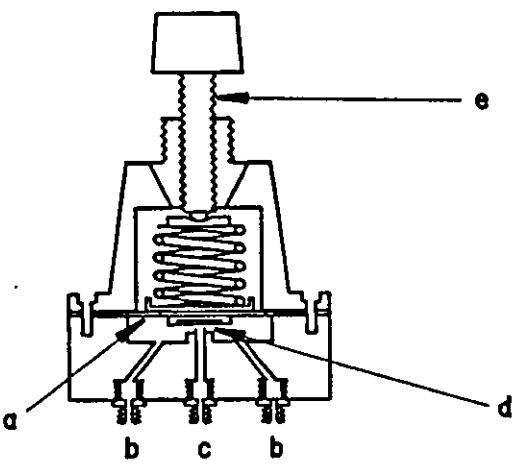

a : The diaphragm
b : The inlet/gauge ports
c : The outlet port
d : The valve seat
e : The spring-loading screw.

The introduction of the downstream BPR has isolated the gas system directly from pressure fluctuations but is itself sensitive to these changes, in that the venting pressure depends on atmospheric pressure. The solution to this is to seal the spring chamber as effectively as possible. Once gas-tight the set pressure may drift with temperature but should be insensitive to sudden changes. The spring chamber has a vent hole which was, presumably, intended to allow equilibration of the pressure

inside the chamber with atmosphere. This can be sealed off with insulation tape or, more permanently, with epoxy resin. The panel-mounting thread and screw guide is part of an insert pushed into the spring chamber casting. Any gaps existing between the insert and the casting are effectively sealed using epoxy resin or vacuum grease. The final non-gas-tight area is the loading screw thread. This can be sealed with PTFE thread-sealing tape or with vacuum grease but these methods are only effective when winding in onto fresh tape or fresh grease. If the pressure is reduced by winding the screw out, the seal becomes unreliable. The problem was resolved by using a locking nut which contained a PTFE (or similar) washer which can be 'squashed' down after the pressure has been set. Once both BPRs (one at the downstream end and one in the flow-setting system) have been so modified the system should be almost completely isolated from atmospheric pressure fluctuations. Of course, a sufficiently large pressure disturbance could propagate through the downstream BPR but its effect will be reduced if the pressure-drop distributions in each of the two flow channels are well-matched.

3.6 Summary

The effect of pressure noise can be greatly reduced by :

a) making each of the flow channels as identical as possible so that any pressure disturbance is propagated at the same rate up each channel and so the pressures at each side of the transducer will change together.

b) isolating the system from atmosphere using a suitably modified back-pressure regulator at the gas outlet so that the gas vents at a pressure slightly above atmospheric. The BPR used in the flow-setting system should also be desensitised to atmospheric pressure fluctuations.

c) pressure noise was worst when the TCD was included in the system so, the TCD should not be included unless it is required.

The configuration of a typical sorption-effect chromatograph protected against atmospheric pressure fluctuations is shown in Figure 3.18.

Figure 3.18 - The Configuration of a Typical Sorption-Effect Chromatograph Protected against Atmospheric Pressure Fluctuations.

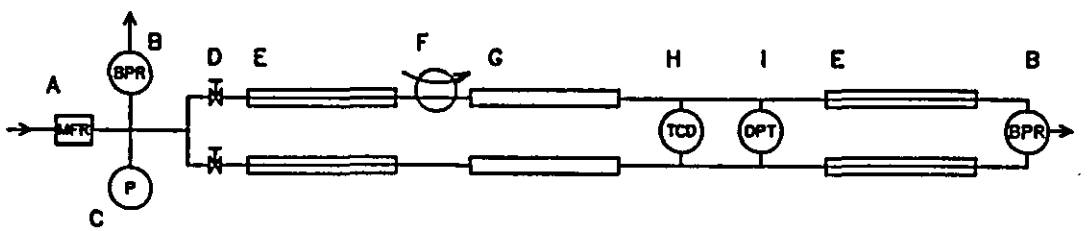

A	Mass-Flow Regulator
B	Back-Pressure Regulator
C	Pressure Gauge
D	Needle Valve
E	Flow-Restricting Capillary
F	Sample Valve
G	Column
H	Thermal Conductivity Detector
I	Differential Pressure Transducer

CHAPTER FOUR - THERMAL NOISE

4.1 Introduction

Random fluctuations in temperature, both in the oven and the environment, are a major source of baseline noise and drift during sorption-effect chromatography. Baseline noise generated within the chromatograph could be imagined to be caused by pockets of warmer or colder air which momentarily come into contact with parts of the apparatus. Additionally, the ambient temperature is subject to drifting over long periods of time and could affect any component not contained within the chromatographic oven. Thermal noise only becomes apparent when one flow channel is affected by a temperature change or the noise-generating mechanisms (outlined below) happen at different rates in one channel compared to the other. If both channels were affected in exactly the same way at exactly the same rate then although the respective flow rates would be altered during the time that the temperature change was taking place there would be no relative change and the output of the differential pressure transducer would remain constant. Considering a chromatograph such as that shown in Figure 3.18 there are three ways in which a changing temperature may perturb the gas flow rate :

a) any expansion or contraction of pipework, column tubing, flow-setting and flow-detecting capillaries, or needle valves, will change the volume of the flow channel and cause the volumetric flow rate in that channel to change.

b) if the gas passing through the system is subjected to heating or cooling, the density of the gas will change and so the volumetric flow rate will change.

c) the amount of gas adsorbed varies with temperature so if the temperature of any part of the column changes the amount of gas that is adsorbed at that point in the column will change. Adsorption is an exothermic process so if the column temperature is increased, gas will be desorbed, and if the column temperature is decreased, gas will be adsorbed.

The random noise generated within the thermostatted oven which houses the columns may be the result of a complex interaction of all three causes.

The susceptibility of the gas in the columns to temperature fluctuations can be seen by comparing Figures 4.1a and 4.1b. Figure 4.1a is the baseline produced with the columns in the system, Figure 4.1b is that produced without the columns. Both traces show pressure noise which appears as sharp spikes but without the columns, the gentle meandering of the baseline due to thermal noise is much less pronounced. This indicates that most of the thermal noise is generated within the isothermal oven.

Figure 4.1 - Baseline Noise Caused by Temperature Fluctuations

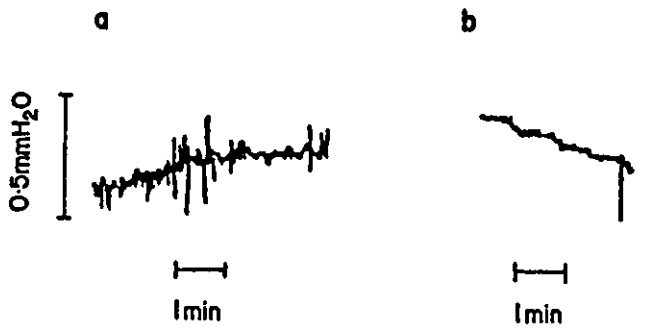

a : With columns
b : Without columns.

Examples of the effect of a cold spot on the column can be seen in Figures 4.2 to 4.7. Figure 4.2 shows the passage of an argon sample through a column purged with helium carrier gas. Evidently the column is not perfect because of the oscillations between the injection peak and the desorption peak. A length of wet string was wrapped around the column at various positions and the shape of the oscillations was seen to be altered according to the position of the string (Figures 4.3 to 4.7). The string has the effect of causing a cold spot in the column which results in the affected part of the column being able to adsorb more gas relative to the remainder of the column.

Figure 4.2 - The Passage of an Argon Sample Through an Imperfectly Packed Column in Helium Carrier Gas

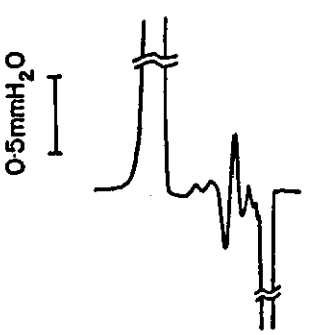

The trace runs from right to left so that the right-hand peak is the combined injection/adsorption peak and the left-hand peak is the desorption peak. The oscillations between the two main peaks are caused by changes in the amount of gas adsorbed as the argon moves through the column, caused by non-uniformity in the packing.

Figures 4.3 to 4.7 - The Passage of an Argon Sample in Helium Carrier Gas Through an Imperfectly Packed Column with a Cold Spot

Figure 4.3 - With the Cold Spot Located at 12 o'clock on the First Loop of the Column

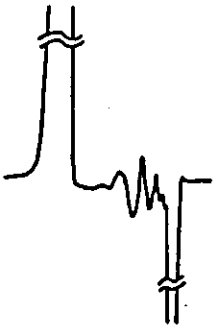

Figure 4.4 - With the Cold Spot Located at 12 o'clock on the Second Loop of the Column

Figure 4.5 - With the Cold Spot Located at 6 o'clock on the First Loop of the Column

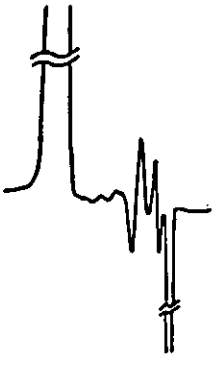

Figure 4.6 - With the Cold Spot Located at 6 o'clock on the Second Loop of the Column

Figure 4.7 - With the Cold Spot Located at 6 o'clock on the Third Loop of the Column

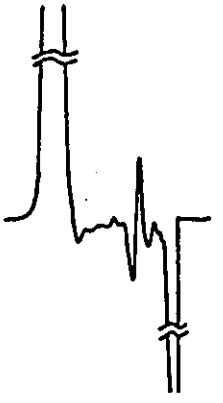

The need for good temperature control in the context of sorption-effect chromatography is obvious. With regard to conventional chromatography Goedert and Guiochon (1973) investigated the effect of temperature fluctuations and temperature gradients using an oil bath to thermostat the columns. They concluded that, using commercial equipment, with gradients in the order of 0.1°C and fluctuations up to 1°C, typical errors were in the range 0.5-2%. They had previously (1969) developed an apparatus for high-precision work. To set a stable gas flow rate they used a three-stage pressure control system. The reference pressure for the third stage was fixed by using a mechanical vacuum pump and varied between 0.04 and 0.05 millibar. The delivery pressure of the carrier gas was found to be steady to within ±0.3millibar. All the pressure regulators were contained in an oil bath, the temperature of which was controllable to within 0.1°C. The main part of the chromatograph : the sampling valve, column and detector were contained in a second oil bath the temperature of which was controllable to within 0.01°C. All sources of pressure drop were positioned in one or other of the two oil baths. Adlard, Khan and Whitham (1960) used a vapour jacket to heat their columns which in turn was surrounded by a silvered, evacuated jacket. The maximum temperature difference was measured to be 0.08°C. Their reason for needing such precise temperature control is not made obvious. Munari and Trestianu (1983) reported an oven design to overcome the characteristic "Christmas tree" shape of a peak caused by temperature fluctuations during capillary gas chromatography. They investigated the source of thermal disturbances in the region of a capillary column and concluded that the cause was an uneven air-flow pattern inside the oven. They developed an oven with what they claim to be an

unconventional design but which has similar features to those of the Pye 104 (see Section 4.2.1). They also increased what they refer to as the thermal inertia of the column by using a metal cage. Alternative suggestions were to wrap the columns in aluminium foil, or, a glass fibre sleeve. This oven is marketed by Carlo Erba. Yang *et al.* (1984) reported the design and performance of an oven. They shielded the oven heater from the columns with the fan blades and a screen to reduce heat radiation to the columns. They implicate radiation as the largest cause of temperature variation. With this design they claim temperature uniformity to be better than ±0.04°C at 46.7°C and ±0.14°C at 151.5 °C. This oven is marketed by Varian.

4.2 The Pye Model 104 Chromatograph

4.2.1 General Description

The Pye 104 was designed over twenty-five years ago but modern day chromatographs bear a remarkable similarity to it. Most chromatographic ovens are simply a box containing a heater and a means of air circulation. Conventional ovens almost invariably have a resistance-wire heater suspended around a radial-flow fan, and a control circuit to regulate the input of power. The columns are usually suspended in the air space.

The trend in chromatography has been to sell an oven by its associated extras (often involving a microprocessor). The only feature of real interest, in the development of sorption-effect chromatography, is the temperature controlled box in which the chromatographic columns (and sometimes the detector) are housed and this does not change significantly from one manufacturer to another. The Pye 'box' (Figure 4.8) is constructed of substantial asbestos blocks giving it a high thermal mass. Four walls are permanently fixed, the base, the two side walls and the rear wall through which protrudes the shaft on which the fan is mounted. The connections for the heating element and a platinum resistance thermometer enter the oven through the rear wall. The oven is protected from over-heating by a thermal fuse which is also inserted through the back wall and is connected in series with the heating coil. The front wall is an opening door, hinged at the bottom, and the lid is removable. There are holes in the lid for the columns and detector. Several different detectors were available with the Pye but the design of the lid is very similar in each case. At the rear of the box is housed the fan motor and part of the electrical system. The complete apparatus is enclosed in a metal casing around the inside of which air is blown by a second fan mounted on the motor shaft between the motor and the outside of the rear wall to prevent the metal becoming too hot when the oven is operating at high temperatures and to cool the electrical system. The fan has

two speeds, high and low, and is of the radial flow type. Temperature controllers and detector power supplies are separate stacking modules whose electrical connections plug into the rear panel of the main box. The means of carrier gas flow control is mounted on the top panel. On some models this is a pair of mass flow regulators and on others, a set of crimped-tube flow restrictors.

Figure 4.8 - Front and Side Views of the Pye 104 Oven Shown with the Lid Separated From the Main Oven

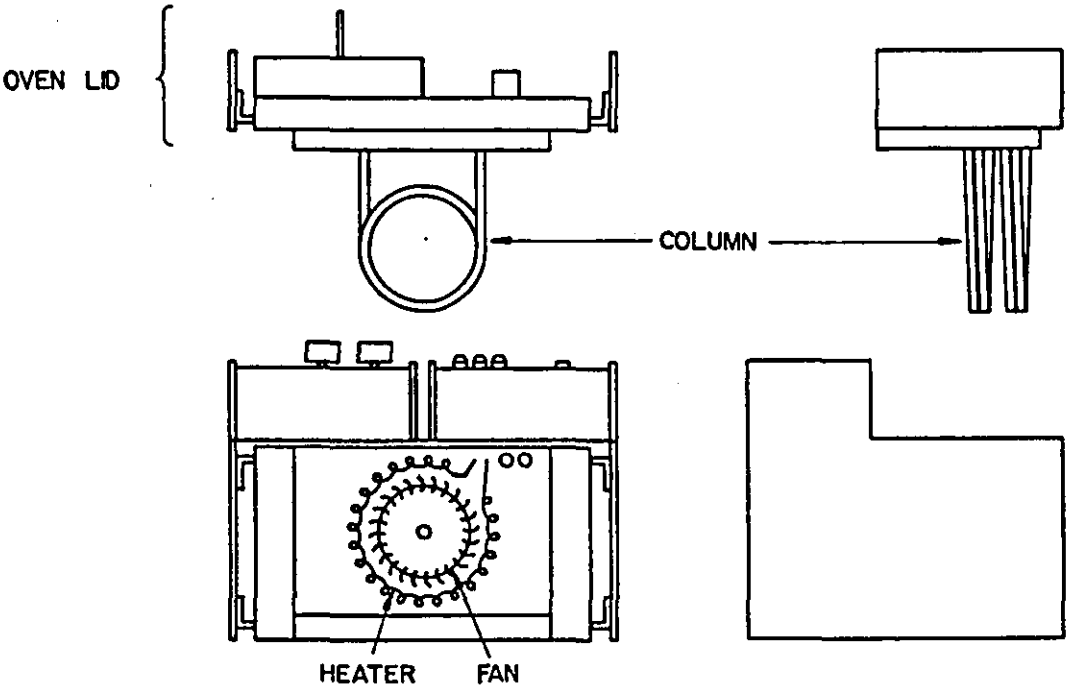

4.2.2 Heat Losses

Most of the chromatographic work reported in this thesis was performed on a Pye Model 104 Chromatograph with modifications. This is because, for the purposes of sorption-effect chromatography, it performs more satisfactorily than more recent machines and so has been used as a yardstick for testing oven performance.

Given the oven configuration, described above, of a heating element suspended in the air space, there inevitably exists a temperature gradient within the oven when heat is being lost to the atmosphere. Heat can be lost by conduction through the oven walls and by warm air leaking out of gaps and holes and being replaced by colder air. Heat is transferred to the walls mainly by forced convection, but whilst the air may be well

mixed, the heater wire is always at a higher temperature than the surrounding air. Heat is also radiated to the walls. This temperature gradient can be minimised by having as low a heat load as possible.

Conduction of heat through the walls is unavoidable. The Pye 104 has an advantage for isothermal work in that it has such a high thermal mass. The trend in chromatographic oven design has been toward low thermal mass to assist temperature ramping and fast cooling. Some manufacturers incorporate a flap which opens and closes in accord with the signal from the temperature controller to allow warm air to be vented.

4.2.3 Heat Transfer to Chromatographic Columns

The mechanism by which temperature fluctuations manifest themselves upon the column is not known. Glass is a relatively poor conductor of heat and the number of points of contact between column packing and column wall results in a small area for heat conduction, yet the amount of baseline noise can be substantial.

A series of experiments were conducted to investigate two parameters using a leak-proof* Pye 104 oven (*see Section 4.3.1 Reducing the Effect of Leaks). These were :

i) the number of points of contact between column packing and column wall. Two different grades of packing were used : 4-8 mesh and 8-12 mesh.

ii) heat transfer through the column wall. Three column materials were used : 3/8" o.d. Copper tubing, 3/8" o.d. Thin-walled glass tubing, and, 3/8" o.d. Thick-walled glass tubing. All columns were 18" (45cm) long.

Nitrogen carrier gas was used because, of the gases which were readily available in the laboratory, it is the most strongly adsorbed and therefore the most susceptible to temperature variations. The baseline was monitored with heater input and with air circulation only for each packing/column wall material combination.

Figure 4.9 - Thermal Noise Generated within 3/8" o.d. Copper-Walled Columns

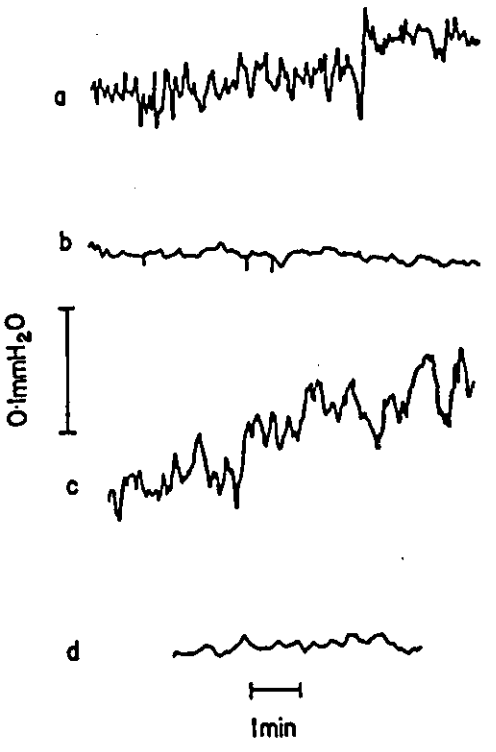

a : 4-8 mesh 5A Molecular Sieve packing, temperature controller set to 50°C
b : 4-8 mesh, fan circulation only (no temperature control)
c : 8-12 mesh, temperature controller set to 50°C
d : 8-12 mesh, fan circulation only (no temperature control)

Table 4.1 is a summary of the results obtained from Figures 4.9 to 4.11. Noise is expressed as a proportion of full-scale deflection on the chart recorder.

Figure 4.10 - Thermal Noise Generated within 3/8" o.d. Thin-Walled Glass Columns

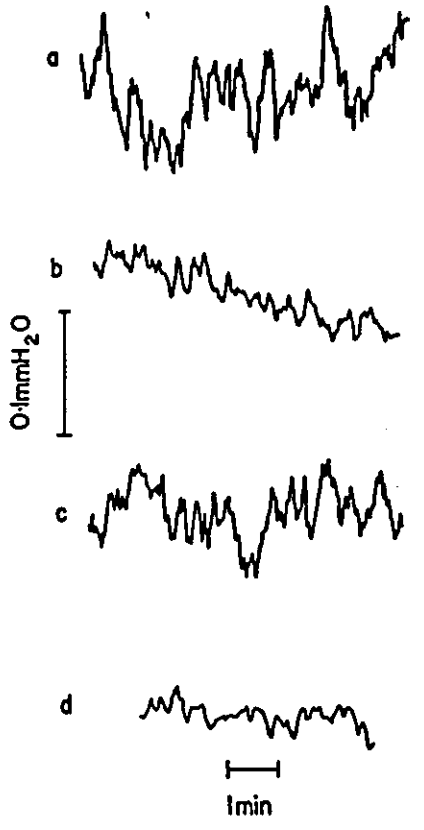

a : 4-8 mesh 5A Molecular Sieve packing, temperature controller set to 50°C
b : 4-8 mesh, fan circulation only (no temperature control)
c : 8-12 mesh, temperature controller set to 50°C
d : 8-12 mesh, fan circulation only (no temperature control)

The results of these tests were inconclusive. The baseline noise which has been attributed to temperature fluctuations seems to take two forms. One is a relatively rapid flow rate variation which is superimposed on a much more gradual baseline drift. The smoothest baseline obtained using heat input was with the coarsest packing and the worst column for heat conduction, i.e. 4-8 mesh in the heavy-walled glass (Figure 4.11a). With no heater input (using only air circulation by the fan) there is little to choose between the copper columns and the heavy-walled glass columns (Figure 4.9b, 4.9d, 4.11b and 4.11d) but all are smoother than the best trace under heater input. This implies that the column should be insulated and have the minimum number of points of contact between the packing and the column wall by using the coarsest possible packing size.

Table 4.1 -An Investigation of the Influence of the Column Wall Material and Packing Size on Thermal Noise

Tube Material	Packing Size	Baseline Noise Deviation		Run Duration	Comments	Figure
	(Mesh)	Maximum	Average	(mins)		
3/8"	4-8	0.09	0.03	19	55.3°C	4.9a
Copper	4-8	0.02	0.01	32	Fan only -	4.9b
					no heater	4.9c
	8-12	0.06	0.03	18	55.7°C	4.9d
	8-12	0.02	0.01	11	Fan only	
3/8"	4-8	0.11	0.08	19	≈ 50°C	4.10a
Thin	4-8	0.05	0.02	10	Fan only	4.10b
-Walled	8-12	0.08	0.04	36	≈ 50°C	4.10c
Glass	8-12	0.03	0.02	8	Fan only	4.10d
3/8"	4-8	0.05	0.03	6	≈ 50°C	4.11a
Thick	4-8	0.03	0.01	9	Fan only	4.11b
-Walled	8-12	0.07	0.03	60	≈ 50°C	4.11c
Glass	8-12	0.02	0.01	10	Fan only	4.11d

Figure 4.11 - Thermal Noise Generated within 3/8" o.d. Thick-Walled Glass Columns

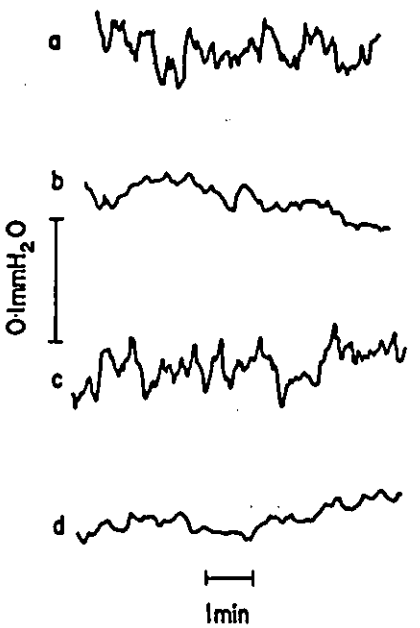

a : 4-8 mesh 5A Molecular Sieve packing, temperature controller set to 50°C
b : 4-8 mesh, fan circulation only (no temperature control)
c : 8-12 mesh, temperature controller set to 50°C
d : 8-12 mesh, fan circulation only (no temperature control)

These experiments did highlight two important factors :

a) the circulation of air within the oven

b) the method of heat input.

4.3 Modifications Made to the Pye 104 Chromatographic Oven

4.3.1 Reducing the Effect of Leaks

As stated earlier, the Pye oven is constructed of blocks of asbestos, with a removable lid and a door. It is unlikely that these blocks form a leak-tight seal. Heat losses would occur if warm air was leaking out of the oven and/or cool air was being drawn into the oven. The effect of leaks was reduced by sealing all the joints between the fixed asbestos blocks of the Pye oven with fire cement. The door and lid can be sealed by casting a high-temperature resistant silicone rubber seal onto one of the surfaces, or, creating a sandwich of ordinary silicone rubber between two layers of aluminium foil, one for the lid and one for the door, reassembling the oven, thus squashing down the sandwich, and allowing the rubber to set. This second method produces a removable seal, should the

operating conditions exceed the maximum working temperature of the seal, for instance, during column conditioning. Any access holes in the lid and walls are easily plugged with, for instance, glass wool.

4.3.2 Air Circulation

The manner in which the air in the oven is circulated is important. If eddies of warmer or colder air are the cause (or one of the causes) of baseline instability, then the less turbulent the air flow, the smoother the baseline. But if no mixing of the air takes place then temperature differences will obviously exist within the oven.

As stated earlier, the oven has a radial flow fan. Ideally, air would be blown radially out of the fan, past the heating element and along the side-walls, floor and lid, becoming uniform in temperature in the process. It would then be drawn past the columns which are suspended in the centre of the front of the oven, moving axially back into the fan to begin another circuit of the oven (Figure 4.12). In this way, all the air which comes into contact with the columns would be at the same temperature and the column could be regarded as isothermal.

Figure 4.12 -Ideal Oven Air Circulation in the Radial Plane of the Fan

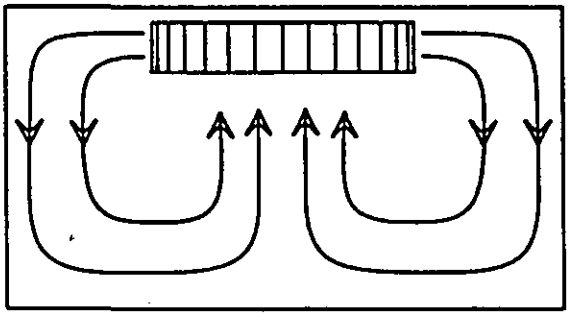

To allow the actual flow pattern around the oven to be observed, the door was replaced with a piece of perspex and small pieces of tissue paper placed inside to act as flow followers. With the fan at full speed the circulation of the air was very turbulent with stagnant regions in the lower corners. The lower fan speed gave a smoother, more consistent air flow but still with stagnant areas. The introduction of baffles, in the lower corners of the oven improved the air circulation but more elaborate baffles designed to encourage radial exit from the fan and axial entry were not noticeably effective, perhaps because even at the lowest fan speed the air circulation was still too turbulent. Figure 4.13 shows the baseline recorded when a cardboard 'honeycomb' was positioned in the

centre of the oven inside the coils of the column for the purpose of straightening the flow as it returns to the fan. Comparison with Figure 4.1a suggests that the inclusion of the baffle may have improved the air circulation slightly. If the complete oven space is filled with honeycomb baffling there is very definitely a drop in oven performance (Figure 4.14) even though this baffle arrangement, in principle, ought to approach the air circulation ideal in that the air is encouraged to flow in a fashion similar to that shown in Figure 4.12.

Figure 4.13 - Baseline Noise Recorded with Axial Flow Straighteners Positioned in the Centre of the Column Coils

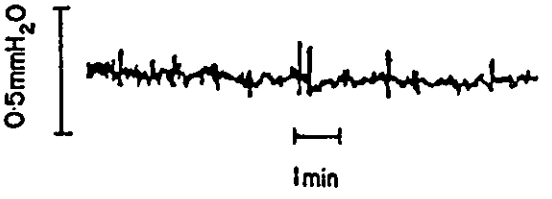

Figure 4.14 - Baseline Noise Recorded with Axial Flow Straighteners Completely Surrounding the Column Coils

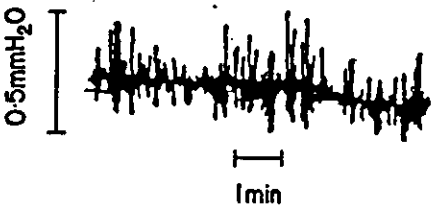

4.3.3 Fan Speed

A variable auto-transformer ("Variac") was connected into the low fan speed circuit so that the voltage to the fan motor, and thus the fan speed, could be varied. Figure 4.15a shows the baseline noise with the fan set on its low speed setting (before the Variac was connected into the fan circuit) with no temperature control. At low speed, the voltage supplied to the fan motor by the oven circuitry is 110V. Figures 4.15b, 4.15c and 4.15d show the baseline noise recorded when the fan motor is supplied with 60V, 70V and 80V respectively. The baseline is smoother with 60V (Figure 4.15b) than with 110V supply (Figure 4.15a) but there is no discernible difference between the baseline noise

in Figures 4.15b, 4.15c and 4.15d. The minimum voltage is set by the point at which the friction in the motor bearings cannot be overcome. The modification which could be made was to incorporate a Variac as above and set the fan speed somewhere close to its minimum. However, there is a range of speeds above the minimum over which baseline quality does not deteriorate significantly and a more convenient modification was to connect a high-power resistor in series with the motor winding. The resistor was sized during tests on one particular motor, to give a motor speed of the right order, and that one size used to modify several motors at different stages of wear. The optimum speed for another motor was set with a Variac to 200 r.p.m., whereas with the resistor in series, the fan speed was 370 r.p.m. with no discernible loss of oven performance.

Figure 4.15 - Baseline Noise Recorded with Oven Air Circulation Only

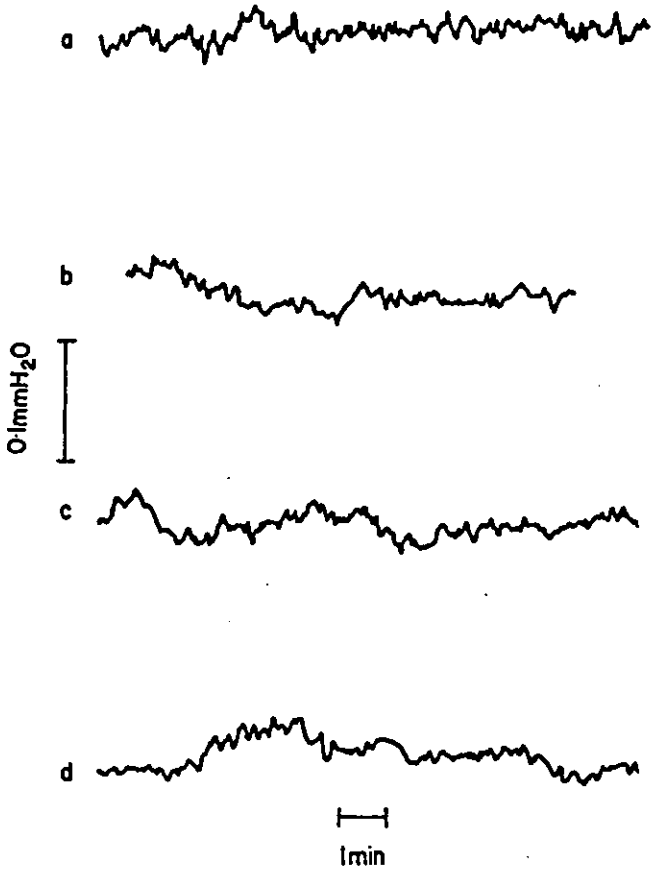

Voltage applied to the fan motor
a : 110V
b : 60V
c : 70V
d : 80V

4.3.4 Heater Power Input

There is a variety of different ways of supplying power to the heating element which could be used by oven manufacturers. The heating element is usually a resistance wire suspended around a radial flow fan as found in the Pye 104. The Pye element has a resistance of 20Ω giving it a potential output of around 3kVA (operated with mains electricity) and an operating range of around 35°C to 500°C (although for operation above 420°C the thermal fuse must be exchanged for one with a higher melting temperature). In the case of the Pye 104, the temperature controller supplies any part, and as much of, each mains half-cycle as required. This means that the power is turned on and off one hundred times a second. This is known as phase angle control and leads to a relatively smooth heat input. More modern ovens employ a time cycle (cycle length is typically about one second but in some cases may be alterable by reprogramming the temperature controller) putting in the required amount of power at the beginning of each cycle, then off until the end of the cycle. This leads to saw-toothing of the temperature within the oven, to a greater or lesser extent, and is not ideal for sorption-effect chromatography. This move away from phase angle control is probably because of more stringent rules on radio frequency noise within a works environment.

Four ways of powering up the heater were devised and compared to the performance of the standard Pye 104. The basic element of all these methods is the temperature controller (Eurotherm Model 821 : Full specification 821 -070 -049 -070 -713 -412 -512 -018 -00) using a platinum resistance thermometer as the temperature sensor.

4.3.4.1 Heat Input Method 1

Method 1 was a commercially available system using a Eurotherm thyristor stack (Model 461-081-13-19-008-002-00) in conjunction with the controller and shown schematically in Figure 4.16a. The thyristor is essentially a power 'valve' which opens and closes with the controller output. Four different power input modes (Figure 4.17) are selectable with this model (via a DIL switch) :

a) phase angle

b) single cycle i.e. decides before each cycle whether or not to take it

c) fast cycle i.e. timed cycle for which power is on part of the time

d) phase angle start fast cycle i.e. beginning of timed cycle takes phase angle power.

Figure 4.16 - Four Different Methods of Inputting Heat to the Oven Air Space

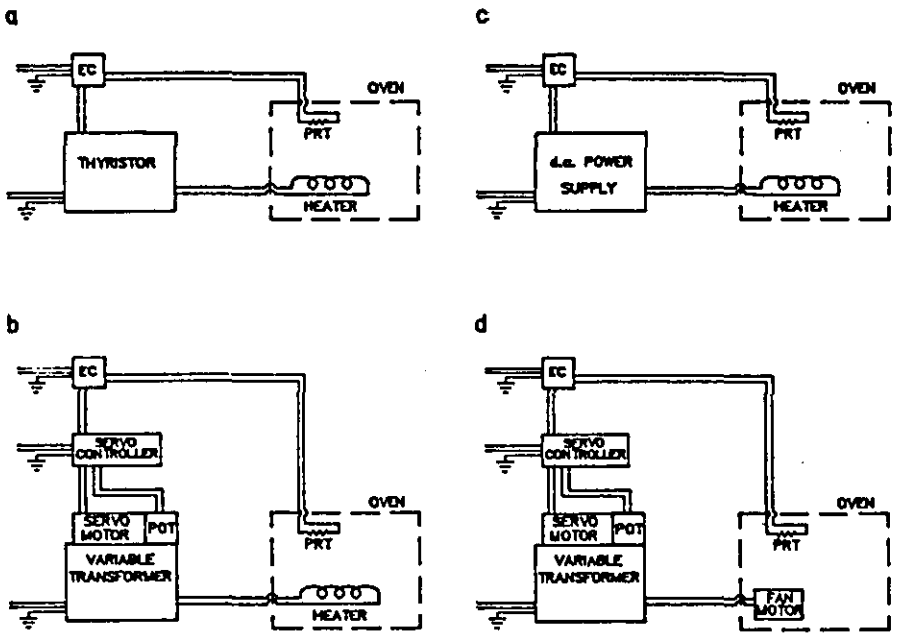

a : Method 1 - the commercially available system using a temperature controller in conjunction with a thyristor to regulate power to the heating element.

b : Method 2 - the temperature controller output is used to drive a servo motor which moves the rotor arm of a variable transformer thus altering the voltage applied across the heating element.

c : Method 3 - the temperature controller is used to vary the output of a direct current power supply which is connected to the heating element.

d : Method 4 - the transformer output in Method 2 is used to vary the voltage applied to the fan motor. This method uses the friction of the fan blades in the oven air as the means of heating.

4.3.4.2 Heat Input Method 2

Method 2 involves the use of a variable auto-transformer (Variac). If the power to the heater were set at a constant value, then the temperature in the oven would settle at steady state, but the temperature would not be controllable. If the output of the Variac were alterable according to the oven temperature then control would be possible. Figure 4.18 shows a diagram of a modified Variac with a servo motor gearbox and clutch arrangement. The Variac (Zenith Electric Co. Type Y16 HM) was purchased with an extended shaft so that the motor and gearbox could be mounted on top of the casing. The motor (RS Components Stock Number 336-292) and gearbox (RS 336-286) were off-the-shelf items along with the servo control unit (RS 591-663). The clutch was required because the Variac does not have 360° movement and it was possible that the controller might try and drive the Variac brush arm when it was up against a stop. The

Figure 4.17 - The Four Power Input Modes of the Thyristor

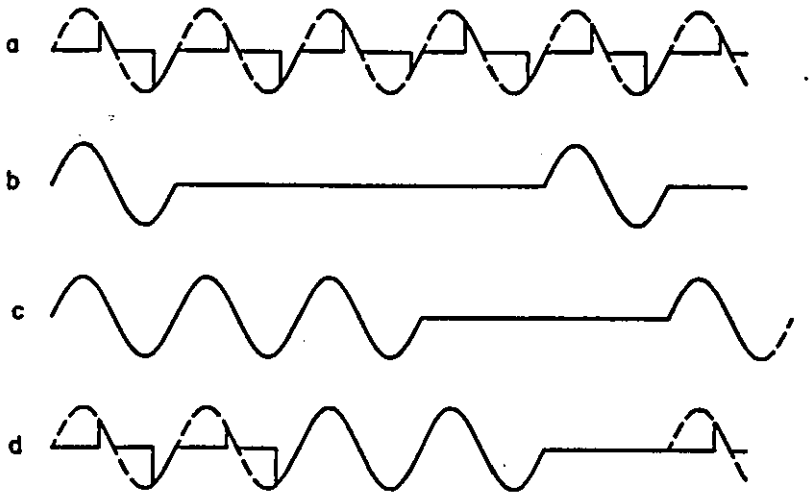

a : Phase angle
b : Single cycle
c : Fast cycle
d : Phase angle start fast cycle

clutch consists of a nylon friction washer and a loading spring. The tension in the spring is set by the loading nut (plus locking nut) and determines the torque at which the gear cog and the nylon ring will slip. The position of the brush arm is set so that at zero controller output it is resting against the zero volts stop. The servo motor controller is intended for use with two potentiometers, a master and a slave. The master is usually a joy-stick and the slave (5kΩ RS 173-574) is coupled to the gearbox output shaft (mounting kit RS 336-214). Movement of the master potentiometer is followed by the motor until the potential difference across the slave potentiometer matches some prerequisite control criterion. The full range of movement of the motor is realised when the potential difference across the master potentiometer changes from -5V to +5V. When the gearbox ratio is 2560:1 this movement is ±162°. In this application the master potentiometer is replaced by the output of the temperature controller (0-5V) so the maximum permissible rotation of the Variac arm is 162° which allows the Variac output voltage to vary by about 130Va.c. (N.B. The gearbox output shaft to Variac shaft gear ratio is 1:1). The control circuit is shown schematically in Figure 4.16b.

Figure 4.18 - The Servo Transformer Assembly

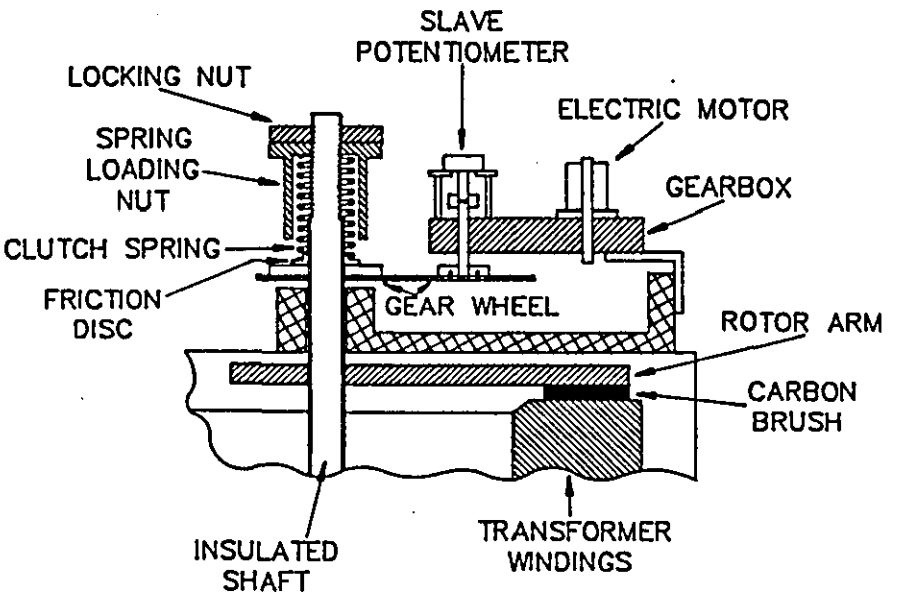

Figure 4.19 - Power Variation Versus Voltage Applied Across the Heater Element

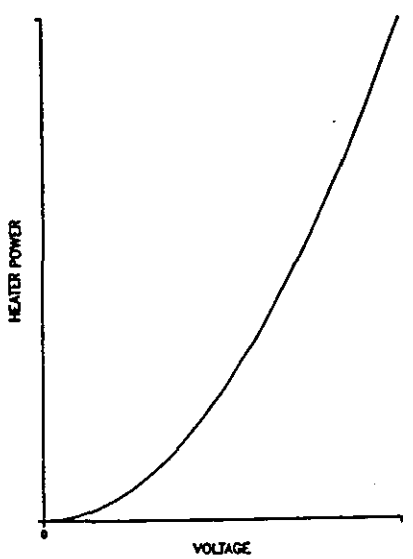

One advantage of this system is that the heater power varies as the square of the applied voltage so when the heater is working at low load (when control is more critical) a small increase in voltage does not give such a large change in heater power as it would at higher voltage (Figure 4.19).

4.3.4.3 Heat Input Method 3

Method 3 was to use a precision d.c. power supply (Electronic Measurement Inc. TCR Model $150^{S}7$-2) to power the heater. One mode of operation for the power supply is to use a remote setting voltage (0-5V) to vary the power output. The control signal from the Eurotherm temperature controller was connected to act as the setting voltage, consequently varying the voltage to the heater between 0V and 150V d.c. (i.e. 0-1kW using the 20Ω Pye element) with the temperature sensed in the oven (shown schematically in Figure 4.16c).

4.3.4.4 Heat Input Method 4

The fourth method makes use of the fact that the blades of the fan actually increase the temperature of the air inside the oven because of friction. The Pye oven will attain a temperature about seventeen degrees Centigrade above ambient with the fan at full speed and about twelve degrees above on the low speed setting. Taking into consideration the importance of the air circulation there is a range of fan speed above the minimum for which the oven performance is still satisfactory so it should be possible to vary the temperature by varying the fan motor speed. The servo-driven Variac was used to drive the fan motor so that it is the rotational speed of the fan which varies with the control signal. The limits of this system are that the fan will stop if the voltage is too low and obviously if the fan speed is too fast there are problems with random temperature fluctuations caused by the air turbulence. The controller does however have a facility for limiting the maximum output. The fan motor voltage at zero controller output had to be adjusted to the minimum at which the fan kept moving. This was achieved by moving the Variac shaft gear relative to the gearbox output shaft gear. This control system proved to be very difficult to tune. With the controller set to the most favourable control settings found, the temperature is only controllable within about half a degree of setpoint and the setpoint must be only a few degrees above ambient temperature (but this is an advantage over other ovens - most commercial ovens have a minimum operating temperature which is usually around ten degrees above ambient). Unless the work requires a very accurate temperature this is not a problem. The advantage of this system for sorption-effect chromatography is that the temperature changes are so smooth and slow. The system could perhaps be used in conjunction with a conventional heater for

operation at higher temperatures. A constant voltage could be applied to the conventional heating element to set the temperature roughly and the fan speed then be used to fine tune the temperature.

Some problems were experienced during the operation of the servo-Variac mechanism. The clutch spring was initially set at too low a tension. This would not have been a problem but the contact surface of the carbon brush on the Variac arm was rough and uneven which caused sparking between the brush and the windings. This caused the brush, and also the insulation in which the copper windings are set, to burn away, roughening the two surfaces even more. This eventually led to the clutch slipping when the friction between the brush and the windings was greater than that between the two surfaces in the clutch mechanism. This was overcome by polishing the contact surfaces of the brush and the windings with fine emery paper which eliminated the sparking and reduced the friction. The clutch spring was also set to a greater tension.

4.3.5 Controller Tuning

4.3.5.1 Introduction

The Eurotherm 821 is a proportional-integral-derivative (PID) controller meaning that it can combine proportional action with either integral action or derivative action, or both.

Proportional action is where the controller output is proportional to the error, that is, the difference between the set-point and the measured value. The magnitude of the action is determined by one of two related parameters, controller gain (K_c), or proportional band (PB). The relationship is :

$$K_c = \frac{100}{PB} \tag{4.1}$$

Integral action causes the controller output to change as long as an error exists. This is to eliminate steady-state offset.

Derivative action is intended to speed up the control action by anticipating where the process is going by measuring the rate of change of the error and applying corrective action.

The tuning of the control system for each method of power input was something of an empirical process. There are two recognised methods of determining initial controller settings.

4.3.5.2 Loop Tuning (Ziegler-Nichols (1942))

The controller is set to proportional action only. The controller gain is then gradually increased until the system is on the point of instability indicated by continuous cycling of the measured variable. Each time the gain has been changed, a change in set-point may be required to initiate cycling. The gain at which the system oscillates is known as the ultimate gain (K_u) and the period of the oscillation, the ultimate period, P_u (Figure 4.20).

Figure 4.20 - Controller Tuning by the Ziegler-Nichols Method

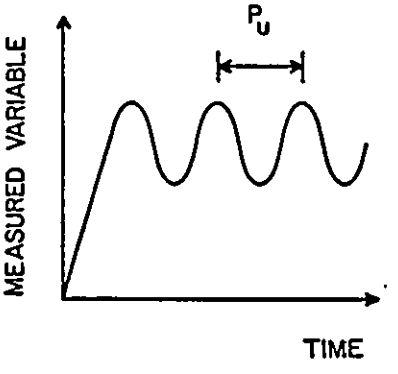

The gain is gradually increased until the closed-loop system cycles continuously.

From these values, the controller settings can be estimated using the Ziegler-Nichols rules which are summarised in Table 4.2. Specifications for PD control cannot be made from only K_u and P_u.

Table 4.2 - Controller Settings based on the Loop Tuning Method (Wherry and Miller (1973))

Controller Action	Gain	Integral Time	Derivative Time
P	$0.5K_u$	-	-
PI	$0.45K_u$	$0.833P_u$	-
PID	$0.6K_u$	$0.5P_u$	$0.125P_u$

The Eurotherm controller uses proportional band (as opposed to gain) so the point of instability was reached by gradually increasing the proportional band and so was approached from the unstable side. In these circumstances, allowing the system to go

unstable did not cause any problems but in certain cases this practice may be unacceptable because of the consequences of going unstable, e.g. tuning of an exothermic reactor temperature control loop.

4.3.5.3 Reaction Curve Method (Cohen and Coon (1953))

This method uses the open-loop response (i.e. no control action) to a step change to derive the dynamic characteristics of the loop. For certain processes the controller settings can be estimated.

The step change, ΔM, should give a response as shown in Figure 4.21 if the controller settings are to be approximated by this method. The maximum rate of change is R and the dead-time L. The rate of change per unit step change in the manipulated variable is $R_1 = R/\Delta M$. The controller settings are given in Table 4.3.

Figure 4.21 - Controller Tuning by the Reaction Curve Method

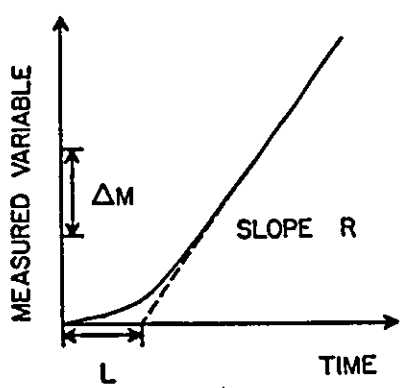

The open-loop response to a step change.

4.3.5.4 Fine Tuning

Once the initial settings have been established the control loop, in all probability, requires some trial and error adjustments.

4.3.6 Controller Tuning for Heat Input Methods 1 to 4

The loop tuning method seemed suitable for the first three methods of heater power input because the oven temperature could be made to oscillate and reasonable control could be achieved on the basis of the Ziegler-Nichols rules.

Table 4.3 - Controller Settings based on the Reaction Curve Method (Wherry and Miller (1973))

Controller Action	Gain	Integral Time	Derivative Time
P	$\frac{1}{R_1 L}$	-	-
PI	$\frac{0.9}{R_1 L}$	3L	-
PID	$\frac{1.2}{R_1 L}$ to $\frac{2}{R_1 L}$	2.5L to 2L	0.5L to 0.3L

Neither tuning method mentioned above was suited to tuning the friction-of-the-fan-blades input mode. The system could not be made to oscillate even after hours of monitoring at the lowest proportional band and the process reaction curve was not of the correct form and so could not be used to predict the controller settings. The shape of the reaction curve obtained is probably due to an initial rapid rise in the air temperature followed by the more gradual heating of the walls (Figure 4.22).

Figure 4.22 - The Reaction Curve Obtained When a Step Change in the Fan Motor Voltage is Applied Using Heater Power Input Method 4

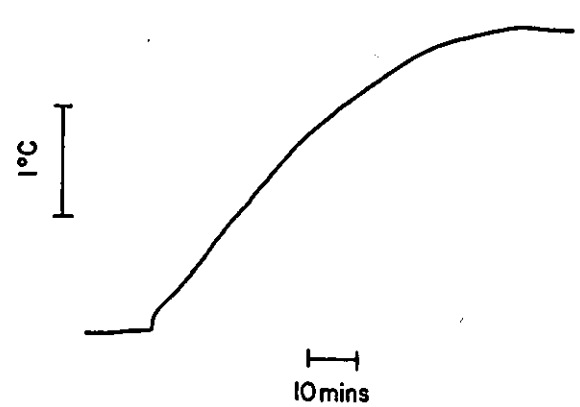

On the advice of a Eurotherm engineer, the controller was set for proportional-integral control with a long reset time and high proportional band. The resolution of the control system was also increased in two ways :

The controller has 12 bit resolution (4096 divisions) over the configured temperature range. This was altered from 0-500°C to 0-100°C by reconfiguring the controller in set-up mode giving 40 divisions per degree instead of 8 divisions per degree.

Two resistors, 1kΩ and 1.5kΩ, were connected in series across the controller output terminals and the voltage at either side of the 1k resistor connected to the servo control system inputs (Figure 4.23). This meant that instead of the controller output being 0(0%)-5V(100%) and giving the corresponding Variac arm movement (162° ≅ 130Va.c.) via the servo control unit, the controller output becomes 0(0%)-2V(100%) thereby reducing the maximum arc through which the arm can move to approximately 65° (≅50Va.c.). The change in the output of the Variac to a 1% change in the control signal is 0.5Va.c. with this modification compared to 1.3Va.c. with the previous configuration.

Figure 4.23 - Increasing the Resolution of the Control System

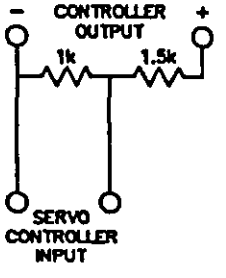

4.4 Testing Commercial Ovens

A study of the operation of several makes of modern oven was carried out. Chromatographic columns were installed and the thermal noise monitored. The flow-generating system and flow-detector were as described in Chapter 2.

4.4.1 Analytical Instruments Model 93 Oven

This oven follows the 'classic' design but with low thermal mass walls to assist rapid heating and cooling. In addition, there is a motor-driven flap built into the rear wall for cooling and for operation at temperatures close to ambient. Whilst the flap is

open it is unlikely that the oven temperature can be either stable or uniform. The temperature is controlled by an Eurotherm 812 controller working on a time cycle of around one second (Figure 4.17a, heater input mode c). The position of the flap depends on the controller output in the following manner :

0-1% output	flap opening
2-11%	flap stationary
12-18%	flap closing at a speed proportional to output
19-100%	flap closing at full speed.

Modifications made to try and improve the oven performance included re-tuning the control system (optimum PID settings were found which differed from those set in the factory), slowing down the fan speed (using a Variac), inserting baffles like those used in the Pye, using heater input method 1 (the Eurotherm controller and thyristor stack - as described earlier) and disabling the flap. No improvements to temperature stability were made that surpassed the performance of the modified Pye.

For sorption-effect chromatography and good temperature uniformity, the AI oven possesses all the disadvantages of the Pye oven (oven geometry, high fan speed, heater in air space) plus the flap, but none of the advantages (phase-angle control, high thermal mass). One advantage over the Pye is the ease with which temperature ramping can be achieved i.e. for isobaric work.

4.4.2 Packard Model 436 and 427 Ovens

The Packard range of ovens has a U-shaped chamber which houses the columns. The fan in the Model 427 is positioned behind the grille which is the rear wall of the oven. In the Model 436 (a more modern design) the fan is enclosed in a cage protruding from the rear wall which is located in the rear centre part of the oven. The heating element is mounted around the outside of the curved face and zigzags front to back from the top left part of the U around to the top right. The oven space is enclosed by a second U-shaped wall on the outside of the heater which makes a seal with the roof and door. Air is blown by the fan, past the heater, to enter the chamber around the lip of the inner U-shaped wall, and then is drawn back into the fan. The manufacturers claim temperature stability to within 0.01°C however this is in fact the difference in the average temperature of separate seventy-two hour runs. Temperature gradients within the oven are claimed to be less than 0.1°C. The temperature controller inputs power to the heater over a half second cycle. The power required for the cycle is supplied at the beginning of the cycle and switched off for the remainder. This leads to saw-toothing of the temperature. Figure 4.24 shows the power pulses triggered by the controller to maintain a temperature of 40°C. These were measured by use of a power meter. The power meter is an induction

coil which encircles the wire to the heater. A pulse to the heater induces a current in the coil. A resistor is connected across the meter outputs which are in turn connected to a chart recorder so that the induced voltage can be observed.

Figure 4.24 - Pulses of Power Being Input to the Heater by the Packard Temperature Controller

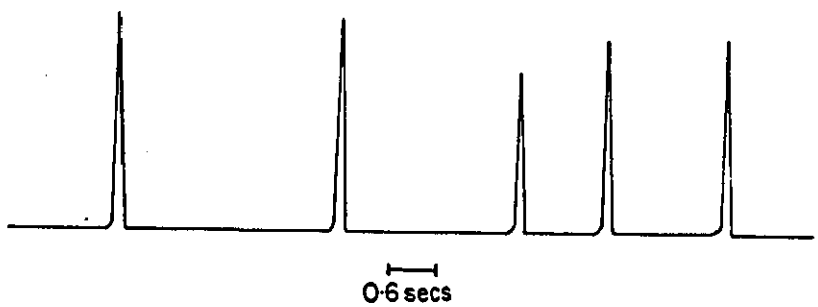

The temperature and air velocity at twelve different points around the lip of the inner shell where the air enters the column chamber vary as in Figure 4.26. These measurements were taken on the Model 427. The twelve positions are shown in Figure 4.25. The air velocity was measured by taking a pressure reading at each point using one side of a differential pressure transducer with the other side blanked off. The units on the right-hand axis of Figure 4.26 are arbitrary. The air temperature at each point was measured by using a thermocouple.

As can be seen, the air velocity is greatest at the bottom of the U and it follows that this air is the coldest. A U-shaped baffle was fabricated from aluminium sheet with twelve variable flaps so that the flow distribution could be made more even. The dotted line in Figure 4.26 shows the flow distribution after 'tuning'. The performance of the oven was not improved upon sufficiently to warrant using this model in preference to the modified Pye 104.

4.4.3 Carle Series 400 AGC

One make of oven tested which does not follow the conventional design is the Carle Series 400 AGC. The manufacturers claim that the oven has "a 'hot floor' diffusion system with a very high capacity heat sink". "Heat is uniformly conducted from the floor and walls of the column oven". Presumably, heat is transferred to the columns by convection (in the absence of a circulating fan) and this design does not seem likely to be capable of isothermality. No temperature specification is quoted by the manufacturers. The columns are wound in different diameter coaxial coils. Temperature measurements

Figure 4.25 - The Positions Around the Packard Heater Element Shell at Which Temperature and Pressure Measurements were Taken

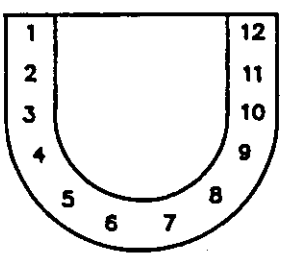

Figure 4.26 - . Temperature (Lower Line) and Air Flow (Upper Line) Variation Around the Packard Heater Element Shell

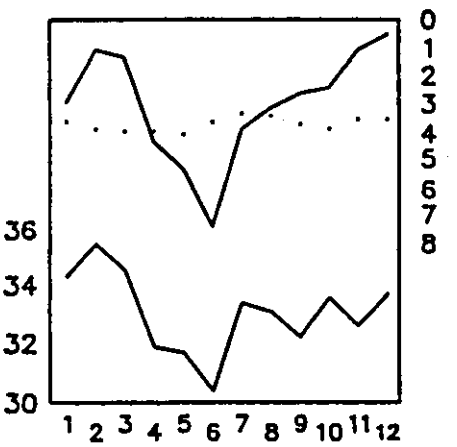

at various positions, in the proximity of the column wall, are listed in Table 4.4. The oven set-point temperature was 50 °C. All measurements were made with the same probe. However, the oven had to be opened and the probe moved between readings thus the temperature in the oven had to be allowed to reach equilibrium.

Table 4.4 - Temperature Variation within the Carle Oven

Column	Position (o'clock)	Temp °C
Outer Column	3	52.4
	6	51.9
	9	51.8
	12	50.9
Inner	6	50.9

4.4.4 Carlo Erba (Munari and Trestianu (1983))

Carlo Erba have established "a reputation which is second to none in High Resolution Gas Chromatography". Figure 4.27a shows the flow rate trace from a sorption-effect chromatograph which has the columns contained within a Carlo Erba oven at 50°C. Figure 4.27b shows the trace where there is no heater input but the fan is circulating.

Figure 4.27 - Baseline Noise Experienced Using the Carlo Erba Oven

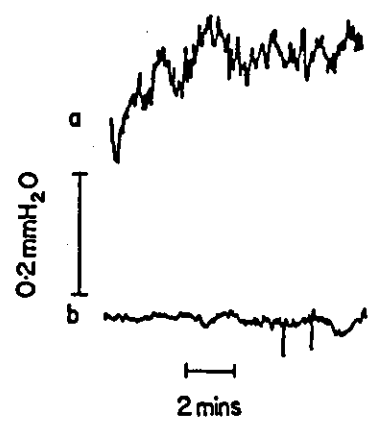

a : with heater input
b : with only air circulation.

4.4.5 Summary

Most of the modern ovens available for test were similar in design to that of the Pye. Unmodified, the performance of an oven is very poor in the context of Sorption-Effect Chromatography. There was no advantage in trying to improve every oven tested because there was an adequate, modified Pye oven available so the quest to find a suitable modern oven was abandoned.

4.5 Development of an Isothermal Oven

4.5.1 Introduction

Most commercial ovens, as has been stated before, seem to be based on designs similar to that of the Pye 104. A novel isothermal oven was designed and built with the heating elements making up the inner surfaces of the walls. Any heat lost through the walls can, in theory, be provided by the heaters and not the circulating air. With this design, a uniform temperature within the oven is more feasible than with the conventional design. The same problems exist as with commercial ovens, how to circulate the air, and, how to supply the power to the heaters.

4.5.2 Design

The oven was built as a box 32cm x 32.5cm x 22.5cm (external dimensions) contained within a framework which also houses the fan motor, electrical wiring, temperature controller, etc...(Figure 4.28).

Figure 4.28 - The Framework Designed and Used to Build an Isothermal Oven

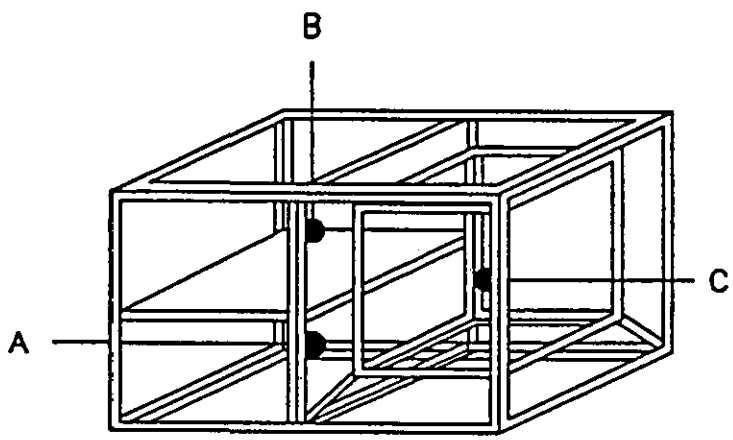

A : Temperature controller and thyristor compartment
B : Fan motor and wiring block compartment
C : Heated chamber housing the columns and fan.

The walls consisted of aluminium sheets with the heater elements attached to the inner face of each wall. For each heater the wire was wound onto an insulating board which was then sealed inside a mica envelope.

The fan motor was bolted to the shelf behind the rear wall of the oven with the shaft protruding through this wall on the vertical centre line but about an inch above the horizontal centre line. The fan was of the radial exit flow type, positioned on the shaft near to the rear wall.

4.5.3 Operation

The seal made by the aluminium sheets was not completely airtight which caused unnecessary heat losses, and the whole framework acted as a cooling fin so there was uneven heat loss by conduction. Sheets of cardboard were inserted between the aluminium walls and the heaters and every joint sealed with adhesive tape. After controller tuning, the temperature control was at least as good as that of a commercial oven and the thermal noise generated within a column with the heaters connected in parallel (Figure 4.29a) compared favourably with the Carlo Erba oven trace (Figure 4.27a). The Carlo Erba trace was recorded at half the sensitivity of the prototype oven

trace. Figures 4.29b and 4.29c show the flow trace for fan motor supply voltages of 50V and 70V. The significance of this is that the fan speed is faster at 70V than at 50V and so the noise is greater. Reducing the heat conductivity of the oven walls improved the temperature control but the use of cardboard as heat insulation restricts the working temperature range of the oven. The cardboard/aluminium plates were replaced by a non-asbestos heat resistant board donated by Turner and Newell plc, Manchester. The material (8mm Syndanyo L21) is based on Portland cement blended with man-made fibres and density modifiers and has a thermal conductivity of 0.34W/mK compared to aluminium (2370W/mK@25°C: Weast and Astle (1982)) and cardboard (8W/mK: Liley and Gambill (1973)). The coefficient of linear expansion for Syndanyo L21 is 10^{-5}/°C.

Figure 4.29 - Baseline Noise Experienced Using the Prototype Isothermal Oven

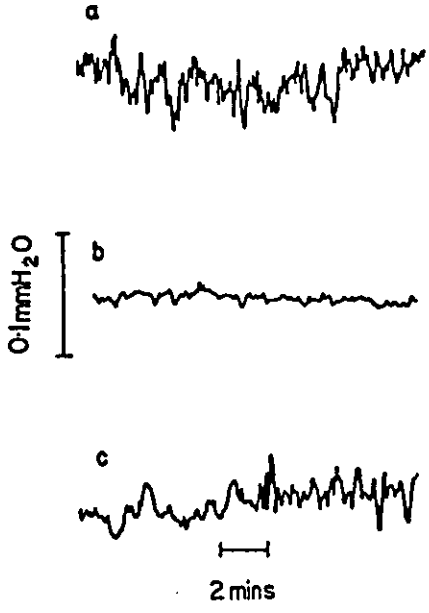

a : with heater input
b : with air circulation only, fan motor voltage 50V
c : with air circulation only, fan motor voltage 70V.

4.5.4 Heater Power Input

The three methods of supplying power to a heating element devised for the Pye were all as good as each other, within the limits of the test procedure, so the combination of the Eurotherm controller and thyristor was chosen because it is the most convenient to use.

4.5.5 Heater Configuration

The heaters were made as three pairs :

Front/Back (F/Ba)	85Ω	(28cm x 30cm)
Left/Right (L/R)	160/158Ω	(18cm x 30cm)
Top/Bottom (T/Bo)	153/162Ω	(18cm x 28cm)

It seemed sensible to have the same heat output per unit area for each wall. The power output per unit area is inversely proportional to the product of the heater element resistance multiplied by the heater area and directly proportional to the square of the potential difference across the heater.

$$\frac{W}{A}=\frac{V^2}{RA} \tag{4.2}$$

where V is the potential difference across the heater element

$$\frac{W}{A}=\frac{(pV_T)^2}{RA} \tag{4.3}$$

where p is the proportion of the total voltage, V_T, across the heater element.

Four possible configurations are dealt with below.

Figure 4.30a : Configuration 1: Heaters in Parallel

Figure 4.30b : Configuration 2: Heaters in Pairs in Parallel

Figure 4.30c : Configuration 3: Heaters in Threes in Parallel

Figure 4.30d : Configuration 4: Heaters in Series

Figure 4.30 - Possible Heating Element Configurations

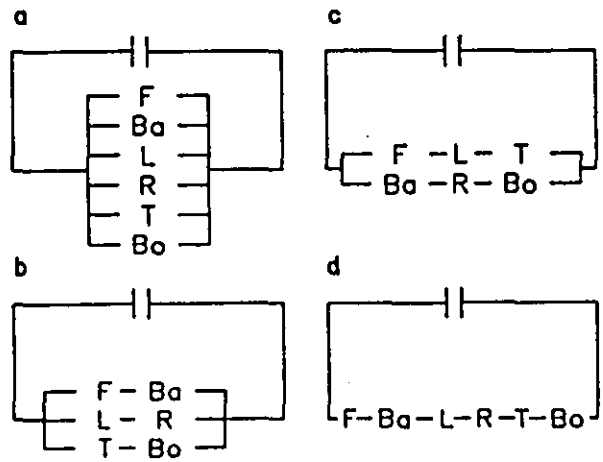

F - front wall heater
Ba - back wall heater
L - left-hand wall heater
R - right-hand wall heater
T - roof heater
Bo - floor heater

The working temperature range of the oven can be altered by choosing a different heater configuration.

From Table 4.5 it can be seen that the relative heat output per unit area for each of the three pairs of heaters is quite close using configurations 1 and 2. The output could be made more equal by connecting a 10Ω power resistor in series with both front and back heaters in configuration 1 (Figure 4.30a and Table 4.6). These extra resistors remain outside the oven and make no contribution to the heating of the oven space. The resistor should be rated to 64VA if the oven was to be operated over its full power range but for operation up to around 100°C the rating can be considerably lower, in keeping with the ranges that are readily available.

Table 4.5 - Relative and Total Heater Output for Configurations 1 to 4.

Configuration /Heater Pair	Proportion of Total Voltage, p	$\left(\frac{p^2}{RA}\right)$ $(\Omega m^2)^{-1}$	Relative Heat Output / Unit Area	Total Heater Power $\left(\frac{(pV_T)^2}{R}\right)$ for 240V a.c. (VA)
1 F/Ba	1	0.140	1.0	1355
L/R	1	0.116	0.83	724
T/Bo	1	0.126	0.9	731
			TOTAL	2810
2 F/Ba	0.5	0.035	1.0	339
L/R	0.5	0.029	0.83	181
T/Bo	0.5	0.031	0.9	183
			TOTAL	703
3 F/Ba	0.212	0.0063	1.0	61
L/R	0.396	0.0182	1.87	114
T/Bo	0.392	0.0194	1.85	112
			TOTAL	287
4 F/Ba	0.106	0.0016	1.0	15
L/R	0.198	0.0046	1.87	28
T/Bo	0.196	0.0048	1.85	28
			TOTAL	71

Note : Power output for 240V a.c. is calculated for each pair, using the average resistance i.e. the front and back heaters put in 1355VA (2 x 677.5) between them and the total output for all six heaters is 2810VA when the elements are connected in parallel (Configuration 1) with full mains supply.

Table 4.6 - Relative and Heater Output for Configuration 1 Modified

Configuration /Heater	p	$\frac{p^2}{RA}$ $[\Omega m^2]^{-1}$	Relative Heat Output / Unit Area	Total Heater Power $\left(\frac{(pV_T)^2}{R}\right)$ for 240V a.c. (VA)
1 F/Ba	0.895	0.112	1.0	1086
10Ω Outside oven	0.105	-	-	64
L/R	1	0.116	1.03	724
T/Bo	1	0.126	1.09	731
			TOTAL	2541(+64)

4.5.6 Air Circulation

Judging from earlier experiments, this area is where the most improvement in oven performance seemed to be possible. The goal was to achieve a stable air flow around the oven. This would not be helped by the oven space being rectangular and the fact that the fan shaft does not enter the oven at the centre of the rear wall. As with the Pye, ideally the air would flow radially out of the fan, along the side walls, ceiling and floor to the front wall then back past the columns to enter the fan axially. The actual flow pattern could be observed by using shreds of tissue paper through a perspex lid. The corners in the oven were "rounded off" using triangular pieces of cardboard to discourage the formation of stagnant areas. A rectangular piece of cardboard with a hole in the centre was fixed in front of the fan to encourage air to flow out past the edge of the cardboard and into the fan through the hole. Strips of tissue paper were attached to the edge of this baffle and at some points on the walls. If the flow around the oven were stable, these strips of tissue paper would be blown in the same direction all the time. Baffles of different complexities were constructed and tested but in all cases regions of unstable flow were observed. The baffles were designed to 'peel' air off the fan blades radially and encourage flow along the oven walls to the front, returning past the columns to the centre of the fan. A significant factor could be the asymmetry of the fan position but this could not be altered easily because the motor shaft passed through a hole in the heater for the rear

wall. Figures 4.31a to 4.31c show the view looking towards the rear wall of the oven from the front wall. The outer rectangle represents the rear wall of the oven looking along the surfaces of the side walls, floor and roof. The inner rectangle is the baffle in front of the fan and there are vanes on the rear side of this baffle to modify the flow of air from the fan. The fan is situated behind the hole at the centre of the vanes. The direction of the flow of air passing between the walls and the edge of the rectangular baffle is shown for three different arrangements of vanes where : "+" represents a region of stable air flow towards the rear wall, "•" represents a region of stable air flow away from the rear wall, "*" represents a region of unstable flow where flow direction changes are indicated by the tissue paper streamers. Three straight vanes gave a largely unexpected flow pattern (Figure 4.31a). A large proportion of the flow is towards the rear wall with unstable flow along one of the walls. Increasing the number of straight vanes to six produced a more ideal flow pattern (Figure 4.31b) with only one small region of unstable flow along the wall. Making the six vanes curved (Figure 4.31c) made the flow pattern less stable than if the vanes were straight. The baffle with six straight vanes appears to be the most suitable for achieving the desired air circulation flow pattern for this geometry of oven.

Figure 4.31 - Air Flow Directions Using Different Baffle Configurations

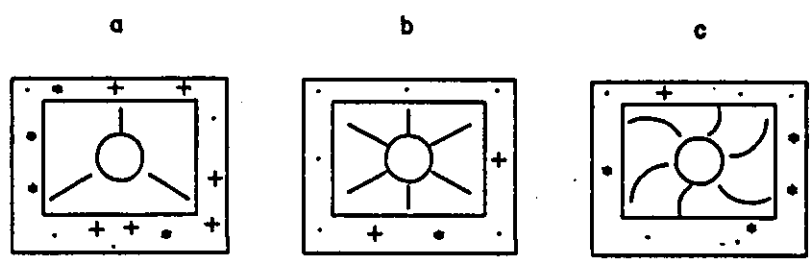

The view is towards the rear of the oven. The inner rectangle is a baffle in front of the fan. The vanes shown protrude only from the back of this baffle.

4.5.7 Isothermal Oven Performance

From the outset this oven performed better than any commercial oven that had been tested previously (Figure 4.29a :New oven vs Figure 4.27a :Carlo Erba).

The method of power supply was found to be satisfactory with the proviso that the controller must be tuned adequately.

The air circulation tests showed that improvements are possible but, with this particular prototype, completely consistent flow patterns were not attained. This can be attributed to the oven geometry. The shortfalls of this oven were the internal shape and the off-centre position of the fan. It would be better to have obtuse corner angles and the fan in the exact centre of one face. If the fan rotor entered the oven through the floor it is possible that flow symmetry could be achieved in any vertical plane. Air circulation is probably the area in which most improvement can occur.

For work performed at around ambient temperatures the modified Pye oven with fan blade temperature control is still the least noisy but its operation is limited to low temperatures.

4.5.8 Summary

The prototype isothermal oven had a performance similar to that of the Pye. The limits of the prototype oven had been reached and a new mechanical design was required. Consequently, it was decided, that rather than try and further improve the design, a readily-available, modified Pye oven would be used in the experiments.

CHAPTER FIVE - THE EFFECT OF VISCOSITY IN THE CAPILLARY FLOWMETER

5.1 Introduction

The theoretical response to a sample gas moving through a sorption-effect chromatograph has been described in Chapter 1 Section 2.2. To reiterate, the capillary flowmeter is expected to respond when sample gas is injected into a chromatograph such as that shown in Figure 5.1a, when the sample band reaches the start of the column and sample gas is adsorbed, and when the sample band reaches the end of the column and sample gas is eluted. In some cases the desorption of solutes results in peaks on the flow chromatogram which resemble conventional chromatograms but in other cases the responses could be described as anomalous. Previous published work (Buffham, Mason and Meacham (1986)) contained a seemingly unambiguous sorption-effect chromatogram for the injection of air into a helium carrier gas. The flow chromatogram showed a peak as the sample was injected, a pause in flow as some of the sample gas was adsorbed and two desorption peaks, the first due to the elution of the oxygen component and the second due to the elution of the nitrogen component. However, a hydrogen sample produced an anomalous double peak as the hydrogen band left the column instead of the expected single peak (described in Chapter 1). It was mooted that this was a viscosity effect because the viscosity of hydrogen is much different from that of the other gases used in the study. If the anomaly is caused by viscosity differences, then the sorption-effect chromatogram, for hydrogen at least, does not provide a record solely of the amount of gas adsorbed so it is important to identify the causes of this odd behaviour.

Attempts have been made in the past to use viscosity changes as a means of composition detection in gas chromatography. Griffiths, James and Phillips (1952) reported the detection of chromatographic peaks using a capillary viscometer. When they incorporated appreciable dead volume between their column and their viscometer they observed a sharp peak at the beginning of their normal displacement step. This modification to the response was most likely due to the sorption effect.

Scott (1964) monitored the pressure effects in a chromatographic column using a flame thermocouple detector. To ensure that the detector responded only to changes in flow rate (which were caused by the pressure effects) he used a second column to adsorb the sample irreversibly before it reached the detector. To isolate the pressure effects in each of the columns a length of copper tubing was used as a delay line.

Figure 5.1 - The Sorption-Effect Chromatograph

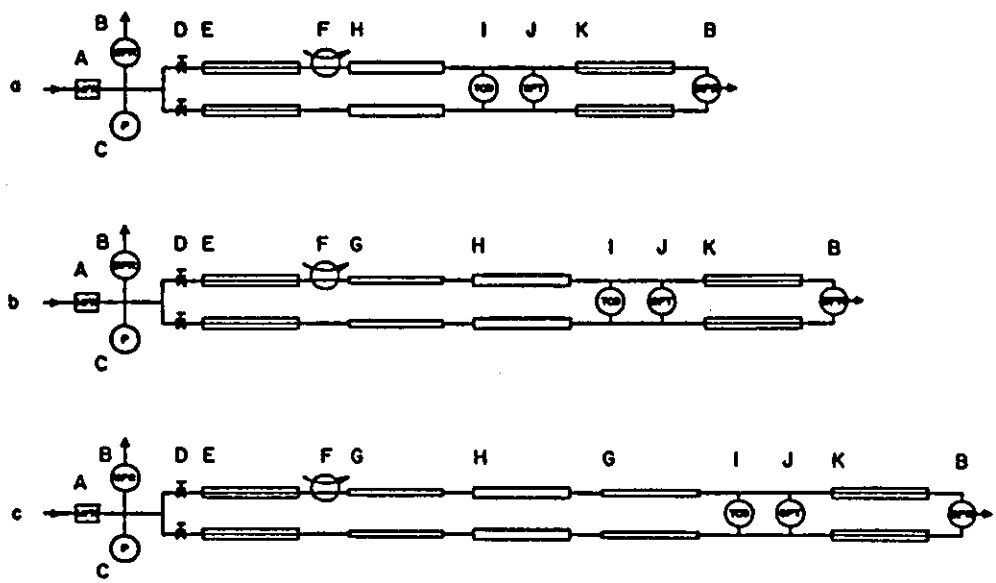

a : A typical sorption-effect chromatograph as used previously

b : A sorption-effect chromatograph incorporating a delay line upstream of the column to separate the injection peak from the adsorption peak

c : A sorption-effect chromatograph incorporating delay lines both upstream and downstream of the column.

A : Mass-flow regulator
B : Back-pressure regulator
C : Pressure gauge
D : Trimming needle valve
E : Flow-setting choke
F : Sample valve
G : Delay line
H : Chromatographic column
I : Thermal conductivity detector
J : Differential pressure transducer
K : Flow-detecting capillary

To investigate the anomalous hydrogen response and also to isolate the various effects which occur in a sorption-effect chromatograph, a series of experiments was devised using different combinations of a chromatographic column and delay lines.

5.2 Sorption-Effect Chromatography with Delay Lines

5.2.1 In Principle

Consider a chromatograph with a detector which is sensitive not only to flow but also to viscosity and is positioned immediately downstream of the column. A sample gas eluting from the column will pass directly into the detector and the flow change caused by the sorption effect will be combined with any viscosity effect.

If there is a small volume of pipework between the column outlet and the detector, the flow surge caused by sample desorption will precede any viscosity effect caused by a composition change within the detector.

In Chapter 2 the effect of a change in flow rate at constant viscosity, and of a change in viscosity at constant flow rate in the 'sorption-effect detector' was described theoretically. The downstream end of each of the two matched capillaries is held at a constant pressure. The pressure at the upstream end of each capillary is monitored by a differential pressure transducer. If the flow rate in one channel is increased relative to that in the other (whilst the gas contained within the capillaries is of constant composition) the pressure at the upstream end of the detecting capillary in that channel will increase because the pressure drop down the capillary has increased and the downstream end of the capillary vents at constant pressure. Similarly, if the flow rate drops in one channel only, the pressure drop down the capillary in that channel will decrease and the DPT will detect a decrease in pressure.

If the flow rate in each channel is constant but the viscosity of the gas flowing in one detecting capillary changes because the composition changes, then the pressure drop across that capillary will be modified. A greater gas viscosity will cause the pressure drop to increase and an increase in upstream pressure will be detected. A lower gas viscosity will cause the pressure drop to decrease and a decrease in the upstream pressure will ensue.

Consider a chromatograph of the configuration shown in Figure 5.1b with the capillary flow meter positioned immediately downstream of the columns. For an argon sample in helium carrier gas, any effect of altered viscosity is in the same sense as the sorption effect and there is but a single peak (Figure 5.2a, peak C). Note that peak A, the injection peak, and peak B, the adsorption peak, have been completely separated by the addition to the system of a length of delay line between the sample valve and the column. In the case of a hydrogen sample in helium carrier gas the two effects are in opposite senses (Figure 5.2b, peak C). This is shown schematically in Figure 5.3.

Figure 5.3a is a schematic representing the channel of a sorption-effect chromatograph into which the sample gas is introduced. A sample of inviscid, adsorbable gas (at a higher pressure than that of the non-adsorbed carrier at that point) will cause a surge in flow as soon as the sample valve is switched (Figure 5.3b). When the band reaches the start of the column it is preferentially adsorbed and there is a pause in flow (Figure 5.3c). Upon reaching the end of the column, sample gas is desorbed which causes an increase in flow (Figure 5.3d). When the band of lower viscosity reaches the capillary

Figure 5.2 - Sorption-Effect Chromatography as Reported Previously (Buffham, Mason and Meacham (1986))

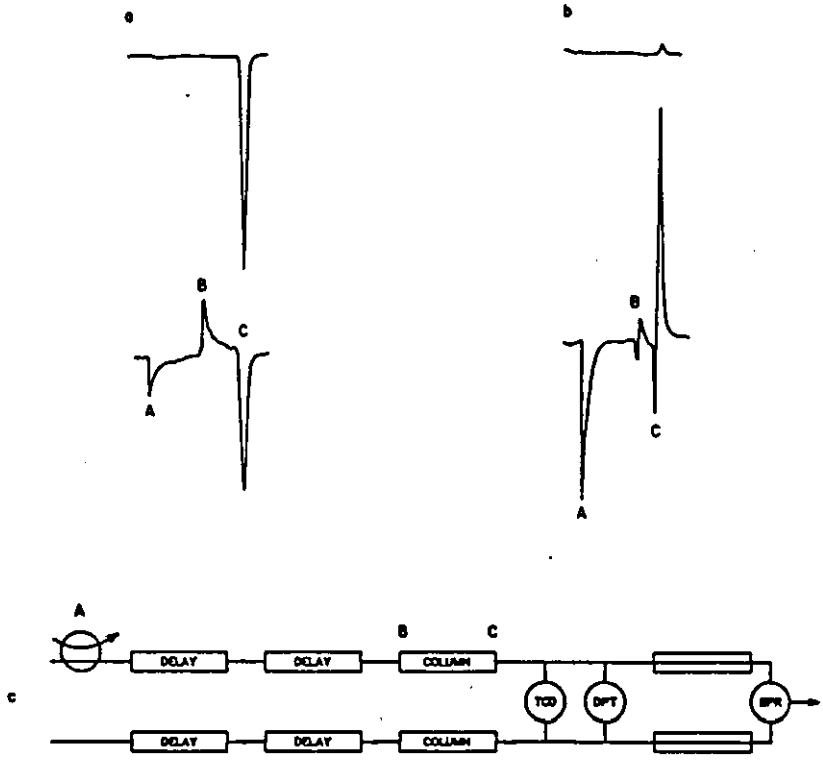

a : A typical sorption-effect chromatogram (lower trace) showing (A) the injection peak - the pressure surge as sample gas (argon) is introduced into helium, (B) the adsorption peak - the pause in flow rate as sample gas is adsorbed at the start of the column, and (C) the desorption peak - the surge in flow rate as previously adsorbed gas leaves the column. The TCD response (upper trace) shows only the sample gas passing through the detector situated at the column exit.

b: The anomalous sorption-effect chromatogram produced by hydrogen injected into helium (lower trace) showing (A) - the injection peak, (B) the adsorption peak, preceded by an atypical blip in the opposite direction, and (C) the desorption peak, consisting of an initial surge in flow followed by a larger pause in flow. This coincides with the peak found by the TCD (upper trace).

c: The experimental configuration (downstream of the flow-setting chokes) used to produce similar results to those previously reported. A, B and C indicate the sample position when the peaks A, B and C in a and b occurred.

flow meter, the pressure drop across the capillary is reduced. Since the pressure downstream from the capillary is constant, there is a decrease in the pressure upstream from the capillary for the period that the band remains in it (Figure 5.3e). So, a band of inviscid, adsorbable gas moving through the system in a non-adsorbed carrier gas gives the idealised sorption-effect chromatogram shown in Figure 5.3f.

Figure 5.3 - An Inviscid, Sorbable Band Passing Through a Chromatograph that has a Flow Meter at the Column Exit

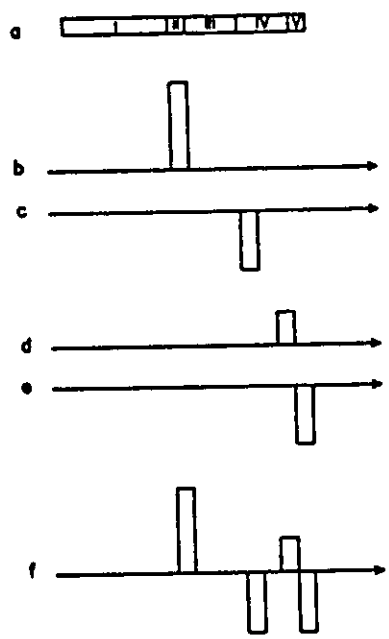

Figure 5.4 - An Inviscid, Sorbable Band Passing Through a Chromatograph that has Appreciable Dead Volume Between the Column Exit and the Flow Meter

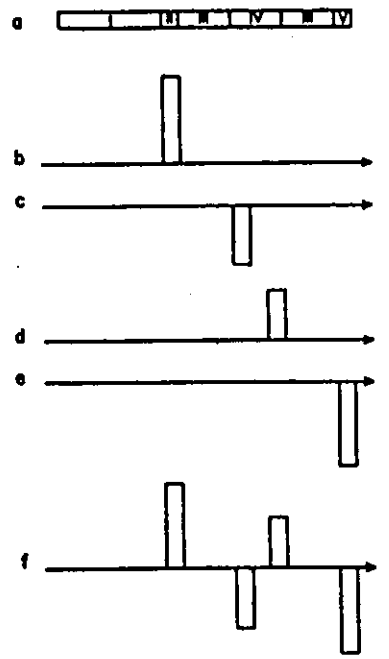

a : I - upstream pipework
II - sample valve
III - delay line
IV - chromatographic column
V - capillary flow meter

b : the injection peak

c : the adsorption peak

d : the desorption peak

e : the viscosity peak

f : the entire chromatogram for an inviscid adsorbable sample gas passing through the chromatogram

Note the separation of peaks d and e in Figure 5.4 compared with those in Figure 5.3.

Sufficient volume between the column end and the capillary meter (such as in the configuration shown in Figure 5.1c) would allow the entire sorption effect to be observed followed some time later by the composition peak. This is shown schematically in Figure 5.4. Figure 5.4a shows the sample channel of a chromatograph incorporating downstream delay lines. Figures 5.4b, 5.4c and 5.4d correspond to Figures 5.3b, 5.3c and 5.3d and

show, respectively, the responses when the sample valve is switched, allowing the higher pressure sample gas to expand into the system, when the sample gas reaches the column and is adsorbed, and when the sample band desorbs from the end of the column. Finally, after the band has traversed the delay line, it affects the capillary meter (Figure 5.4e). The entire schematic sorption-effect chromatogram caused by a band of inviscid adsorbed sample gas moving through a chromatograph containing delay lines between column and detector is shown in Figure 5.4f. The capillary meter acts first as a flow meter to record desorption and then as a viscometer when gas of changed composition arrives at the capillary.

There will be small pressure changes throughout the chromatograph as the band passes through the system (see Chapter 6). The chromatographs in Figure 5.1 have four principal sources of pressure drop. These are associated with, in sequence, the flow-setting chokes, the columns, the TCD connecting pipework, and the flow-detecting restrictors. Typically, the greatest pressure drop is across the flow-setting chokes with the column pressure drop being the second most important. The ratios of the pressure drops across the flow-setting chokes, the columns, the TCD and pipework, and the flow-detecting restrictors that were measured in previous experiments were 150 : 20 : 3 : 1 respectively.

Imagine a band of non-adsorbed inviscid gas passing through one of the channels of the system shown in Figure 5.1c. During the time that the band is within the system it reduces the pneumatic resistance. If the upstream and downstream pressures remain constant, the flow rate must be slightly greater than it otherwise would be. The size of the increase depends on the position of the inviscid band. Figure 5.5a shows how the pressure profile is modified by the band being at various positions in the system. Line a on Figure 5.5a is the pressure profile when the viscosity is uniform. The sample enters the system via the injector. As this is downstream from the flow-setting choke, zone 1, the pressure drop through the high-resistance flow-setting choke remains substantially unaffected.

During the time the sample remains in the column, the total pressure drop in the column is reduced by some relatively small amount and consequently a higher pressure is recorded by the transducer. The pressure profile while the sample slug is in the column is referenced b in Figure 5.5a. As the slug leaves the column there is a pause in flow (Chapter 6 Section 2.1). Pressure changes due to the sorption effect have been ignored: the profiles in Figure 5.5 correspond to the case where the column is inert. When the sample is in a delay line it produces a negligible effect on the pressure distribution because there is then hardly any pressure drop across the delay line. Consequently, the flow rate

Figure 5.5 - How the Pressure Varies in the Chromatograph When a Less Viscous Sample is Introduced

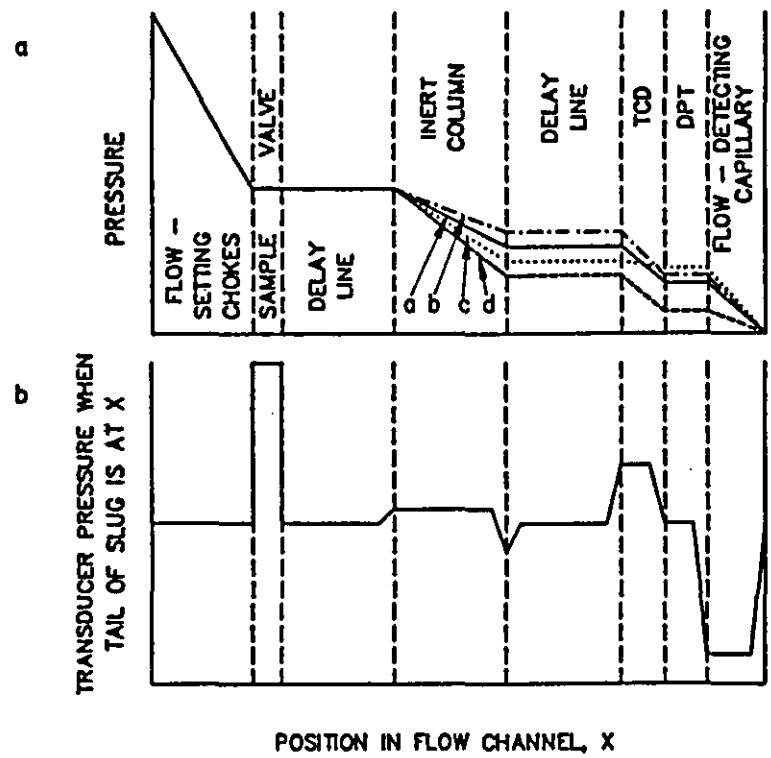

a : The pressure profile along the chromatograph.

Line a - the normal profile when only carrier gas flows through the system and the viscosity is uniform.

Line b - how the pressure changes when the inviscid slug is within the column (flow changes due to gas sorption are ignored).

Line c - the pressure profile as the slug passes through the high pressure drop tubing connecting the TCD.

Line d - the effect of the inviscid slug within the flow-detecting capillary.

b : The DPT response as the slug passes through the system.

will return to its initial value and will be recorded as such by the capillary flow meter.

When the sample is in the pipework connecting the delay line to the detector, it reduces the pressure drop across this section and, just as when the sample was in the column, the capillary flow meter indicates the actual increase in flow (line c on Figure 5.5a).

When the sample passes into the flow-sensing restrictor (see line d on Figure 5.5a), the pneumatic resistance in the flow-detecting restrictor is reduced because of the decrease in viscosity. This is seen as a reduction in pressure at the capillary flow meter

because the downstream pressure remains constant and the upstream pressure (at the pressure transducer) falls. The flow rate chromatogram is the response of the differential pressure transducer plotted against time. Figure 5.5b shows how the DPT responds as the sample moves through a system containing an inert column. A more viscous sample gas would have the effect of adding pneumatic resistance and the responses of the DPT would be the reverse of those just described.

5.2.2 In Practice

The experimental apparatus used to investigate the combined effects of flow rate and viscosity changes is similar to that described previously (Buffham, Mason and Meacham (1986)) but with the addition of delay lines both upstream and downstream of the column (Figure 5.1c). The columns were 1.5m x 6mm o.d. x 4mm i.d. packed with 5A molecular sieve (500-250μm). The delay lines were 10m lengths of 3mm o.d. x 1.5mm i.d. nylon tubing and had approximately the same internal volume as an empty column. The delay lines and TCD were arranged so that they could easily be moved to different parts of the system. The dimensions of the delay lines were arrived at empirically as a compromise between diameter and length. The amount of peak spreading increases with increasing diameter and with increasing length.

The helium carrier gas flow rate was 30mL/min.

The injection heads were dispensed with and a Specac 5μL sample valve (P/N 34.001) was connected into one of the parallel streams. In these experiments argon and hydrogen were used as the sample gases. Argon was included because it behaved as expected in previous experiments and hydrogen, because of its anomalous behaviour. The argon sample size was 5μL @ 4 bar (i.e. approximately 20μL at NTP) and the hydrogen sample size was 5μL @ 8 bar (i.e. approximately 40μL @ NTP).

The TCD was used to indicate when the sample gas reaches a certain point in the system. (A flow-through type TCD could not be used because it would be sensitive to flow rate as well as composition. A semi-diffusion type TCD is relatively insensitive to flow and will respond only when the sample gas is inside it.) It was possible to position the TCD anywhere in the system between the end of the column and the flow detector. The TCD and DPT outputs were recorded simultaneously on a two-pen chart recorder to give conventional and sorption-effect chromatograms.

5.3 Experiments

5.3.1 Configuration 1 : Basic Configuration

The configuration used in the first experiment was intended to duplicate that which gave rise to the anomalous flow chromatogram previously reported (Buffham, Mason and Meacham (1986)). The delay lines were placed upstream from the columns as shown in Figure 5.6a and the TCD and DPT were close together. (Part a of each of Figures 5.6 to 5.10 show only the configuration downstream of the flow-setting chokes and valves.) Figure 5.6b shows the chromatogram produced when an argon sample is introduced into helium carrier gas. The flow chromatogram shows a surge in flow when the sample is injected because, in this case, the sample gas was at a higher pressure than the helium carrier gas passing through the sample valve. This is followed some time later by a pause in flow as the sample reaches the column and is adsorbed to some extent. There is a single desorption peak which occurs at the same time as the peak detected by the TCD, that is, when the sample leaves the column. Figure 5.6c shows what happens when a hydrogen sample is injected into helium carrier. There is a surge in flow as the hydrogen sample is introduced. After the surge the flow rate returns to its previous (base-line) value and remains there until the hydrogen reaches the column. There is then a second, smaller, and as yet unexplained, small positive peak (which might be due to the difference in viscosity between hydrogen and helium) followed by a larger negative peak that indicates the reduction in flow as hydrogen is adsorbed slightly from the carrier. If helium were the more adsorbed of the two gases, this peak would be positive. It is worth noting that flow rate experiments of this kind give a very sensitive way of determining whether the carrier or the sample is the more adsorbed. Finally there is the anomalous double peak, first positive and then negative, which had been observed before with hydrogen samples. The composition (TCD) chromatogram shows that the anomalous peak occurs at almost the same instant that the hydrogen enters the series of detectors.

Figure 5.6 - The Chromatograms Produced Using Configuration 1

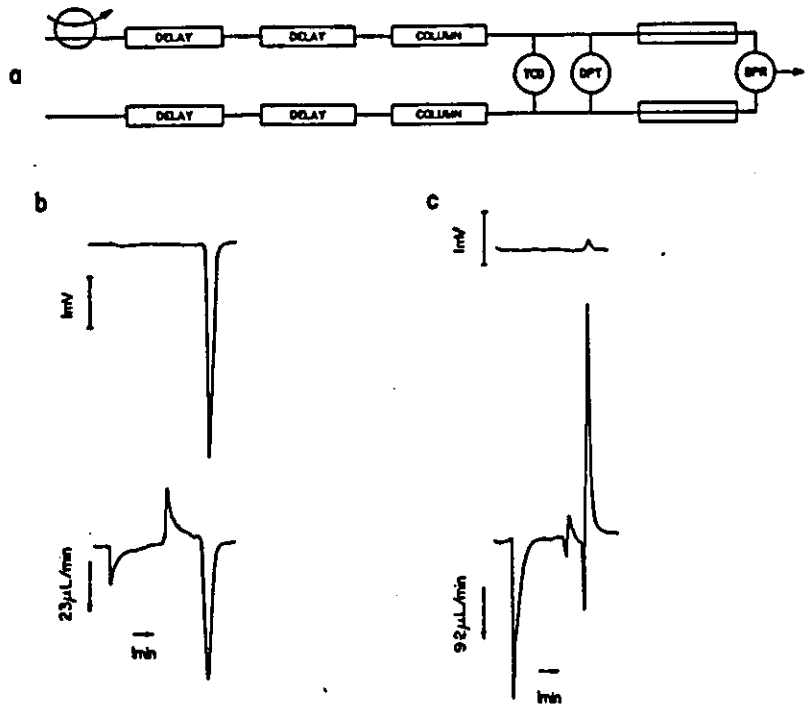

a : The configuration downstream of the flow-setting chokes with both detectors immediately downstream of the columns.

b : 20µL argon sample in helium carrier. The flow trace (lower) shows the injection peak, the adsorption peak, and an unambiguous desorption peak. The composition trace (upper) shows a peak which coincides with the desorption peak.

c : 40µL hydrogen sample in helium carrier. The flow trace (lower) shows the injection peak, the adsorption peak (preceded by a blip in the opposite direction), and the anomalous desorption peak. The composition trace (upper) shows a peak which coincides with the anomalous peak.

5.3.2 Configuration 2 : Observation of Peaks Leaving Delay Lines

In this experiment one delay line was moved (Figure 5.7a) to a position downstream from the column and upstream from the detectors. This delay line separates the sorption-effect response from the viscosity-change response.

The TCD is placed to reveal when the sample leaves the delay lines. This should correspond to the time when the viscosity change affects the differential capillary meter, the desorption peak still occurring when the sample leaves the column.

Figure 5.7b gives a flow chromatogram obtained by using an argon sample. It shows the same sample injection and adsorption peaks as before (Figure 5.6b), but, unexpectedly, the desorption peak has been resolved into two smaller, positive peaks. The first of these peaks occurs when the sample leaves the column (the desorption peak)

the second when the sample gas reaches the detectors, as can been seen by comparing the DPT response with the TCD response. The introduction of a more viscous gas into the flow-detecting capillaries has increased the pressure drop across them. Because the pressure at the downstream end is constant, the DPT detects an increase in pressure.

The first three peaks of the flow chromatogram shown in Figure 5.7c are the same as those in Figure 5.6c, but the anomalous fourth response has been separated into a positive peak that occurs when hydrogen is desorbed from the column and a negative peak that occurs at about the same time as the TCD response. The pressure drop across the capillary used to measure the flow rate changes has been reduced during the passage of the lower viscosity gas. Because the downstream pressure is held constant, the upstream pressure (at the DPT) must be reduced and thus gives rise to a negative peak on the sorption-effect chromatogram. This experiment confirms that the anomalous response previously reported is actually caused by the relatively large viscosity difference between the carrier gas and the sample.

Figure 5.7 - The Chromatograms Produced Using Configuration 2

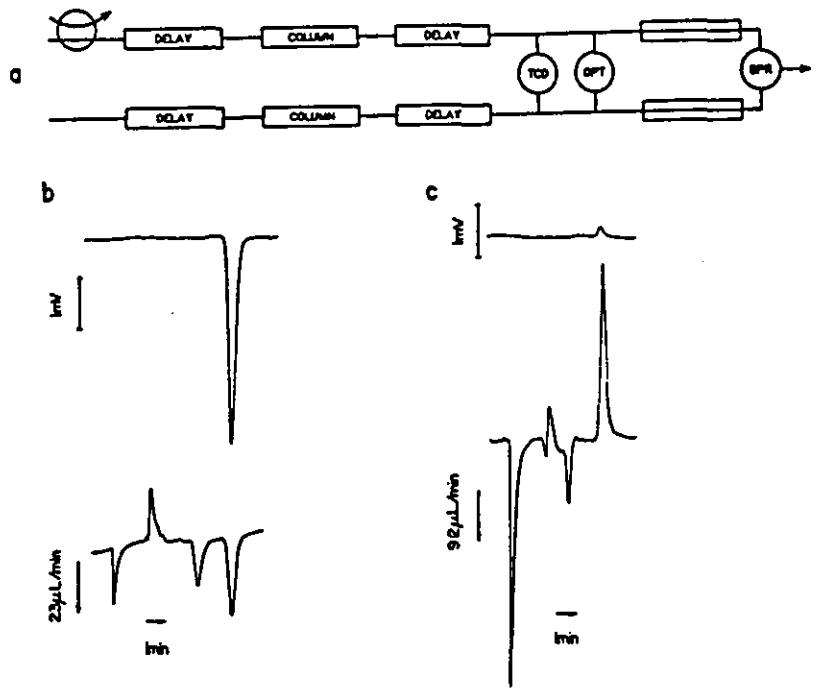

a : The columns and detectors are separated by delay lines.

b : 20μL argon sample in helium carrier. The flow trace (lower) is similar to that in Figure 5.6b except that the desorption peak has been resolved into two positive peaks, namely a desorption peak when the sample leaves the column and a second peak which coincides with the sample reaching the detectors (compare with composition (upper) trace).

c : 40μL hydrogen sample in helium carrier. The flow trace (lower) shows the same injection and adsorption peaks as Figure 5.6c. However, the negative surge of the anomalous peak has become the desorption peak, followed by a peak in the opposite direction occurring when the sample gas reaches the detectors, as indicated by the composition (upper) trace.

5.3.3 Configuration 3 : Observation of the Sample Leaving the Column

This configuration (Figure 5.8a) is the same as was used in the previous experiment (Figure 5.7a) except that the TCD is connected between the columns and the delay lines. It should now respond when the sample leaves the column, that is, at the same time as the sorption effect. The flow rate chromatograms, Figures 5.8b and 5.8c, are identical to those in Figures 5.7b and 5.7c, but, because the TCD is directly downstream from the column, its response confirms that the third peak on each flow chromatogram is caused by the desorption of the sample component from the column.

Figure 5.8 - The Chromatograms Produced Using Configuration 3

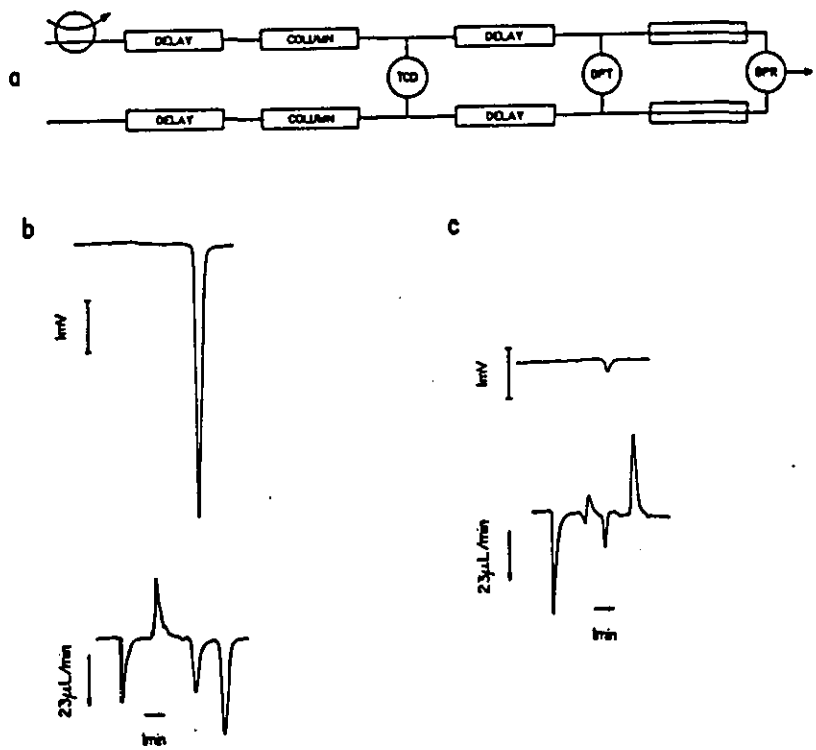

a : The TCD is immediately downstream of the columns but the DPT is separated from the columns by delay lines.

b : 20µL argon sample in helium carrier. The flow trace (lower) is the same as Figure 5.7b. The TCD trace (upper) shows that the third peak occurs as the sample leaves the column.

c : 40µL hydrogen sample in helium carrier. The flow trace (lower) is the same as Figure 5.7c. The TCD trace (upper) indicates when the sample desorbs from the column.

5.3.4 Configuration 4 : Without Columns

Without chromatographic columns being present, Figure 5.9a, there is no sorption effect on the flow chromatogram. The injection peak is now very sharp because of the much improved pneumatic connection of upstream and downstream ports as a result of a relatively resistive column being removed. The TCD again responds as the sample leaves the delay lines. The flow chromatograms in Figures 5.9b and 5.9c show only the injection peak and the viscosity peak; the TCD response in each case occurs at a similar time to the viscosity peak. In both cases the larger viscosity peak is preceded by a smaller peak in the opposite direction. This is caused by a change in viscosity of the gas in the TCD-connecting pipework upstream from the DPT. An increase in viscosity, such as is the case with the argon sample (Figure 5.9b) causes an increase in pressure drop immediately upstream of the DPT and consequently the DPT detects a lower pressure.

Once the high viscosity band passes downstream from the DPT (into the flow-detecting capillaries) the increased pressure drop is detected as an increase in pressure at the DPT. The lower viscosity hydrogen band causes the pressure drop to decrease and the viscosity effects on the flow chromatogram in Figure 5.9c are in the opposite sense to the corresponding peaks in Figure 5.9b. Previously, when the columns were included, the sample band was sufficiently broad that the concentration changes were too gradual to cause a noticeable viscosity effect in the TCD-connecting pipework but without the columns the sample band is much narrower and the concentration change is more abrupt. Comparison of Figure 5.9 with Figures 5.6, 5.7 and 5.8 confirms the previous identification of adsorption and desorption peaks because due to there being no columns in the system these peaks are now absent.

Figure 5.9 - The Chromatograms Produced Using Configuration 4

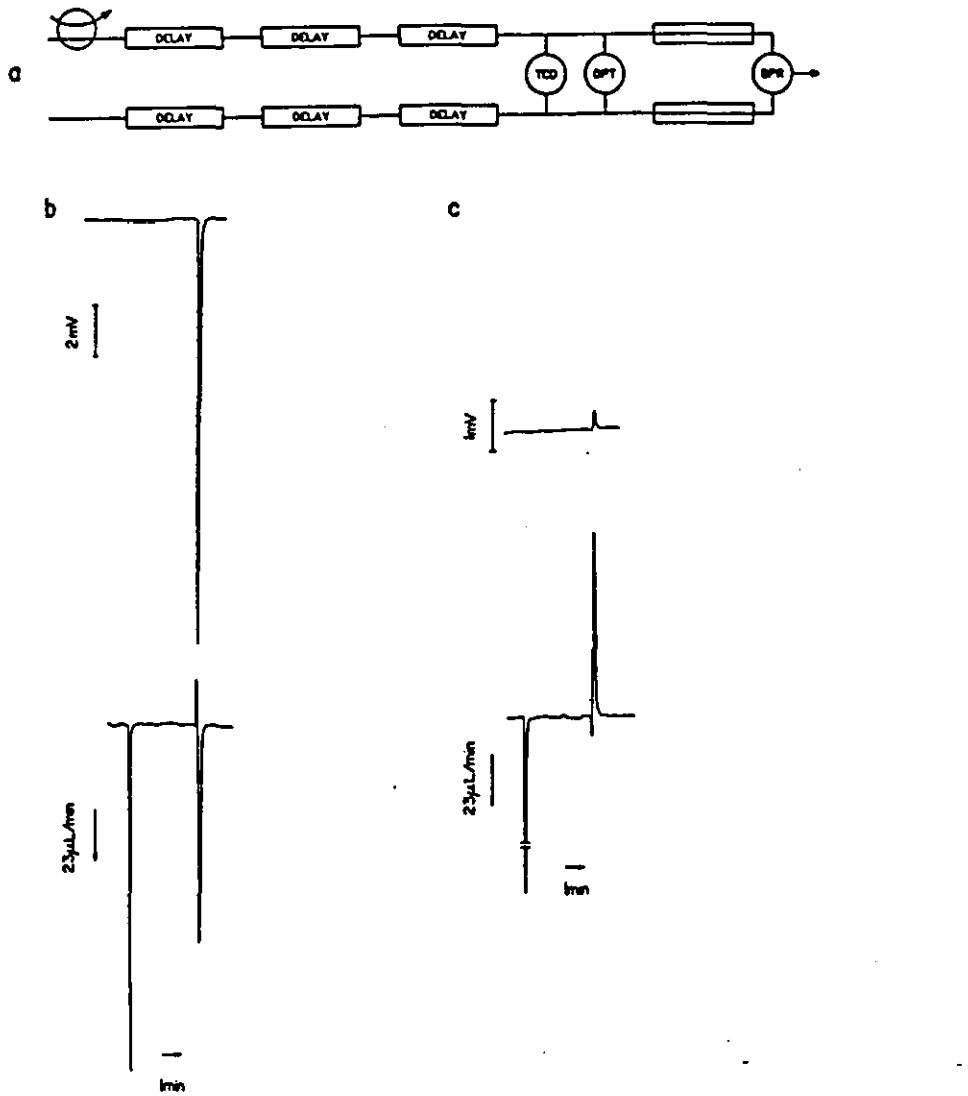

a : The columns have been replaced by delay lines.

b : 20µL argon sample in helium carrier. The flow trace (lower) shows the injection peak followed by a positive peak caused by increased viscosity in the capillary flow meter. The negative blip which precedes this peak is the effect of increased viscosity in the TCD connecting pipework.

c : 40µL hydrogen sample in helium carrier. The flow trace (lower) shows only the injection peak and the negative peak caused by the effect of decreased viscosity in the flow-detecting capillary. This second peak is also preceded by an opposite blip.

5.3.5 Configuration 5 : With Neither Columns Nor TCD

In this experiment, the previous experiment was repeated, but without the TCD, so that the effect of flow through its narrow-bore connecting pipework was absent.

The effect of removing the TCD and its connecting pipework (1.5mm o.d., 0.8mm i.d.) (Figure 5.10a) is to remove the positive blip that occurs before the larger response caused by gas of different viscosity reaching the flow-detecting restrictors (compare Figure 5.10b with 5.9b and Figure 5.10c with 5.9c). This is because the sample gas no longer affects the pressure drop in the capillary tubing connecting the TCD with the system upstream of the DPT. The response after the sample gas enters the flow-detecting chokes downstream of the DPT is identical with that found when using Configuration 4. The injection peak is not a direct measure of the amount of sample used, but of the difference in pressure between the sample gas and the carrier gas when the sample valve was switched. The TCD responses were recorded at the same sensitivity (bridge current 200mA, unattenuated signal). Comparison of the response to an argon sample in helium with that to a hydrogen sample in helium verifies that the TCD is not the most suitable for detecting hydrogen in helium. This is because the thermal conductivities of hydrogen and helium are so similar.

Figure 5.10 - The Chromatograms Produced Using Configuration 5

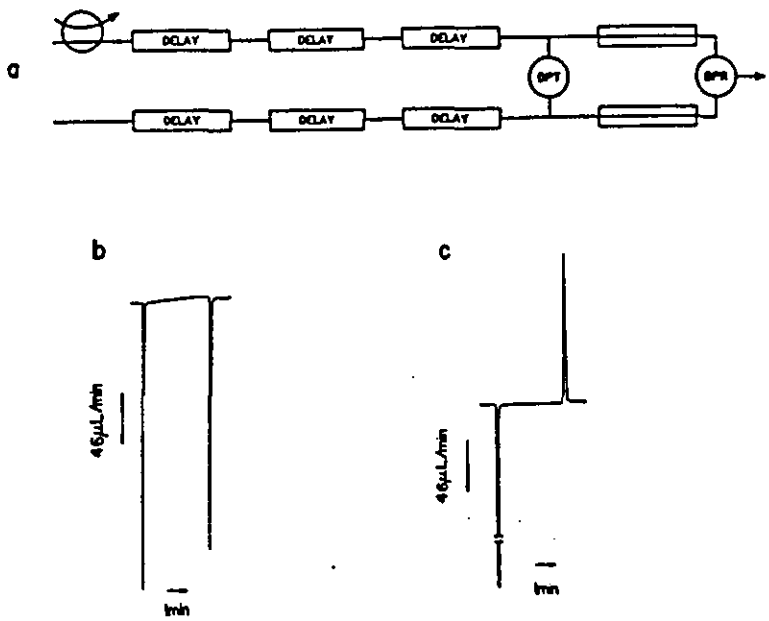

a : The TCD and its pipework have been removed from the system completely.

b : 20μL argon sample in helium carrier. The negative blip before the viscosity peak in Figure 5.9b has disappeared because there is no longer a significant pressure drop immediately upstream of the flowmeter.

c : 40μL hydrogen sample in helium carrier. Removing the TCD and connecting pipework has eliminated the positive blip immediately prior to the viscosity peak in Figure 5.9c.

5.4 Viscosities of Binary Mixtures

The viscosities of the pure gases (Weast and Astle (1982)) used in these experiments were:

Argon	221.7×10^{-7} Ns/m^2 (20°C)
Helium	194.1×10^{-7} Ns/m^2 (20°C)
Hydrogen	87.6×10^{-7} Ns/m^2 (20.7°C)

It might be thought that, as well as causing the response to be in the opposite sense, injecting hydrogen into helium would cause a larger viscosity effect at the flow-detecting capillaries than injecting argon into helium, because the viscosity difference between hydrogen and helium is greater than that between argon and helium. However, gas-mixture viscosities only vary linearly with composition for small ranges of composition (Dyson and Littlewood (1967(I))) and the viscosity of a mixture cannot in general be obtained by linear interpolation between the viscosities if the pure components. On the flow chromatograms, the injection of argon produces a greater

viscosity effect than the injection of hydrogen. This is the reverse of what might be expected, especially because the hydrogen sample was approximately twice the size of the argon sample. The reason that one's expectation is false is that the gradient of the argon-helium viscosity versus composition curve for virtually pure helium is far steeper that of the more nearly "ideal" hydrogen-helium curve for virtually pure helium. So, smaller composition changes produce larger viscosity changes when argon is the sample gas than when hydrogen is the sample gas (See Appendix III).

5.5 Conclusions

Five different experimental configurations were used in an experimental programme to explain the anomalous behaviour of hydrogen during sorption-effect chromatography and to compare with the seemingly explicable behaviour of argon.

1. A typical sorption-effect chromatogram was recreated by using argon sample in helium carrier gas. By using delay lines between the column and the DPT, it was possible to separate the desorption peak of the typical chromatogram into two peaks. This shows that argon also behaves "anomalously", but that this was not noticed before because the two peaks were both in the same direction.

2. The anomalous response of a hydrogen sample in helium carrier gas was reproduced and, again with the use of delay lines, the desorption peak was separated into two peaks, one positive one negative.

3. By using a conventional TCD at different positions in the system it has been shown that, of the two newly resolved peaks, the former occurs when the sample reaches the end of the column and the later occurs when the sample has reached the flow detector.

4. With the use of delay lines between the columns and the flow detector, four main peaks are observed as a sample of a single adsorbable gas passes through the system in a non-adsorbed carrier:

   i) an injection peak as the sample gas is introduced;
   ii) an adsorption peak as a sample gas is adsorbed at the start of the column;
   iii) a desorption peak as sample gas is desorbed at the end of the column;
   iv) a peak caused by the effect of viscosity changing in the flow-detecting capillaries – the "viscosity effect".

5. The viscosity effects for hydrogen and argon are in opposite senses because diluting helium with trace quantities of these gases causes the viscosity of the gas mixture to decrease and increase respectively.

6. There is an effect caused by the viscosity of the gas mixture changing in any region of significant pressure drop in the system, for example, the TCD and its connecting capillary tubing upstream of the DPT.

CHAPTER SIX - PRESSURE DROP

6.1 Introduction

During its development the basic sorption-effect chromatograph has been improved and the sensitivity has increased. This has meant that other effects have become apparent which may or may not interfere with the sorption effect. The effects described in this chapter are associated with the distribution of pressure drop down the system. There are essentially three major regions of pressure drop in a chromatograph that does not include a TCD :

a) the flow-setting chokes

b) the chromatographic columns, and

c) the flow-detecting capillaries.

No problems have been attributed to the values chosen for the pressure drop in regions a) and c), both relative and absolute, so there has been no reason to alter either set of capillaries. Up to this stage in the development of the method, separations were performed using the Pye glass columns (1.5m×6mm o.d.×4mm i.d.) packed with 500-710μm 5A molecular sieve. Relatively large samples had been separated and the resultant sorption effect had caused a comparatively large flow rate deviation.

6.2 The Importance of Pressure Drop Down the Column

6.2.1 The Effect of Viscosity in the Column

The practice has been to re-condition the columns only when there was a noticeable drop in performance. This is caused by water from the carrier and sample gases gradually saturating the columns (although it is not unknown for volatile material to bleed from regulator diaphragms and poison the columns). This highlights what good practice it is to use a guard column to 'clean up' the gases before they reach the columns. A noticeable drop in performance becomes apparent through the incomplete separation of sample components when all, or a large proportion of the column is affected. When the saturation with water vapour is partial and only the front part of the column is affected, there is a flow deviation before the reduction in flow caused by the adsorption of sample gas (Figure 6.1). This can also be seen in Figures 5.2b and 5.6c. That is, there is an effect due to the entry of the sample band into the packed column which ordinarily is lost in the adsorption peak.

To investigate this further a 3m×4mm i.d.×6mm o.d. piece of tubing was packed with 200-300μm sand (on which no adsorption takes place) and used in place of the adsorbent column. The TCD was also removed from the system. Different sample gases

Figure 6.1 - The Sorption-Effect Chromatogram Produced When a Hydrogen Sample is Injected into a Helium Carrier Gas Using a Column Which is Non-Sorbing at the Upstream End

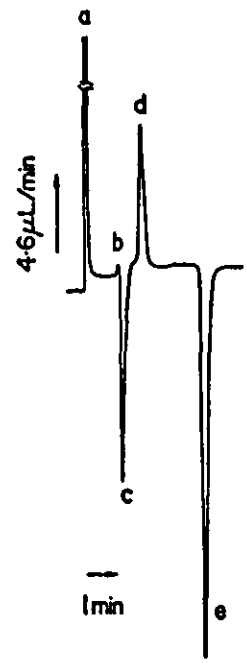

a injection peak
b a pre-adsorption peak increase in flow
c adsorption peak
d desorption peak
e viscosity peak

were introduced into helium carrier gas. Figures 6.2, 6.3 and 6.4 show the passage of argon, hydrogen and nitrogen samples respectively. The samples were all of 10μL @NTP. There are two chart recordings in each figure. The gas flow through the inert column was reversed for the second trace. The second trace in each figure confirms that the oscillations observed are due to non-uniformity of the packing because the oscillations are also reversed. The number of oscillations corresponds to the number of coils in the column suggesting that they may be caused by settling of the packing at the top of each coil. In each case there is firstly an injection peak, as the high-pressure sample gas is introduced, and lastly, a viscosity peak, as described in chapter 5. Between the two there is a net shift in the baseline (onto which are superimposed the flow oscillations due to packing irregularity), followed by a surge in the opposite direction, followed by a return to the original baseline. All this can be explained from a knowledge of the viscosity of helium slightly diluted with the individual sample gases. Consider the case

of an argon sample (Figure 6.2). Diluting helium with argon increases the gas viscosity (as shown in Appendix III Figure 1) so there is a band of higher viscosity gas introduced into the system. In the parts of the system with a lower pressure drop, changes in gas viscosity do not alter the pressure drop distribution significantly so there is no noticeable change in the pressure measured by the transducer. As the higher viscosity band enters the column it momentarily stops the flow of gas whilst the downstream pressure subsides sufficiently for there to be a large enough pressure difference to push the band along the column. (Note : the column is non-adsorbing.) Because there is now more pressure drop down the column than before (and because the total pressure drop through the system remains constant) the pressure drop down the flow-detecting capillaries must be decreased and the DPT records a lower pressure. The baseline is offset in the opposite direction to the injection peak. Because the flow-setting chokes constitute such a large proportion of the total pressure drop the volumetric flow will hardly have changed. This state of affairs continues all the time the sample band remains within the column. When the band reaches the end of the column its influence on the pressure drop is about to be removed almost instantaneously. On moving out of the column into a relatively low pressure drop region the band speeds up and there is a pressure surge until the pressure in the system re-equilibrates and the baseline returns to its original value. That this is merely a re-equilibration of pressures can be seen by comparing the rate of return to baseline after this surge with that occurring after the injection pulse.

With a lower viscosity mixture, such as an hydrogen sample gas in helium carrier gas (Figure 6.3), the opposite happens. Upon entering the column, less pressure is required to push the band through the column so a higher pressure is recorded at the DPT and the baseline is offset in the same direction as the injection peak. As the band leaves the end of the column the pressure must build up again and the band is momentarily stopped. Accordingly, the DPT records a negative pressure surge followed by a gradual return to baseline. The viscosity of a helium-hydrogen mixture varies almost linearly with composition between the viscosities of the pure components (Appendix III Figure 4).

Figure 6.2 - The Injection of an Argon Sample Gas into a Helium Carrier Gas Flowing Through a System Containing a Non-Sorbing Column

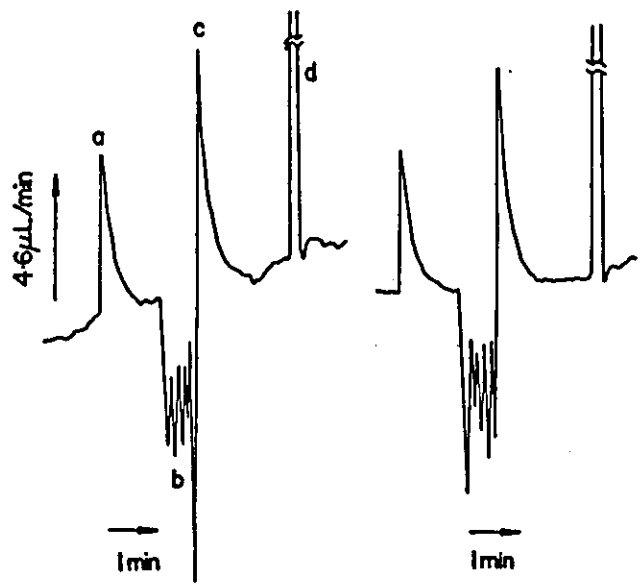

a The injection peak.
b The reduction in flow rate due to the more viscous gas entering the column.
c The flow surge as the sample slug leaves the column.
d The viscosity peak.
The column was reversed to produce the second trace.

Figure 6.3 - The Injection of a Hydrogen Sample Gas into a Helium Carrier Gas Flowing Through a System Containing a Non-Sorbing Column

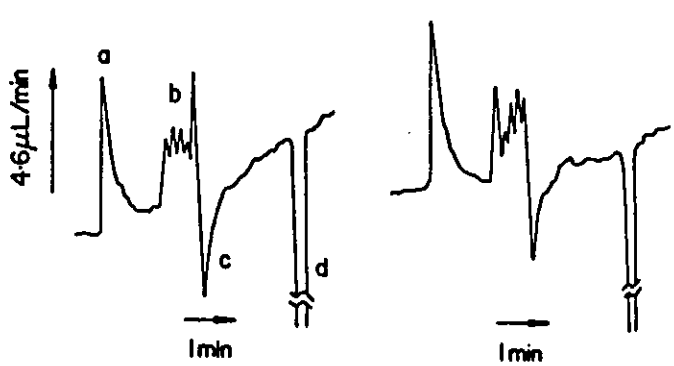

a The injection peak.
b The increase in flow rate as the less viscous gas enters the column.
c The flow surge as the sample slug leaves the column.
d The viscosity peak.
The column was reversed to produce the second trace.

The introduction of a nitrogen sample (Figure 6.4) generates a chart trace that suggests the mixture viscosity is higher than that of the pure carrier whereas the viscosity of pure nitrogen is less than that of pure helium. Appendix III Figure 5 confirms that the viscosity of helium does increase with increasing mole fraction of nitrogen up to around 20 per cent nitrogen.

Figure 6.4 - The Injection of a Nitrogen Sample Gas into a Helium Carrier Gas Flowing Through a System Containing a Non-Sorbing Column

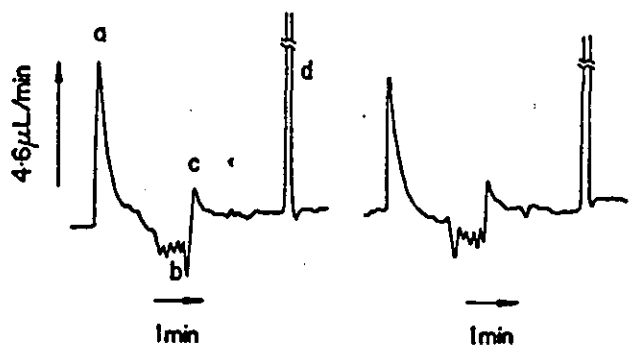

a The injection peak.
b The reduction in flow rate as the more viscous gas enters the column.
c The flow surge as the sample slug leaves the column.
d The viscosity peak.
The column was reversed to produce the second trace.

These results bear a remarkable resemblance to those of Dyson and Littlewood (1967(I)(II)). They attribute the shift in baseline to changed gas viscosity in the column but the surge in the opposite direction as the sample leaves the column, they accredit to the elution of the sample from the adsorbent (the sorption effect), combined with the effect of changed viscosity in the capillary flowmeter as dealt with in Chapter 5. This may be the case if the gas passes directly from the adsorbent column into the flowmeter but in the work reported here both these effects were eliminated because no adsorption took place on the column and the flowmeter was separated from the end of the column by delay lines. These authors do not appear to have experienced any flow deviation at the start of the column as the sample gas enters and is initially adsorbed!

6.2.1.1 Errors Caused by the Column Viscosity Effect

The possible errors caused by a gas of altered viscosity traversing an adsorbent column are illustrated in Figure 6.5. The theoretical trace due solely to the sorption effect is shown in Figure 6.5a. The schematic trace due solely to the change in viscosity is

shown in Figure 6.5b. Four different combinations of these two effects are possible. The sample gas may have a higher or lower partition coefficient to that of the carrier gas, and, the carrier gas when slightly diluted with sample gas may have a higher or lower viscosity than that of the pure carrier gas.

Figure 6.5 - A Schematic Diagram of the Possible Errors Caused by Viscosity Changes in an Adsorbent Column with High Pneumatic Resistance

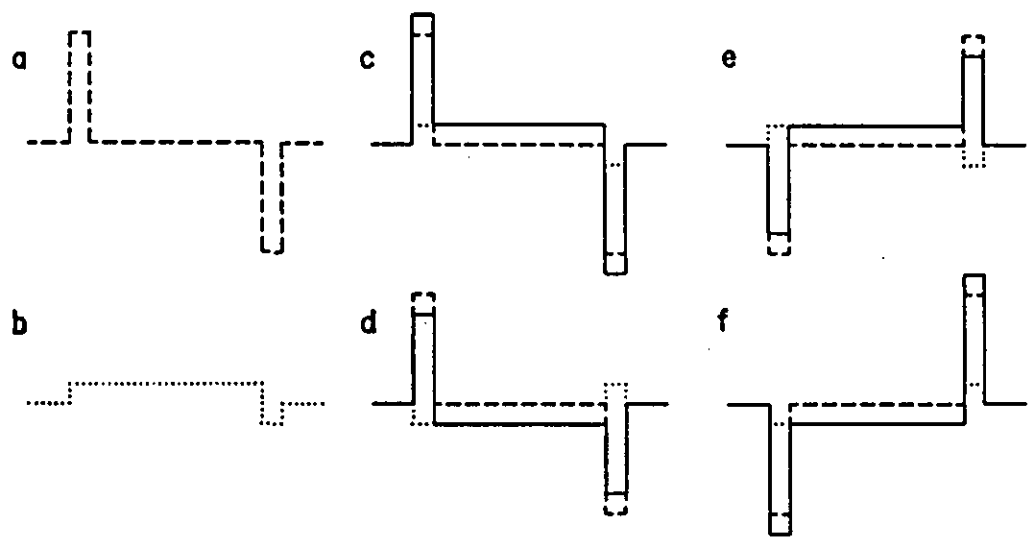

a The flow rate changes caused by a less sorbed sample gas being injected into a more sorbed carrier gas showing the flow surge as more carrier gas is desorbed at the start of the column than sample gas is adsorbed and the flow pause as more carrier gas is resorbed at the end of the column than sample gas is desorbed.

b The flow changes caused by a less viscous sample gas entering the column showing a step increase after the sample gas enters the column and reduces the pneumatic resistance followed by a flow pause as the sample gas moves from a region of high resistance (in the column) to a region of low resistance (in the delay line downstream of the column) and the influence of the viscosity difference is removed.

c The combined effects of a less sorbed/less viscous sample gas in a more sorbed/more viscous carrier gas. The observed peaks are larger because of the altered viscosity.

d The combined effects of a less sorbed/more viscous sample gas in a more sorbed/less viscous carrier gas. The observed peaks are smaller because of the altered viscosity.

e The combined effects of a more sorbed/less viscous sample gas in a less sorbed/more viscous carrier gas. The observed peaks are smaller because of the altered viscosity.

f The combined effects of a more sorbed/more viscous sample gas in a less sorbed/less viscous carrier gas. The observed peaks are larger because of the altered viscosity.

For the sake of simplicity, the peak caused by the entry of the sample band into the column will be referred to as the adsorption peak, and, the peak caused by the exit of the sample band from the column will be referred to as the desorption peak. If the sample

gas has a lower partition coefficient than the carrier, the adsorption peak is in fact a flow surge caused by more carrier gas being desorbed than sample gas adsorbed. Similarly, the desorption peak is actually a pause in flow caused by more carrier gas re-adsorbing at the end of the column than sample gas desorbing.

In the cases where the sample gas has a higher partition coefficient than the carrier gas and forms mixtures of greater viscosity than that of the pure carrier gas, or, where the partition coefficient is lower and the mixture viscosity lower, the adsorption peak is larger than it would be if it solely represented the net difference in the number of moles of gas adsorbed. The desorption peak is similarly enhanced because of the pressure surge (Figures 6.5c and 6.5f). The net transducer output is indicated by the continuous line.

Figure 6.6 - The Magnitude of the Column Viscosity Effect in an Inert Column Which has a Similar Pneumatic Resistance to that of the Adsorbent Column Used Previously

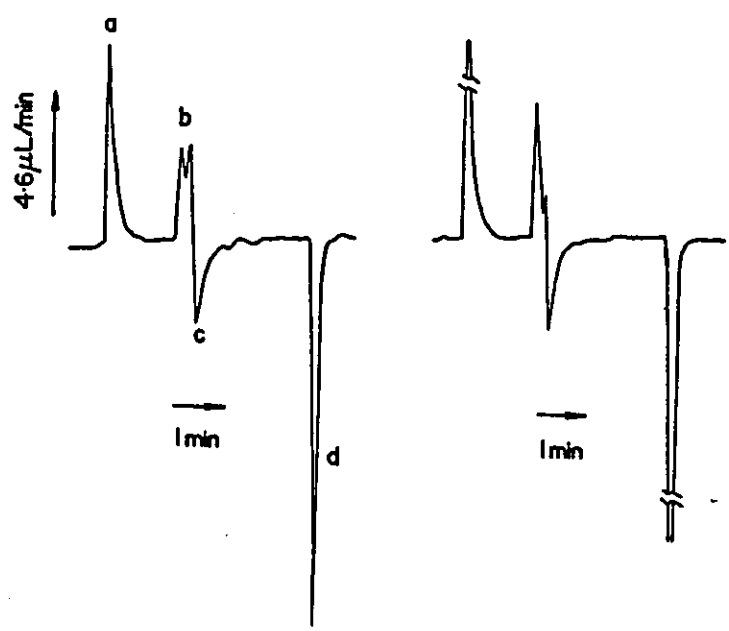

a The peak caused by the injection of hydrogen into a helium carrier gas.
b The increase in flow rate due to the band of lower viscosity gas entering the column.
c The reduction in flow rate caused by the sample band leaving the column.
d The viscosity peak.
The column was reversed for the second trace.

Where the sample gas has a higher partition coefficient and lower viscosity, or, lower partition coefficient/higher viscosity, the sorption peaks are smaller than they would otherwise be (Figures 6.5d and 6.5e). Again, the continuous line indicates the net transducer output.

Figure 6.6 shows the magnitude of this effect in Pye columns (1.5m×6mm o.d.×4mm i.d.) packed with 500-710μm silica - the same size packing that had been used previously, so that the pressure drop would be similar, only with no capacity for adsorption. The sample gas is hydrogen being injected into a helium carrier gas. The sample size was 5μL @ 4 bar (20μL at NTP). Figure 6.7 is the sorption-effect chromatogram recorded for a 10μL NTP sample of hydrogen and argon injected into helium carrier gas using a Pye column as above but packed with 500-710μm 5A molecular sieve. The ratio of the peaks caused by the viscosity effects will remain the same for the same system. The two traces shown in Figure 6.6 show the carrier flow in opposite directions through the dummy column. The average baseline offset is about 0.19 times the capillary viscosity peak height. The peak height of the pressure surge in the opposite direction is about one-fifth of the capillary viscosity peak height. The ratio of the desorption peak height to the capillary viscosity peak height in Figure 6.7 is approximately 0.5 so it appears that the errors introduced by the column viscosity effect could be appreciable. In order to minimise errors produced in this way, the pressure drop down the column must be reduced as much as possible whilst maintaining satisfactory column performance. A typical pressure profile down a system containing columns such as these, and a TCD, (as shown in Figure 6.8) is given in Table 6.1. The possible error on each pressure reading is approximately ±0.001bar.

Figure 6.7 - The Injection of a Hydrogen/Argon Sample into Helium Column Using an Adsorbent Column

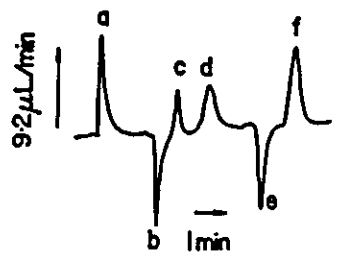

a The injection peak.
b The adsorption peak.
c The hydrogen desorption peak.
d The argon desorption peak.
e The hydrogen viscosity peak.
f The argon viscosity peak.

Table 6.1 - Pressure Measurements Taken at the Points Indicated in Figure 6.8

Flow Rate	Pressure (bar)								
(mL/min/ channel)	A	ΔP_{AB}	B	ΔP_{BC}	C	ΔP_{CD}	D	ΔP_{DE}	E
≈20	0.972	0.805	0.167	0.114	0.053	0.016	0.037	0.006	0.031
		150	:	20	:	3	:	1	

Figure 6.8 - The Points at Which the Pressure Measurements Given in Table 6.1 Were Taken

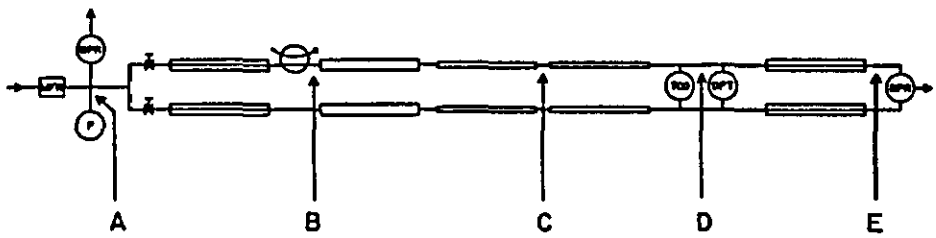

A Upstream of the flow-setting chokes.
B Immediately upstream of the column.
C At the mid-point of the delay line.
D Immediately upstream of the DPT.
E At the exit of the flow-detecting chokes.

6.2.1.2 Column Efficiency

Van Deemter *et al.* (1956) derived an equation, taking into account the various mechanisms which cause peak spreading, which gives some measure of the column efficiency in terms of a height equivalent to a theoretical plate (HETP). Martin and Synge (1941) first attempted to apply concepts developed for distillation to chromatography. The efficiency of a packed-type of distillation column can be expressed in terms of the number of theoretical equilibrations it achieves. The HETP is therefore the total height of the column divided by the number of theoretical equilibrations (or theoretical plates). In the context of chromatography, the HETP is defined as "the thickness of the layer such that the solution issuing from it is in equilibrium with the mean concentration of solute in the non-mobile phase throughout the layer".

$$HETP = A + \frac{B}{u} + Cu \qquad (6.1)$$

where :

A is the contribution of eddy diffusion
B that of longitudinal diffusion
C the term relating to the resistance to mass transfer, and,
u is the linear velocity of the gas.

A plot of HETP versus u has an optimum value of u for which the HETP is a minimum. This is the carrier gas velocity at which the column is most efficient. This

treatment is specific for a particular sample gas and is not a complete expression of the separating power of a column (Giddings (1964)). For a multi-component sample, each component will (in all probability) have a different optimum flow rate.

A more useful treatment is the extent of the separation (Horvath (1967)). The resolution is the ratio of the difference in the mean retention times of two neighbouring peaks to the mean base width of the peaks (Figure 6.9).

Figure 6.9 - The Extent of Separation of Two Peaks

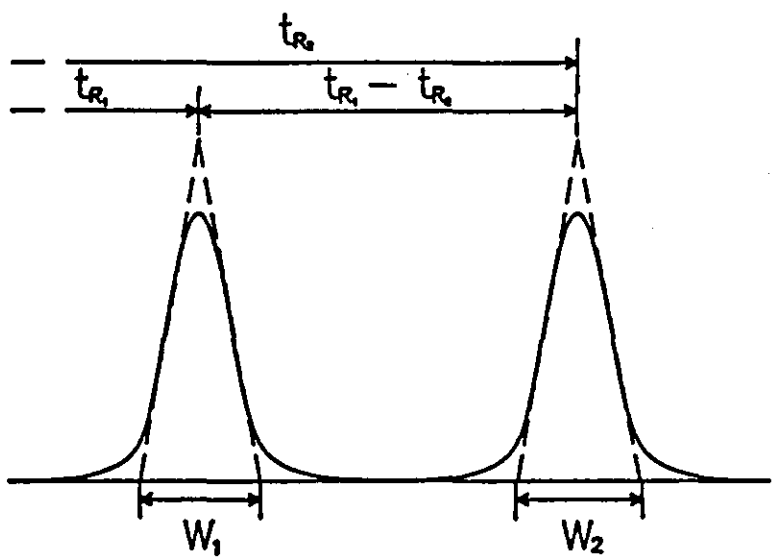

$$R = \frac{2(t_{R_2} - t_{R_1})}{(W_1 + W_2)} \qquad (6.2)$$

The separation is 99.7% complete when R=1.5 but for R=1 the separation is still 98% complete and Horvath suggests that this is adequate in practice.

For the further development of sorption-effect chromatography it is evident that the column must satisfactorily perform the separation with only a minimal pressure drop (to minimise the error contribution of the column viscosity effect). A satisfactory separation would be one where all peaks are completely separate but not so broad that the beginning and end of a peak is lost in the baseline. As has been mentioned, the Pye columns (1.5m×6mm o.d.×4mm i.d.) which were used initially proved to have too great a column viscosity effect under suitable separating conditions.

There are three parameters which could be altered in the search for a suitable column. These are :

packing size
column diameter
column length.

6.2.1.3 Packing Size

The efficiency of a column increases with decreasing packing size (Purnell 1967) and increasing the packing size can seriously impair the column efficiency (Gordon, Krige and Pretorius (1964)). The pressure drop ($-\Delta P$) down the column of length l can be determined using the Carmann-Kozeny equation.

$$\frac{-\Delta P}{l} = K\mu u\left(\frac{6}{\psi d}\right)^2\left(\frac{(1-\varepsilon)^2}{\varepsilon^3}\right) \qquad (6.3)$$

where :

K is the Kozeny constant and its commonly accepted value is 5
μ is the fluid viscosity
u is the average fluid velocity
d is the average particle diameter
ψ is the particle sphericity (=1 for spherical particles), and,
ε is the bed voidage.

The pressure drop decreases with increasing voidage and also with increasing particle diameter. It is worth noting that Griffiths, James and Phillips (1952) achieved satisfactory performance with relatively crude columns. They used a fairly coarse packing by chromatography standards (BSS 40 - 420μm). This suggests that there should be a column which meets the conflicting requirements of low pressure drop and satisfactory resolution

As the packing size is changed so the column voidage changes. 5A molecular sieve, ground down and graded, is irregularly shaped but Table 6.2 gives some indication how the voidage might change as particle size is increased. 5A molecular sieve is commercially available as 4-8 mesh (4-2mm) or 8-12 mesh (2-1.4mm) beads and 1/16" (1.5mm) or 1/8" (3mm) pellets (however some chromatographic suppliers will provide a nominated packing size range). A range of particle sizes was produced by crushing and sieving the molecular sieve as supplied. This was then washed with distilled water to remove any fines (relatively little crushing produces large quantities of powder <250μm). The size ranges were :

1200-1400μm (14-12 mesh)

1000-1200μm	(16-14 mesh)
855-1000μm	(18-16 mesh)
710-855μm	(22-18 mesh)
500-710μm	(30-22 mesh)
250-500μm	(60-30 mesh)

in addition to 1/16" pellets and the 8-12 mesh beads.

Table 6.2 - How Bed Voidage Varies with Packing Size and Packing Density (Coulson and Richardson (1980(II)))

Spheres		Cubes	
Diameter (")	Voidage	Size (")	Voidage
1/32	0.393	1/8	0.190
1/16	0.405	1/8	0.425
1/8	0.393	1/4	0.318
1/4	0.405	1/4	0.455
5/16	0.416		

6.2.1.4 Column Diameter

Littlewood (1970) reports that the HETP does not increase significantly between column diameters of 3mm to 30mm, the major factor being flow unevenness in wider columns. If a column were perfectly uniformly packed it would be equivalent to a number of narrow columns in parallel and the plate height would be independent of diameter. Horvath (1967) suggests that 2-3mm i.d. columns are the most adequate for analytical purposes whilst Purnell (1967) reports that above column diameters of 10mm the plate height increases rapidly with diameter.

6.2.1.5 Column Length

The length of the column should be the shortest that will perform the required separation (Horvath (1967)), this is borne out by Gordon, Krige and Pretorius (1964). Peaks that have long retention times may be so diffuse that the sample gas is not discernible above the baseline.

6.2.1.6 Column Optimisation

The procedure adopted for finding a satisfactory packing size was to prepare the column, condition it, and then, by varying the volumetric flow rate, see if a satisfactory separation of the chosen mixture could be achieved. Complete separation of the adsorption peak, the hydrogen desorption peak and the argon desorption peak was desired, but with each peak narrow enough to be accurately analysed. (Remember, the peak area is a measure of the number of moles adsorbed so the sum of the desorption peak areas should equal the area of the adsorption peak provided none of the components is irreversibly adsorbed.) Complete separation would be indicated by a section of baseline between each peak. Any significant offset of the baseline between peaks would suggest that the pressure drop in the column were too high. Reducing the volumetric flow rate has the effect of reducing any baseline offset but increasing the peak widths.

The 1.5m columns could not be packed with anything greater than 850μm and no satisfactory column was found using packing sizes smaller than this. A pair of columns were manufactured (enclosed in a glass envelope to reduce the effects of thermal noise) of approximately equal volume to those previously used but of a larger diameter glass tubing. These were 0.4m×9.5mm o.d.×7.5mm i.d. and could easily be packed with the full range of prepared packing sizes. No satisfactory column could be prepared to meet the desired criteria using this length of column. The packing size was chosen to be 1200-1400μm. Various lengths of copper tubing (9.5mm o.d.×7.5mm i.d.) were packed and the performance evaluated. The columns which seemed best suited for the chosen separation were found to be 0.75m×9.5mm o.d.×7.5mm i.d. packed with 1200-1400μm 5A molecular sieve. These columns, whilst perhaps still not the most suitable, seemed to meet the requirements although the selection procedure was quite subjective. The pressure profile down the system containing the 'optimum' columns for two different carrier flow rates is given in Table 6.3. The configuration of the chromatograph and the points of measurement are shown in Figure 6.10.

Figure 6.10 - The Points at Which the Pressure Measurements Given in Table 6.3 Were Taken

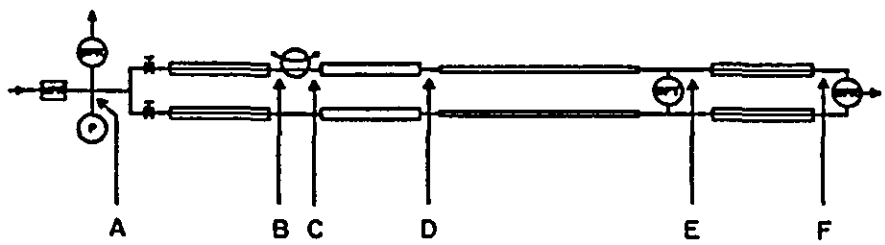

A Upstream of the flow-setting chokes.
B Immediately upstream of the sample valve.
C Immediately upstream of the column.
D Immediately downstream of the column.
E Immediately upstream of the flow-detecting capillaries.
F Immediately downstream of the flow-detecting capillaries.

Table 6.3 - Pressure Measurements Taken at the Points Indicated in Figure 6.10

Flow Rate	Pressure (bar)										
(mL/min/ channel	A	ΔP_{AB}	B	ΔP_{BC}	C	ΔP_{CD}	D	ΔP_{DE}	E	ΔP_{EF}	F
42.5	1.6	1.475	0.125	0.016	0.109	0.001	0.108	0.016	0.092	0.005	0.087
		1400	:	15	:	1	:	15	:	5	
23.9	1.007	0.899	0.108	0.009	0.099	0.001	0.098	0.009	0.089	0.002	0.087
		900	:	9	:	1	:	9	:	2	

6.2.2 The Effect of Viscosity Elsewhere in the System

6.2.2.1 The Presence of Extra Peaks

As has been shown, the band of different composition has an effect in the flow-detecting capillaries and can affect the pressure drop in the column. In Chapter 5 Figures 5.9a and 5.9b, a flow deviation was observed which was shown to be the effect of the sample band moving through the connecting pipework to the TCD and the TCD itself. It was surmised that in this relatively high pressure drop region upstream of the DPT, reduced viscosity causes the DPT to record a higher pressure, and vice versa for increased viscosity. These 'stray' effects can and do occur anywhere where due care is not taken. Figure 6.11 and 6.12 show pure hydrogen and pure argon samples respectively,

being injected into helium carrier gas, using the 'optimum' size column. The carrier gas flow rate was around 20 mL/min per channel. These traces could be described as excellent because the peaks are well defined with a steady baseline before and after each peak. As usual, the peaks in order are : the injection peak, the adsorption peak, the desorption peak and the viscosity peak. However, if the carrier flow is increased to around 55 mL/min in each channel there is a flow disturbance immediately after the desorption peak (the third peak) on the hydrogen injection trace (Figure 6.13) and also another immediately before the viscosity peak (the last peak). The same effect (only in the opposite direction) can be seen immediately before the viscosity peak in Figure 6.14 and there could possibly be the same, but opposite effect as the argon sample elutes from the column but it is not easily identifiable. If these flow perturbations are due to changed viscosity then argon and hydrogen would cause opposite effects.

Figure 6.11 - The Injection of Hydrogen into Helium Carrier Gas Flowing at 20mL/min Using 'Optimal' Columns

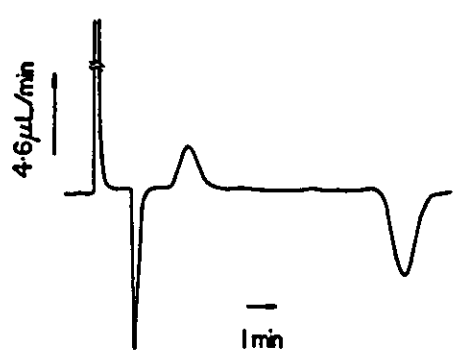

Figure 6.12 - The Injection of Argon into Helium Carrier Gas Flowing at 20mL/min Using 'Optimal' Columns

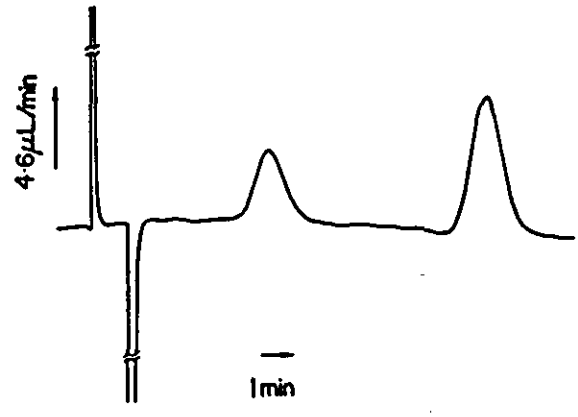

Figure 6.13 - The Injection of Hydrogen into Helium Carrier Gas Flowing at 55mL/min Using 'Optimal' Columns

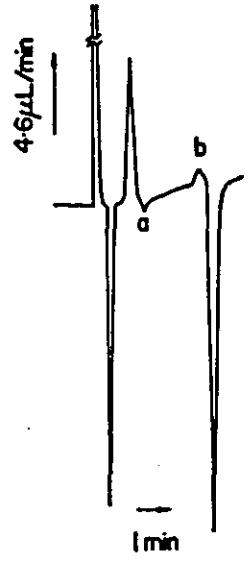

a An apparent flow reduction after the desorption peak.

b An apparent flow increase before the viscosity peak.

The addition of 1.8m×6mm o.d.×4mm i.d. Nylon tubing between the column end and the 3mm o.d. delay lines appears to eliminate this first 'new' disturbance (Figures 6.15 and 6.16). This was intended to reduce the abruptness of the change in cross-sectional area from the column (8mm i.d.) to the delay line (1.5mm i.d.). However, if the perturbation were a column-end effect it would be lost in the desorption peak so

Figure 6.14 - The Injection of Argon into Helium Carrier Gas Flowing at 55mL/min Using 'Optimal' Columns

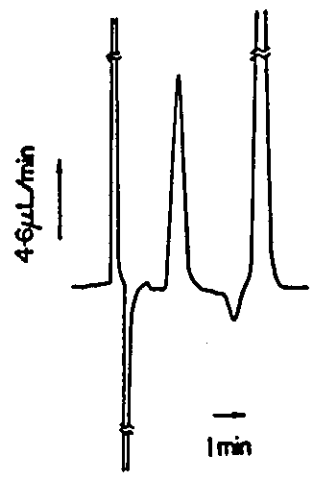

the origins of this peak were probably somewhere in the delay lines or fittings. Nevertheless, the more gradual change in cross section seemed a worthwhile modification.

Figure 6.15 - The Injection of Hydrogen into a Helium Carrier Gas Using 4mm i.d. Delay Lines Immediately Downstream of the Column

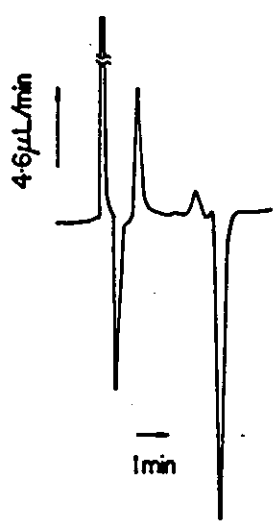

Figure 6.16 - The Injection of Argon into a Helium Carrier Gas Using 4mm i.d. Delay Lines Immediately Downstream of the Column

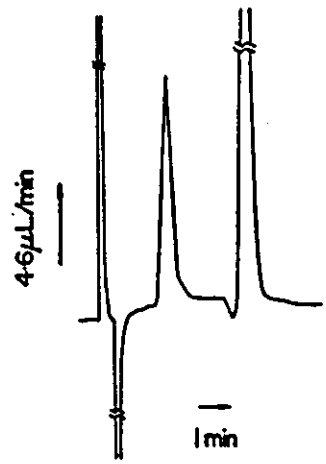

The cause of the second perturbation, just prior to the viscosity peak, must be upstream of the DPT inlet. It could be caused by the passage of the band of changed viscosity moving to a region of relatively high flow resistance thereby modifying the pressure drop causing the pressure at the DPT to change (see Chapter 5).

The extent of these supposed viscosity effects is seen better if the columns are removed from the system. The actual changes in cross section are, moving downstream from the sample valve with the columns removed :

0.8mm i.d. (sample valve to delay line connecting tubing)
1/16"-1/8" reducing union (all fittings are "Swagelok")
1.5mm i.d. (delay line #1 - upstream of column)
1/8"-1/4" reducing union (this replaces 1/8"-3/8" to 8mm i.d. packed column to 3/8"-1/4")
4mm i.d. (delay line #2 - downstream of column)
1/4"-1/8" reducing union
1.5mm i.d. (second delay line (#3) - downstream)
1/8" straight connector
1.5mm i.d. (third delay line (#4) - downstream)
1/8" bulkhead (DPT inlet port)
1.5mm i.d. (DPT tubing)
0.8mm i.d. (flow-detecting chokes)

Figures 6.17, 6.18 and 6.19 are the recorded passages of hydrogen, argon and dichlorodifluoromethane (CCl_2F_2) samples respectively, in helium carrier flowing at the same rate as before (around 55mL/min). Five peaks (or flow deviations) can be observed. The two peaks at either end of each trace are immediately recognisable. The first is the injection peak and the final peak is the flow-detecting-capillary viscosity effect. The intermediate effects could be related to viscosity or density variations depending on whether the restriction is acting more like a tube or more like an orifice. With a given pressure drop, the flow rate through an orifice is dependent on density (Equation 2.1) whereas the flow rate through a tube depends on the fluid viscosity (Equation 2.2).

Figure 6.17 - The Passage of a Hydrogen Sample in a Helium Carrier Gas Through a System Containing No Column

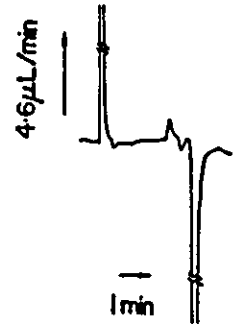

The two large peaks are immediately identifiable as the injection peak the (earlier peak) and the viscosity peak (the later peak). Immediately after the injection peak there is a small pause in flow. Before the viscosity peak there is a flow surge followed by another flow pause.

CCl_2F_2 was included in the experiment because, when pure, it has a high density and low viscosity (c.f. hydrogen;low density/low viscosity and argon;high density/high viscosity). If CCl_2F_2/He mixtures are ideal with respect to density, and if the effects are density related, then CCl_2F_2 will have the largest effect because it is the most dense of the sample gases and the effect will be in the same sense as the effects caused by argon. Hydrogen would have relatively little effect because its density is so similar to that of helium compared to the densities of the other two sample gases.

If the effects are viscosity related, and if CCl_2F_2/He mixtures are ideal with respect to viscosity (experience suggests caution in making this assumption), then CCl_2F_2 would cause effects in the same sense as those caused by hydrogen.

Figure 6.17 shows the passage of a 10μL @NTP hydrogen sample through the system in helium carrier gas. The first peak is the injection peak (the pressure disturbance caused by the expansion of a high pressure slug of sample gas into the carrier stream),

the last peak is the viscosity peak, (the peak caused by a band of changed viscosity passing through the flow detector). Immediately after the injection peak is a smaller effect, in the same direction as the viscosity peak. Prior to the viscosity peak are two more effects, the earlier in the opposite direction to the viscosity peak, and the later, in the same direction.

Figure 6.18 - The Passage of an Argon Sample in a Helium Carrier Gas Through a System Containing No Column

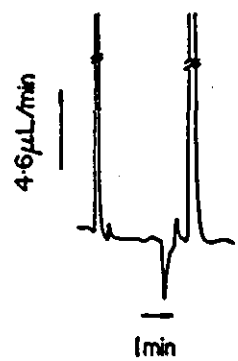

The trace shows the injection peak followed by a flow surge. Later, there is a flow pause followed by a flow surge, both preceding the viscosity peak. The direction of all peaks, apart from the injection peak, is reversed compared to those in Figure 6.17

A 10μL @NTP argon sample (Figure 6.18) shows the same main peaks although, of course, the viscosity peak is in the same sense as the injection peak. The direction of each of the intermediate effects is reversed from those due to the hydrogen sample in Figure 6.17.

The magnitude and direction of the effects shown in these traces are consistent with predictions based on published viscosity data for argon and hydrogen in helium. The magnitude of the effect is determined by the gradient of the viscosity versus composition curve over the appropriate range. If the effect were due to density differences then, for the same sample size, argon (molecular mass 40) should have a much larger effect than hydrogen (m.m. 2) in helium (m.m. 4).

Instead of providing conclusive evidence, the CCl_2F_2 sample confuses the issue. It was not possible to generate a consistent size of sample of CCl_2F_2 because of a faulty valve (the supply of CCl_2F_2 came from sealed canisters instead of cylinders and these must be punctured using a special valve) however Figure 6.19 does show the passage of a CCl_2F_2 sample of indeterminate size. The magnitude of the effects is **not** directly comparable to those in Figures 6.17 and 6.18. The two main peaks can be seen, the

Figure 6.19 - The Passage of a Dichlorodifluoromethane Sample in a Helium Carrier Gas Through a System Containing No Column

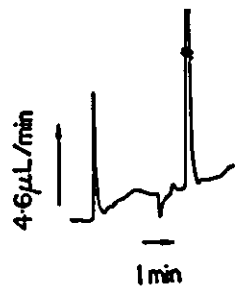

The sample is much smaller than those of hydrogen and argon in Figures 6.17 and 6.18, so the injection peak is correspondingly smaller. There is no discernible flow perturbation after the injection peak. There is a flow pause and a flow surge preceding the larger flow surge caused by the changing viscosity in the flow-detecting capillaries.

viscosity peak indicates an increase in gas viscosity due to the CCl_2F_2. The two later intermediate peaks correspond in direction to those caused by the argon sample. As no data could be found for the viscosity of CCl_2F_2/He mixtures, a plot of mixture viscosity versus composition was produced (Appendix III Figure 6) using the method outlined in Appendix II. The graph shows that dilute concentrations of CCl_2F_2 in helium cause an increase in viscosity up to around ten per cent CCl_2F_2. This is entirely consistent with the effects observed in Figure 6.19.

6.2.2.2 Identification of the Extra Peaks

These extra effects were thought to be caused by changes in cross-sectional area in the flow path, so in order to identify where each of these extra peaks is caused, a short length of high impedance tubing was inserted at various likely positions in the system and the change in response to the passage of a sample gas was observed. The narrow-bore tubing was intended to exaggerate the change in cross-sectional area and thus give a larger effect. Figure 6.20 shows the effect of an argon sample being injected into hydrogen flowing at around 60 ml/min per channel through a system containing no columns. Again, the injection peak and the viscosity peak caused by the flow-detecting capillary are immediately identifiable as the first and last peaks. Soon after the injection peak there is a pressure surge followed later on by two reductions in pressure before the viscosity peak.

Figure 6.20 - The Passage of an Argon Sample in a Hydrogen Carrier Gas Through a System Containing No Column

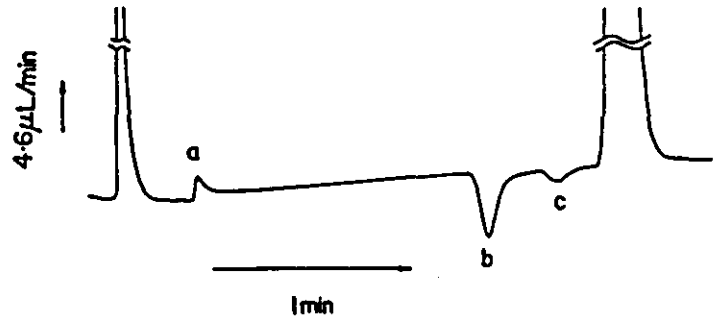

Hydrogen was used as the carrier gas because the gradient of a plot of hydrogen/argon mixture viscosity versus composition is steeper than that for helium and argon over the relevant composition range. The trace is slightly modified compared to Figure 6.18 but the three extraneous peaks (a, b and c) can be observed.

Approximately 8cm of 0.8mm i.d. tubing was inserted at the join of the two 3mm o.d. delay lines (#3 and #4) furthest downstream to investigate whether this fitting is the cause of one of the extraneous peaks. The fourth peak from Figure 6.20 is spectacularly transformed proving that the effect is caused in the 1/8" straight connector joining delay lines #3 and #4 (Figure 6.21). The effect was eliminated (Figure 6.22) by making the delay line out of one length of tubing instead of two. A specially-made length of tube, tapered from 4mm i.d. to 1.5mm i.d., inserted between the 4mm delay line (#2) and the one-piece 1.5mm delay line (#3/4) only slightly reduces the third peak (compare with Figure 6.20).

Figure 6.21 - Identification of the Extra Peaks

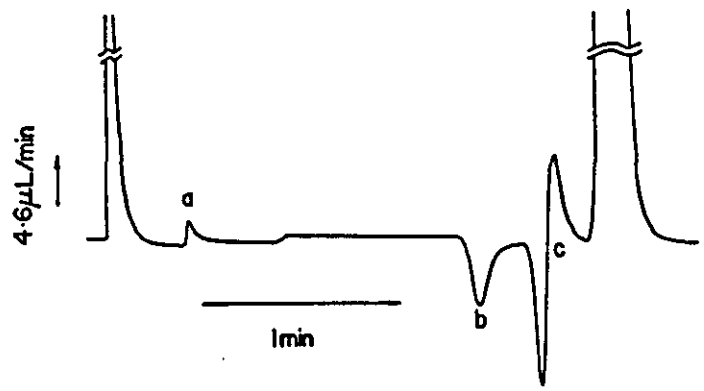

A length of high impedance tubing was inserted at the join of the delay lines #3 and #4. Peak c from Figure 6.20 is spectacularly transformed.

Figure 6.22 - Identification of the Extra Peaks

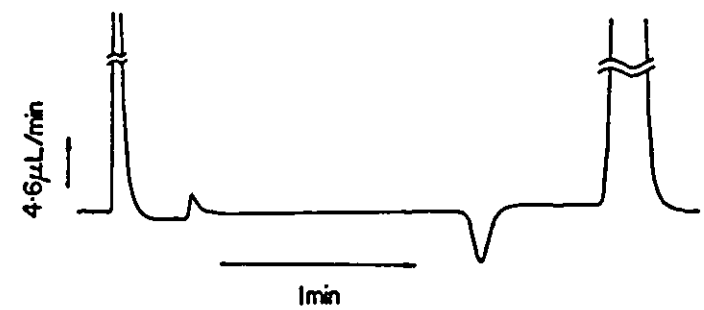

Delay lines #3 and #4 were replaced by a single length of tubing thus eliminating peak c from Figures 6.20. A 4mm i.d. to 1.5mm i.d. tapered tube inserted between delay lines #2 and #3/4 only slightly reduces peak b in Figure 6.20.

If the 0.8mm i.d. tube is inserted between the first length of 3mm o.d. delay line (#1) and the 6mm o.d. delay line (#2) the second peak is affected (Figure 6.23). This shows that it is caused by the sample band crossing this union.

Figure 6.23 - Identification of the Extra Peaks

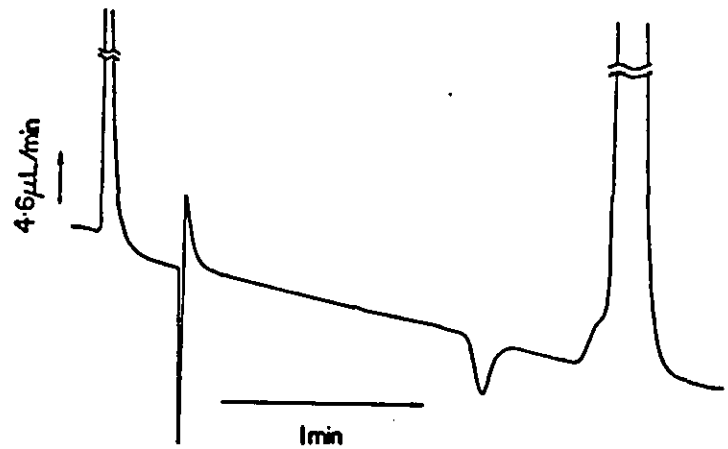

Insertion of a length of high impedance tubing between delay lines #1 and #2 transforms peak a from Figure 6.20.

Inserting the 0.8mm i.d. tube at the downstream end of the tapered tube but before the 3mm o.d. one-piece delay line (#3/4) confirms that the third peak is caused by the presence of the sample band at this union (Figure 6.24). The apparent step between the second and third peaks is probably only a random shift because it occurs while the sample band is within the 6mm o.d. delay line. The sense of the effects has changed between Figures 6.23 and 6.24. This is because the connections to the DPT inlets were inadvertently switched between experiments.

Figure 6.24 - Identification of the Extra Peaks

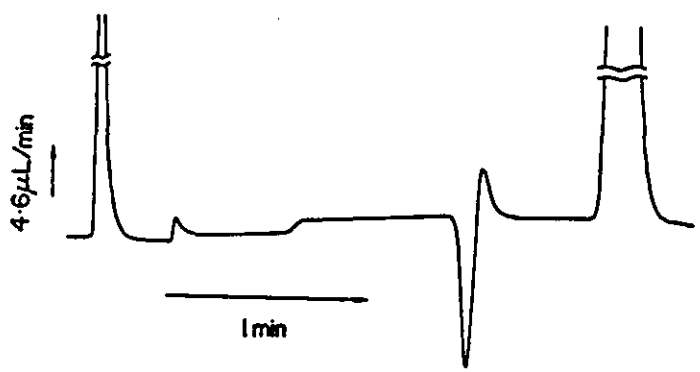

The high impedance tubing was inserted between the tapered tube and delay line #3/4. Peak b from Figure 6.20 is modified.

These two peaks (caused at the entry to the column, and at the union of 6mm o.d. (#2) and 3mm o.d. delay lines (#3/4)), which have not been eliminated, can be observed in Figure 7.7 as small baseline deviations before the adsorption peak and before the viscosity peak.

These effects are relatively large because :

i) the volumetric flow rate is high so the pressure drop is relatively high

ii) the gradient of a plot of the viscosity of a hydrogen/argon mixture versus composition is very steep at low argon concentrations (Appendix III Figure 2).

Conder (1982) recommends minimising sudden changes of diameter and dead pockets because they are both sources of band spreading and asymmetry. During sorption-effect chromatography, sudden changes in cross-sectional area are also a cause of baseline perturbations.

6.3 Density Effects

6.3.1 Introduction

During the course of identifying the column viscosity effect, another, reproducible effect was noticeable at very high sensitivity. The sensitivity could be increased because an inert column was in use so thermal noise was almost completely absent. Figure 6.25 shows a trace of an argon slug being introduced into this system. The peculiarity is the presence of oscillations immediately after the injection i.e. whilst the slug travels through the coils of the pre-column delay line. As the slug leaves the column there is a negative blip. Finally, there is the positive, capillary viscosity effect. The 'blips' are due to the band of different viscosity moving to a larger bore tube on entry to the column and to a narrower bore tube on exit. This can be clarified using the arguments proffered in Chapter 5 and Section 6.2.2.

The oscillations caused by the passage of the sample slug down one delay line previously unobserved, and in the course of chromatographic analysis (at usual sensitivities) would probably be unobservable.

6.3.2 Confirmation of the Density Effect

The columns were removed from the system and replaced by a delay line so that the system contained three lengths of coiled delay line, joined by Swagelok straight connectors.

Figure 6.25 - The Effect of an Argon Sample in a Helium Carrier Gas Passing Through a System Containing a Low Pressure Drop Inert Column at High Detector Sensitivity

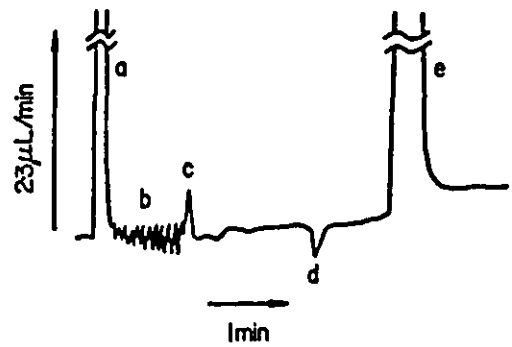

a The injection peak.

b Oscillations in flow rate produced by the passage of the sample slug through the upstream delay line.

c An effect of the sample band passing through the fitting at the upstream end of the column.

d An effect of the sample band passing through the fitting at the downstream end of the column.

e The viscosity effect.

An argon sample into helium carrier gas in this system produces similar oscillations as those in Figure 6.25 for the passage of the sample through the first delay line. Oscillations of greater amplitude are produced in the second delay line. There is a negative viscosity blip at the pipe union between the second and third delay lines and then the passage of the sample through the final delay line is marked by more flow oscillations. The number of oscillations corresponds approximately to the number of coils in the tubes. The characteristic injection peak and viscosity peak can be seen as positive peaks at the beginning and end of the trace. These oscillations could be caused by the sample band having a different density to pure helium carrier gas. The density of argon is ten times the density of helium. This is endorsed by the trace produced when a hydrogen sample is introduced into this configuration (Figure 6.27). The density of hydrogen is half that of helium whilst there is an appreciable viscosity difference between the two gases yet there are no noticeable oscillations. If the oscillations in Figure 6.26 were related to viscosity they would appear with a hydrogen sample gas as well (Figure 6.27). The trace shows the positive injection peak and the negative peak attributable to reduced viscosity in the flow-detecting capillaries. In between the two is a positive blip which is a fitting effect i.e. the effect of a band of changed viscosity moving through the pipe union between the second and third delay lines.

Figure 6.26 - The Effect of an Argon Sample in a Helium Carrier Gas Passing Through Three Similar, Coiled Delay Lines

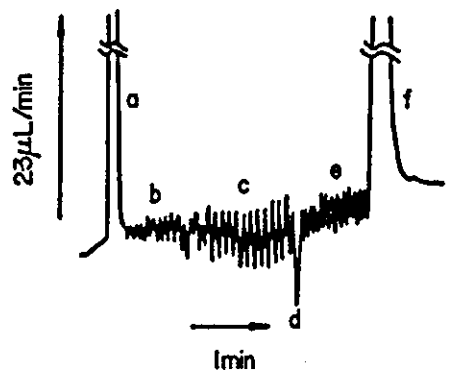

a The injection peak.

b The oscillations in flow rate produced by the passage of the sample band through the first delay line.

c The oscillations in flow rate produced by the passage of the sample band through the second delay line.

d The effect of the sample band passing through the pipe fitting connecting the second and third delay lines.

e The oscillations in flow rate produced by the passage of the sample band through the third delay line.

f The viscosity effect.

Confirmation of this density effect is obtained using dichlorodifluoromethane as the sample gas. CCl_2F_2 is thirty times more dense than helium and produces substantial oscillations (Figure 6.28). The sample size was unknown because of the nature of the gas supply and was probably smaller than the sample sizes of argon and hydrogen (25μL) yet the effect was largest for CCl_2F_2. The maximum pressure deviation was in the region of 0.0025mmH_2O compared to typical desorption peak maximum of 0.2mmH_2O.

Figure 6.27 - The Effect of a Hydrogen Sample in a Helium Carrier Gas Passing Through Three Similar, Coiled Delay Lines

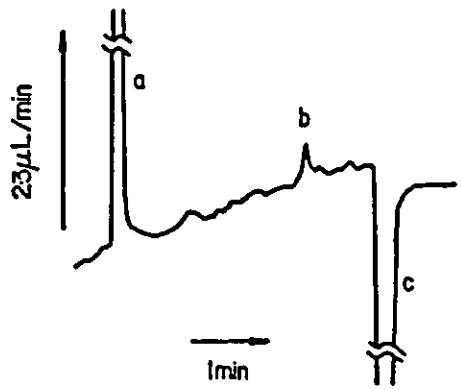

a The injection peak.

b The effect of the sample band passing through the pipe fitting connecting the second and third delay lines.

c The viscosity effect.

Note there are no oscillations whilst the sample passes through the delay coils because the respective densities of hydrogen and helium are so similar.

Figure 6.28 - The Effect of a Dichlorodifluoromethane Sample in a Helium Carrier Gas Passing Through Three Similar, Coiled Delay Lines

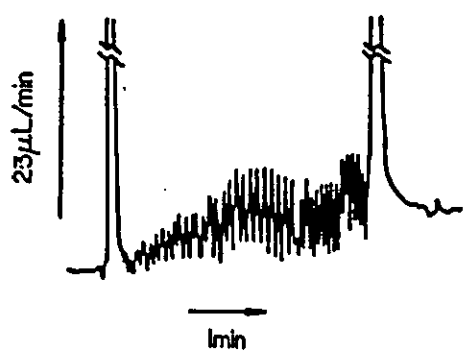

Nitrogen has a similar viscosity to helium yet is seven times more dense. Figure 6.29 is the result of injecting nitrogen into the helium carrier gas. The oscillations are present as would be expected if the effect were density related. The presence of the viscosity peak implies that despite the fact that nitrogen is slightly less viscous than

helium, a dilute mixture of nitrogen in helium has a greater viscosity than pure helium. Appendix III Figure 5 that up to around 15% nitrogen, the mixture viscosity does in fact increase.

Figure 6.29 - The Effect of a Nitrogen Sample in a Helium Carrier Gas Passing Through Three Similar, Coiled Delay Lines

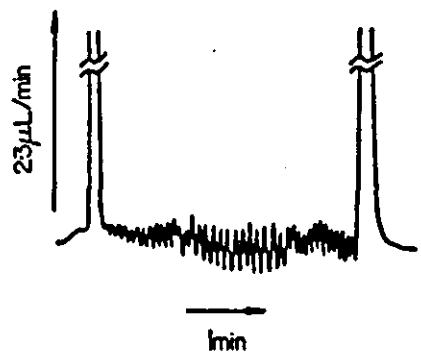

The source of these flow oscillations is the effect of a slug of different density gas passing around the coils of the delay line. It may be the orientation of the delay lines that produces the effect. If the coil is not horizontal, a denser slug can be imagined to accelerate under gravity in the down side of a vertical coil and decelerate in the up side. The opposite could be imagined for a less dense slug of gas. These density effects are of a very small magnitude but regardless of this, if they were super-imposed on a peak, the peak area would be calculated the same as for a smooth baseline because positive and negative oscillations would tend to cancel each other.

6.4 Volumetric Flow Rate Measurement

The phenomenon caused by gas of changing viscosity flowing through changes in cross-sectional area has been used to calculate the volumetric flow rate of gas. A slug of tracer gas is introduced into the flow that is to be measured and the perturbations which result from the movement of the slug through a part of the system where there are changes in the cross-sectional area are used to time the rate at which the gas flows through a certain volume of pipe.

6.4.1 Introduction

Several chromatographers have developed novel ways of measuring the volumetric flow rate of gas. Van Swaay (1963) described an automatic flowmeter which could also be used to detect sample elution from a column as mentioned earlier. Methods based

more on chromatography were used by Bosanquet and Morgan (1957) and by Chen and Parcher (1971). Bosanquet and Morgan measured the passage of a slug of slightly soluble gas through a chromatographic column using a TCD. Chen and Parcher measured the transit time of an air peak through an empty column. They could not use a soap bubble flowmeter because of the large hydrocarbon concentration and variations in viscosity were too great to use a capillary flowmeter. A robust capillary flowmeter using a pressure gauge which could be calibrated to give a direct flow rate reading was developed by Munns and Frilette (1965). Hussey and Parcher (1974) measured the retention distance of a nitrogen sample in pure carrier gas at known flow rates in order that they could determine the flow rate of solute/carrier gas mixtures from a plot of reciprocal retention time versus flow rate. Testerman and McLeod (1964(II)) described how the ultrasonic frequency produced by gas flowing through an orifice could be used to measure the mass flow rate of gas.

The method of measuring volumetric flow rate described here uses the principle that a slug of sample gas can be detected at either end of a known volume of flow path using a TCD or by detecting the flow perturbations caused by changes in cross-sectional area of the flow path (as described in the previous sections) hence the time of flight of the gas can be determined.

The bubble flowmeter is commonly used to establish the rate of flow of carrier gas and, in many cases, is the most reliable method. For this reason it has been used to calibrate the flowmeter volumes. The operator generates a film of soap solution the passage of which along a graduated tube is timed thus giving the flow rate. Where great accuracy is required, the calculated flow rate must be corrected for temperature, pressure and the vapour pressure of water (which is assumed to saturate the gas flow). Drawbacks with this method are that the gas may diffuse through the bubble, it may be highly soluble in the soap solution, and the graduations on the flow meter may be inaccurate. Light sensors have been incorporated in the design by some manufacturers to register when the bubble passes and calculate the flow rate electronically (SGE, Horiba).

6.4.2 Determination of Volumetric Flow Rate

This experiment shows how two chromatographic detectors, the sorption-effect detector and the TCD, can be used to measure volumetric flow rate.

6.4.3 Principles

A tracer gas is used to determine the volumetric flow rate of a bulk gas. The entry and exit of the tracer gas into and out of a length of tube are timed. Knowledge of the volume of the flow path between events will enable the volumetric flow rate to be calculated.

6.4.4 Apparatus

The position of the tracer is indicated by the two detectors. Figure 6.30 shows the experimental configuration. The flowmeter tube is connected across the two channels of the TCD. The outlet of one side of the TCD is connected to one channel of the capillary flowmeter. In order to be able to measure a differential pressure, a make-up gas is required on the second channel of the capillary meter. A mass-flow regulator is used to set the make-up flow such that the pressures on either side of the DPT are nearly equal before a measurement is taken.

Figure 6.30 - The Apparatus Used to Measure Volumetric Flow Rate

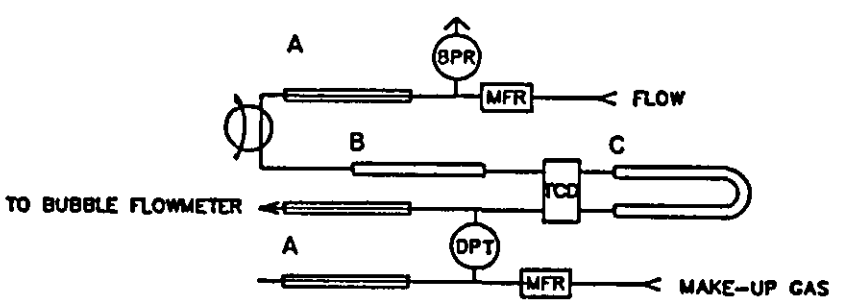

A The flow-restricting capillary.
B A delay line.
C The flowmeter volume.

Upstream from the TCD is a delay line to allow the pressures to equilibrate after the tracer is injected via the sample valve. The capillary restrictor, BPR and MFR constitute a single channel version of the constant flow rate generating system (described in Chapter 2) which is used to make up a flow rate to be measured.

A suitable tracer is one that has a different thermal conductivity and a different viscosity to the bulk gas. The entry of the tracer into the measuring volume is detected by one channel of the TCD and, the exit, detected in the second channel of the TCD. In addition, the passage of the tracer into, and/or out of, the detection chamber causes a flow perturbation due to the change in cross section and to the change in viscosity so

the capillary flowmeter also detects the entry of the tracer into the flowmeter volume. The exit of the tracer is marked by any effect of passing through the TCD combined with the viscosity effect as it passes into the capillary flowmeter.

6.4.5 Experimental Method

Three different flowmeter volumes were used at three different flow rates of nitrogen, nominally 40, 65 and 90 mL/min. For each flow rate, the make-up gas flow rate was adjusted to zero the DPT output. A slug of hydrogen tracer gas was introduced and the TCD and DPT responses logged using the BBC Master-based data-logging system, and, also on a conventional chart recorder. The start time and the finish time can be determined from the logged data.

6.4.6 Results

Figure 6.31 displays the responses of the two detectors as recorded by a chart recorder. The TCD trace is as expected: the 'start' peak is the first peak and the 'finish' peak, the second. The two peaks are in opposite directions because, for the first, the sample slug is passing through one side of the detector, and for the second, the slug is in the other side of the detector. The 'start' peak recorded by the DPT is actually a doublet, a pressure swing in one direction followed by a swing in the opposite direction. The 'finish' peak is an ordinary viscosity peak combined with any flow effects caused by the tracer passing through the second channel of the TCD.

The two methods of analysing the data differ in the way that the characteristic times are determined.

Method 1 - First Moments

When the peaks are non-symmetrical, the correct method of finding a mean time is to take the first moment of the detector response because this takes account of the asymmetry. The mean time is defined by :

$$\bar{t} = \frac{\int_0^\infty \overline{V} t dt}{\int_0^\infty \overline{V} dt} \qquad (6.4)$$

where, $\overline{V}$ is the difference between baseline signal and the signal at time t.

Figure 6.31 - The Output of the Two Detectors Used in the Configuration Shown in Figure 6.30

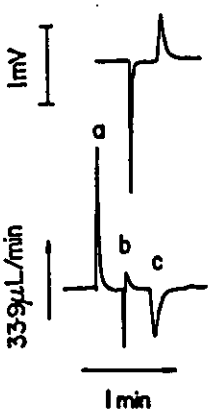

The lower trace shows the DPT response.

a The injection peak.

b The sample slug passing through one channel of the TCD.

c The sample slug passing through the second channel of the TCD and the capillary flowmeter.

The upper trace shows the TCD output. The two peaks correspond to peaks b and c on the DPT trace.

The data-processing program described in Chapter 8 (and listed in Appendix VIII) was adapted to calculate this (Appendix IX). Great care must be taken to locate peak start and peak end correctly otherwise errors can be introduced because $\overline{V}$ is not necessarily zero outside the limits of the peak because of baseline noise. This is not the case when calculating the peak area because the start/end points can lie anywhere on the baseline.

Method 2 - Time of Peak Maximum

If the peaks are symmetrical, the first moment and the time of the peak maximum are the same. However, the peak maximum is much more easily determined than the first moment. The data-processing program displays this information for every peak it finds and integrates, so no program modifications were necessary.

Both first moments and the times of the peak maxima were determined for all data. On the basis of these timings, and knowing the volumetric flow rate, the volume of the system between the timing points, "the flowmeter volume", was calculated. Because of the shape of the first flow perturbation, the flowmeter volumes based on the DPT response and calculated by Methods 1 and 2, will not be exactly the same. The calculated flowmeter volume for the TCD-based measurements ought to be the same regardless of which method is used because the first moment of the peak and the peak maximum ought to be the same. It is unlikely that the DPT and TCD flowmeter volumes will be exactly the

same because the detection points which define the flowmeter volume for the TCD are somewhere in each filament chamber whereas the flow perturbation points are likely to be at the inlet port and/or the outlet port of the TCD for the start peak and somewhere between the TCD inlet port and the end of the flow-detecting capillary for the finish peak. Because the flow rates are relatively high, any discrepancies are small. The flowmeter volume is not merely the volume of the delay line connected between the ports of the TCD. The volume of the delay line may give a good approximation to the actual flowmeter volumes and can be calculated from a knowledge of the internal diameter and the length. The tube dimensions, however, are only nominal. Consider Table 6.5, the average flowmeter volume is around 100mL but the internal volume of 6m x 4mm nominal i.d. tube is only 75mL. Similarly, for the 3m x 4mm i.d. (Table 6.6), the average flowmeter volume is around 50mL whereas the calculated pipe volume is 37.5mL. If the difference were the extra volume, other than that of the delay line, the discrepancy would remain constant. Because halving the length of delay line halves the discrepancy, it must be due to the volume of the delay line being calculated inaccurately. The 10m x 1.5mm i.d. delay line has an average volume of 29mL (Table 6.7) but the nominal volume of this tubing works out at around 18mL. So, no independent check on the calculated volumes is available.

The flow rates were then back calculated using the average volume from each set of data and each timing method (Tables 6.8 to 6.13). From only six data-logging runs for each delay line it is difficult to draw accurate conclusions. The smallest delay volume (10m x 1.5mm i.d.) gave the largest errors and would appear to be unsuitable for this range of volumetric flow rate. The 3m x 4mm i.d. delay line gave the best results and would appear to be the optimum of the three for the test flow rates. It is probable that for lower flow rates, a smaller volume will be optimal. The method of timing by peak maximum yields the more accurate results, especially for the TCD data. In the main, calculations based on the TCD peak maxima are accurate to less than 1% error. The DPT based errors are consistently higher but still mostly less than 1%.

There must be a pressure drop in the flow-detecting capillaries for the DPT to be able to register the flow perturbations. The pressure at the upstream end of the capillaries is calculated for each of the test flows in Table 6.4. Because of the pressure drop, the volume of the flowmeter calculated above will be greater than it would be if the gas were at atmospheric pressure.

On rearranging the Hagen-Poiseulle equation for compressible laminar flow :

$$P_1 Q_1 = \frac{\pi d^4}{256 \mu L}(P_0^2 - P_1^2) \tag{6.5}$$

where Q_1 =the volumetric flow at the outlet (m^3/s)

P_1 (atmospheric pressure) = $1.013 \times 10^5 N/m^2$

$d = 0.5 \times 10^{-3} m$

$L = 0.15 m$

$\mu_{N_2} = 1.75 \times 10^{-5} Ns/m^2$ @ NTP

$\rho_{N_2} = 1.167 kg/m^3$ @ NTP

it becomes :

$$P_0^2 = 3.566 \times 10^{14} Q_1 + P_1^2 \tag{6.6}$$

where Q_1 is in m^3/s and P in N/m^2.

$$N_{Re} = \frac{\rho v d}{\mu} = \frac{4 \rho Q}{\pi \mu d} \tag{6.7}$$

calculated for the worst case, for helium gas,

$$N_{Re} = \frac{4 \times 1.167 \times 1.5 \times 10^{-6}}{\pi \times 1.75 \times 10^{-5} \times 0.5 \times 10^{-3}}$$

$$N_{Re} \approx 255$$

therefore the flow is laminar.

If there is no pressure drop in the flowmeter delay line, the calculated volume of this pipe at the highest flow rate is approximately 2.6% too large. At the lowest flow rate, the error is around 1.1%. Expressed another way, the volumetric flow rates within the flowmeter volume will be 97.5%, 98.1% and 98.9% of the respective values measured at the outlet. The random errors make it difficult to distinguish a trend of an apparent increase in flowmeter volume with increasing flow rate. A significant pressure drop in the delay line itself will affect the calculations even further because the average pressure

Table 6.4 - Calculated Values of the Pressure at the Upstream End of the Flow-Detecting Capillary (P_0) for the Test Flow Rates

Flow Rate mL/min ($m^3/s \times 10^6$)	Capillary Upstream Pressure (bar)
90 (1.5)	1.026
65 (1.083)	1.019
40 (0.667)	1.011

within the delay line will be higher. These errors increase with increasing flow rate. A knowledge of the mean pressure of the gas in the delay line would be needed to calculate the flow rate more accurately.

If there is no significant pressure drop in the TCD and in the delay lines, then the removal of the capillary flowmeter would remove this source of error.

Table 6.5 - Flowmeter Volume Using a 6m Delay Line

Data File	Flow rate (mL/min)	Flowmeter Volume based on First Moment (mL)		Flowmeter Volume based on Peak Maximum (mL)	
		DPT	TCD	DPT	TCD
FLOW151	49.11	99.59	100.38	101.90	100.88
FLOW152	49.11	99.91	101.27	101.49	99.65
FLOW153	65.59	98.79	100.54	101.66	99.75
FLOW154	65.59	100.90	101.36	101.39	99.75
FLOW161	91.21	104.70	101.01	105.65	101.09
FLOW162	91.21	104.59	103.52	102.99	101.09
	AVERAGE	101.41	101.35	102.51	100.37

Table 6.6 - Flowmeter Volume Using a 3m Delay Line

Data File	Flow Rate (mL/min)	Flowmeter Volume based on First Moment (mL)		Flowmeter Volume based on Peak Maximum (mL)	
		DPT	TCD	DPT	TCD
FLOW221	89.99	51.18	49.79	50.62	49.12
FLOW222	89.99	52.12	50.21	50.99	49.12
FLOW223	66.81	48.72	50.78	50.39	49.27
FLOW224	66.81	50.25	49.94	50.66	49.27
FLOW225	43.44	50.75	51.29	50.32	49.05
FLOW226	43.44	49.92	50.93	50.14	49.05
	AVERAGE	50.49	50.49	50.52	49.15

Table 6.7 - Flowmeter Volume Using a 10m Delay Line

Data File	Flow Rate (mL/min)	Flowmeter Volume based on First Moment (mL)		Flowmeter Volume based on Peak Maximum (mL)	
		DPT	TCD	DPT	TCD
FLOW111	90.25	29.86	27.45	29.71	28.58
FLOW112	90.25	30.35	26.70	30.08	31.59
FLOW113	65.79	29.66	28.92	29.33	27.41
FLOW114	65.79	29.41	28.65	28.78	28.51
FLOW115	42.40	28.76	29.33	28.97	28.09
FLOW116	42.40	29.71	30.03	28.44	27.91
	AVERAGE	29.62	28.51	29.22	28.68

Table 6.8 - Back-Calculated Flow Rates for the 6m Delay Line based on First Moments

Data File	Flow Rate from DPT Timings (mL/min)	% Error	Flow Rate from TCD Timings (mL/min)	% Error
FLOW151	50.01	1.8	49.59	1.0
FLOW152	49.85	1.5	49.15	0.8
FLOW153	67.29	2.6	66.18	0.9
FLOW154	65.88	0.4	65.58	0.1
FLOW161	88.34	3.1	91.51	0.3
FLOW162	88.44	3.0	88.29	2.1

Table 6.9 - Back-Calculated Flow Rates for the 6m Delay Line Based on Time of Peak Maximum

Data File	Flow Rate from DPT Timings (mL/min)	% Error	Flow Rate from TCD Timings (mL/min)	% Error
FLOW151	49.40	0.6	48.86	0.5
FLOW152	49.60	1.0	49.46	0.7
FLOW153	66.13	0.8	66.00	0.6
FLOW154	66.31	1.1	66.00	0.6
FLOW161	88.50	3.0	90.56	0.7
FLOW162	90.78	0.5	90.56	0.7

Table 6.10 - Back-Calculated Flow Rates for the 3m Delay Line based on First Moments

Data File	Flow Rate from DPT Timings (mL/min)	% Error	Flow Rate from TCD Timings (mL/min)	% Error
FLOW221	88.77	1.3	91.25	1.4
FLOW222	87.18	3.1	90.50	0.6
FLOW223	69.24	3.6	66.43	0.6
FLOW224	67.13	0.5	67.54	0.1
FLOW225	43.21	0.5	42.76	1.6
FLOW226	43.94	1.1	43.06	0.9

Table 6.11 - Back-Calculated Flow Rates for the 3m Delay Line Based on Time of Peak Maximum

Data File	Flow Rate from DPT Timings (mL/min)	% Error	Flow Rate from TCD Timings (mL/min)	% Error
FLOW221	89.81	0.2	90.04	0.1
FLOW222	89.15	0.9	90.04	0.1
FLOW223	66.99	0.3	66.64	0.2
FLOW224	66.62	0.3	66.64	0.2
FLOW225	43.61	0.4	43.53	0.2
FLOW226	43.77	0.8	43.53	0.2

Table 6.12 - Back-Calculated Flow Rates for the 10m Delay Line based on First Moments

Data File	Flow Rate from DPT Timings (mL/min)	% Error	Flow Rate from TCD Timings (mL/min)	% Error
FLOW111	89.55	0.8	93.73	3.8
FLOW112	88.10	2.4	96.37	6.8
FLOW113	65.71	0.1	64.86	1.4
FLOW114	66.26	0.7	65.48	0.5
FLOW115	43.67	3.0	41.20	2.8
FLOW116	42.27	0.3	40.25	5.1

Table 6.13 - Back-Calculated Flow Rates for the 10m Delay Line Based on Time of Peak Maximum

Data File	Flow Rate from DPT Timings (mL/min)	% Error	Flow Rate from TCD Timings (mL/min)	% Error
FLOW111	88.77	1.6	90.57	0.3
FLOW112	87.66	2.9	81.94	9.2
FLOW113	65.54	0.4	68.83	4.6
FLOW114	66.79	1.5	66.18	0.6
FLOW115	42.76	0.8	43.29	2.1
FLOW116	43.56	2.7	43.56	2.7

6.5 Column Pressure Drop Using a Highly-Sorbed Carrier Gas

Consider the case where a non-sorbed sample species is injected into a highly sorbed carrier gas. The entry of the sample band into the column causes desorption of carrier gas and a surge in flow. When the band leaves the column, carrier gas is resorbed and there is a pause in flow. In practice, when the carrier gas flow rate is high, immediately after the desorption of carrier gas (the 'adsorption peak'), the baseline is offset in the

opposite direction indicating that the pressure drop down the column has increased because more gas than before is moving in the gas phase (Figures 6.32 to 6.34). The pressure drop rapidly decreases towards the initial baseline value until the sample band reaches the end of the column and the excess carrier gas is resorbed (the 'desorption peak').

Figure 6.32 - The Sorption-Effect Chromatogram Produced Using a Carrier Gas (Hydrogen) which is More Highly Adsorbed than the Sample Gas (Helium)

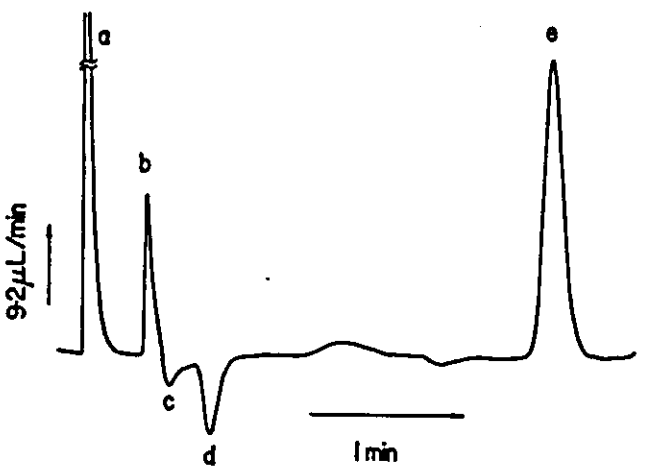

a The injection of helium into hydrogen carrier gas.

b A peak indicating a net increase in flow caused by more hydrogen desorbing from the column than the amount of helium adsorbing as the sample band enters the column.

c A net drop in flow rate caused by the presence of the sample band in the column followed by a gradual increase in flow until....

d The peak produced by the sample band leaving the column when a greater amount of hydrogen resorbs than the amount of helium that desorbs from the column.

e The viscosity peak.

Figure 6.32 is the trace obtained when a helium sample is introduced into a hydrogen carrier gas. Hydrogen is more strongly adsorbed than helium. The trace shows five peaks. The first peak is the injection peak. When the helium band enters the column, the concentration of hydrogen within the band becomes less than for pure carrier so hydrogen gas desorbs within the band to approach a new equilibrium. Some helium may be adsorbed but the amount is less than the amount of hydrogen desorbing and there is an increase in flow rate. The trace is then offset on the opposite side of the original baseline. The flow rate then begins to increase to its original value until the band reaches the end of the column, when there is a pause in flow as hydrogen is adsorbed to the original extent - the 'desorption peak'. The fifth peak is the viscosity effect.

Similar traces are obtained by injecting helium into nitrogen (Figure 6.33) and argon into nitrogen (Figure 6.34). Nitrogen is adsorbed more strongly than argon which is adsorbed more strongly than helium.

Figure 6.33 - The Sorption-Effect Chromatogram Produced Using a Carrier Gas (Nitrogen) which is More Highly Adsorbed than the Sample Gas (Helium)

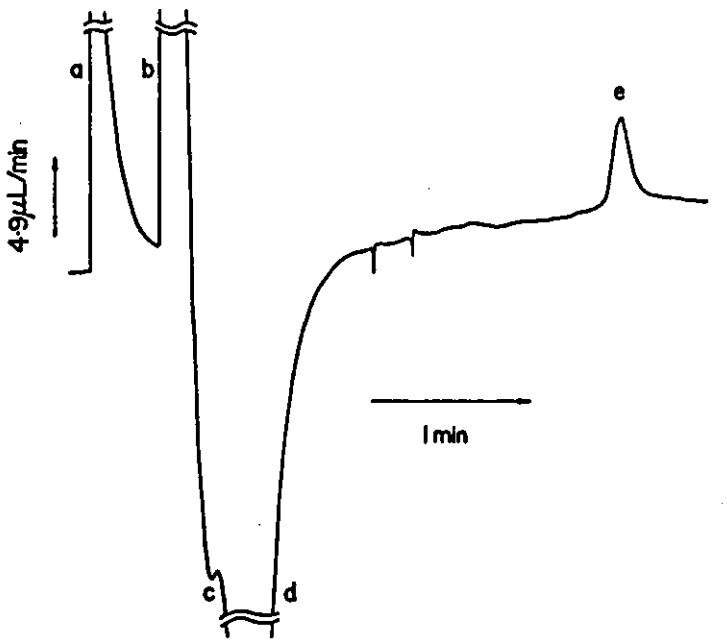

a The injection of helium into a nitrogen carrier gas.

b The desorption of more nitrogen than the amount of helium adsorbing at the start of the column.

c The net drop in flow rate followed by a gradual increase in flow rate until....

d The sample reaches the end of the column whereupon a greater quantity of nitrogen is resorbed than helium is desorbed causing a drop in flow rate.

e The viscosity peak.

The baseline offset following the adsorption peak is not due to the viscosity of the band. In the above cases, the band viscosity will be greater than that of pure carrier. A hydrogen sample in nitrogen has the effect of decreasing the gas viscosity but the baseline offset is in the same direction as before (Figure 6.35). The pressure drop down the column represents only a small fraction of the total pressure drop even at the high flow rates used to produce Figures 6.32 to 6.35 so it is unlikely that this mid-column baseline drift is caused by increased pressure drop in the column.

Figure 6.34 - The Sorption-Effect Chromatogram Produced Using a Carrier Gas (Nitrogen) which is More Highly Adsorbed than the Sample Gas (Argon)

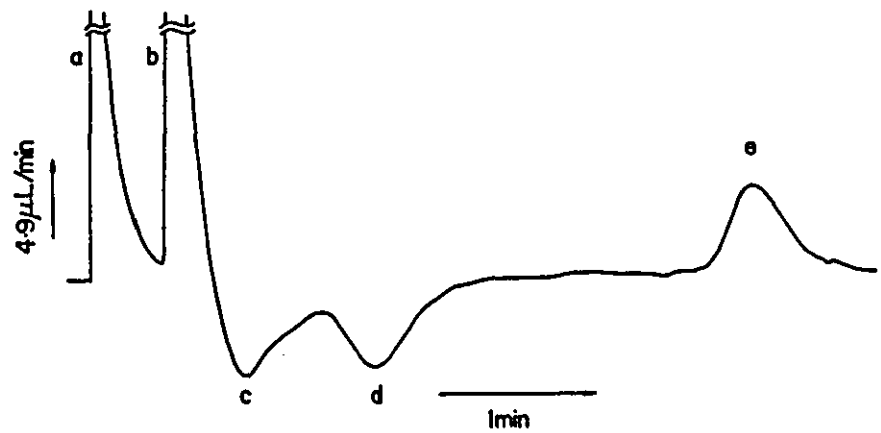

a The injection of argon into nitrogen carrier gas.

b The net increase in flow rate when the argon sample enters the column and causes a greater amount of nitrogen to desorb than the amount of argon which is adsorbed.

c The net drop in flow rate followed by a gradual increase as the sample slug passes through the column.

d The net decrease in flow as the argon desorbs from the column being replaced by a greater amount of resorbing nitrogen.

e The viscosity peak.

Figure 6.35 - The Sorption-Effect Chromatogram Produced Using a Carrier Gas (Nitrogen) which is More Highly Adsorbed than the Sample Gas (Hydrogen)

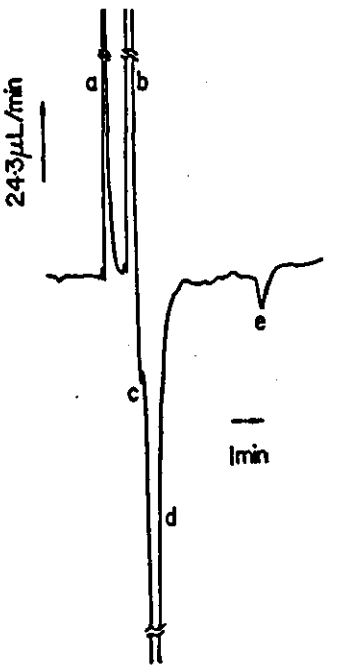

a The injection of hydrogen into nitrogen carrier gas.

b More nitrogen gas desorbing than hydrogen gas adsorbing as the sample enters the column.

c The net reduction in flow rate caused by the presence of the sample band in the column followed by a gradual increase in flow as it moves along the column.

d Nitrogen gas resorbing in a greater amount then the amount of hydrogen desorbing at the end of the column.

e The viscosity peak.

Weinstein (1961) explained that, because more carrier is eluted than sample adsorbed, the pressure in the sample band is higher than that existing normally. Because of this, he states, "carrier gas ahead of the band is forced from the column at a faster rate", and a continuous flow change takes place. No alternative explanation can be proffered at this time.

At lower flow rates, the baseline drift is much less pronounced. This is because there is time for the pressures to re-equilibrate. Use of a highly sorbed carrier gas offers a method of detecting less strongly sorbed (and non-sorbed) species which otherwise would cause only a small, if any, desorption peak.

CHAPTER SEVEN - QUANTITATIVE ANALYSIS

7.1 Peak Measurement

In conventional chromatography, the output of the detector changes when the sample species enters the detector. The detector response moves gradually from its baseline value to a maximum (or minimum) deflection and then gradually returns to the baseline value. The analyst's problem is how to determine peak size, and, how to relate the peak size to the quantity of material (Debbrecht (1985)). The size of the chromatographic peak is proportional to the amount of material contributing to the peak. Peak size can be either the peak height or the peak area. Provided that, for a given component on a given column, the ratio of the retention time to peak width remains constant, the peak height can be used as the measure of peak size. This is the simplest and easiest of the measurement techniques. There are many different ways of calculating peak area and these are listed by many authors, amongst them, Simpson (1970); Dimbat, Porter and Stross (1956); Purnell (1967); and Debbrecht (1985). Peak area can be approximated by the product of the peak height and the peak width at half the height, or, by constructing tangents to the peak at the inflection points and using the area of the constructed triangle to represent the peak area. More accurate areas are obtained by a method known as "cutting and weighing" where each peak is cut out of the chart paper and weighed. This method relies on the paper being homogenous and it does destroy the chromatogram. Apart from being a most tedious method, the area can be determined by counting of squares. Planimetry is a technique where the perimeter of the peak is traced using an instrument known as a planimeter. This method is both tedious and unreliable with small areas (Purnell (1967)). Automatic methods include the use of mechanical and electronic integrators. Debbrecht (1985) evaluates the different methods but his conclusions suggest that any particular method may be suitable under certain circumstances.

7.2 Detector Calibration (Standardisation)

In the absence of an absolute method of chromatographic analysis, there are three ways of relating peak size to the amount of sample (Debbrecht (1985)).

7.2.1 External Standard

This usually involves processing a known mixture of the sample components and obtaining the corresponding peak sizes. Unknown compositions are obtained by comparison of the known sample peak sizes with the unknown sample peak sizes. If the detected property varies non-linearly with composition the calibration mixture must be close in composition to the unknown mixture. The approximate composition can be

determined using the first calibration mixture then a second calibration mixture having this composition is made up and used to determine the sample composition more accurately.

7.2.2 Internal Normalisation

This method takes account of the fact that two different samples of the same weight may not necessarily give identical peak areas when chromatographed because the detector responds differently to different components. Here a known sample mixture is analysed and the area of each component peak evaluated. The concentration per unit area is calculated for each component. One component is then assigned a response factor of unity. The corresponding response factors for the other components are determined by dividing the relevant concentration per unit area by that of the component with the response factor of one. The unknown sample is then chromatographed and the peak areas evaluated. The original sample mixture composition can be calculated from knowing the concentration per unit area for each component. The calculated response factors should be constant whilst the operating conditions remain constant.

7.2.3 Internal Standard

This is used where only one component is of interest. A second component not included in the sample to be analysed is prepared in a standard with the component of interest and the relative response factor evaluated. A measured quantity of the second component is then added to the unknown sample. The amount of the component of interest is calculated from the area measurements resulting from the analysis and the relative response factor.

7.3 The Analysis of Sorption-Effect Chromatograms

A variety of the methods described for peak measurement have been attempted in this work. Unfortunately, there is no fundamental technique for comparison, such as the bubble flow meter in volumetric flow rate determination. Peak integration by computer can be the most accurate and is undoubtedly the most convenient.

7.3.1 Quantitative Analysis of Sorption-Effect Chromatograms

A single-component sample gas passing through a sorption-effect chromatograph produces four peaks, namely, the injection peak, the adsorption peak, the desorption peak and the viscosity peak. The desorption peak has an area which represents the volume of sample gas desorbing from the end of the column less the volume of carrier gas which resorbs as the sample gas leaves the column and the column returns to steady-state conditions. The area of the adsorption peak represents the volume of carrier gas which

is desorbed by the entry of the sample gas into the column less the volume of the sample gas which is adsorbed at the start of the column. Assuming that the equilibrium properties do not alter as the sample traverses the column then the amount of sample gas within the band which is adsorbed remains the same. This means that the area of the adsorption peak should equal that of the desorption peak. For a binary component sample gas the area of each desorption peak again represents the volume of sample gas desorbing from the end of the column less the volume of carrier gas which resorbs as each sample gas leaves the column. The adsorption peak represents the total volume of sample mixture which is adsorbed less the volume of the displaced carrier gas. In the absence of interaction, the sum of the areas of the two desorption peaks should equal the area of the adsorption peak. This gives a method of checking that all the sample gas is accounted for.

Sorption-effect chromatograms do not readily lend themselves to analysis by conventional commercial integrators.

The initial objective was to process data produced by sample injection. These chromatograms always feature both positive and negative peaks. Negative peaks can be accommodated by the off-the-shelf integrator. However, if the output of a TCD is required for comparison as well as the sorption-effect detector output, a dual-channel machine is needed and these were neither common nor inexpensive.

The secondary objective was to develop the system to process step-change data for the determination of gas-solid equilibrium isotherms (Buffham, Mason and Yadav (1985)) where both composition and flow chromatograms may be required. Software to do this would have to be specially written and the commercial integrator would have to be used in programmable mode (if it had one). For these reasons there was no advantage in using an off-the-shelf integrator.

A data-logging and data-processing system has been specifically developed for the quantitative analysis of sorption-effect chromatograms.

7.3.2 Sorption-Effect Chromatography Correction Factor

A change in flow rate due to the sorption effect occurs whenever there is a change in the net quantity of gas which is adsorbed onto the column. This happens when the sample gas enters and when the sample gas leaves the column. When the sample species enters the column the amount of carrier gas adsorbed within the sample band will be reduced because of the presence of the sample (Figure 7.1).

Figure 7.1 - How the Relative Amounts of Adsorbed Carrier and Sample Gas Vary Within the Sample Band

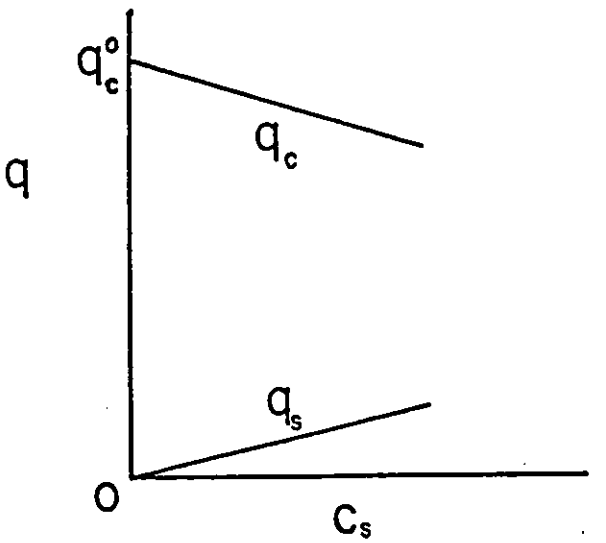

q is the molar concentration of adsorbed gas per unit of solid volume
c_s is the instantaneous molar concentration of sample species in the gas phase
subscripts c and s refer to the carrier and sample species respectively.

Prior to the introduction of the sample gas the number of moles of carrier gas adsorbed per unit of solid volume at any point in the column, q_c^o, is given by :

$$q_c^o = \left(\frac{dq_c}{dc_c}\right) c_c^o \qquad (8.1)$$

Once the sample has been introduced, the number of moles of carrier gas adsorbed at any point within the sample band, q_c, is given by :

$$q_c = \left(\frac{dq_c}{dc_c}\right) c_c \qquad (8.2)$$

where :

$\left(\frac{dq_c}{dc_c}\right)$ is the gradient of the carrier gas equilibrium isotherm,

c_c^o is the steady-state molar concentration of the carrier gas, and,
c_c is the instantaneous molar concentration of carrier gas within the sample band.

If the assumptions are made that :

the total molar density remains constant i.e. $c_c + c_s = c_c^\circ$ (constant), and,

$\left(\frac{dq}{dc}\right)$ is linear over the concentration range within the sample band (See Appendix IV), then

$$q_c = q_c^\circ - \left(\frac{dq_c}{dc_c}\right)c_s \tag{8.3}$$

where c_s is the molar concentration of the solute.

The number of moles of solute that are adsorbed at any point, q_s, is given by

$$q_s = \left(\frac{dq_s}{dc_s}\right)c_s \tag{8.4}$$

At any point in the sample band there will be less carrier adsorbed than if there were no sample gas present and some proportion of the sample gas will be adsorbed. Hence the net amount of gas that would desorb if that particular point were to return to steady-state conditions would be

$$q_{NET} = q_s + q_c - q_c^\circ = \left(\left(\frac{dq_s}{dc_s}\right) - \left(\frac{dq_c}{dc_c}\right)\right)c_s \tag{8.5}$$

If the sample band is completely enclosed in a volume V of the packed column then the net amount of gas desorbing from this volume is

$$V_{NET} = \left(\left(\frac{dq_s}{dc_s}\right) - \left(\frac{dq_c}{dc_c}\right)\right)(1-\varepsilon)\int_0^V c_s dV \tag{8.6}$$

where ε is the fractional voidage, εV is the volume of gas space and $(1-\varepsilon)V$ is the volume of packing which encloses the sample band.

Now, the total amount of sample gas is the sum of that proportion which remains in the gas phase and that which is adsorbed.

$$V_{TOT} = \varepsilon\int_0^V c_s dV + (1-\varepsilon)\left(\frac{dq_s}{dc_s}\right)\int_0^V c_s dV \tag{8.7}$$

i.e.

$$V_{TOT} = \left(\varepsilon + (1-\varepsilon)\left(\frac{dq_s}{dc_s}\right)\right)\int_0^V c_s dV \tag{8.8}$$

The area of a desorption peak represents the amount of sample gas which is desorbed less the amount of carrier gas which is adsorbed and must be multiplied by the ratio of the total amount of solute to the net change in the amount of gas adsorbed as the sample band exits the column to depict the total amount of sample species present in the sample band.

$$\frac{V_{TOT}}{V_{NET}} = \frac{\left(\varepsilon + (1-\varepsilon)\left(\frac{dq_s}{dc_s}\right)\right)\int_0^V c_s dV}{\left(\left(\frac{dq_s}{dc_s}\right) - \left(\frac{dq_c}{dc_c}\right)\right)(1-\varepsilon)\int_0^V c_s dV} \tag{8.9}$$

Now, the mean retention time of a gas (Ruthven (1984))

$$\bar{t} = \frac{L}{v}\left[1 + \left(\frac{1-\varepsilon}{\varepsilon}\right)\left(\frac{dq}{dc}\right)\right] \tag{8.10}$$

where L is the length of the column and v is the gas velocity.

Therefore, the correction factor, CF, is

$$CF = \frac{V_{TOT}}{V_{NET}} = \frac{\bar{t}_s}{\bar{t}_s - \bar{t}_c} \tag{8.11}$$

where $\bar{t}_s$ and $\bar{t}_c$ are the retention times of sample and carrier gases respectively.

If the carrier gas is non-sorbed then $\bar{t}_c$ is the gas hold-up time $\frac{L}{v}$ or $\frac{\varepsilon V}{Q}$ where Q is the volumetric flow rate through the column, V is the volume of the column. Care must be taken to use the correct values of ε, Q and V if this route is used.

Alternatively, the retention times can be evaluated using a carrier gas which is not one of the gases used in the experiments. The same temperature and pressure was used as for the experiments although how the calculated correction factor will vary with the conditions is not certain.

Each of the sample gases, and the carrier gas used in the experiments, is then injected as an individual sample into the new carrier gas. The mean retention time is then strictly the first moment of the desorption peak but peak maximum has been used here because of the difficulty in evaluating the first moment with the developed software. The correction factor for each of the resolved species can then be applied to each of the desorption peak areas to give a relative measure of the total quantity of that species present.

i.e. Peak Area = Correction Factor × Net Desorption Peak Area

The correction factor is applied to the net desorption peak. In the case where the carrier gas is less adsorbed than the sample gas, the elution of the sample band results in a surge in flow. Let the desorption peak caused by a surge in flow be regarded as a positive peak. The correction factor will also be positive because the retention time of the carrier gas is less than that of the sample gas.

Consider how the correction factor varies with the carrier gas retention time :

Correction Factor (equation 7.10) $\quad CF = \frac{\bar{t}_s}{\bar{t}_s - \bar{t}_c}$

When $\bar{t}_s \geq \bar{t}_c$

$$1 \leq CF \leq \infty$$

When $\bar{t}_s \leq \bar{t}_c \leq 2\bar{t}_s$

$$-\infty \leq CF \leq -1$$

When $\bar{t}_c \geq 2\bar{t}_s$

$$-1 \leq CF \leq 0$$

In physical terms, if the sample is very highly adsorbed and the carrier gas is non-sorbed ($\bar{t}_s \gg \bar{t}_c$) then $CF \rightarrow 1$ and the desorption peak approaches being a direct measure of the number of moles of that sample species present. This was postulated by Buffham, Mason and Meacham (1986).

If the sample species and the carrier gas are adsorbed to an equal extent ($\bar{t}_s = \bar{t}_c$) then $CF = \infty$. In terms of the sorption effect, this situation results in there being no flow change when the sample gas elutes from the column : there is no desorption peak.

When the sample species is less adsorbed than the carrier gas ($\bar{t}_c > \bar{t}_s$), a negative peak results from the elution of the sample species. This peak is a measure of the number of moles of carrier gas being resorbed less the number of moles of sample gas being desorbed at the end of the column and in this case is a reduction in flow. The correction factor is negative. When $\bar{t}_c = 2\bar{t}_s$ the desorption peak is negative but the peak area represents the total number of moles of sample species present ($CF = -1$).

Now,

$$\frac{\partial CF}{\partial t_s} = \frac{-t_c}{(t_s - t_c)^2} \tag{8.12}$$

$$\frac{\partial CF}{\partial t_c} = \frac{-t_s}{(t_s - t_c)^2} \tag{8.13}$$

In practical terms this means that each sample gas should ideally have a retention time which differs by as much as possible from that of the carrier gas to ensure that errors in determining the retention times have as little as possible effect on the value of the correction factor. The rate of change of the correction factor with small errors in the retention times will be low when the denominator has a high value.

7.4 Data-Logging Hardware

The system is composed of a differential input interface (CIL Model PCI1281) linked via an RS232 port to the RS423 port of a BBC Master 128 computer (Figure 7.1). The interface receives the output voltage from the DPT and converts it into a number in the range -32768 to +32768 (i.e. 16 bit resolution). The DPT output is also logged on a conventional chart recorder. There are sixteen input channels (which could be read simultaneously) configured as follows :

channels 0 - 7 ± 100mV
channels 8 - 11 ± 1V
channels 12 - 15 ± 5V

In addition the interface contains 32K of memory for data and program storage.

7.5 Data-Logging Software

There are three main programs :

interface initialisation
data recovery
data processing.

These are accessible via a menu program. Before the computer can run the data-processing program, the available memory must be expanded by using "Basic 128" and a screen dump routine must also be loaded. "Basic 128" is a disk-based version of BBC BASIC which allows access to the whole of the BBC Master 128 memory. This is done by 'booting up' the program disk (<shift>+<break>). The menu program is automatically loaded by boot up. All ancillary programs are listed in Appendix V.

Figure 7.2 - A Schematic Diagram of the Data-Logging System

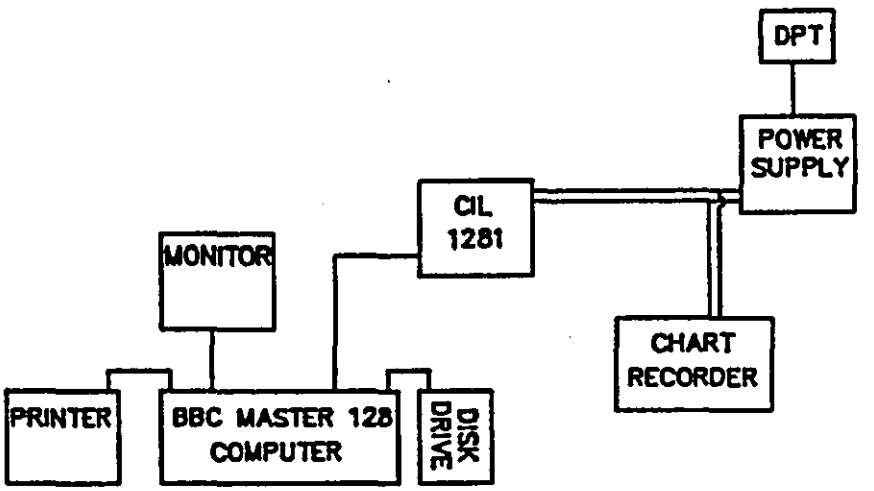

The BBC Master computer is supported by a monitor, disk drive and printer. The transducer output is amplified by the power supply unit and fed simultaneously to a conventional chart recorder and the computer interface which converts the analogue signal to a digital signal. This is fed into the computer via its RS423 port.

7.5.1 Initialisation

The interface is instructed via the computer; when to begin data collection, on which channel(s), how many data to collect, and at what time interval (0-255ms). This is known as initialising the interface. A test run in real time can be performed as a menu option to check the initialisation before an actual logging run is attempted but the computer is only acting as a chart recorder in this mode. Once a run is executed, each channel is read at the specified interval and the data is stored in the memory of the interface until the logging run is completed. The settings for the run are saved in a disk file so that the data can be recovered from the interface. Appendix VI shows a listing of the initialising program.

7.5.2 Data Recovery

Once the interface has finished collecting data, the data can be recovered from the interface memory. The data recovery program (Appendix VII) reads the run settings file, collects that amount of data and writes it to a data disk. Run settings (channel numbers, logging interval, etc) are also stored in the data file.

7.5.3 Data Processing

7.5.3.1 Data In

Data are loaded in from the previously saved disk file. Each item of data is in the range ± 32768. 32768 is added to each piece of data as it is read in from the disk file which enables the computer to store it as only two bytes of memory compared to four bytes taken up by negative numbers of this magnitude. In this way data storage space needed is halved.

7.5.3.2 Peak Area Calculation Parameters

A single component sample injection will produce up to four main peaks. At least one of these peaks will be in the opposite sense to the remainder. Which peaks are negative and which are positive depends on which channel the sample is injected into and the relative partition coefficients and roles of the gases involved.

The computer program (Appendix VIII) developed using the BBC Master uses five parameters to define the conditions under which a peak is found and integrated. These are :

Baseline Noise Level (B) - defines the normal level of variation between consecutive data.

Countback from Peak Start or End (H) - when a peak is discovered, the data have deviated by a sufficient amount from baseline. This parameter defines how far backwards (or forwards with asymmetric peak factor) from the detected point data are included so that the lower portion of the peak is not lost.

Asymmetric Peak Factor (L) - this parameter allows the integrator to accommodate peak leading (apf<1) and peak tailing (apf>1).

Maximum Height of a 'Noise' Peak (P) - if the peak maximum is below a set value the peak is ignored. This parameter is also used to identify and eliminate baseline spikes. If the current data is larger (or smaller) than both the previous and the next data points by an amount greater than the product of this parameter and the baseline noise level, the point is replaced by the average of the two neighbouring data points.

Data Filter Constant (F) - gives the opportunity to average data and smooth out the baseline. (0<dfc<1). With an amplified transducer signal it has been found that the data needs no filtering. The transducer can be adjusted, as is, to output up to ±7.5V over the pressure range or easily modified to give ±10V.

All these options are available via the menu options by selecting the appropriate letter. The menu is displayed at various points in the program or by pressing the escape key.

Other menu options include :

Range (R) - sets the vertical scale of the screen plot. A range of unity means that the height of the screen represents the full range of the logging channel, a range of two represents half the range of the channel, etc, etc.

Vertical Position of the Trace (Z) - the position of the trace can be changed from its intended default position of halfway up the screen.

Window (W) - this option allows the integrator to select a portion of the trace, by defining start and finish times, and process it individually.

Change Channel (X) - if more than one channel is logged, each is processed separately. Channels are renumbered in sequence for computer processing, beginning at channel 0. For instance, if channels 0, 8 and 15 are logged on the interface they become channels 0,1 and 2 in the computer.

New Data (N) - restarts the program for a new data file.

Plot Chart on Screen (C) - data is plotted for the chosen settings on the screen. When the plot is complete there is a regular sound prompt. Pressing <H> will obtain a hard copy of the screen contents plus the integration parameters, any other key returns the user to the menu. (Note - menu option <H> is not the same).

Quit (Q) - returns the user to the menu program.

Out (O) - quits the program but retains the listing in the memory.

7.6 Peak Area Calculation

7.6.1 Criteria used by Commercial Integrators for Peak Integration (Dyson (1986))

Integration is performed in real time using the trapezoidal rule. The software compares the area of each 'slice' with its n^{th} predecessor and decides whether a peak has been found, or whether it is merely signal noise, using pre-programmed parameters. This is done by either setting a noise threshold (i.e. maximum permissible deviation from baseline value which is not a peak) or setting a maximum baseline gradient (once the slope exceeds this value a peak has been found).

Once a peak start has been identified, the area below the peak is calculated by summing the areas of the slices which make up the peak until the end of the peak is identified (by comparison with the area of a baseline slice). Obviously the peak threshold must be small enough to ensure that as little as possible of each end of the peak is missed but it must be large enough for the integrator to be able to ignore noise and slight baseline drift.

The detector signal should be set at around 5mV above the integrator zero. Littlewood (1970) tabulated the errors possible by the integrator 'zero' being above the detector baseline value. If the displacement is only 0.5% of the peak height above the baseline the error is 1.42%. He also examined the influence of the noise threshold. When the lower 5% of the peak height is excluded the error is again 1.42%.

The program can usually accommodate baseline drift, negative peaks, incomplete peak separation and small peaks superimposed on the tails of large peaks.

If sampling is too frequent, baseline noise may cause a problem. If it is too infrequent, event markers such as peak start, peak end and peak maximum, will be late.

7.6.2 How the Peak Area is determined by the Data-Processing Program

A peak is discovered when there is a significant deviation of the data from the average baseline. The program then backtracks a user-specified number of data to the real peak start. Data is now summed from this point until the difference between consecutive data is less than the noise level. The program counts forward the number of data which it counted back at the start of the peak, multiplied by the asymmetric peak factor. Altering the asymmetric peak factor allows peak tailing and peak leading to be accommodated.

The peak is designated positive or negative depending on whether the maximum is above or below the baseline. For a positive peak (Figure 7.3) the peak area (BCD) is the signal sum (ABCDE) less the trapezoidal area below the peak (ABDE). For a negative peak (Figure 7.4) the peak area (BCD) is the trapezoidal area (ABDE) less the signal sum (ABCDE). The area is in terms of the digital signal and the unit logging interval. Conversion to more useful units (for comparison with other methods) is straightforward :

Peak Area (mVs) = Peak Area × Logging Interval (ms) / 1000 × Interface Channel Range (mV) / 2^{16}

Figure 7.3 - Calculating the Area of a Positive Peak

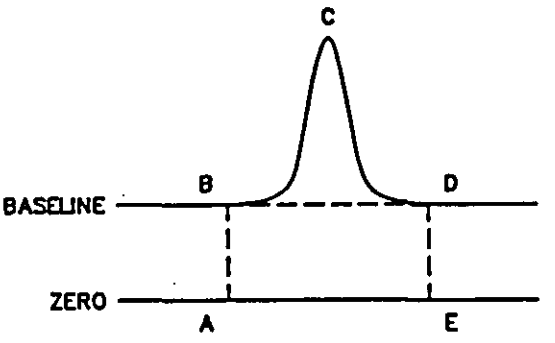

Ideally the baseline value would correspond to a differential pressure (and therefore transducer output) of zero. The zero line shown corresponds to the negative full-scale deflection of the logging channel i.e. -100mV, -1V or -5V.

Figure 7.4 - Calculating the Area of a Negative Peak

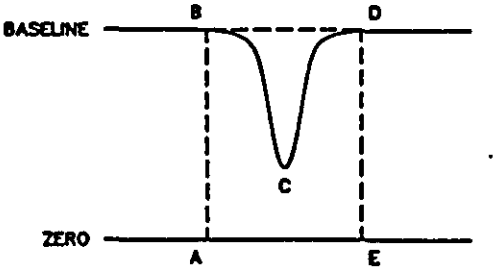

At the end of a peak area calculation, a baseline counter is activated so that at the beginning of the next peak a new average baseline can be calculated. This takes account of any long term baseline drift.

7.6.3 Processing Peaks with Known Areas

The program can be run for artificially produced calibration data to see how accurately the peak area is calculated. The program listed in Appendix X was written to produce a peak of known area which could be processed by the integrating program. The facilities to superimpose a wandering baseline, in the form of a cubic equation, and random noise are incorporated. Some measure of the errors due to baseline drift and noise can be determined using these facilities. The peak generated in the program is a good mimic of the sort of peaks produced during sorption-effect chromatography.

Figure 7.5 - Processing Peaks of Known Areas

a

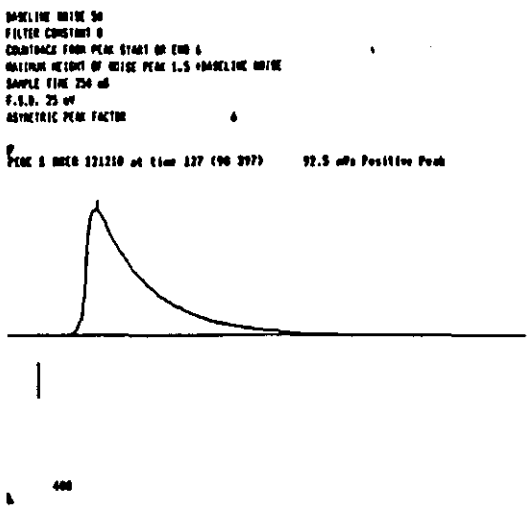

d

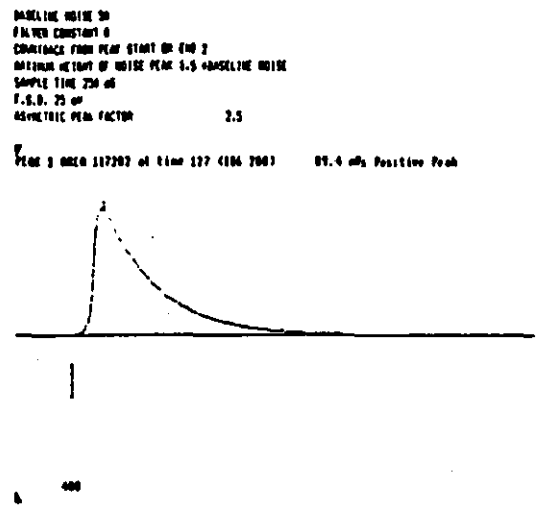

b

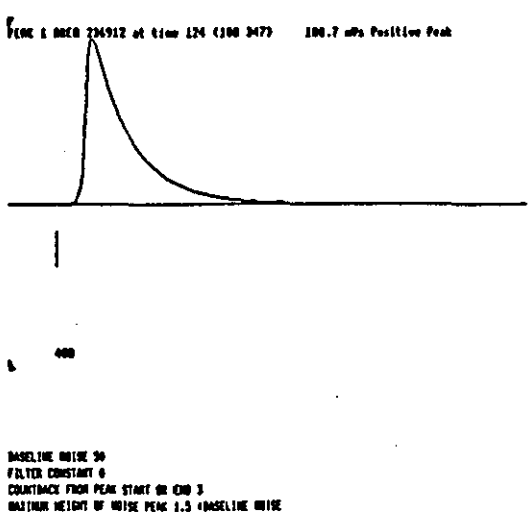

e

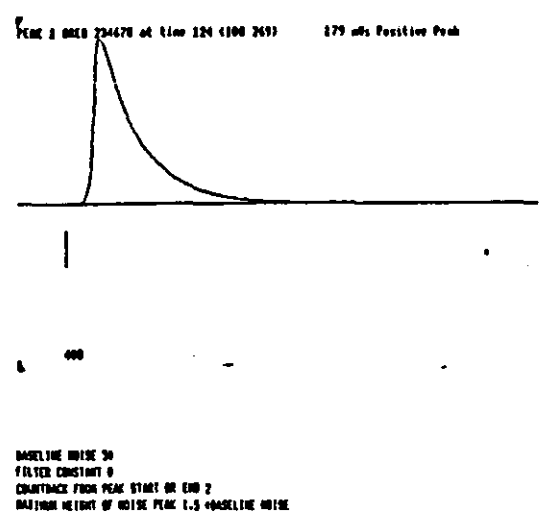

c

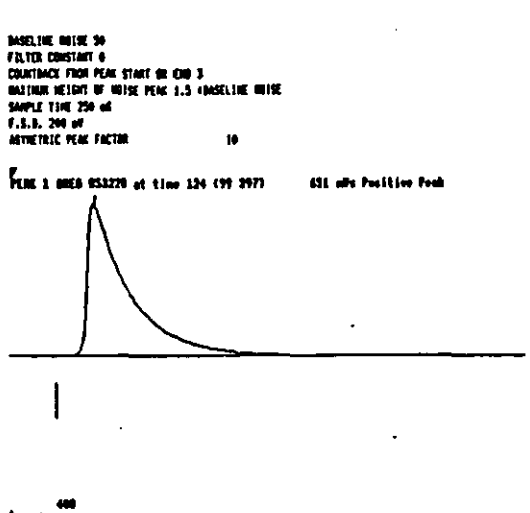

f

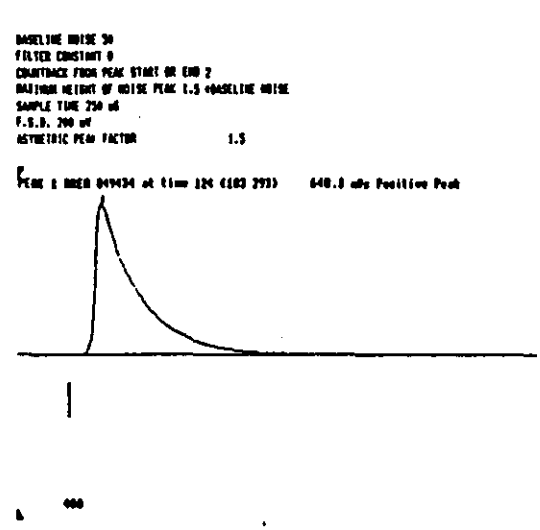

Three different peak sizes were produced. The calibration peaks have a very long tail which contributes somewhat to the total area. From a knowledge of the peak start and end, the integrating program could be encouraged to calculate the peak area exactly (Figures 7.5a, 7.5b and 7.5c). Without this knowledge there would be no reason to include such a long peak tail (refer to asymmetric peak factor). Processing the peak as a complete unknown yields Figures 7.5d, 7.5e and 7.5f. These analyses are summarised in Table 7.1.

Table 7.1 - The Processing of Peaks of Known Area

Figure	Known Peak Area	Figure	Measured Peak Area	Error (%)
7.5a	121210	7.5d	117202	-3.3
7.5b	236912	7.5e	234678	-0.9
7.5c	853220	7.5f	849434	-0.4

The middle peak was selected as being representative size. The 'tail' was cut off sooner because a tail as long as before would usually be lost in the baseline. The effect of random noise and baseline drift was investigated.

Four parameters A,B,C and D are used to superimpose baseline drift and random noise on the calibration peak. Baseline drift is of the form

$$Ax + Bx^2 + Cx^3$$

and D is a multiplication factor for random noise.

For three different noise values, data was generated to see over what range the peak size varied. Data with baseline drift was also generated and processed. Table 7.1 shows the variation of the calibration peak area. Whilst the generated peak is always the same, its area changes with drift and noise. For the peaks with random noise superimposed, several peaks were generated for the same noise factor, and an average value calculated, and one of these was processed (columns 5,6,7 and 8). For the peaks without random noise (D=0) the area generated was always the same.

Peak start is marked by a vertical line to the left of the peak maximum. Peak end is marked with a vertical line half the height of the peak start marker. The accuracy of the integration can only be judged by how well the area enclosed by a line drawn between

Table 7.2 - The Effect on Analytical Accuracy of Random Noise and Baseline Drift

A,B,C,D	Mean Area	σ_{n-1}	Difference of Mean from Standard* (%)	Test Area	Measured Area	Error from test area (%)	Error from standard area	Peak Height / Noise
0,0,0,0	233702*	-	-	233702	234678	+0.4	+0.4	-
0,0,0,100	234667	4517	+0.4	233494	234142	+0.3	+0.2	19.0
0,0,0,200	235120	9188	+0.6	240602	232047	-3.6	-0.7	11.9
0,0,0,300	230386	9064	-1.4	249718	237641	-4.8	+1.7	14.3
1,1,1,0	233331	-	-0.2	233331	230266	-1.3	-1.5	-
10,10,10,0	229517	-	-1.8	229517	227814	-0.7	-2.5	-

the peak start and end matches the area that the analyst thinks should be included. The line is extended beyond these two points and should coincide with the baseline before and after the peak ends.

The error between the known area and what was judged to be a good analysis was up to 1.7% for the noisiest signal. For the medium noise data the error was 0.7%. Appendix XI contains the computer analyses for the calibration peak data.

7.6.4 BBC Integrating Program versus Shimadzu C-R3A Integrator

Both the data-logging system and the Shimadzu integrator were connected to a chromatograph set up to examine the water content of glacial acetic acid. The printout of the Shimadzu was compared to the results obtained via the developed system.

The Shimadzu finds up to four peaks on each run. Only the two later peaks, the water peak and the acid peak respectively, were integrated using the developed software. The first two were deemed to be too small to yield any worthwhile results.

A line was fitted to each set of data in Table 7.3 yielding the following equations (y is the area calculated by the BBC program, x, the area calculated by the Shimadzu. The Shimadzu prints out the area in units of μVs - these were rounded off into mVs.

Water Peak $y = 0.987x - 0.131$

Acid Peak $y = 0.990x + 0.791$

According to this treatment the areas agree to around one per cent.

Table 7.3 - Peak Integration by Two Different Methods

	Area of Acid Peak (mVs)		Area of Water Peak (mVs)	
Run Number	C-R3A	BBC	C-R3A	BBC
AC05	8520	8423	27.5	27.2
AC9	8677	8594	63.8	64.4
AC10	8692	8573	55.4	55.4
AC11	9100	9052	106.2	104.1
AC12	6292	6218	21.8	20.4
AC13	6599	6530	17.2	14.2
AC14	7832	7698	18.3	17.9
AC15	7008	6918	27.5	27.6
AC16	6556	6499	17.5	20.0
AC17	8773	8622	13.8	14.0
AC18	7087	7000	13.5	14.0

The computer analyses for this data are given in Appendices XII and XIII.

7.7 Comparison of the Amount of Gas Adsorbed at the Start of the Column and the Amount Desorbed at the End of the Column

7.7.1 Sorbed Material Balance on the Column

As was reasoned out earlier (Section 7.3.2), if the major contribution to the flow perturbations at the beginning and end of the column is caused by changes in the amount of sorbed material then the area of the adsorption peak should equal the area of the desorption peak (assuming that the equilibrium properties do not change along the column).

Table 7.4 shows the calculated areas for the adsorption and desorption of hydrogen in a helium carrier gas. The areas have been calculated using a planimeter on the chart trace and also by processing data collected using the developed system. The area calculated using the planimeter is in conventional units of area e.g. cm^2. Conversion to mVs is straightforward.

Peak Area (mVs) = Peak Area (cm^2) x Chart Range (mV) / [Full Scale Deflection (cm) x Chart Speed (cm/s)]

Figure 7.6 is an example of the chart recorder output for a hydrogen sample.

Where the sample sizes are the same, the areas have been averaged and the ratio of the average size of the desorption peak to the average size of the adsorption peak calculated. If the ratio is close to unity the areas can be considered to be the same.

Figure 7.6 - A Flow Chromatogram of a Hydrogen Sample in Helium Carrier Gas Where the Predominant Cause of the Adsorption and Desorption Peaks is the Sorption Effect

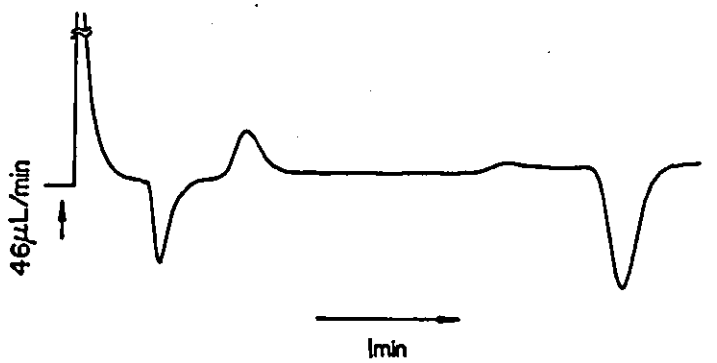

For the planimeter areas the ratios are 0.886 and 1.028. A difference of 2.8% is not unreasonable but an 11.4% difference is not acceptable. The discrepancy could be a reflection on the quality of the chromatograms from which the data was taken and/or the method of evaluating the areas. The integrating program gives the average desorption peak to be 96.6% and 102.5% of the average adsorption peak for the two series of samples. The integrating program gives better agreement but the first set of data raises doubts about the assumption. The computer analyses are given in Appendix XIV.

For an argon sample (Figure 7.7 and Table 7.5), the planimeter areas give ratios of 0.954 and 0.977 for the two different sample sizes whereas the integrating program gives much better agreement (0.995 and 1.008). Argon has a longer retention time than hydrogen and it is perhaps the better separation of the adsorption and desorption peaks that causes the argon data to appear better. The computer analyses are given in Appendix XV.

It can be concluded, on the basis of these results, that planimetry is not only more tedious but also a less consistent method of area calculation when compared with the developed data-logging system.

Figure 7.7 - A Flow Chromatogram of a Argon Sample in Helium Carrier Gas Where the Predominant Cause of the Adsorption and Desorption Peaks is the Sorption Effect

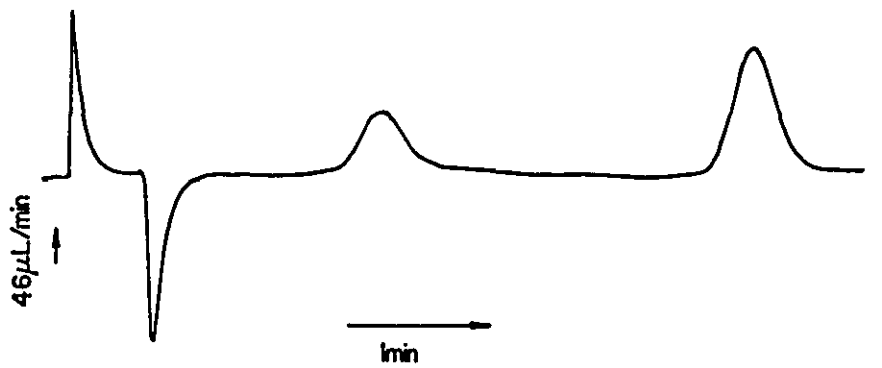

The assumption is ratified that gas sorption is the major, if not the only, cause of flow surges and pauses at either end of the column during sorption-effect chromatography.

Table 7.4 - Analyses of Hydrogen Injections into Helium Carrier Gas

Data File and Peak		Planimeter Area (mVs)	Integrating Program Area (mVs)
HHE911	a	195.6	183.1
	d	167.3	167.5
HHE1011	a	213.8	187.8
	d	196.1	183.3
HHE1012	a	200.2	184.7
	d	174.7	178.3
HHE1013	a	206.1	184.4
	d	179.6	181.9
HHE1014	a	196.6	182.7
	d	186.9	180.9
HHE1015	a	200.7	184.0
	d	170.5	177.1
Average	a	202.2	184.5
	d	179.2	178.2
	d/a	0.886	0.964
HHE1111	a	164.2	160.4
	d	168.1	153.4
HHE1112	a	167.0	157.6
	d	162.9	164.2
HHE1113	a	169.6	164.4
	d	166.3	166.3
HHE1114	a	156.6	158.8
	d	162.7	153.8
HHE1115	a	167.4	161.3
	d	188.3	185.5
Average	a	165.0	160.5
	d	169.7	164.6
	d/a	1.028	1.025

Table 7.5 - Analyses of Argon Injections into Helium Carrier Gas

Data File and Peak		Planimeter Area (mVs)	Integrating Program Area (mVs)
AHE311	a	-	363.1
	d	-	370.0
AHE312	a	358.2	358.4
	d	336.4	350.7
AHE313	a	368.4	364.6
	d	366.2	369.0
AHE511	a	371.0	355.8
	d	348.0	340.8
AHE512	a	367.7	365.5
	d	347.0	368.0
Average	a	366.3	361.5
	d	349.4	359.7
	d/a	0.954	0.995
AHE513	a	451.0	449.3
	d	448.1	451.1
AHE514	a	471.1	445.5
	d	452.8	451.2
Average	a	461.0	447.4
	d	450.5	451.2
	d/a	0.977	1.008

7.7.2 Sorbed Material Balance for Binary Gas Mixtures on the Column

Three known mixtures of hydrogen and argon were prepared using the gas mixing system (Appendix I) and chromatographed.

The three sorption peaks, adsorption, hydrogen desorption and argon desorption (Figure 7.8), were integrated and the areas averaged for all analyses of the same mixture (Table 7.6). The sum of the average desorption peak areas agrees with the average adsorption peak area to within 1% for all three sample sizes. Furthermore, for each individual analysis, the discrepancy is not more than 2%. However, whilst the total amount of adsorbed material matches the total amount of desorbed material very well, the individual desorption peak areas differ by an appreciable amount for analyses 7 and 8. The computer analyses are given in Appendix XVI.

Figure 7.8 - A Flow Chromatogram of a Hydrogen and Argon Sample Mixture in Helium Carrier Gas Where the Predominant Cause of the Adsorption and Desorption Peaks is the Sorption Effect

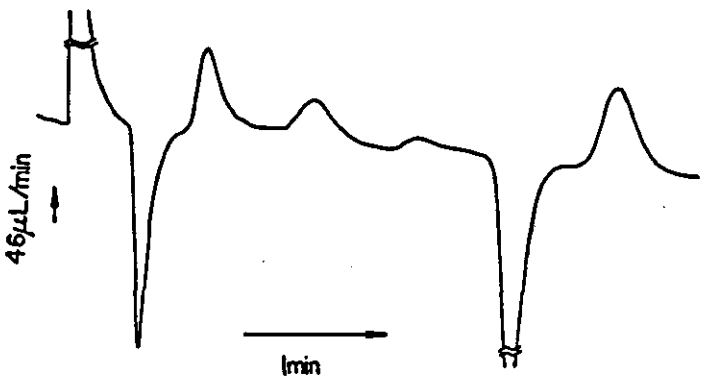

These calculated areas represent amounts of sorbed gas and not the total quantity of the component present (because some of each sample component remains in the gas phase) so the correction factor must be applied to these results to find the sample composition.

Table 7.6 - Calculated Sorption Peak Areas for Binary Mixtures

Data File	Peak	Area (mVs)
HAHE1811	a	294.8
	d_{H_2}	72.5
	d_{Ar}	222.5
	$\left(\frac{d_{H_2}+d_{Ar}}{a}\right)$	(1.001)
HAHE1812	a	286.8
	d_{H_2}	72.8
	d_{Ar}	217.7
	$\left(\frac{d_{H_2}+d_{Ar}}{a}\right)$	(1.013)
HAHE1813	a	302.6
	d_{H_2}	81.4
	d_{Ar}	222.1
	$\left(\frac{d_{H_2}+d_{Ar}}{a}\right)$	(1.003)
Average	a	294.7
	d_{H_2}	75.6
	d_{Ar}	220.8
	$\left(\frac{d_{H_2}+d_{Ar}}{a}\right)$	(1.006)

HAHE1814	a	273.8
	d_{H_2}	92.6
	d_{Ar}	179.5
	$\left(\frac{d_{H_2}+d_{Ar}}{a}\right)$	(0.994)
HAHE1815	a	277.5
	d_{H_2}	93.1
	d_{Ar}	181.7
	$\left(\frac{d_{H_2}+d_{Ar}}{a}\right)$	(0.990)
HAHE1816	a	277.4
	d_{H_2}	93.2
	d_{Ar}	185.6
	$\left(\frac{d_{H_2}+d_{Ar}}{a}\right)$	(1.005)
Average	a	276.2
	d_{H_2}	93.0
	d_{Ar}	182.3
	$\left(\frac{d_{H_2}+d_{Ar}}{a}\right)$	(0.997)
HAHE1817	a	255.1
	d_{H_2}	121.8
	d_{Ar}	136.8
	$\left(\frac{d_{H_2}+d_{Ar}}{a}\right)$	(1.014)
HAHE1818	a	240.7
	d_{H_2}	90.2
	d_{Ar}	150.6
	$\left(\frac{d_{H_2}+d_{Ar}}{a}\right)$	(1.000)
Average	a	247.9
	d_{H_2}	106.0
	d_{Ar}	143.7
	$\left(\frac{d_{H_2}+d_{Ar}}{a}\right)$	(1.007)

7.8 Calculation of the Original Sample Mixture Composition using Correction Factors

Using nitrogen as a carrier gas, under the same conditions as experimental runs HAHE1811-HAHE1818 were performed, samples of helium, hydrogen and argon were injected separately and their respective retention times determined based on the time of the peak maxima. The computer analyses are given in Appendix XVII. The correction factors for hydrogen in helium and argon in helium under these experimental conditions was then calculated (Table 7.7). How the correction factors vary with the conditions has not been determined.

Table 7.7 - Calculation of Correction Factors

Data File	Time of Peak Maximum (units of 250ms)		Retention Time	Correction Factor (in helium)
	d	a		
HEN34A	247	179	68	-
HEN34B	239	171	68	-
H2N34A	261	172	89	4.2381
H2N34B	268	179	89	4.2381
AN34A	398	173	225	1.4331
AN34B	392	169	223	1.4387
				(av. 1.4359)

These correction factors are then applied to the average desorption peak areas calculated earlier (Table 7.8).

The mixing system calibration data is given in Appendix I.

Table 7.8 - Calculation of the Original Sample Mixture Composition

Data File	Peak	Desorption Peak Area (mVs)	Corrected Peak Area (mVs)	Calculated Mixture (mole fraction)	Actual Mixture (mole Fraction)
HAHE1811-3	H_2	75.6	320.4	0.503	0.4907
	Ar	220.8	317.0	0.497	0.5093
HAHE1814-6	H_2	93.0	394.1	0.601	0.5814
	Ar	182.3	261.8	0.399	0.4186
HAHE1817-8	H_2	106.0	449.2	0.685	0.6864
	Ar	143.7	206.3	0.315	0.3136

CHAPTER EIGHT - SUMMING UP

The objective of this work has been to develop an understanding of the changes in volumetric flow rate that occur during chromatography so that flow rate measurements can be used as the basis of an analytical method. During the course of the experiments it was found that the sorption effect is not the only cause of changes in the flow rate during chromatography; other effects, both random and systematic, are superimposed on the chromatogram.

Random surges in atmospheric pressure were observed to cause rapid fluctuations in flow rate. This was found to be because of volume distribution imbalances between the two flow channels of the chromatograph so that an external pressure fluctuation causes a pressure surge to be propagated through the two sides of the chromatograph at different rates and to affect the DPT at different times. The sensitivity of the apparatus to external pressure fluctuations was reduced by isolating the system from the atmosphere by using modified back-pressure regulators and by attempting to make both flow channels as similar to each other as possible.

The source of baseline meandering was found to be the effect of temperature fluctuations both inside and outside the 'isothermal' oven. The effects of ambient temperature fluctuations were satisfactorily minimised by insulating all parts of the system outside the oven. Protecting the chromatographic columns from temperature fluctuations within the Pye oven proved to be a more difficult task and several commercial chromatographic ovens were tested against the performance of the Pye oven and in some cases modified in attempts to reduce the temperature variations which existed within all the ovens (regardless of the manufacturers' claims). The reported chromatographic experiments were performed using a leak-proofed Pye 104 oven with a temperature control system which uses the heat generated by the friction of the fan blades to maintain the air temperature. A prototype 'isothermal oven' was built and developed but this work was abandoned at the point where the limits of the oven's performance had been reached and recommendations for an improved design could be made.

Four events which cause peaks on the baseline have been reported. These are, in chronological order, the injection of the sample, the entry of the sample into the column, the exit of the sample from the column and the passage of the sample through the capillary flowmeter. In the preliminary experiments the sample was introduced immediately upstream from the column resulting in the injection peak and the adsorption peak being superimposed upon each other to some extent. The capillary flowmeter was positioned immediately downstream from the column so the desorption peak and the viscosity peak

were also superimposed in part. Lengths of tubing were connected between the point of injection and the column and between the column and the flowmeter to act as delay lines and isolate the peaks which were previously superimposed. The injection peak then gave an indication of the size of sample. If the sample gas is at a higher pressure than the carrier gas at the injection point then the introduction of the sample via a sample valve causes a pressure surge. If the pressures are identical there will be no flow disturbance when the sample valve is switched and a lower sample pressure will cause a temporary decrease in flow when the sample valve is switched. The adsorption and desorption peaks indicate whether the sample gas is adsorbed more or adsorbed less than the carrier gas. A flow pause as the sample gas enters the column indicates that the sample gas is more adsorbed than the carrier gas. There is a flow surge when the more highly sorbed sample gas desorbs from the column to be replaced by the adsorption of a smaller amount of carrier gas. If both carrier and sample gas are adsorbed to the same extent there will be neither an adsorption peak as the sample gas enters the column nor a desorption peak as the sample gas leaves the column. Where the carrier gas is more highly sorbed than the sample gas, more carrier gas will desorb at the start of the column then sample gas adsorbs and the entry of the sample species into the column will be marked by a flow surge. When this sample gas leaves the column there will be a flow pause as the amount of sample gas previously adsorbed is replaced by a greater amount of carrier gas. The direction of the viscosity peak is determined by how the viscosity of the sample/carrier gas mixture varies with composition. The pressure drop down the flow-detecting capillaries will be increased if the gas mixture viscosity increases and an apparent increase in flow is indicated on the chromatogram. Similarly, if the gas mixture viscosity is decreased, a decrease in flow is indicated.

The distribution of pressure drop in the system was found to be a possible cause of error. The size of both adsorption and desorption peaks could be affected by the use of a high-pressure-drop column. During the time that a band of different viscosity gas remains in a high-pressure-drop column, the pressure profile in the system is modified and the peaks produced are either larger or smaller than they would be if there were no viscosity effect in the column. The solution was to find a column which would still perform the desired separation but with a low enough pressure drop to have relatively little effect on the peak areas. The band of gas with viscosity different from that of the carrier gas was also found to cause minor flow perturbations as it passed through regions of changing cross-sectional area. In the main, these regions were identified and then eliminated. This effect did throw up a method for measuring volumetric flow rate where other ways i.e. the bubble flowmeter would not be suitable. The method uses the time

taken for a tracer gas to travel through a measuring volume. Entry and exit from the measuring volume were marked by a flow deviation due to the change in cross-sectional area. A TCD was used to provide an abrupt change in cross-sectional area and also to provide event markers for comparison. Three different flowmeter volumes (100mL, 50mL and 29mL) were used to measure three different volumetric flow rates (90mL/min, 65mL/min and 40mL/min). The time of flight of the tracer gas was determined by taking the first moments of each of the event markers and also by taking the time of the peak maximum. The flowmeter volume was then calculated using the volumetric flow rate as measured using a bubble flowmeter and the flow rates then back calculated. The calculated flow rates were found to agree best with the measured flow rate when the flowmeter volume was 50mL and the time-of-peak-maximum measurements were used. The results calculated from the TCD output for this case were better than those from the DPT output although all agreed to within one per cent. The method is subject to an error proportional to the volumetric flow rate to be measured because of the pressure developed across the flow-detecting capillary but no obvious trend could be discerned from the results.

With no columns in the system and at very high flow sensitivity, flow rate oscillations were observed which are attributable to the passage of a band of gas with density different from that of the carrier gas. These oscillations were caused in the coiled, delay lines and were of very small magnitude and consequently do not affect the adsorption and desorption peak areas.

A computer-based data-logging and peak processing system was developed for the quantitative analysis of the sorption-effect chromatogram. This system was also used to evaluate the first moments of peaks and the times of peak maxima during the volumetric flow rate measurement experiment. The system was tested against a commercially available system. Peak areas calculated by the two different systems agreed to within one per cent but the newly developed system is far more versatile in the context of sorption-effect chromatography. Data collected for single component samples were processed to test the hypothesis that the adsorption peak area equals the of the desorption peak area. This would be the case if the peaks were solely caused by the sorption effect and the equilibrium relationship remains constant throughout the column. These results were compared to peak areas measured by using a planimeter. The ratio of the average desorption peak area to the average adsorption peak area for two different sets of data generated using a hydrogen sample in helium carrier gas was 0.964 and 1.025 using the computer analyses and 0.886 and 1.028 for the planimeter based areas. For an argon sample in helium carrier gas, the computer analyses yielded average desorption peak

area to adsorption peak area ratios of 0.995 and 1.008 for the two sets of data, and the planimeter, 0.954 and 0.977. The computer generated areas for the single component sample experiments showed agreement to within 4% for the hydrogen sample and 1% for the argon sample. Based on these results it was assumed that the sorption effect was the sole cause of the flow deviations which form the adsorption and desorption peaks. The sum of the average desorption peak areas for binary mixtures of hydrogen and argon was calculated to within one per cent of the respective average adsorption peak areas. The peak areas represent a net volume of gas adsorbing or desorbing and a correction factor must be applied to calculate the actual quantity of sample gas present. The correction factor is the ratio of the total amount of sample gas present to the amount of sample gas which is adsorbed by the column less the amount of carrier gas which is desorbed by the presence of the sample gas and can be expressed in terms of the retention times of the carrier and sample species. These can be evaluated using a carrier gas which is not one of the experimental gases and measuring the retention time of each of the experimental gases in that carrier gas under the same experimental conditions. The original composition for three different sample mixtures was determined using the calculated correction factors. The measured mixture compositions do not differ by more than two per cent from the actual mixture compositions. This discrepancy could be attributed to the resolution with which the retention times used to calculate the correction factors were determined. The retention times are accurate to the nearest 250 milliseconds and this is enough to cause the error in the calculated composition assuming that there is negligible error on the peak areas. This assumption is justified by the good agreement of the adsorption peak area with the sum of the desorption peak areas. The correction factor for hydrogen in helium is very sensitive to variation in the retention times because the retention times of hydrogen and helium are so similar. The correction factor for argon in helium is less susceptible to errors in the retention times because argon has an appreciably longer retention time to that of helium.

This technique has been developed specifically for the separation of hydrogen and argon in a helium carrier gas. The columns and delay lines have been tailored for the separation of hydrogen and argon in helium carrier gas and these are not necessarily suitable for another separation. The length of the delay line upstream of the column is determined by the carrier gas flow rate and it is intended to allow the pressure to equilibrate after sample injection and before the sample gas reaches the column. The downstream delay line was made long enough for all the resolved sample bands to emerge

from the column before the earliest band reaches the capillary flowmeter to produce a viscosity peak. The method would be more versatile if the column and delay lines did not have to be customized for each separation.

The error in calculating the original sample mixture composition can attributed to the resolution with which the retention times of the gases involved are measured. The computer interface can be programmed to collect data at intervals of 1ms to 255ms so the retention times could easily be measured with greater accuracy. The retention times were evaluated using the same column pressure drop as for the sample runs and the resultant correction factors enabled the sample compositions to be calculated with acceptable accuracy. No work was undertaken to investigate how the correction factors vary with the conditions under which the retention times are measured.

Gases which are not very strongly adsorbed such as hydrogen only cause relatively small desorption peaks which are more difficult to integrate accurately. Additionally, the correction factor for a weakly sorbed gas in a weakly sorbed carrier gas will be relatively large and sensitive to errors in the retention time measurements. The area of the desorption peak would be larger if a highly sorbed carrier gas were used for a weakly sorbed sample gas. The desorption peak would then be the net result of an amount of sample gas desorbing at the end of the column as a larger quantity of carrier gas is resorbed. Provided that the carrier gas retention time is greater than twice the retention time of the sample gas the correction factor will lie between 0 and -1 and the correction factor will be less sensitive to errors in the retention time evaluation procedure. Weakly sorbed samples could be analysed more accurately using a highly sorbed carrier gas if a way could be found to eliminate the baseline drift associated with highly sorbed carrier gases.

The sensitivity of the detector would be increased by reducing the sensitivity of the chromatographic columns to the effects of thermal noise within an isothermal oven. Improvements could indubitably be made to the performance of the prototype oven which was developed during the course of this project and recommendations for design modifications have been suggested.

CHAPTER NINE - PUBLISHED WORK

The following papers concerning some of the work reported in this thesis have been published.

"Sorption-Effect Chromatography"
Buffham,B.A.; Mason,G.; Meacham,R.I. *J. Chrom. Sci.* 1986,24,265-269.

Abstract

In gas chromatography, sorption of gas species by the stationary phase causes changes in flow rate and pressure (the "sorption effect"). By following these changes with a suitable instrument, a chromatogram can be drawn that shows the quantity of gas injected and the net quantity sorbed as separate peaks in addition to peaks corresponding to the resolved species. Modifications to a standard chromatograph are described that allow these measurements to be made while leaving the chromatograph able to function normally. The modifications include a sorption-effect detector in the form of a sensitive differential capillary flow meter. Examples of sorption-effect chromatography are reported.

"The Role of Viscosity in Sorption-Effect Chromatography"
Meacham,R.I.; Buffham,B.A.; Mason,G. *J. Chrom. Sci.* 1990,28,34-41.

Abstract

In sorption-effect chromatography, a band of sample gas is detected when it enters and leaves a chromatographic column by monitoring changes in flow rate. The differential capillary flow meter that has been used to detect the changes caused by gas adsorption also responds to changes in composition. In previous work on sorption-effect chromatography, the results obtained when a hydrogen sample gas was injected into helium carrier gas were inexplicable. In comparison, it seemed possible to explain results obtained using argon or nitrogen in helium. In the present work, analyses are carried out with and without dead volume between the column and flow meter—with different combinations of packed columns and empty tubing—in order to determine why hydrogen should act differently. A large dead volume between the column and the flow meter splits both the inexplicable hydrogen peak and also the seemingly explicable single argon peak into two separate peaks. The explanation is that the first peak is due to the sorption effect when gas desorbs from the column and the second is caused by the changing viscosity in the flow meter as the composition changes.

CHAPTER TEN - BIBLIOGRAPHY

Adlard,E.R.; Khan,M.A.; Whitham,B.T. in *Gas Chromatography*; Scott,R.P.W. Ed.; Butterworths: London, 1960.

Amy,J.W.; Brand,L.; Baitinger,W. in *Progress in Industrial Gas Chromatography Vol. 1*; Szymanski,H.A. Ed.; Plenum: New York, 1961.

Annino,R.; Curren,J.; Kalinowiski,R.; Karas,E.; Lindquist,R.; Prescott,R. *J. Chromatogr.* **1976**,126,301-314.

Annino,R.; Voyksner,R. *J. Chromatogr.* **1977**,142,131-143.

Annino,R. *Chemtech* **1981**,482-487.

Barrer,R.M. *Zeolites and Clay Minerals as Sorbents and Molecular Sieves*; Academic, 1978.

Bevan,S.C.; Gough,T.A.; Thorburn,S. *J. Chromatogr.* **1969**,42,336-348.

Boer,H. in *Vapour Phase Chromatography*; Desty,D.H. Ed.; Butterworths: London 1957.

Bosanquet,C.H.; Morgan,G.O. in *Vapour Phase Chromatography*; Desty,D.H. Ed.; Butterworths: London, 1957.

Boucher,D.F.; Alves,G.E. *Chemical Engineers' Handbook*, 5th ed.; Perry,R.H.; Chilton,C.H. Eds.; McGraw-Hill: 1973.

Buffham,B.A. *Proc. R. Soc. London A.* **1973**,333,89-98.

Buffham,B.A. *Proc. R. Soc. London A.* **1978**,364,443-455.

Buffham,B.A.; Mason,G.; Meacham,R.I. *J. Chrom. Sci.* **1986**,24,265-269.

Buffham,B.A.; Mason,G.; Yadav,G.D. *J. Chem. Soc., Faraday Trans. 1* **1985**,81,161-173.

Chen,C.J.; Parcher,J.F. *Anal. Chem.* **1971**,43,1738-1744.

Cohen,G.H.; Coon,G.A. *Trans. ASME* **1953**,75,827-834.

Conder,J.R. *Chromatographia* **1974**,7,387-394.

Conder,J.R. *Journal of High Resolution Chromatography & Chromatography Communications* **1982**,5,397-403.

Conder,J.R.; Purnell,J.H. *Trans. Faraday Soc.* **1968**,64,3100-3111.

Conder,J.R.; Young,C.L. *Physiochemical Measurement by Gas Chromatography*; Wiley: 1979.

Coulson,J.M.; Richardson,J.F. *Chemical Engineering Volume 1*; Pergamon: 1980.

Coulson,J.M.; Richardson,J.F. *Chemical Engineering Volume 2*; Pergamon: 1980.

David,D.J. *Gas Chromatographic Detectors*; Wiley: 1974.

Debbrecht,F.J. in *Modern Practice of Gas Chromatography*; Grob,R.L. Ed.; Wiley: 1985.

Dimbat,M.; Porter,P.E.; Stross,F.H. *Anal. Chem.* **1956**,28,290-297.

Dyson,N. Presented at Loughborough University of Technology Short Course on Gas-Liquid Chromatography 1986.

Dyson,N.; Littlewood,A.B. *Anal. Chem.* **1967**(I),39,638-641.

Dyson,N.; Littlewood,A.B. *Trans. Faraday Soc.* **1967**(II),63,1895-1905.

Giddings,J.C. *J. Gas Chromatogr.* **1964**,2,167-169.

Giddings,J.C.; Kao,J.T.F.; Kobayashi,R. *J. Chem. Phys.* **1966**,45,578-586.

Goedert,M; Guiochon,G. *J. Chrom. Sci.* **1969**,7,323-339.

Goedert,M; Guiochon,G. *Anal. Chem.* **1973**,45,1180-1187.

Golay,M.J.E. *Nature* **1964**,202,489-490.

Gordon,S.M.; Krige,G.J.; Pretorius,V. *J. Gas Chromatogr.* **1964**,2,246-251.

Greene,S.A.; Moberg,M.L.; Wilson,E.M. *Anal. Chem.* **1956**,28,1369-1370.

Griffiths,J.; James,D.; Phillips,C. *Analyst* **1952**,77,897-904.

Guiochon,G.; Jacob,L. *Chromatogr. Rev.* **1971**,14,77-120.

Haarhoff,P.C.; van der Linde,H.J. *Anal. Chem.* **1965**,37,1742-5.

Horvath,C. in *The Practice of Gas Chromatography*; Ettre,L.S.; Zlatkis,A. Eds.; Wiley: 1967.

Huber,J.F.K.; Gerritse,R.G. *J. Chromatogr.* **1971**,58,137-158.

Hussey,C.L.; Parcher,J.F. *J. Chromatogr.* **1974**,92,47-54.

James,A.T. in *Vapour Phase Chromatography*; Desty,D.H. Ed.; Butterworths: London, 1957.

James,D.H.; Phillips,C.S.G. *J. Sci. Instr.* **1952**,29,362-3.

Janak,J; Novak,J. *Abhandl. Deut. Akad. Wiss. Berlin. Kl. Chem., Geol. Biol.* **1964**(6),99-104(1963); *Chem. Abstr.* **1965**,63,5250e.
See also - British Patent 1 046 162,1966; US Patent 3 354 696,1967.

Keulemans,A.I.M.; Kwantes,A.; Rijnders,G.W.A. *Anal. Chim. Acta* **1957**,16,29-39.

Krige,G.J.; Pretorius,V. *Anal. Chem.* **1965(I)**,37,1186-1190.

Krige,G.J.; Pretorius,V. *Anal. Chem.* **1965(II)**,37,1191-1195.

Liley,P.E.; Gambill,W.R. in *Chemical Engineers' Handbook*, 5th ed.; Perry,R.H.; Chilton,C.H. Eds.; McGraw-Hill: 1973.

Littlewood,A.B. *Gas Chromatography*, 2nd ed.; Academic: 1970.

Martin,A.J.P.; James,A.T. *Biochem. J.* **1956**,63,138-143.

Martin,A.J.P.; Synge,R.L.M. *Biochem. J.* **1941**,35,1358-1368.

Mason,G.; Buffham,B.A. Presented at the Third International Conference on Fundamentals of Adsorption, Sonthofen, Bavaria, May 1989.

McWilliam,I.G. *J. Appl. Chem.* **1959**,9,379-388.

Meacham,R.I.; Buffham,B.A.; Mason,G. *J. Chrom. Sci.* **1990**,28,34-41.

Munari,F.; Trestianu,S. *J. Chomatogr.* **1983**,279,457-472.

Munns,G.W.; Frilette,V.J. *J. Gas Chromatogr.* **1965**,3,145-6.

O'Brien,M.J. in *Modern Practice of Gas Chromatography*; Grob,R.L. Ed.; Wiley: 1985.

Perry,R.H.; Chilton,C.H. *Chemical Engineers' Handbook, 5th ed.*; McGraw-Hill: 1973.

Peterson,D.L.; Helfferich,F. *J. Phys. Chem.* **1965**,69,1283-1293.

Purnell,H. *Gas Chromatography*; Wiley: 1967.

Rathor,M.N.; Buffham,B.A.; Mason,G. *J. Chromatogr.* **1987**,404,33-40.

Rathor,M.N.; Buffham,B.A.; Mason,G. *J. Chromatogr.* **1988**,445,37-48.

Ruthven,D.M. *Principles of Adsorption and Adsorption Processes*; Wiley: 1984.

Schettler,P.D.; Giddings,J.C. *Anal. Chem.* **1965**,37,835-840.

Schmauch,L.J. *Anal. Chem.* **1959**,31,225-230.

Schmauch,L.J.; Dinerstein,R.A. *Anal. Chem.* **1960**,32,343-352.

Scott,R.P.W. *Anal. Chem.* **1964**,36,1455-1461.

Sewell,P.A.; Stock,R. *J.Chromatogr.* **1970**,50,10-18.

Simpson,C. *Gas Chromatography*; Kogan Page: 1970.

Testerman,M.K.; McLeod,P.C. U.S. Patent 3 144 762,1964(I).
See also - *Chem. Eng. News* **1961**,39,49.

Testerman,M.K.; McLeod,P.C. U.S. Patent 3 144 767,1964(II).

Touloukian,Y.S.; Saxena,S.C.; Hestermans,P. *Thermophysical Properties of Matter : The TPRC Data Series Volume 11 - Viscosity*; IFI/Plenum 1975.

Tranchant,J. in *Practical Manual of Gas Chromatography*; Tranchant,J. Ed.; Elsevier: 1969.

Valentin,P.; Guiochon,G. *J. Chrom. Sci.* **1976**(I),14,56-63.

Valentin,P.; Guiochon,G. *J. Chrom. Sci.* **1976**(II),14,132-139.

Van de Craats,F. *Gas Chromatography*; Desty,D.H. Ed.; Academic: New York, 1958.

Van Deemter,J.J.; Zuiderweg,F.J.; Klinkenberg,A. *Chem. Eng. Sci.* **1956**,5,271-289.

Van Swaay,M. *J.Chromatogr.* **1963**,12,99-103.

Waters,A.W. *Aust. J. Instr.* **1976**,32,121-125.

Weast,R.C.; Astle,M.J. *CRC Handbook of Chemistry and Physics, 63rd ed.*; CRC, Boca Raton, Florida, 1982.

Weinstein,A. *Anal. Chem.* **1960**,32,288-290.

Weinstein,A. *Anal. Chem.* **1961**,33,18-22.

Wherry,T.C.; Miller,E.C. in *Chemical Engineers' Handbook*, 5th ed.; Perry,R.H.; Chilton,C.H. Eds.; McGraw-Hill: 1973.

Yang,F.J.; Guidinger,D.; Matthews,R.; DeFord,D.; Iwao,R.; Ray,C.; Ogden,G. *American Laboratory*, May, **1984**.

Yeroshenkova,G.V.; Volkov,S.A.; Sakodynskii,K.I. *J. Chromatogr.* **1980**,198,377-388.

Ziegler,J.G.; Nichols,N.B. *Trans. ASME* **1942**,64,759-768.

APPENDICES

Appendix I - The Generation of Known Gas Mixtures

A three-way gas mixing system was used to make up known mixtures for quantitative analysis, and also for measuring the viscosities of gas mixtures. The calibration information needed to make up the gas mixtures to be analysed is given in Table I.1.

Table I.1 - Percentage Argon in Hydrogen/Argon Mixtures for Different Flow Regulator Settings (Delivery Pressure to Mixing System 30psig)

Regulator Setting/Flow (mL/min) $H_2 \rightarrow$ Ar $\downarrow$	10.5/29.28	10.0/38.86	9.5/51.70	9.0/65.16
10.0/13.38	31.36*	25.61	20.55	17.04
9.0/21.08	41.86*	35.17	28.96	24.44
8.0/30.4	50.93*	43.89	37.02	31.81

* denotes the mixtures used in runs HAHE1811-8.

Appendix II - Measurement of Gas Mixture Viscosity

Introduction

This method was used to measure the viscosities of mixtures of dichlorodifluoromethane and helium. No published data could be found for this particular mixture.

For a constant pressure drop down a given capillary tube, the volumetric flow rate is inversely proportional to the gas viscosity (see Chapter 2), i.e.

$$Q_1 = \frac{\pi d^4}{256 \mu L} \frac{(P_0^2 - P_1^2)}{P_1} \qquad \text{(II.1)}$$

$$= \frac{k}{\mu}$$

Apparatus

The apparatus consisted of the mixing system mentioned in Appendix I with 10m of 1.5mm o.d.×0.5mm i.d. connected to the gas mixture delivery port.

Method

The gas mixture delivery pressure was set to 1.5 bar. Ensuring that the mixing system was always venting excess gas mixture, the volumetric flow rate leaving the capillary tube was measured for different, known gas mixtures. One mass-flow regulator had previously been calibrated for each specific gas.

Results

The value of the system constant, k, can be calculated from a knowledge of the pipe geometry and the experimental conditions. Alternatively, the constant can be determined as the product of the viscosity of each pure component at the relevant temperature and its respective volumetric flow rate through the measuring capillary at the test pressure drop.

Perry 3.211 gives :

$$\mu_{He} = 0.0186 \text{cP} \; @ \; 20°\text{C}$$

$$\mu_{CCl_2F_2} = 0.0123 \text{cP} \; @ \; 20°\text{C}$$

The flow rates of the pure components were :

$$Q_{He} = 11.5 mL/min \therefore k_{He} = 0.2139 cPmL/min$$

$$Q_{CCl_2F_2} = 17.6 mL/min \therefore k_{CCl_2F_2} = 0.2165 cPmL/min$$

This gives an average system constant of 0.2152cPmL/min. The viscosity of each mixture can be determined using this average value (Table II.1).

Table II.1 - Calculation of the Viscosities of Dichlorofluoromethane and Helium Mixtures

Calibration Flow CCl_2F_2 (mL/min)	Calibration Flow He (mL/min)	Mole Fraction He	Mixture Flow (mL/min)	$\mu\left(=\frac{k}{Q}\right)$
-	39.2	1.00	11.5	187.1
8.4	239	0.97	10.8	199.3
8.4	165	0.95	10.7	201.1
8.4	122	0.93	10.8	199.3
8.4	86	0.91	10.9	197.4
8.4	60.4	0.88	11.2	192.1
8.4	39.2	0.82	11.7	183.9
8.4	23.6	0.74	12.4	173.5
14.0	23.6	0.63	13.5	159.4
20.8	23.6	0.53	14.2	151.5
28.8	23.6	0.45	14.7	146.4
38.4	23.6	0.38	15.1	142.5
49.2	23.6	0.32	15.4	139.7
60.6	23.6	0.28	15.6	137.9
60.6	10.6	0.15	15.9	135.3
107	-	0.00	17.6	122.3

Conclusion

The mixture viscosity is plotted against mole fraction of helium in Appendix III. The plotted curve does not fit the data very well at low helium concentrations. The scatter may be connected to the unreliable nature of the CCL_2F_2 supply. The source was a canister as opposed to bottled gas and the supply valve used to access the gas was faulty so the

measurements had to be taken in a short space of time before the contents of the canister leaked away. Some of the measurements may therefore have been subject to error because of the haste with which they were taken.

The data does show that the mixture viscosity does increase from pure helium up to around 90% helium. As the dichlorodifluoromethane content increases after 10% the mixture viscosity decreases. This rise to a maximum is consistent with observations reported in Chapter 6.

Appendix III - The Viscosity of Binary Gas Mixtures

1 Argon - Helium (Touloukian, Saxena and Hestermans (1975))
2 Argon - Hydrogen (Touloukian, Saxena and Hestermans (1975))
3 Argon - Nitrogen (Touloukian, Saxena and Hestermans (1975))
4 Helium - Hydrogen (Touloukian, Saxena and Hestermans (1975))
5 Helium - Nitrogen (Touloukian, Saxena and Hestermans (1975))
6 Helium - Dichlorofluoromethane
7 Hydrogen - Nitrogen (Touloukian, Saxena and Hestermans (1975))

SMOOTHED VISCOSITY VALUES AS A FUNCTION OF COMPOSITION FOR GASEOUS ARGON–HELIUM MIXTURES AT 291.1K

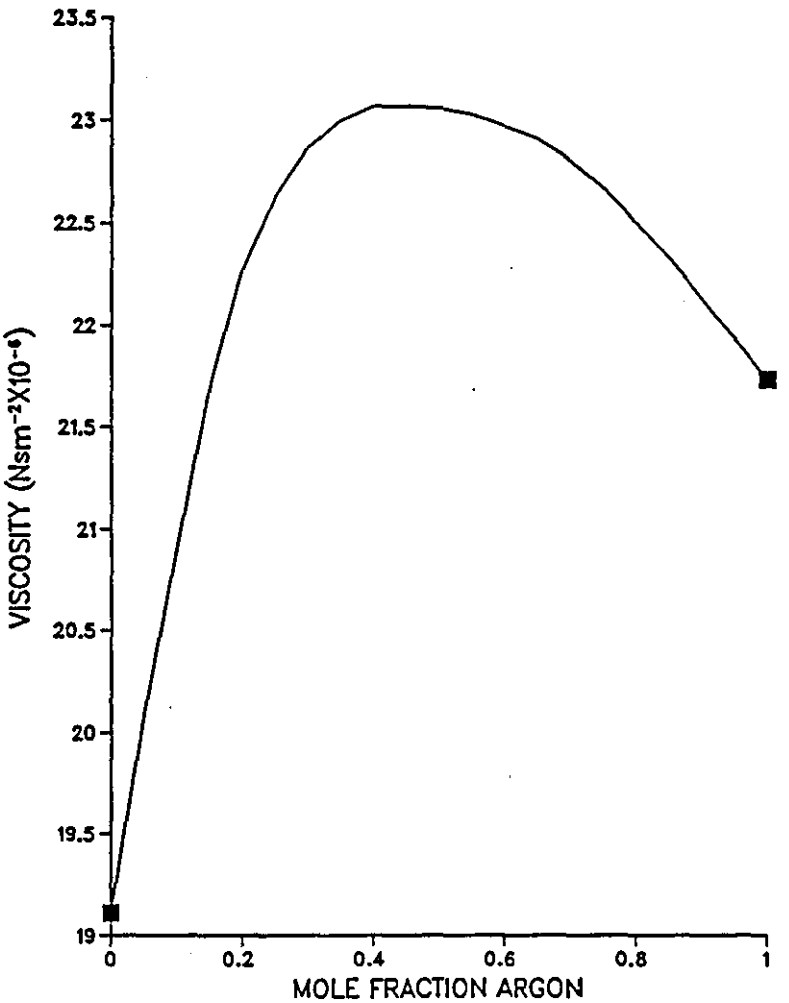

SMOOTHED VISCOSITY VALUES AS A FUNCTION OF COMPOSITION FOR GASEOUS ARGON–HYDROGEN MIXTURES AT 293K

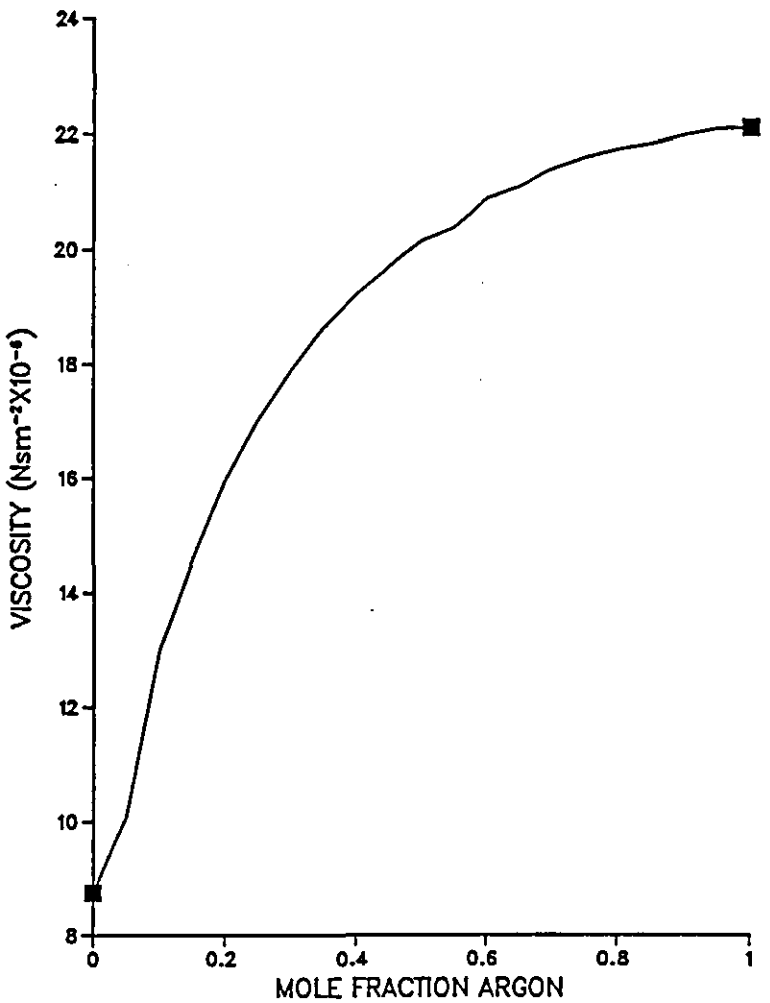

VISCOSITY VALUES AS A FUNCTION OF COMPOSITION FOR GASEOUS ARGON–NITROGEN MIXTURES AT 293.2K

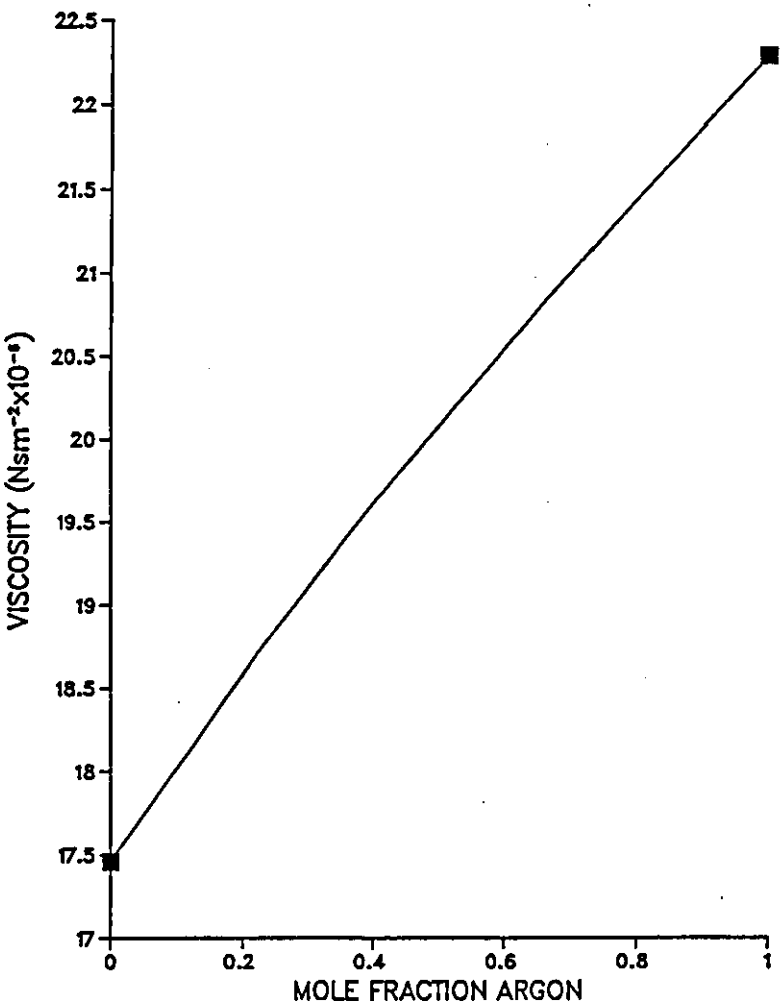

SMOOTHED VISCOSITY VALUES AS A FUNCTION OF COMPOSITION FOR GASEOUS HELIUM–HYDROGEN MIXTURES AT 293.0K

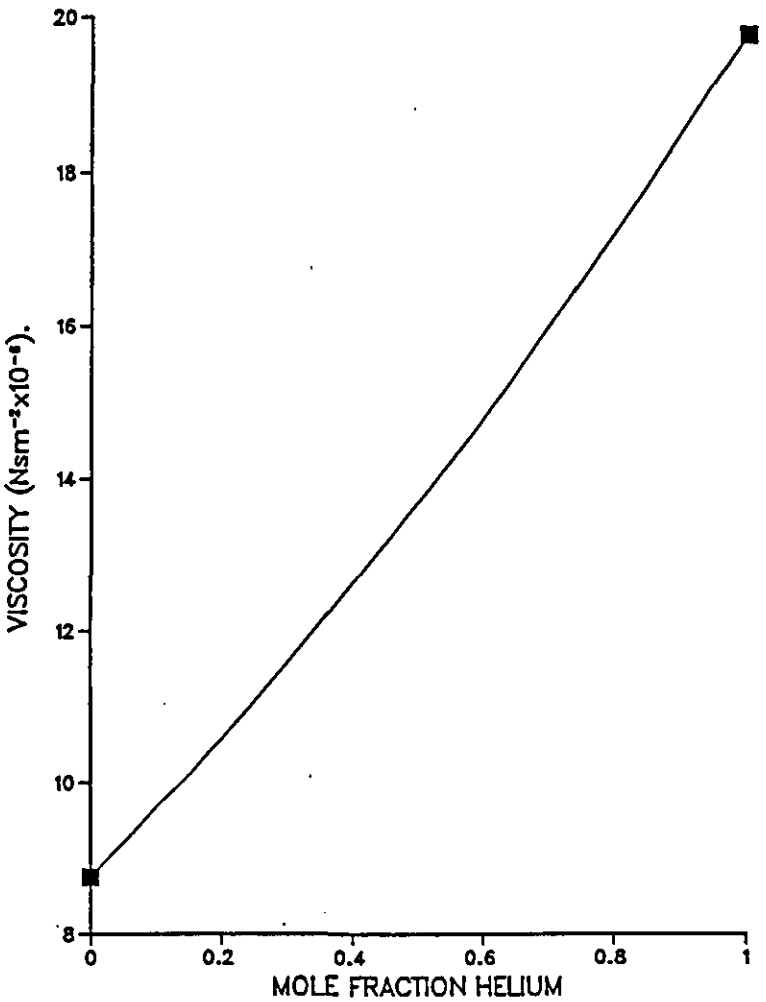

VISCOSITY VALUES AS A FUNCTION OF COMPOSITION FOR GASEOUS HELIUM–NITROGEN MIXTURES AT 293.2K

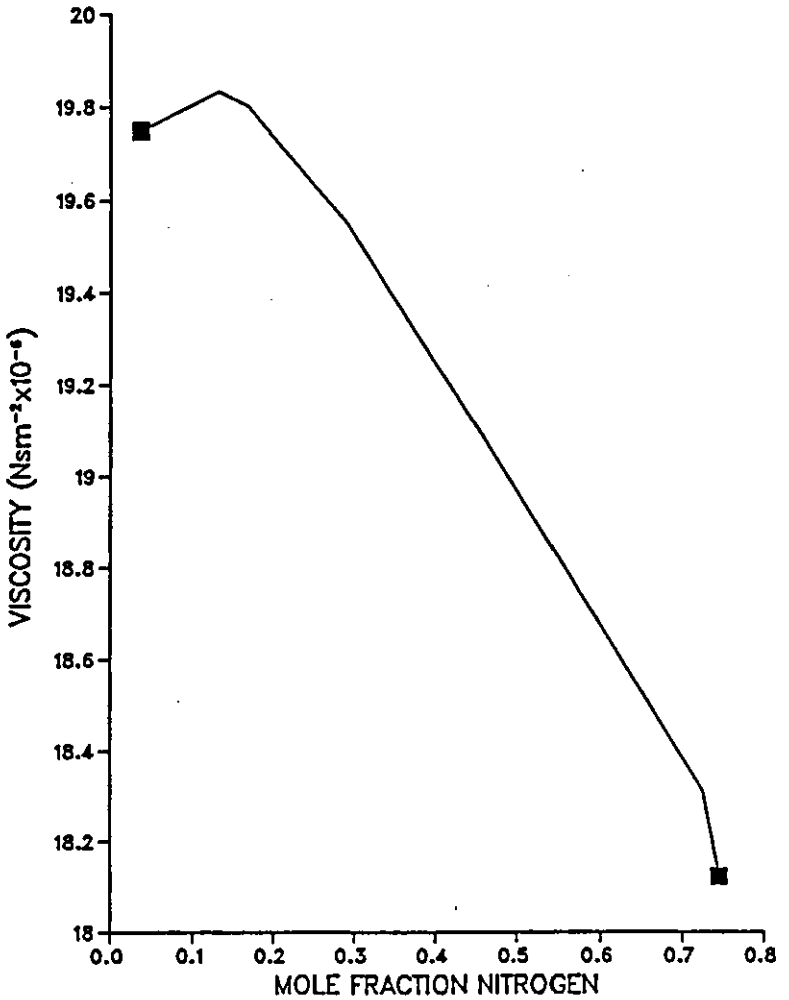

VISCOSITY OF DICHLORODIFLUOROMETHANE/HELIUM MIXTURE AT 293K

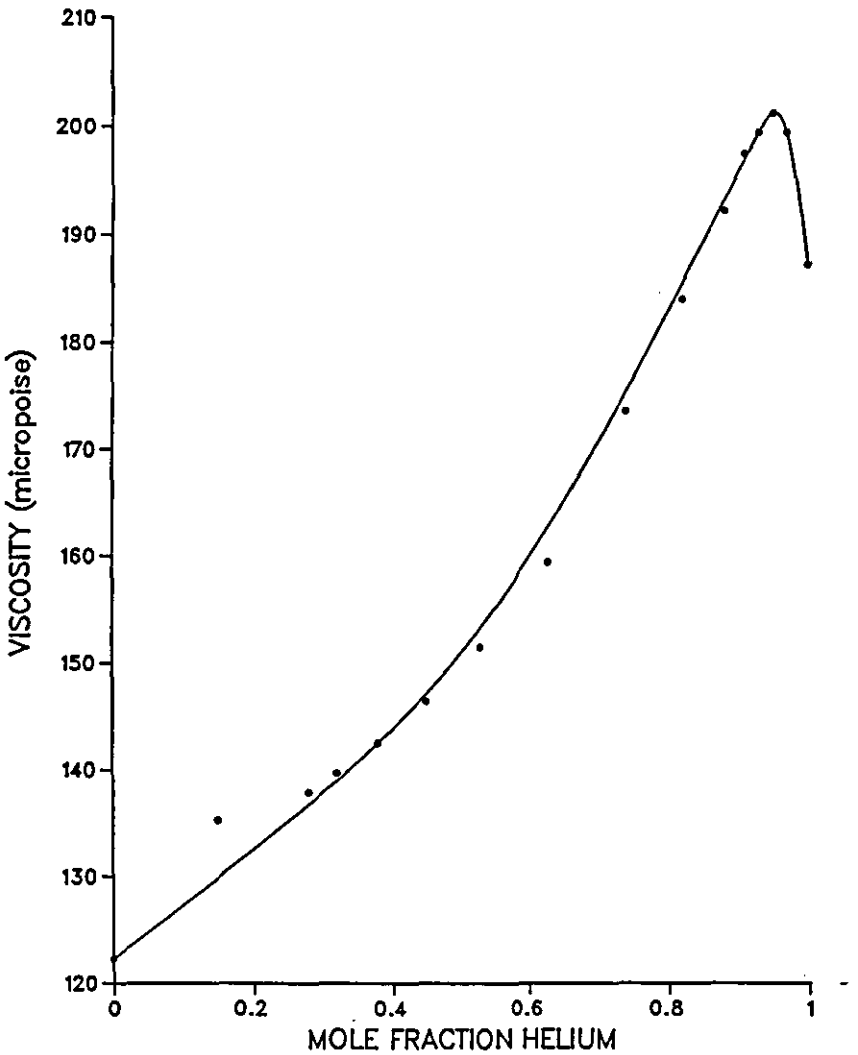

SMOOTHED VISCOSITY VALUES AS A FUNCTION OF COMPOSITION FOR GASEOUS HYDROGEN–NITROGEN MIXTURES AT 291.2K

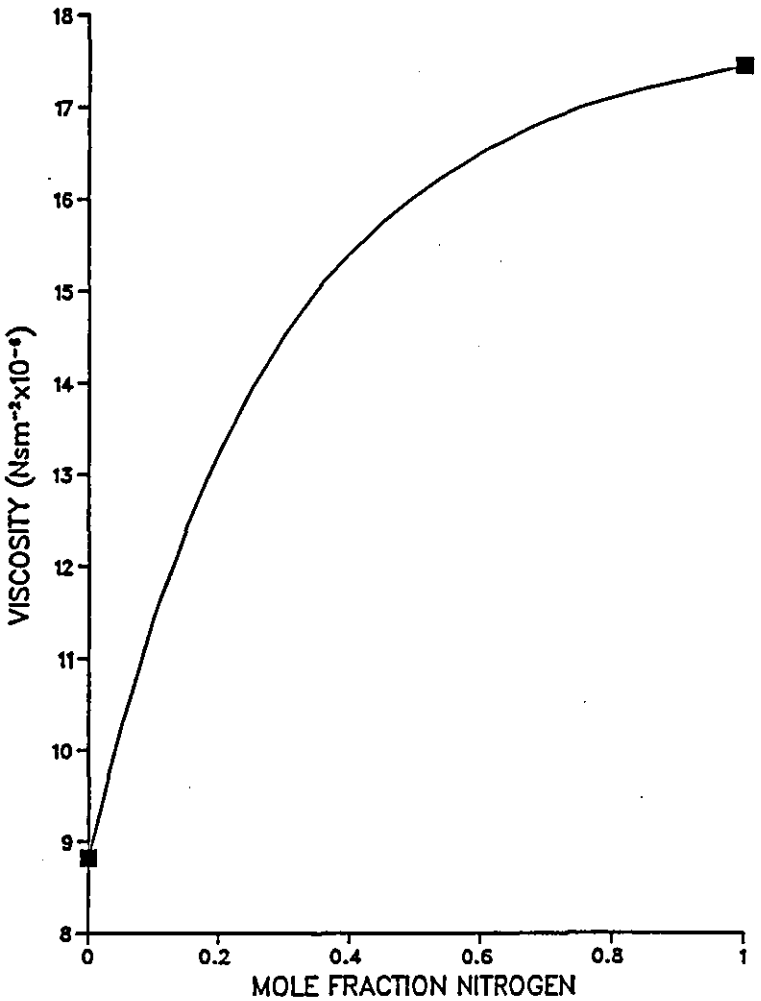

Appendix IV - Estimation of the Sample Gas Concentration at the Peak Maximum

Assume that the sample band travels with a concentration profile corresponding to a normal distribution. Consider a desorption peak that completely elutes in approximately 29 seconds (Appendix XIV). The helium carrier gas rate is 0.55mL/s per channel and the sample size is 15μL (i.e. 5μL at 3 bar).

The average sample gas concentration is then :

$$\frac{15\times10^{-3}}{29\times0.55+15\times10^{-3}}\times100\%$$

$$=0.094\%$$

Consider now a strip $\pm0.1\sigma$ either side of the peak maximum (where 99.73% of the peak is contained between $\pm3\sigma$ and σ is the standard deviation). From Perry and Chilton (1973), the proportion of the total peak in the strip is

$$\frac{0.0797}{0.9973}=0.08$$

The strip is $\frac{0.1}{3}\times29s=0.97s$ wide.

The percentage sample gas at the maximum is therefore

$$\frac{0.08\times15\times10^{-3}}{0.97\times0.55+0.08\times15\times10^{-3}}\times100\%$$

$$=0.224\%$$

Hydrogen was used for this calculation because it has a relatively high maximum concentration. The less adsorbed a sample gas is, the more sample gas remains in the gas phase, and, the narrower the desorption peak. The calculated peak concentration is for the worst case, when no sample gas is removed from the gas phase by adsorption. Obviously, any adsorption will reduce the maximum concentration. Even in the worst case, the calculated concentration is so low that the gradient of the equilibrium curve can be considered constant over the concentration range encountered across the sample band.

Appendix V - Listings of Ancillary Programs

1 Boot Up

```
A$=CHR$1+CHR$&1B+CHR$1+"N"+CHR$1+CHR$3
VDU2 : P.A$ : VDU 3
CH."GDUMP0"
*BAS128
CH."MENU"
```

2 Screen Print

```
L.
  10REM EPSMONO Screen Dump on EPSON. M/C stored at BASE
  20BASE=&C00:REM In place of User Defined Characters
  30MODE3
  40xpointlo=&70:xpointhi=&71:ypointlo=&72:ypointhi=&73:pixelvalue=&74:printer:
yte=&75:bitcount=&76:mode0=&77:step=&78:OSWRCH=&FFEE:OSWORD=&FFF1:OSBYTE=&FFF4
  50FOR pass=0 TO 3 STEP 3
  60P%=BASE
  70[OPT pass
  80LDA£2:JSR&FFBC
  90.ScreenDump LDA£&FF:STAypointlo:LDA£&3:STAypointhi
 100LDA£0:STAmode0:LDA£4:STAstep:LDA£135:JSROSBYTE:TYA:BNELineGap:INCmode0:LSR
tep
 110.LineGap LDA£27:JSRPrinter:LDA£65:JSRPrinter:LDA£8:JSRPrinter
 120.NewLine LDA£0:STAxpointlo:STAxpointhi
 130LDA£27:JSRPrinter:LDAmode0:BEQModeAbove0:LDA£76:JSRPrinter:LDA£128:JSRPrin
er:LDA£2:JSRPrinter:BNENewColumn
 140.ModeAbove0 LDA£75:JSRPrinter:LDA£64:JSRPrinter:LDA£1:JSRPrinter
 150.NewColumn LDA£8:STAbitcount
 160.ReadPixel LDX£xpointlo:LDY£0:LDA£9:JSROSWORD
 170CLC:LDApixelvalue:BEQSetPrinterByte:SEC
 180.SetPrinterByte ROLprinterbyte
 190LDAypointlo:SEC:SBC£4:STAypointlo:BCSCheckColumnEnd:DECypointhi
 200.CheckColumnEnd DECbitcount:LDAbitcount:BNEReadPixel
 210.Print LDAprinterbyte:JSRPrinter
 220.NextColumn CLC:LDAstep:ADCxpointlo:STAxpointlo:BCCCheckLineEnd:INCxpointh
 230.CheckLineEnd LDAxpointhi:CMP£5:BEQEndLine
 240.ColumnTop LDA£32:CLC:ADCypointlo:STAypointlo:BCCNewColumn:INCypointhi:BCS
ewColumn
 250.EndLine LDA£10:JSRPrinter
 260.CheckEnd LDAypointhi:BMIEnd:JMPNewLine
 270.End LDA£10:JSRPrinter:LDA£27:JSRPrinter:LDA£64:JSRPrinter
 280LDA£2:JSR&FFBC:RTS
 290.Printer PHA:LDA£1:JSR&FFEE:PLA:JSR&FFEE:RTS
 300]NEXT pass
```

3 Master Menu

```
1000 REM SAVE "MENU"
1010 REM 8 SEPT 88
1020 MODE 0
1040 *KEY0 0
1060 *KEY1 1
1080 *KEY2 2
1090 *KEY3 3
1100 *FX 7,5
1120 *FX 8,5
1140 VDU 23;8202;0;0;0;
1160 PROCstatus
1180 PROCmenu
1200 MODE 7
1220 PRINT"Program terminated.":VDU 10,10
1240 END
1260 DEF PROCstatus
1280 LOCAL count%,i%,i2%,a$
1300 count%=0
1320 VDU 28,0,8,79,0
1340 COLOUR 0 : COLOUR 129
1360 CLS
1380 PRINTTAB(0,1);STRING$(46,"_");
1400 FOR i%=1 TO 64 STEP 16
1420 IF count%<3 PRINTTAB(i%,0);"f";count%;
1440 count%=count%+1
1460 IF count%=1 THEN NEXT
1480 FOR i2%=0 TO 5 : PRINTTAB(i%-3,i2%);"¦";:NEXT i2%
1500 NEXT
1520 :
1540 REM display channels
1560 :
1580 PRINTTAB(0,2);" Initialise"
1600 PRINTTAB(0,4);" CIL reading"
1620 :
1640 REM display delay time
1660 :
1680 PRINT TAB(16,2);"Read data"
1700 PRINT TAB(16,4);"from CIL"
1720 :
1740 REM display scans
1760 PRINTTAB(32,2);"Process data"
1780 PRINTTAB(32,4);"from disk"
1800 PRINTTAB(0,5);STRING$(46,"_");
1820 REM now fill the rest
1840 COLOUR 1 : COLOUR 130
1860 PRINTTAB(48,1);"CIL control MENU program";
1880 PRINTTAB(48,3);"HIT f key or Q to quit.";
1900
1920 ENDPROC
1940 DEF PROCmenu
1960 on=1
1980CILON=0
2000 IF on THEN ?&D3=255 ELSE ?&D3=0
2020 IF on=0 THEN ?&D3=0
2040 PRINTTAB(48,3);"HIT f key or Q to quit.";
2060 A=0 : A=INKEY(100)
2080 IF on=1 THEN on=0 ELSE on=1
2100 IF A=0 THEN 2000
2120 IF A=81 THEN ENDPROC
2140 IF A<48 OR A>51 THEN 2000
2160 CLS : PRINTTAB(3,10);
2180 ON (A-47) GOSUB 2300,2340,2360,2380
2200 PROCstatus
2220 PROCreset_scan
2240 GOTO 2000
2260 ENDPROC
2280 :
2300 CHAIN"PRGASA"
2320 :
2340 CHAIN"PRGREADMC"
2360 CHAIN"INT3TA"
2380 CHAIN"FLOW-M"
```

Appendix VI - Listing of Initialisation Program

```
 1000 REM SAVE "PRGASA"
 1020 MODE 128
 1040 chanls%=2
 1060DIM RANGE(16),ZERO(16),COL(4),X(16),A(16),FC(16),SUM(16),Z(16)
 1080 DIM SCALE(chanls%),LOT(chanls%),BL(chanls%),IBL(chanls%),max%(chanls%)
 1100SCALE=1
 1120 VDU 23;8202;0;0;0;
 1140 PROCstart
 1160 CHAIN"MENU"
 1180 DEFPROCkeyin(L):LOCALX,Y,B,C,K,A,I:T$="":X=POS:Y=VPOS:PRINTTAB(X,Y);"[";TA
B(X+L+1,Y);"]";TAB(X+1,Y);:REPEAT
 1200K=GET:B=POS:C=VPOS:IFK=13THEN1300ELSEIFK=127THEN1260
 1220T$=T$+CHR$K:PRINTCHR$K;
 1240UNTIL LENT$=L OR K=13:PRINT:ENDPROC
 1260A=LENT$:IFA=0THEN1200
 1280T$=LEFT$(T$,A-1):PRINTTAB(B-1,C);" ";:PRINTTAB(B-1,C);:GOTO1200
 1300FOR I=B TO (X+L):PRINT" ";:NEXT:GOTO1240:PRINT" ";:NEXTI:GOTO1240
 1320 DEF PROCvariables
 1340 channels$="IOI1":delay$="QD250":scans$="QS2880":delay%=250:mins=14:scans%=
2880:file$=""
 1360FOR I = 0 TO chanls%-1
 1380SCALE=1
 1400IF RANGE(I)THEN 1440
 1420RANGE(I)=1
 1440IF ZERO(I)THEN 1480
 1460ZERO(I)=500
 1480IF COL(I) THEN 1520
 1500COL(I)=I+1
 1520IF FC(I) THEN 1560
 1540FC(I)=0
 1560IF Z(I) THEN 1600
 1580Z(I)=640
 1600NEXTI
 1620 CILON=0
 1640 FOR i%=0 TO 5
 1660 OSCLI("KEY"+STR$(i%)+" "+STR$(i%))
 1680 NEXT
 1700 ENDPROC
 1720 DEF PROCout(string$)
 1740 IF LEN(string$)=0 THEN VDU 7 : ENDPROC
 1760 *FX 3,7
 1780 PRINT string$
 1800 *FX 3,0
 1820 ENDPROC
 1840 DEF PROCcil_out
 1860 LOCAL out$
 1880 out$="A,"+channels$+CHR$13+scans$+CHR$13+delay$+CHR$13+",T2"+CHR$13+"QE"+C
HR$13
 1900 *fx 21,1
 1920 PROCout(out$)
 1940 CILON=1
 1960 ENDPROC
 1980 DEF PROCgetchannels
 2000 LOCAL i% : channels$=""
 2020 PRINT"How many channels ";: PROCkeyin(2)
 2040 chanls%=VAL(T$)
 2060FORI=0TOchanls%-1
 2080IF SCALE THEN GOTO 2120
 2100SCALE=1
 2120IF RANGE(I)THEN 2160
 2140RANGE(I)=1
 2160IF ZERO(I)THEN 2200
 2180ZERO(I)=500
 2200IF COL(I) THEN 2240
 2220COL(I)=I+1
```

```
 2240IF FC(I) THEN 2280
 2260FC(I)=0
 2280NEXTI
 2300 PROCcheckok
 2320 IF err=1 THEN PRINT"Not enough memory." : PRINT"Continue? ";:PROCkeyin(1)
: IF T$<>"Y" THEN ENDPROC
 2340 FOR i%=0 TO chanls%-1
 2360 PRINT"Channel £";i%;"  ";:PROCkeyin(3)
 2380 channels$=channels$+"I"+T$+","
 2400 NEXT i%
 2420 channels$=LEFT$(channels$,(LEN(channels$)-1))
 2440 ENDPROC
 2460 DEF PROCscans
 2480 PRINT"Enter time period in minutes "; : PROCkeyin(4)
 2500 mins=VAL(T$)
 2520 GOTO 2560
 2540 DEF PROCreset_scan
 2560 scans%=INT((1000/delay%)*60*mins)
 2580 IF ( scans% * chanls%) >16384 THEN PRINT"Not enough memory." : err=1 : END
PROC
 2600 scans$="QS"+STR$(scans%)
 2620 ENDPROC
 2640 DEF PROCdelay
 2660 PRINT"Enter delay between scans ";:PROCkeyin(4)
 2680 delay%=VAL(T$)
 2700 IF delay%>255 IF delay%<0 THEN PRINT"0-255mS only ":GOTO2660
 2720 delay$="QD"+STR$(delay%)
 2740 ENDPROC
 2760 :
 2780 DEF PROCfile
 2800 LOCAL i%,handle%
 2820 CLS
 2840 OSCLI("*CAT :0.$.FILE")
 2860 PRINT:PRINT
 2880 PRINT "Enter Filename "; : PROCkeyin(10)
 2900 file$="$.File._"+T$
 2920 handle%=OPENOUT(file$)
 2940 PRINT£handle%,chanls%,channels$,delay$,scans$,delay%,mins,scans%
 2960 CLOSE£handle%
 2980 ENDPROC
 3000 DEF PROCfileread
 3020 OSCLI("*CAT :0.$.FILE")
 3040 LOCAL i%,handle%
 3060 PRINT "Enter Filename "; : PROCkeyin(10)
 3080 file$="$.File._"+T$
 3100 handle%=OPENIN(file$)
 3120 INPUT£handle%,chanls%,channels$,delay$,scans$,delay%,mins,scans%
 3140 CLOSE£handle%
 3160 ENDPROC
 3180 DEF PROCexecute
 3200 PRINT"Do you wish to save settings."
 3220 PRINT:PRINT"You MUST if they are not already saved!";
 3240 VDU 11,11,8,8,8,8,8,8
 3260 PROCkeyin(1) : IF T$="N" THEN 3300
 3280 PROCfile
 3300 PROCcil_out
 3320 ENDPROC
 3340 DEF PROCcheckok
 3360 IF ( scans% * chanls%) >16384 THEN PRINT"Not enough memory." : err=1 ELSE
err=0
 3380 ENDPROC
 3400 DEF PROCstart
 3420 PROCvariables
 3440 PROCstatus
 3460 CLS
 3480 PROCmenu
```

```
3500 :
3520 ENDPROC
3540 DEF PROCstatus
3560 LOCAL count%,i%,i2%,a$
3580 count%=0
3600 PROCreset_scan
3620 VDU 28,0,8,79,0
3640 COLOUR 0 : COLOUR 129
3660 CLS
3680 PRINTTAB(0,1);STRING$(80,"_");
3700 FOR i%=1 TO 80 STEP 16
3720 PRINTTAB(i%,0);"f";count%;
3740 count%=count%+1
3760 IF count%=1 THEN NEXT
3780 FOR i2%=0 TO 4 : PRINTTAB(i%-3,i2%);"¦";:NEXT i2%
3800 NEXT
3820 :
3840 REM display channels
3860 :
3880 PRINTTAB(0,2);chanls%;" Channels" : PRINT
3900 FOR i%=1 TO LEN(channels$)
3920 a$=MID$(channels$,i%,1) : IF a$="I" THEN 3960
3940 IF a$="," THEN PRINT" "; ELSE PRINTa$;
3960 NEXT
3980 :
4000 REM display delay time
4020 :
4040 PRINT TAB(16,2);"Delay (ms)"
4060 IF delay%<255 THEN PRINTTAB(16,3);"FAST DATA"
4080 PRINT TAB(16,4);RIGHT$(delay$,LEN(delay$)-2)
4100 :
4120 REM display scans
4140 :
4160 PRINTTAB(32,2);"Time scan"
4180 PRINTTAB(32,4);mins;"Mins."
4200 :
4220 REM now fill the rest
4240 :
4260 PRINTTAB(48,2);"Load file"
4280 PRINTTAB(64,2);"Execute"
4300 PRINTTAB(0,5);STRING$(80,"_")
4320 PRINTTAB(20,6);"There are ";scans%*chanls%;" scans initiated."
4340 VDU 28,0,30,79,7
4360 COLOUR 1 : COLOUR 130
4380 CLS
4400 ENDPROC
4420 DEF PROCmenu
4440 PRINTTAB(15,10);"Hit appropiate function key or Q to quit."
4460 PRINTTAB(15,7);"f5 - BASELINE LOGGING"
4480 A=GET
4500 IF A=81 THEN ENDPROC
4520 IF A<48 OR A>53 THEN 4480
4540 CLS : PRINTTAB(3,10);
4560ON (A-47) GOSUB 4640,4700,4760,4820,4900,4960
4580 PROCstatus
4600 PROCreset_scan
4620 GOTO 4440
4640 :
4660 PROCgetchannels
4680 RETURN
4700 :
4720 PROCdelay
4740 RETURN
4760 :
4780 PROCscans
4800 RETURN
```

```
4820 :
4840 PROCfileread
4860 RETURN
4880 :
4900 PROCexecute
4920 RETURN
4940:
4960PROCbaseline
4980RETURN
5000DEF PROCbaseline
5020 IF CILON =1 THEN ENDPROC
5040 VDU 22,129
5060CLS:CLG:dsc=0:time=0
5080MOVE640,1023
5100MENU$="SRZQTCMPFAE"
5120*FX3,7
5140PRINT"A"
5160*FX3,0
5180NN=0:nn=0:FORI=0TO chanls%-1:SUM(I)=0:NEXT I:REM SCREEN COUNTER
5200G$=INKEY$(0)
5220 IF TIME-time<INT(delay%/10+.5)THEN5280
5240PROCcharin:time=TIME
5260PROCplot
5280IF G$<>"" THEN PROCdisplay
5300IF G$=""THEN 5200
5320
5340DEF PROCdisplay
5360 IF dsc=1 IF G$<>"E" THEN 5200
5380FORI=1TOLEN(MENU$)
5400A$=MID$(MENU$,I,1)
5420IF A$<>G$THEN5500
5440M=I
5460I=LEN(MENU$)
5480ON M GOSUB 6540,6680,6820,6960,7060,7120,7220,7580,7840,7960
5500NEXTI
5520 G$=""
5540ENDPROC
5560
5580DEF PROCinput
5600PRINTN$,N
5620PRINT"NEW ";N$
5640INPUT V$
5660 NO=VAL(V$):IFNO<>0THEN N=NO
5680ENDPROC
5700
5720DEF PROCplot
5740NN=NN+1:nn=nn+1:I=0
5760 REPEAT
5780XL=X(I)
5800 X1=INT((A(I)+2^15)/2^16*128000+.5)/100
5820SUM(I)=SUM(I)+X1
5840X1 =(X1-ZERO(I))*RANGE(I)+Z(I)
5860X(I)=INT(X1+.5)
5880PRINTTAB(0,20+I)A(I)
5900X(I)=X(I)*(1-FC(I))+XL*FC(I)
5920IFNN=1THEN MOVE X(I),1023
5940 MOVEXL,1024-(NN-1)*SCALE:GCOL 0,COL(I)
5960DRAWX(I),1024-NN*SCALE
5980 I=I+1
6000 UNTIL I=chanls%
6020IF NN>948/SCALE AND NN<950/SCALE THEN VDU7
6040IFNN>1024/SCALE THEN NN=0:CLG:MOVEX(I),1023
6060SEC=INT(TIME/100)
6080PRINTTAB(30,28)SEC;
6100ENDPROC
```

```
6140DEF PROCcharin
6160*FX7,5
6180*FX8,5
6200*FX21,1
6220*FX21,2
6240*FX2,1
6260IF channels$=""THEN GOSUB 4640
6280B$=channels$+"T5"
6300 JJ=0
6320*FX3,7
6340PRINTB$
6360 REPEAT
6380INPUT A(JJ)
6400 JJ=JJ+1
6420 UNTIL JJ = chanls%
6440 *FX3,0
6460 *FX2,0
6480 PRINTTAB(1,2)" "
6500ENDPROC
6520
6540REM CHANGE SCALE (VERTICAL AXIS)
6560 N$="SCALE":N=SCALE
6580PROCinput
6600SCALE=N:CLS
6620GOSUB7060
6640RETURN
6660
6680REM CHANGE RANGE(I) (HORIZONTAL AXIS)
6700PRINTTAB(1,1)"CHANNEL":INPUT IJ
6720 N$="RANGE("+STR$(IJ)+")":N=RANGE(IJ)
6740PROCinput
6760RANGE(IJ)=N :CLS
6780RETURN
6800
6820REM CHANGE ZERO(I) POSITION
6840PRINTTAB(1,1)"CHANNEL":INPUT JI
6860N$="ZERO("+STR$(JI)+")":N=Z(JI)
6880PROCinput
6900Z(JI)=N:CLS
6920RETURN
6940
6960 REM QUIT ON-LINE LOGGING FOR DATA RUN
6980VDU22,128
7000PROCstatus
7020PROCmenu
7040ENDPROC
7060 REM RESET DISPLAY TO TOP
7080NN=0:CLG:FORi%=0TOchanls%-1:SUM(i%)=0:NEXT
7100RETURN
7120REM RESET CLOCK IN 5 SECONDS
7140TIME=0:time =0
7160IF TIME =450 THENVDU7
7180IF TIME =500 THENVDU7:VDU7:TIME=0:RETURN
7200GOTO7160
7220REM MENU
7240CLS
7260PRINT"MENU OPTIONS"
7280PRINT
7300PRINT"  S  -  VERTICAL SCALE PARAMETER"
7320PRINT"  R  -  FULL-SCALE RANGE(I) PARAMETER"
7340PRINT"  Z  -  BASELINE POSITION PARAMETER"
7360PRINT"  T  -  RESETS TRACE TO TOP OF SCREEN"
7380PRINT"  C  -  RESETS CLOCK TO 5 SECS BEFORE "
7400PRINT"        ZERO (TONE AT MINUS 1 SEC AND                AT TIME ZERO)"
7420PRINT"  F     CHANGE FILTER CONSTANT (0-1)"
7440PRINT"  A     AUTO-ZERO TRACE"
```

```
7460PRINT"  Q  -  QUIT OUT OF BASELINE MONITOR"
7480PRINT"  P  -  PEN/BACKGROUND"
7500PRINT"PRESS ANY KEY"
7520 REL$=GET$
7540CLS
7560RETURN
7580 REM CHANGE COLOUR
7600PRINTTAB(1,1)"BACKGROUND OR TRACE"
7620C$=GET$
7640IF C$="B" GOTO 7780
7660IF C$ ="T" THEN 7700
7680GOTO7620
7700PRINT"INPUT CHANNEL,COLOUR"
7720INPUT J,COL(J)
7740GCOL 0,COL(J)
7760GOTO7800
7780INPUT COL:COLOUR COL
7800CLS
7820RETURN
7840REM FILTER CONSTANT (0-1)
7860PRINTTAB(1,1)"CHANNEL":INPUT JI
7880 N$="FILTER CONSTANT("+STR$(JI)+")":N=FC(JI)
7900PROCinput
7920FC(JI)=N:CLS
7940RETURN
7960REM AUTO ZERO
7980FOR J = 0 TO chanls%-1
8000ZERO(J)=SUM(J)/nn
8020PRINTINT(ZERO(J)):SUM(J)=0
8040NEXT J
8060nn=0
8080RETURN
```

Appendix VII - Listing of Data-Recovery Program

```
 1000REM SA."PRGREADMC"
 1020 CLOSE£0
 1040 MODE 0
 1060 VDU 23;8202;0;0;0;
 1080 PROCstart
 1100 OSCLI("DIR $")
 1120 CHAIN"MENU"
 1140 DEFPROCkeyin(L):LOCALX,Y,B,C,K,A,I:T$="":X=POS:Y=VPOS:PRINTTAB(X,Y);"[";TA
B(X+L+1,Y);"]";TAB(X+1,Y);:REPEAT
 1160K=GET:B=POS:C=VPOS:IFK=13THEN1260ELSEIFK=127THEN1220
 1180T$=T$+CHR$K:PRINTCHR$K;
 1200UNTIL LENT$=L OR K=13:PRINT:ENDPROC
 1220A=LENT$:IFA=0THEN1160
 1240T$=LEFT$(T$,A-1):PRINTTAB(B-1,C);" ";:PRINTTAB(B-1,C);:GOTO1160
 1260FOR I=B TO (X+L):PRINT" ";:NEXT:GOTO1200:PRINT" ";:NEXTI:GOTO1200
 1280 :
 1300 DEF PROCvariables
 1320 REM DIMdata(400)
 1340 :
 1360 channels$=""
 1380 delay$   = "QD00"
 1400 chanls%  = 0
 1420 scans$   = "QS00"
 1440 delay%   = 0
 1460 mins     = 0
 1480 scans%   = 0
 1500 file$    = ""
 1520 :
 1540 FOR i%=0 TO 4
 1560 OSCLI("KEY"+STR$(i%)+" "+STR$(i%))
 1580 NEXT
 1600 ENDPROC
 1620 :
 1640 DEF PROCout(string$)
 1660 IF LEN(string$)=0 THEN VDU 7 : ENDPROC
 1680 *FX 3,7
 1700 PRINT string$
 1720 *FX 3,0
 1740 ENDPROC
 1760 :
 1780 DEF PROCdatagrab
 1800 CLS
 1820CILON=0
 1840 LOCAL count%
 1860 PRINTTAB(10,15);"Enter filename for data ";: PROCkeyin(10)
 1880 file$=":1._"+T$
 1900 handle%=OPENOUT(file$)
 1920 PRINT£handle%,chanls%,channels$,delay$,scans$,delay%,mins,scans%
 1940 count%=0 : i%=0
 1960 REPEAT
 1980 PRINTTAB(10,10);
 2000 *FX 2,1
 2020 PROCout("QIT5")
 2040 IF chanls%=1 THEN INPUT data(i%)
 2060 IF chanls%=2 THEN INPUT data(i%),data(i%+1)
 2080 IF chanls%=3 THEN INPUT data(i%),data(i%+1),data(i%+2)
 2100 *FX 2,0
 2120 IF i%=400 THEN PROCwrite : i%=0
 2140 count%=count%+1 : i%=i%+chanls%
 2160PRINTTAB(10,11)count%
 2180 UNTIL count%=scans%
 2200 PROCwrite
 2220 PRINT£handle%,-666.666
 2240 CLOSE£handle%
 2260 ENDPROC
```

```
 2280 :
 2300 DEF PROCfileread
 2320 LOCAL i%,handle%
 2340 file$="$.File._"+T$
 2360 handle%=OPENIN(file$)
 2380 INPUT£handle%,chanls%,channels$,delay$,scans$,delay%,mins,scans%
 2400 CLOSE£handle%
 2420DIM data(410)
 2440 ENDPROC
 2460 :
 2480 DEF PROCwrite
 2500 LOCAL loop%
 2520 PRINT"**************"
 2540 FOR loop%=0 TO i%-1
 2560 PRINT£handle%,data(loop%)
 2580 REM PRINTdata(loop%)
 2600 NEXT loop%
 2620 ENDPROC
 2640 :
 2660 DEF PROCstart
 2680 PROCvariables
 2700 PROCstatus
 2720 CLS
 2740 PROCmenu
 2760 :
 2780 ENDPROC
 2800 :
 2820 DEF PROCstatus
 2840 LOCAL count%,i%,i2%,a$ :count%=0:VDU 28,0,8,79,0:COLOUR 0:COLOUR 129:CLS:P
RINTTAB(0,1);STRING$(80,"_");:FOR i%=1 TO 80 STEP 16:count%=count%+1:IF count%=1
 THEN NEXT
 2860FOR i2%=2 TO 4:PRINTTAB(i%-3,i2%);"¦";:NEXT i2%:NEXT
 2880 REM display channels
 2900 :
 2920 PRINTTAB(0,2);chanls%;" Channels" : PRINT
 2940 FOR i%=1 TO LEN(channels$)
 2960 a$=MID$(channels$,i%,1) : IF a$="I" THEN 3000
 2980 IF a$="," THEN PRINT" "; ELSE PRINTa$;
 3000 NEXT
 3020 PRINT TAB(16,2);"Delay (ms)"
 3040 PRINT TAB(16,4);RIGHT$(delay$,LEN(delay$)-2)
 3060 PRINTTAB(32,2);"Time scan"
 3080 PRINTTAB(32,4);mins;"Mins."
 3100 REM now fill the rest
 3120 :
 3140 PRINTTAB(27,0);"Data collection."
 3160 PRINTTAB(48,2);"File name"
 3180 PRINTTAB(48,4);file$
 3200 PRINTTAB(20,6);"There are ";scans%;" scans initiated per channel."
 3220 PRINTTAB(0,5);STRING$(80,"_");
 3240 VDU 28,0,30,79,7
 3260 COLOUR 1 : COLOUR 130
 3280 CLS
 3300 ENDPROC
 3320 DEF PROCmenu
 3340 CLS
 3360 PRINTTAB(0,0); : OSCLI("*CAT $.File")
 3380 PRINTTAB(10,15);"Enter filename ";:PROCkeyin(10)
 3400 PROCfileread
 3420 PROCstatus
 3440 CLS
 3460 PRINTTAB(10,15);"Everything ok?";:PROCkeyin(1)
 3480 IF T$<>"Y" AND T$<>"y" THEN 3340
 3500 CLS
 3520 PROCdatagrab
 3540 ENDPROC
```

Appendix VIII - Listing of Data-Processing Program

```
 1000  REM SA."INT3TA"
 1020 REM 29 NOV 89
 1040 ON ERROR GOTO 2740
 1060 HIMEM=&18000-5
 1080 MODE 0
 1100 VDU 19,1,6,0,0,0
 1105 VDU 23,240,255,254,252,248,240,224,192,128
 1110 VDU 23,241,128,192,224,240,248,252,254,255
 1120 plot=0
 1140 CLOSE£0
 1160 OSCLI("*CAT :1.$")
 1180 INPUT "Filename (prefix 'CAL' for calibration)";file$:CAL=0
 1200 IF LEFT$(file$,3)="CAL" THEN CAL=1: file$=RIGHT$(file$,LEN(file$)-3)
 1220 file$=":1._"+file$
 1240 handle%=OPENIN(file$)
 1260 IF CAL =1 THEN chanls%=1:channels$="":delay$="":scans$="":delay%=250:mins=
1:scans%=400:GOTO1300
 1280 INPUT£handle%,chanls%,channels$,delay$,scans$,delay%,mins,scans%
 1300 DIM A(20),ZERO(chanls%),RANGE(chanls%),LOT(chanls%),Z(chanls%),BL(chanls%
,IBL(chanls%),max%(chanls%),CC$(LEN(channels$)+1),CHL(chanls%),FSD(chanls%)
 1320 CLS:finish%=scans%
 1340 FORI%=0TOchanls%-1
 1360 RANGE(I%)=1:SCALE=1278/scans%:Z(I%)=480
 1380 NEXT
 1400 PRINT"No. of channels ";chanls%:PRINT"Channels used ";channels$:PRINT"Logg
ing interval (mS) ";delay%:PRINT"No. of scans on each channel ";scans%
 1420 M=&18000
 1440 loop%=0
 1460 REPEAT
 1480 i%=0
 1500 REPEAT
 1520 INPUT£handle%,data%:data%=data%+32768:!M=data%:M=M+2:i%=i%+1
 1540 UNTIL i%=chanls%
 1560 loop%=loop%+1
 1580 UNTIL loop%=INT(scans%)
 1600 CLOSE£handle%
 1620 CC%=0
 1640 FOR I =1 TO LEN(channels$)
 1660 CC$(I)=MID$(channels$,I,1)
 1680 NEXT
 1700 FOR I =1 TO LEN(channels$)
 1720 IF STR$(VAL(CC$(I)))=CC$(I) THEN 1760
 1740 GOTO 1820
 1760 IF STR$(VAL(CC$(I+1)))=CC$(I+1) THEN CHL(CC%)=VAL(CC$(I))*10 +VAL(CC$(I+1)
):CC%=CC%+1:GOTO1800
 1780 CHL(CC%)=VAL(CC$(I)):CC%=CC%+1
 1800 I=I+1
 1820 NEXT
 1840 FOR I=0 TO CC%-1
 1860 IF CHL(I)<8 THEN FSD(I)=2000:GOTO 1920
 1880 IF CHL(I)<12 THEN FSD(I)=20000:GOTO 1920
 1900 IF CHL(I)<16 THEN FSD(I)=100000
 1920 NEXT
 1940 VDU7
 1960 GOTO2220
 1980 DEF PROCmenu
 2000 GOSUB 4880
 2020 MENU$="ZRNCMFBHPLWXQO"
 2040 G$=GET$
 2060 FOR I =1TO LEN(MENU$)
 2080 IF G$=MID$(MENU$,I,1)THEN M=I:I=LEN(MENU$)
 2100 NEXT I
 2120 IF M =13 THEN CHAIN"MENU"
 2140 IF M =14 THEN END
 2160 IF M > 12 THEN 2040
```

```
 2180 ON M GOSUB 3980,4220,4340,4820,4880,5400,5520,5980,6060,6140,6220,6580

 2200 ENDPROC
 2220 :
 2240
 2260 bc=5:bl%=50:dfc=0:mf=1.5:mem=&18000:p%=0:lpc=1.5:begin%=0:window=0:CHANNEL
=0
 2280 v3%=0:fc =10:pc%=0:pp%=0:np%=0:pt%=0:pf%=1:bf%=0:drift%=0:blc%=0:spt%=0:sp
c%=0:ept%=0:last%=0
 2300 IF plot=0 THEN GOSUB 4380
 2320 CLS
 2340 IF plot=0 THEN GOTO 2740
 2360 GOTO 2520
 2380 DEF PROCPRINT
 2400 A$=CHR$1+CHR$&18+CHR$1+CHR$15+CHR$1
 2420 *FX3,10
 2440 PRINTA$:PRINTRIGHT$(file$,LEN(file$)-4):PRINT:PRINT"BASELINE NOISE ";bl%:P
RINT"FILTER CONSTANT ";dfc:PRINT"COUNTBACK FROM PEAK START OR END ";bc:PRINT"MAX
IMUM HEIGHT OF NOISE PEAK ";mf;" *BASELINE NOISE"
 2460  PRINT"SAMPLE TIME ";delay%;" mS":PRINT"F.S.D. ";INT(FSD(CHANNEL)/RANGE(CH
ANNEL)+.5)/10;" mV":PRINT"ASYMETRIC PEAK FACTOR ",lpc:PRINT
 2480 *FX3,0
 2500 ENDPROC
 2520 i%=CHANNEL
 2540 PROCRun
 2560:
 2580 VDU7:VDU7
 2600 GG$=INKEY$(300)
 2620 IF GG$="" THEN 2580
 2640 IFGG$<>"H" THEN 2740
 2660 PRINTTAB(0,0)CHR$(240):PRINTTAB(0,31)CHR$(241);
 2680 PROCPRINT
 2700 VDU2:CALL &C00:VDU3
 2720 GG$="":GOTO2580
 2740 VDU3:PROCmenu
 2760 GOTO2740
 2780
 2800 DEF PROCRun
 2820 v3=0
 2840 loop%=begin%:M=mem+2*loop%*chanls%+2*i%:lo=?M:M=mem+2*loop%*chanls%+2*i%+1
:hi=?M:v%=256*hi+lo:loop%=loop%+1:M=mem+2*loop%*chanls%+2*i%:lo=?M:M=mem+2*loop%
*chanls%+2*i%+1:hi=?M:v2%=256*hi+lo:loop%=loop%+1:sum%=0:LL=0
 2860 MOVE0,(v%/2^16*1024-ZERO(i%))*RANGE(i%)+Z(i%)
 2880 PROCIn:IF pc%=0 THEN LOT(i%)=LOT(i%)+v%:n%=n%+1
 2900 IF pc%=0 THEN LOT(i%)=LOT(i%)+v%:n%=n%+1
 2920 V=(v%/2^16)*1024:V=(V-ZERO(i%))*RANGE(i%)+Z(i%):DRAW (loop%-begin%)*SCALE,
V:IF pc%=1THEN3020
 2960 IF v%>BL(i%)+2*bl% THEN pp%=1:GOSUB3180
 2980 IF v%<BL(i%)-2*bl% THEN np%=1:GOSUB3180:GOTO3020
 3020
 3040 IF pc%=1 IF ABS(v%-BL(i%))> ABS(max%(i%)-BL(i%)) pt%=loop%:max%(i%)=v%
 3060 IF loop%<spt%+spc%+4000/delay% THEN 3160
 3080 IF ABS(v3%-BL(i%))>5*bl% THEN loop%=loop%+1:GOTO2880
 3100 IF pc%=1 IF max%(i%) <> 0 IF ABS(v4%-v%)<bl% IF ABS(v%-v3%)<bl% IF ABS(v3
-v4%)<bl% IF ABS(v%-m%) < bl% THEN GOSUB 3300
 3120 IF np%=1 IFv%>m% IF pc%=1 THEN GOSUB 3300
 3140 IF pc%=1 IF ABS(max%(i%)-BL(i%))<mf*bl% THEN sum%=0:pc%=0
 3160 loop%=loop%+1:GOTO 2880
 3180 REM START PEAK TIME
 3200 IF loop%<ept% THEN RETURN
 3220  m%=v4%:sum%=0:LL=0:LOOP%=loop%:home=INT(1000*bc/delay%+.5):IF p%=0 THEN 3
260
 3240 BL(i%)=LOT(i%)/n%
 3260max%(i%)=BL(i%):last%=0:spf%=1:pc%=1:PROCpeakend:m%=start%:MOVE (spt%-begin
%)*SCALE,300:DRAW (spt%-begin%)*SCALE,400:MOVE (loop%-begin%-1)*SCALE,V:VDU 7:RE
TURN
```

```
 3280 RETURN
 3300 REM END OF PEAK
 3320 VDU 7:m2%=v3%:spf%=0:LOOP%=loop%:home=INT(home*lpc+.5):IF ABS(m2%-BL(i%))>
bl% THEN last%=0:loop%=loop%+1:PROCpeakend:m2%=start%:GOTO 3360
 3340 last%=1:loop%=loop%+1:PROCpeakend:m2%=start%
 3360 LOT(i%)=0:n%=0
 3380 IF pc%=0 THEN RETURN
 3400IF max%(i%)>BL(i%) THENpp%=1:np%=0:pm%=-1
 3420 IF max%(i%)<BL(i%) THENnp%=1:pp%=0:pm%=1
 3440 p%=p%+1
 3460 IF pp%=1 THEN A(p%) =INT(sum% - (m%+m2%)*LL/2)
 3480 IF np%=1 THEN A(p%) =INT((m%+m2%)*LL/2-sum%)
 3520 IF CAL=1 THEN3560
 3540 IF A(p%)<1000THEN PRINT TAB(0,p%)"PEAK ";p%;" IGNORED":GOTO 3660
 3560 mm2=(m2%)/2^16*1024:mm2=(mm2-ZERO(i%))*RANGE(i%)+Z(i%):mm=(m%)/2^16*1024:m
m=(mm-ZERO(i%))*RANGE(i%)+Z(i%):MOVE (ept%-begin%)*SCALE,mm2-50:DRAW (ept%-begin
%)*SCALE,mm2-100
 3570 MOVE(5*(spt%-begin%+1)/4-(ept%-begin%)/4)*SCALE,5*mm/4-mm2/4:DRAW(5*(ept%-
begin%)/4-(spt%-begin%+1)/4)*SCALE,5*mm2/4-mm/4
 3580 mmax=(max%(i%))/2^16*1024:mmax=(mmax-ZERO(i%))*RANGE(i%)+Z(i%):MOVE (pt%-b
egin%)*SCALE,mmax:DRAW (pt%-begin%)*SCALE,mmax-25*pm%:MOVE (LOOP%-begin%)*SCALE
V
 3600 PRINT TAB(0,p%)"PEAK ";p%;" AREA ";A(p%);" at time ";pt%;" (";spt%;" ";ept
%;")";:PRINTINT(A(p%)*delay%/1000*FSD(i%)/65536+.5)/10;" mVs";
 3620 IF pp%=1 THEN PRINT" Positive Peak "
 3640 IF np%=1 THEN PRINT" Negative Peak "
 3660 pp%=0:np%=0:sum%=0:pf%=0:pt%=0:LL=0:loop%=LOOP%:pc%=0
 3680 RETURN
 3700
 3720 DEFPROCIn
 3740 v4%=v%:v%=v2%:v=v3:M=mem+2*loop%*chanls%+2*i%:lo=?M:M=mem+2*loop%*chanls%+
2*i%+1:hi=?M:v2%=256*hi+lo:v3%=INT(v2%*(1-dfc)+v%*dfc+.5):IFpc%=1IFloop%=scans%-
3THENm2%=v%:ept%=loop%:sum%=sum%+v3%:LL=LL+1:GOSUB 3380
 3760 IFpc%=1 THEN sum%=sum%+v3%:LL=LL+1
 3800 PRINTTAB(0,30)loop%
 3820 IF window=1THEN BL(i%)=INT((v3%+v4%+v%)/3):window=0
 3840 IF loop%>finish%-1 THEN 2560
 3860 REM NOISE SPIKE REMOVAL
 3880 IFv%>v3%+mf*bl% IF v%>v4%+mf*bl% THEN 3940
 3900 IFv%<v3%-mf*bl% IF v%<v4%-mf*bl% THEN 3940
 3920 GOTO3960
 3940 sum%=sum%-v%+(v3%+v4%)/2:v%=(v3%+v4%)/2:PRINT," * ";
 3960 ENDPROC
 3980 REM CHANGE ZERO
 4000 CLS
 4020 N$="ZERO("+STR$(CHANNEL)+")":N=Z(CHANNEL)
 4040 PROCinput
 4060 Z(CHANNEL)=N:CLS
 4080 RETURN
 4100 DEF PROCinput
 4120 PRINTN$,N
 4140 PRINT"NEW ";N$
 4160 INPUT V$
 4180 IF V$<>"" THEN N=VAL(V$)
 4200 ENDPROC
 4220 REM CHANGE RANGE
 4240 CLS
 4260 N$="RANGE("+STR$(CHANNEL)+")":N=RANGE(CHANNEL)
 4280 PROCinput
 4300 RANGE(CHANNEL)=N:CLS
 4320 RETURN
 4340 REM RUN NEW DATA
 4360 RUN
 4380 REM
 4400 FOR i%=0TOchanls%-1
 4420 FOR loop%=begin% TO 4000/delay%+begin%
```

```
 4440 GOSUB 4620
 4460 LOT(i%)=LOT(i%)+v3%
 4480 NEXTloop%'
 4500 ZERO(i%)=LOT(i%)/loop%
 4520 BL(i%)=ZERO(i%)*2^16/1024
 4540 max%(i%)=BL(i%):IBL(i%)=BL(i%)
 4560 PRINT TAB(0,30)INT(BL(i%))
 4580 NEXTi%
 4600 RETURN
 4620 REM
 4640 M=mem+2*loop%*chanls%+2*i%
 4660 lo=?M:REM PRINTlo,~M,
 4680 M=mem+2*loop%*chanls%+2*i%+1
 4700 hi=?M:REM PRINThi,~M
 4720 v3%=256*hi+lo
 4740 REMPRINTTAB(0,29)v3%,loop%
 4760 v3%=INT(v3%/2^16*1024 )
 4780
 4800 RETURN
 4820 REM RE-PLOT DATA
 4840 window=1:p%=0:plot=1:CLS:FOR i%=0 TO chanls%-1:BL(i%)=IBL(i%):LOT(i%)=0:NE
XT
 4860 GOTO2280
 4880 REM MENU OPTIONS
 4900 CLS
 4920 PRINT
 4940 PRINT"        MENU OPTIONS"
 4960 PRINT
 4980 PRINT"        R - ALLOWS VERTICAL SCALE TO BE ALTERED"
 5000 PRINT
 5020 PRINT"        Z - ALLOWS VERTICAL POSITION OF TRACE TO BE ALTERED"
 5040 PRINT
 5060 PRINT"        C - PLOT TRACE(S) "
 5080 PRINT
 5100 PRINT"        F - CHANGES FILTER CONSTANT "
 5120 PRINT
 5140 PRINT"        B - CHANGES BASELINE NOISE LEVEL"
 5160PRINT
 5180 PRINT"        H - BACK COUNT FROM PEAK DETECTION POINT"
 5200 PRINT
 5220 PRINT"        P - MAX. HEIGHT OF NOISE PEAK"
 5240 PRINT
 5260 PRINT"        N - LOAD NEW DATA"
 5280PRINT
 5300 PRINT
 5320 PRINT"        Q - QUIT PROGRAM AND RETURN TO MAIN MENU"
 5340 PRINT"        O - ESCAPE"
 5360 PRINT"PRESS ANY KEY"
 5380 RETURN
 5400 REM FILTER CONSTANT
 5420 CLS:PRINT:N$="FILTER CONSTANT":N=dfc
 5440 PROCinput
 5460 dfc=N
 5480 CLS
 5500 RETURN
 5520 REM BASELINE NOISE FACTOR
 5540 CLS:PRINT:N$="BASELINE NOISE":N=bl%
 5560 PROCinput
 5580 bl%=N
 5600 CLS
 5620 RETURN
 5640 DEF PROCpeakend
 5660  s1=v3:s1%=v2%:s2=v:s2%=v%:s3%=v4%:spc%=0:tt%=loop%
 5680 IF spf%=1 THENPROCBack
 5700 REM
 5720 PROCIn
```

```
 5740 IF loop%<3 THEN  5880
 5760 IF loop%>scans%-3 THEN  5880
 5780IF loop%>finish%-3 THEN  5880
 5800 spc%=spc%+1
 5820 IF last%>home THEN5880
 5840 REMIFspf%=1 IF loop%>=LOOP% THEN5265
 5860 last%=last%+1:loop%=loop%+1:GOTO5700
 5880 drift%=0:last%=0
 5900 IF spf%=0 THEN ept%=loop%:start%=v3%:v3=s1:v2%=s1%:v=s2:v%=s2%:loop%=tt%+1
:ENDPROC
 5920 v%=s1%:v4%=s2%:loop%=tt%+1:IF spf%=1 THEN spf%=0
 5940
 5960 ENDPROC
 5980 REM CHANGE BACK COUNT
 6000 CLS:PRINT:N$="BACK COUNT":N=bc
 6020 PROCinput
 6040 bc=N:CLS:RETURN
 6060 REM CHANGE NOISE TOLERANCE
 6080 CLS:PRINT:N$="MAX. NOISE PEAK SIZE":N=mf
 6100 PROCinput
 6120mf=N:CLS:RETURN
 6140 REM LOP-SIDED PEAK FACTOR
 6160 CLS:PRINT:N$="PEAK TAIL ":N=lpc
 6180 PROCinput
 6200 lpc=N:CLS:RETURN
 6220 REM PEAK WINDOW
 6240 CLS:N$="START TIME ":N=begin%:PROCinput:begin%=N
 6260 N$="FINISH TIME ":N=finish%:PROCinput:finish%=N:CLS
 6280 IF finish%>scans%THEN finish%=scans%
 6300 SCALE= 1278/(finish%-begin%)
 6320 window=1:RETURN
 6340 DEFPROCBack
 6360 start%=v3%
 6380 IF loop%=LOOP%-home THEN v3%=v%:v3=v:spt%=loop%:ENDPROC
 6400 IF loop%<6 THEN v3%=v%:spt%=loop%:ENDPROC
 6420loop%=loop%-1
 6440 M=mem+2*loop%*chanls%+2*i%:lo=?M:M=mem+2*loop%*chanls%+2*i%+1:hi=?M:v3%=25
6*hi+lo
 6460 IFdfc=0THENv%=v3%:v2%=v3%:start%=v3%:GOTO6520
 6480 v%=INT(v2%*(1-dfc)+v3%*dfc+.5):v2%=v3%:start%=v3%
 6520 GOTO 6380
 6580 REM CHANGE CHANNEL
 6600 IF chanls%=1 THEN RETURN
 6620 CLS:N$="CHANNEL ":N=CHANNEL
 6640 PROCinput
 6660 IF N>chanls%-1 THEN6640
 6680 CHANNEL=N:CLS:RETURN
>
```

Appendix IX - Modifications to the Data-Processing Program to Enable the Calculation of the 1st Moment of the Peak

```
 2160 DEF PROCRun
 2180 loop%=begin%:M=mem+2*loop%*chanls%+2*i%:lo=?M:M=mem+2*loop%*chanls%+2*i%+1
:hi=?M:v%=256*hi+lo:loop%=loop%+1:M=mem+2*loop%*chanls%+2*i%:lo=?M:M=mem+2*loop%
*chanls%+2*i%+1:hi=?M:v3%=256*hi+lo:loop%=loop%+1:sum%=0:LL=0:v3=v3%
 2400 MOVE0,(v%/2^16*1024-ZERO(i%))*RANGE(i%)+Z(i%)
 2420 PROCIn:IF pc%=0 THEN LOT(i%)=LOT(i%)+v%:n%=n%+1
 2440 IF pc%=0 THEN LOT(i%)=LOT(i%)+v%:n%=n%+1
 2460 V=(v%/2^16)*1024:V=(V-ZERO(i%))*RANGE(i%)+Z(i%):DRAW (loop%-begin%)*SCALE,
V:IF pc%=1THEN2600
 2560 REMIF v%-v4%>bl% IF v3%-v%>bl% IF v3%-v4%>bl% THEN pp%=1:GOSUB2680:GOTO 25
75
 2570 IF v%>BL(i%)+2*bl% THEN pp%=1:GOSUB2680
 2575 IF v%<BL(i%)-2*bl% THEN np%=1:GOSUB2680:GOTO2600
 2580 REMIF v%-v4%<-bl% IF v3%-v%<-bl% IF v3%-v4%<-bl% THEN np%=1:GOSUB2680
 2600
 2620 IF pc%=1 IF ABS(v%-BL(i%))> ABS(max%(i%)-BL(i%)) pt%=loop%:max%(i%)=v%
 2630 IF loop%<spt%+spc%+4000/delay% THEN 2660
 2635 IF ABS(v3%-BL(i%))>5*bl% THEN loop%=loop%+1:GOTO2420
 2640 IF pc%=1 IF max%(i%) <> 0 IF ABS(v4%-v%)<bl% IF ABS(v%-v3%)<bl% IF ABS(v3%
-v4%)<bl% IF ABS(v%-m%) < bl% THEN GOSUB 2860
 2655 IF pp%=1 IFv%<m% IF pc%=1 THEN GOSUB 2860
 2656 IF np%=1 IFv%>m% IF pc%=1 THEN GOSUB 2860
 2657 IF pc%=1 IF ABS(max%(i%)-BL(i%))<mf*bl% THEN sum%=0:sum2%=0:pc%=0
 2660 loop%=loop%+1:GOTO 2420
 2680 REM START PEAK TIME
 2690 IF loop%-20<ept% THEN RETURN
 2700  m%=v4%:sum%=0:sum2%=0:LL=0:LOOP%=loop%:home=1000*bc/delay%:IF p%=0 THEN 2
740
 2730 BL(i%)=LOT(i%)/n%
 2740max%(i%)=BL(i%):last%=0:spf%=1:pc%=1:PROCpeakend:m%=start%:mm=(m%)/2^16*102
4:mm=(mm-ZERO(i%))*RANGE(i%)+Z(i%):MOVE (spt%-begin%)*SCALE,mm:DRAW (spt%-begin%
)*SCALE,mm-75:MOVE (loop%-begin%-1)*SCALE,V:VDU 7:RETURN
 2840 RETURN
 2860 REM END OF PEAK
 2880 VDU 7:m2%=v3%:spf%=0:LOOP%=loop%:home=home*1pc:IF ABS(m2%-BL(i%))>bl% THEN
 last%=0:loop%=loop%+1:PROCpeakend:m2%=start%:GOTO 2940
 2930 last%=1:loop%=loop%+1:PROCpeakend:m2%=start%
 2960 IF pc%=0 THEN RETURN
 2975 p%=p%+1
 2980 mt=INT((sum%/sum2%+spt%)*10+.5)/10
 3060 mm2=(m2%)/2^16*1024:mm2=(mm2-ZERO(i%))*RANGE(i%)+Z(i%):mm=(m%)/2^16*1024:m
m=(mm-ZERO(i%))*RANGE(i%)+Z(i%):MOVE (spt%-begin%)*SCALE,mm:DRAW (ept%-begin%)*S
CALE,mm2:DRAW (ept%-begin%)*SCALE,mm2-50:MOVE (LOOP%-begin%)*SCALE,V
 3080 mmax=(max%(i%))/2^16*1024:mmax=(mmax-ZERO(i%))*RANGE(i%)+Z(i%):MOVE (mt-be
gin%)*SCALE,mmax:DRAW (mt-begin%)*SCALE,mmax-25:MOVE (LOOP%-begin%)*SCALE,V
 3120 PRINT TAB(0,p%);mt
 3160 pp%=0:np%=0:sum%=0:sum2%=0:pf%=0:pt%=0:LL=0:loop%=LOOP%:pc%=0
 3180 RETURN
 3200
 3220 DEFPROCIn
 3240 v4%=v%:v%=v3%:v=v3:M=mem+2*loop%*chanls%+2*i%:lo=?M:M=mem+2*loop%*chanls%+
2*i%+1:hi=?M:v3%=256*hi+lo:v3=v3%*(1-dfc)+v*dfc
 3250 v3%=INT(v3+.5)
 3260 IFpc%=1 THEN sum%=sum%+v%*(loop%-spt%):sum2%=sum2%+v%:LL=LL+1
 3340 PRINTTAB(0,30)(loop%-1)
 3345 REMPRINTv3%,INT(v3*100+.5)/100,v%,INT(v*100+.5)/100,loop%
 3350 IF window=1THEN BL(i%)=INT((v3%+v4%+v%)/3):window=0
 3360 IF loop%>finish% THEN 2060
 3380 IFv%>v3% IF v%>v4% GOTO3440
 3400 IFv%<v3% IF v%<v4% GOTO3440
 3420 GOTO3460
 3440 v%=INT(v3%+v4%)/2
 3460 ENDPROC
>
```

Appendix X - Listing of the Calibration Peak Generating Program

```
  10GOTO2000
 100DEFPROCData
 110DIM I%(1000),A(10),C(14),N(5),K(5)
 125R=20:S=.95:T=.6
 130CLS:Y0=0:Y=0:MOVE0,00:SUM=0
 140FORI=0TO319:J=I/100:X=J*(A+J*(B+J*C))
 150X=X+D*(RND(1)+RND(1)+RND(1))
 160IFI>100 IFI<100+R Y=EXP(6.23*(I-100)/R):Y1=(Y-Y0)*5:Y0=Y
 170IFI>99+R Y=Y+Y1:Y1=Y1*S:Y=Y*T
 180I%(I)=X+INT(Y):SUM=SUM+INT(Y)
 190DRAWI*4,I%(I)
 200NEXT:PRINT"Area = ";SUM
 210ENDPROC
 500STOP
2000REM SAVE "CALIBP"
2020CLOSE£0
2030INPUTA,B,C,D: file$=STR$(A)+STR$(B)+STR$(C)+STR$(D)
2040file$=":1._"+file$+"P"
2050handle%=OPENOUT(file$)
2060 PROCData
2070 i%=319
2200PROCwrite
2220CLOSE£handle%
2230STOP
2240 DEF PROCwrite
2250 LOCAL loop%
2260 FOR loop%=0 TO i%-1
2270 PRINT£handle%,I%(loop%)
2280 PRINTI%(loop%),loop%
2290 NEXT loop%
2300 ENDPROC
>
```

Appendix XI - Calibration Peak Analyses

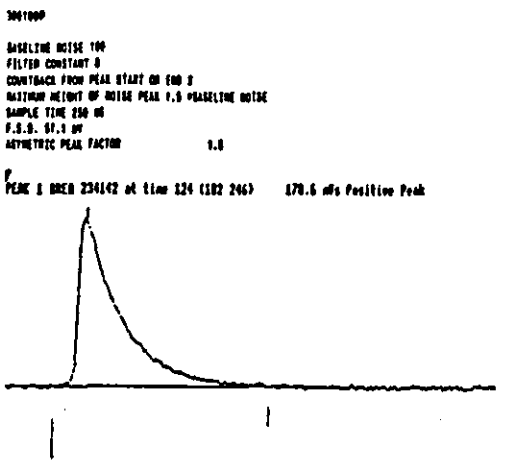

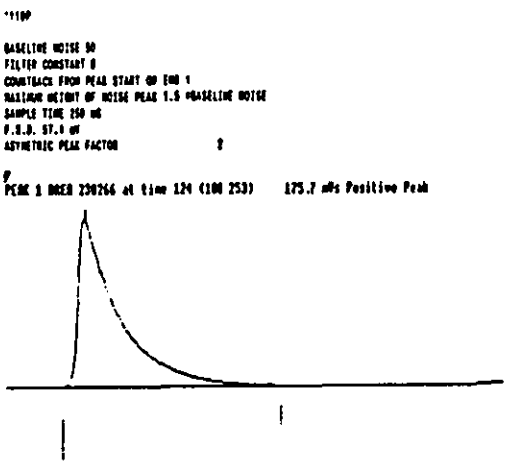

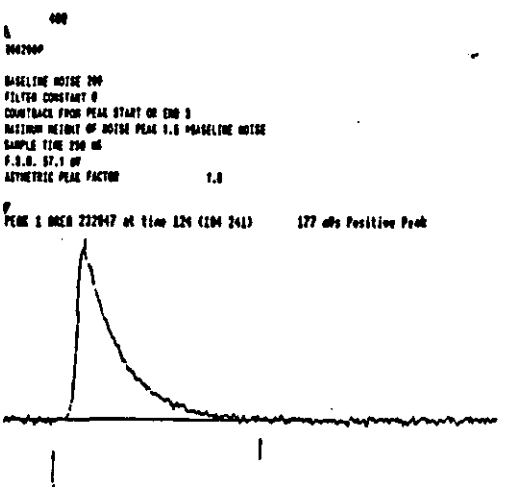

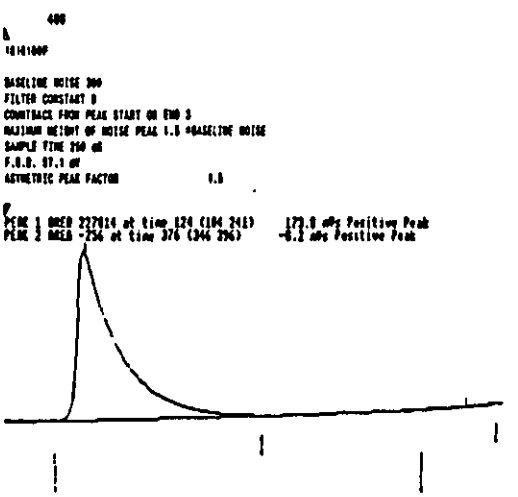

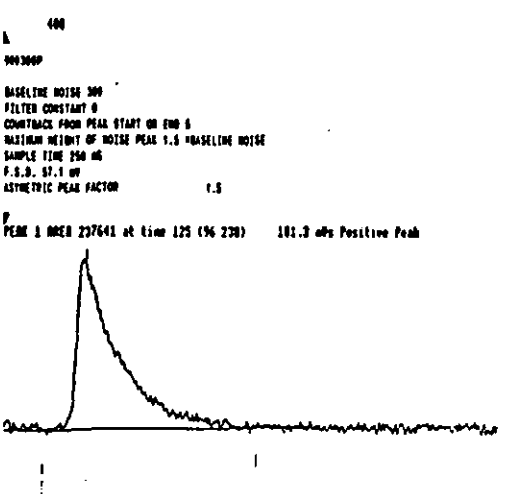

Appendix XII - Acid Peak Analyses

AC10

BASELINE NOISE 200
FILTER CONSTANT 0
COUNTBACK FROM PEAK START OR END 7
MAXIMUM HEIGHT OF NOISE PEAK 1.0 *BASELINE NOISE
SAMPLE TIME 250 mS
F.S.D. 500 mV
ASYMETRIC PEAK FACTOR 5

PEAK 1 AREA 1103945 at time 1126 (1055 1644) 8422.4 mVs Positive Peak

AC3

BASELINE NOISE 200
FILTER CONSTANT 0
COUNTBACK FROM PEAK START OR END 8
MAXIMUM HEIGHT OF NOISE PEAK 1.0 *BASELINE NOISE
SAMPLE TIME 250 mS
F.S.D. 500 mV
ASYMETRIC PEAK FACTOR 8.2

PEAK 1 AREA 1126405 at time 1017 (952 1520) 8593.8 mVs Positive Peak

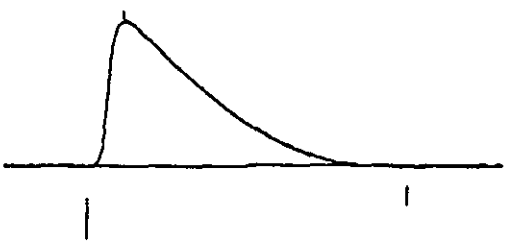

1800

AC11

BASELINE NOISE 200
FILTER CONSTANT 0
COUNTBACK FROM PEAK START OR END 7
MAXIMUM HEIGHT OF NOISE PEAK 1.0 *BASELINE NOISE
SAMPLE TIME 250 mS
F.S.D. 500 mV
ASYMETRIC PEAK FACTOR 5

PEAK 1 AREA 1123666 at time 1075 (1005 1596) 8572.9 mVs Positive Peak

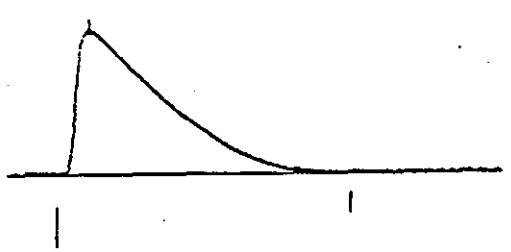

1700

AC19

BASELINE NOISE 200
FILTER CONSTANT 0
COUNTBACK FROM PEAK START OR END 7
MAXIMUM HEIGHT OF NOISE PEAK 1.0 *BASELINE NOISE
SAMPLE TIME 250 mS
F.S.D. 500 mV
ASYMETRIC PEAK FACTOR 4.9

PEAK 1 AREA 1186471 at time 1063 (997 1596) 9052.1 mVs Positive Peak

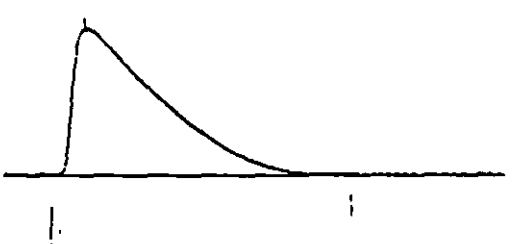

1900

AC17

BASELINE NOISE 200
FILTER CONSTANT 0
COUNTBACK FROM PEAK START OR END 7
MAXIMUM HEIGHT OF NOISE PEAK 1.0 *BASELINE NOISE
SAMPLE TIME 250 mS
F.S.D. 500 mV
ASYMETRIC PEAK FACTOR 5

PEAK 1 AREA 814956 at time 1109 (1037 1581) 6217.6 mVs Positive Peak

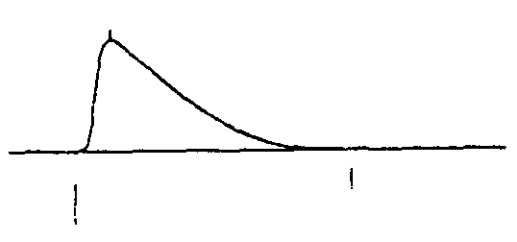

1900

AC13

BASELINE NOISE 200
FILTER CONSTANT 0
COUNTBACK FROM PEAK START OR END 7
MAXIMUM HEIGHT OF NOISE PEAK 1.0 *BASELINE NOISE
SAMPLE TIME 250 mS
F.S.D. 500 mV
ASYMETRIC PEAK FACTOR 5

PEAK 1 AREA 853943 at time 1077 (1006 1561) 6520.3 mVs Positive Peak

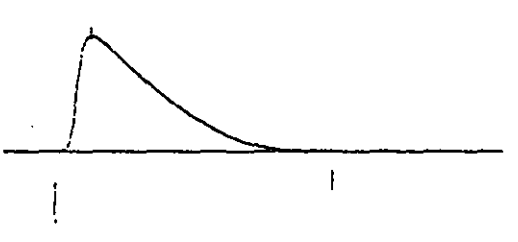

1900

1900

AC10

BASELINE NOISE 200
FILTER CONSTANT 0
COUNTBACK FROM PEAK START OR END ?
MAXIMUM HEIGHT OF NOISE PEAK 1.0 *BASELINE NOISE
SAMPLE TIME 250 uS
F.S.D. 500 mV
ASYMETRIC PEAK FACTOR 4.0

PEAK 1 AREA 1868908 at time 1867 (994 1555) 7697.4 mVs Positive Peak

1900

AC11

BASELINE NOISE 200
FILTER CONSTANT 0
COUNTBACK FROM PEAK START OR END ?
MAXIMUM HEIGHT OF NOISE PEAK 1.0 *BASELINE NOISE
SAMPLE TIME 250 uS
F.S.D. 500 mV
ASYMETRIC PEAK FACTOR 5

PEAK 1 AREA 996737 at time 1880 (1400 1571) 6917.9 mVs Positive Peak

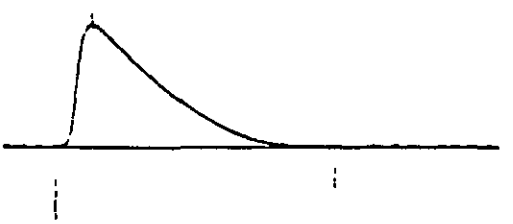

1900

AC16

BASELINE NOISE 200
FILTER CONSTANT 0
COUNTBACK FROM PEAK START OR END ?
MAXIMUM HEIGHT OF NOISE PEAK 1.0 *BASELINE NOISE
SAMPLE TIME 250 uS
F.S.D. 500 mV
ASYMETRIC PEAK FACTOR 5

PEAK 1 AREA 851834 at time 1180 (1031 1505) 6499 mVs Positive Peak

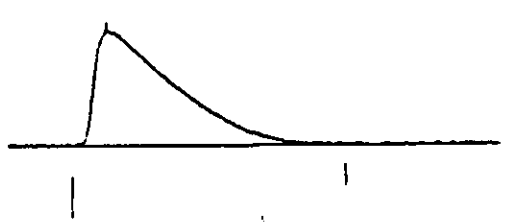

1900

AC17

BASELINE NOISE 200
FILTER CONSTANT 0
COUNTBACK FROM PEAK START OR END ?
MAXIMUM HEIGHT OF NOISE PEAK 1.0 *BASELINE NOISE
SAMPLE TIME 250 uS
F.S.D. 500 mV
ASYMETRIC PEAK FACTOR 5

PEAK 1 AREA 1129973 at time 1946 (979 1566) 8621 mVs Positive Peak

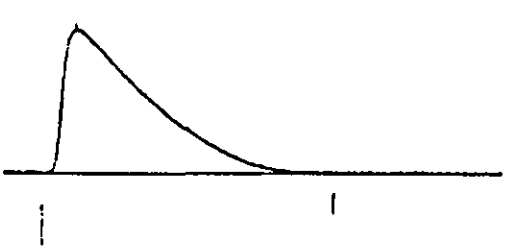

1900

AC18

BASELINE NOISE 200
FILTER CONSTANT 0
COUNTBACK FROM PEAK START OR END ?
MAXIMUM HEIGHT OF NOISE PEAK 1.0 *BASELINE NOISE
SAMPLE TIME 250 uS
F.S.D. 500 mV
ASYMETRIC PEAK FACTOR 4.0

PEAK 1 AREA 917461 at time 1875 (1005 1565) 6999.7 mVs Positive Peak

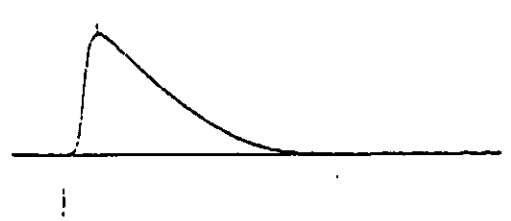

1900

Appendix XIII - Water Peak Analyses

AC06

BASELINE NOISE 50
FILTER CONSTANT 0
COUNTBACK FROM PEAK START OR END 2
MAXIMUM HEIGHT OF NOISE PEAK 1.5 *BASELINE NOISE
SAMPLE TIME 250 mS
F.S.D. 40 mV
ASYMETRIC PEAK FACTOR 1

PEAK 1 AREA 3571 at time 296 (280 319) 27.2 mVs Positive Peak

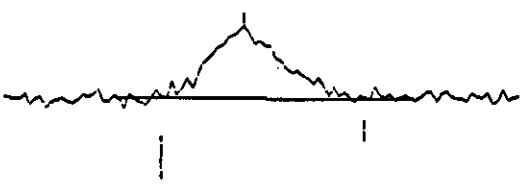

350

AC09

BASELINE NOISE 50
FILTER CONSTANT 0
COUNTBACK FROM PEAK START OR END 3
MAXIMUM HEIGHT OF NOISE PEAK 1.5 *BASELINE NOISE
SAMPLE TIME 250 mS
F.S.D. 40 mV
ASYMETRIC PEAK FACTOR 1

PEAK 1 AREA 8446 at time 189 (168 221) 64.4 mVs Positive Peak

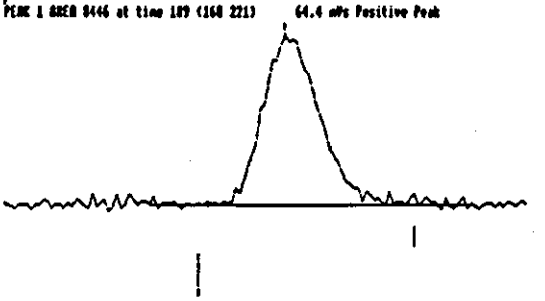

250

AC10

BASELINE NOISE 50
FILTER CONSTANT 0
COUNTBACK FROM PEAK START OR END 1.5
MAXIMUM HEIGHT OF NOISE PEAK 1.5 *BASELINE NOISE
SAMPLE TIME 250 mS
F.S.D. 40 mV
ASYMETRIC PEAK FACTOR 1.0

PEAK 1 AREA 7260 at time 248 (233 274) 55.4 mVs Positive Peak

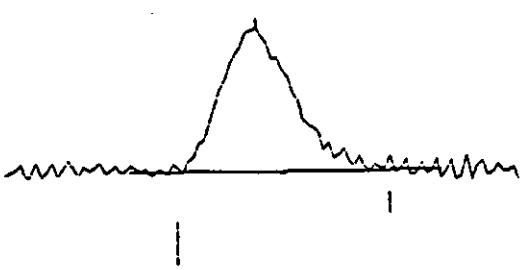

250

AC11

BASELINE NOISE 50
FILTER CONSTANT 0
COUNTBACK FROM PEAK START OR END 2
MAXIMUM HEIGHT OF NOISE PEAK 1.5 *BASELINE NOISE
SAMPLE TIME 250 mS
F.S.D. 80 mV
ASYMETRIC PEAK FACTOR 1.2

PEAK 1 AREA 13639 at time 242 (223 274) 104.1 mVs Positive Peak

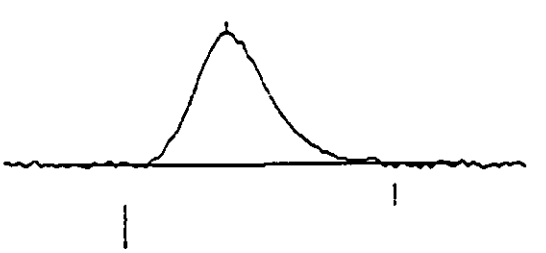

300

AC12

BASELINE NOISE 50
FILTER CONSTANT 0
COUNTBACK FROM PEAK START OR END 3.5
MAXIMUM HEIGHT OF NOISE PEAK 1.5 *BASELINE NOISE
SAMPLE TIME 250 mS
F.S.D. 40 mV
ASYMETRIC PEAK FACTOR 1

PEAK 1 AREA 2671 at time 232 (215 263) 20.4 mVs Positive Peak

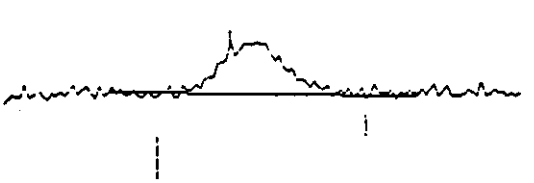

300

AC13

BASELINE NOISE 50
FILTER CONSTANT 0
COUNTBACK FROM PEAK START OR END 3
MAXIMUM HEIGHT OF NOISE PEAK 1.5 *BASELINE NOISE
SAMPLE TIME 250 mS
F.S.D. 40 mV
ASYMETRIC PEAK FACTOR 1.3

PEAK 1 AREA 1864 at time 214 (197 244) 14.2 mVs Positive Peak

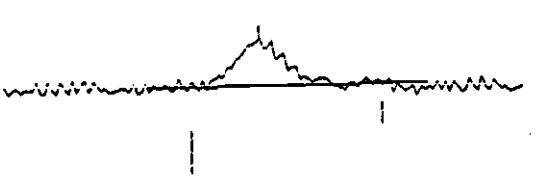

300

200

AC14

BASELINE NOISE 50
FILTER CONSTANT 0
COUNTBACK FROM PEAK START OR END 3.5
MAXIMUM HEIGHT OF NOISE PEAK 1.5 *BASELINE NOISE
SAMPLE TIME 250 mS
F.S.D. 40 mV
ASYMETRIC PEAK FACTOR 0

PEAK 1 AREA 2344 at time 225 (206 239) 17.9 mVs Positive Peak

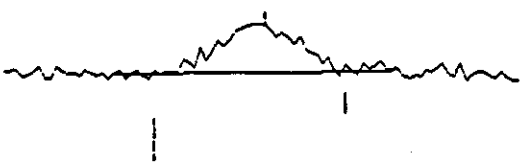

270

AC15

BASELINE NOISE 50
FILTER CONSTANT 0
COUNTBACK FROM PEAK START OR END 3
MAXIMUM HEIGHT OF NOISE PEAK 1.5 *BASELINE NOISE
SAMPLE TIME 250 mS
F.S.D. 40 mV
ASYMETRIC PEAK FACTOR 1

PEAK 1 AREA 3612 at time 222 (204 249) 27.6 mVs Positive Peak

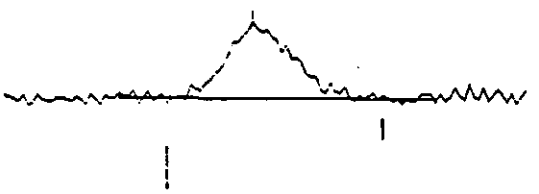

280

AC16

BASELINE NOISE 50
FILTER CONSTANT 0
COUNTBACK FROM PEAK START OR END 3.5
MAXIMUM HEIGHT OF NOISE PEAK 1.5 *BASELINE NOISE
SAMPLE TIME 250 mS
F.S.D. 40 mV
ASYMETRIC PEAK FACTOR 1.2

PEAK 1 AREA 2615 at time 237 (217 267) 20 mVs Positive Peak

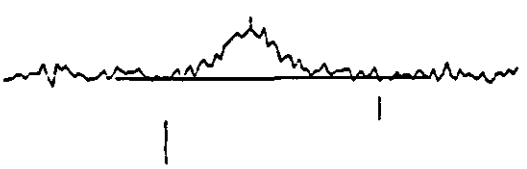

AC17

BASELINE NOISE 50
FILTER CONSTANT 0
COUNTBACK FROM PEAK START OR END 4
MAXIMUM HEIGHT OF NOISE PEAK 1.5 *BASELINE NOISE
SAMPLE TIME 250 mS
F.S.D. 40 mV
ASYMETRIC PEAK FACTOR 0.5

PEAK 1 AREA 1837 at time 220 (207 250) 14 mVs Positive Peak

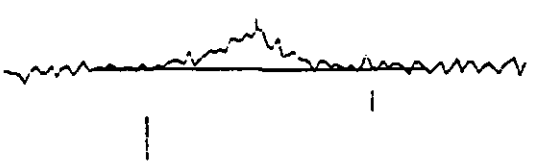

300

AC18

BASELINE NOISE 50
FILTER CONSTANT 0
COUNTBACK FROM PEAK START OR END 4.5
MAXIMUM HEIGHT OF NOISE PEAK 1.5 *BASELINE NOISE
SAMPLE TIME 250 mS
F.S.D. 40 mV
ASYMETRIC PEAK FACTOR 0.5

PEAK 1 AREA 1832 at time 222 (203 249) 14 mVs Positive Peak

270

290

Appendix XIV - Hydrogen Peak Analyses

HHE911

BASELINE NOISE 300
FILTER CONSTANT 0
COUNTBACK FROM PEAK START OR END 2
MAXIMUM HEIGHT OF NOISE PEAK 1.5 *BASELINE NOISE
SAMPLE TIME 250 mS
F.S.D. 100 mV
ASYMETRIC PEAK FACTOR 1.5

PEAK 1 AREA 239929 at time 166 (140 233) 183.1 mVs Positive Peak

270

HHE911

BASELINE NOISE 500
FILTER CONSTANT 0
COUNTBACK FROM PEAK START OR END 9
MAXIMUM HEIGHT OF NOISE PEAK 0.7 *BASELINE NOISE
SAMPLE TIME 250 mS
F.S.D. 40 mV
ASYMETRIC PEAK FACTOR 0.3

PEAK 1 AREA 219530 at time 310 (244 403) 167.5 mVs Negative Peak

450

HHE1011

BASELINE NOISE 300
FILTER CONSTANT 0
COUNTBACK FROM PEAK START OR END 2
MAXIMUM HEIGHT OF NOISE PEAK 1.5 *BASELINE NOISE
SAMPLE TIME 250 mS
F.S.D. 100 mV
ASYMETRIC PEAK FACTOR 1.5

PEAK 1 AREA 246182 at time 163 (136 229) 187.8 mVs Positive Peak

270

HHE1011

BASELINE NOISE 500
FILTER CONSTANT 0
COUNTBACK FROM PEAK START OR END 9
MAXIMUM HEIGHT OF NOISE PEAK 1.5 *BASELINE NOISE
SAMPLE TIME 250 mS
F.S.D. 40 mV
ASYMETRIC PEAK FACTOR 1

PEAK 1 AREA 240283 at time 310 (253 399) 183.3 mVs Negative Peak

450

HHE1012

BASELINE NOISE 300
FILTER CONSTANT 0
COUNTBACK FROM PEAK START OR END 9
MAXIMUM HEIGHT OF NOISE PEAK 1.5 *BASELINE NOISE
SAMPLE TIME 250 mS
F.S.D. 100 mV
ASYMETRIC PEAK FACTOR 1.5

PEAK 1 AREA 242106 at time 167 (144 238) 184.7 mVs Positive Peak

250

HHE1012

BASELINE NOISE 300
FILTER CONSTANT 0
COUNTBACK FROM PEAK START OR END 7
MAXIMUM HEIGHT OF NOISE PEAK 1.5 *BASELINE NOISE
SAMPLE TIME 250 mS
F.S.D. 40 mV
ASYMETRIC PEAK FACTOR 0.7

PEAK 1 AREA 233730 at time 313 (247 396) 178.3 mVs Negative Peak

450

HHE1013

BASELINE NOISE 500
FILTER CONSTANT 0
COUNTBACK FROM PEAK START OR END 2
MAXIMUM HEIGHT OF NOISE PEAK 1.5 *BASELINE NOISE
SAMPLE TIME 250 uS
F.S.D. 100 uV
ASYMETRIC PEAK FACTOR 1.0

PEAK 1 AREA 241760 at time 175 (152 241) 184.4 uVs Positive Peak

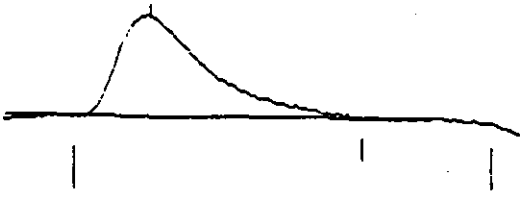

291

HHE1013

BASELINE NOISE 500
FILTER CONSTANT 0
COUNTBACK FROM PEAK START OR END 6
MAXIMUM HEIGHT OF NOISE PEAK 0.7 *BASELINE NOISE
SAMPLE TIME 250 uS
F.S.D. 40 uV
ASYMETRIC PEAK FACTOR 1.0

PEAK 1 AREA 238446 at time 317 (265 412) 181.9 uVs Negative Peak

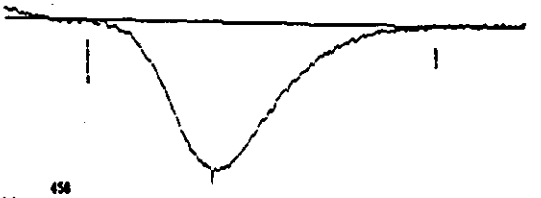

450

HHE1014

BASELINE NOISE 500
FILTER CONSTANT 0
COUNTBACK FROM PEAK START OR END 2
MAXIMUM HEIGHT OF NOISE PEAK 1.5 *BASELINE NOISE
SAMPLE TIME 250 uS
F.S.D. 100 uV
ASYMETRIC PEAK FACTOR 2

PEAK 1 AREA 239475 at time 167 (145 235) 182.7 uVs Positive Peak

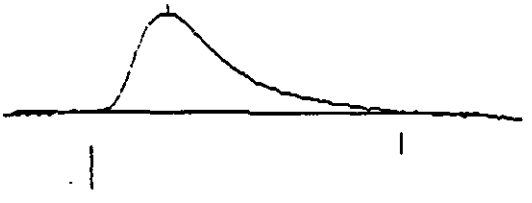

270

HHE1014

BASELINE NOISE 500
FILTER CONSTANT 0
COUNTBACK FROM PEAK START OR END 7
MAXIMUM HEIGHT OF NOISE PEAK 1.5 *BASELINE NOISE
SAMPLE TIME 250 uS
F.S.D. 40 uV
ASYMETRIC PEAK FACTOR 1.0

PEAK 1 AREA 237069 at time 311 (249 411) 180.9 uVs Negative Peak

450

HHE1015

BASELINE NOISE 300
FILTER CONSTANT 0
COUNTBACK FROM PEAK START OR END 2
MAXIMUM HEIGHT OF NOISE PEAK 1.5 *BASELINE NOISE
SAMPLE TIME 250 uS
F.S.D. 100 uV
ASYMETRIC PEAK FACTOR 2.4

PEAK 1 AREA 241225 at time 166 (140 238) 184 uVs Positive Peak

270

HHE1015

BASELINE NOISE 400
FILTER CONSTANT 0
COUNTBACK FROM PEAK START OR END 6
MAXIMUM HEIGHT OF NOISE PEAK 1.5 *BASELINE NOISE
SAMPLE TIME 250 uS
F.S.D. 40 uV
ASYMETRIC PEAK FACTOR 3.1

PEAK 1 AREA 232099 at time 312 (246 393) 177.1 uVs Negative Peak

450

HHE1111

BASELINE NOISE 300
FILTER CONSTANT 0
COUNTBACK FROM PEAK START OR END 1
MAXIMUM HEIGHT OF NOISE PEAK 1.5 *BASELINE NOISE
SAMPLE TIME 250 uS
F.S.D. 100 mV
ASYMETRIC PEAK FACTOR 2.0

PEAK 1 AREA 218385 at time 139 (122 284) 160.4 mVs Positive Peak

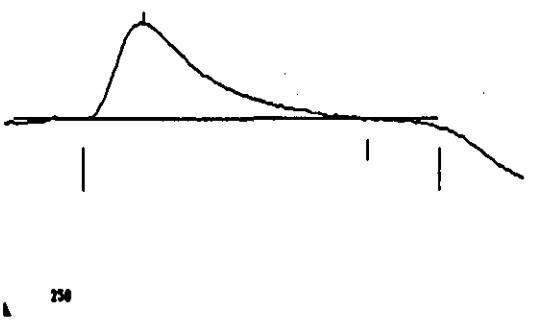

HHE1111

BASELINE NOISE 300
FILTER CONSTANT 0
COUNTBACK FROM PEAK START OR END 2
MAXIMUM HEIGHT OF NOISE PEAK 1.5 *BASELINE NOISE
SAMPLE TIME 250 uS
F.S.D. 40 mV
ASYMETRIC PEAK FACTOR 2.0

PEAK 1 AREA 201092 at time 254 (218 340) 153.4 mVs Negative Peak

HHE1112

BASELINE NOISE 300
FILTER CONSTANT 0
COUNTBACK FROM PEAK START OR END 1
MAXIMUM HEIGHT OF NOISE PEAK 1.5 *BASELINE NOISE
SAMPLE TIME 250 uS
F.S.D. 100 mV
ASYMETRIC PEAK FACTOR 2

PEAK 1 AREA 206588 at time 137 (120 284) 157.6 mVs Positive Peak

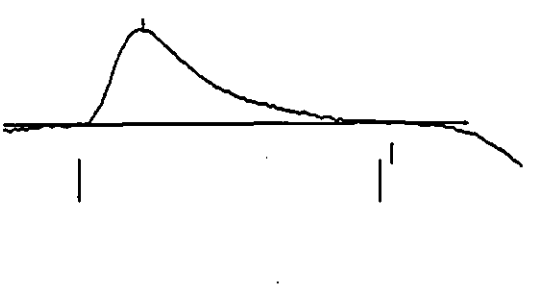

HHE1112

BASELINE NOISE 300
FILTER CONSTANT 0
COUNTBACK FROM PEAK START OR END 4
MAXIMUM HEIGHT OF NOISE PEAK 1.5 *BASELINE NOISE
SAMPLE TIME 250 uS
F.S.D. 40 mV
ASYMETRIC PEAK FACTOR 2

PEAK 1 AREA 215285 at time 253 (204 342) 164.2 mVs Negative Peak

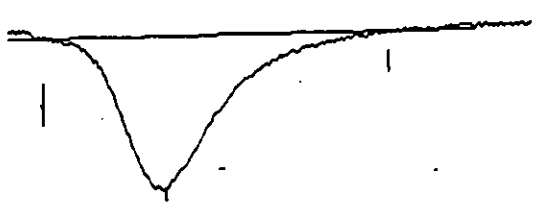

HHE1113

BASELINE NOISE 250
FILTER CONSTANT 0
COUNTBACK FROM PEAK START OR END 1
MAXIMUM HEIGHT OF NOISE PEAK 1.5 *BASELINE NOISE
SAMPLE TIME 250 uS
F.S.D. 100 mV
ASYMETRIC PEAK FACTOR 1.8

PEAK 1 AREA 215520 at time 152 (134 217) 164.4 mVs Positive Peak

HHE1113

BASELINE NOISE 250
FILTER CONSTANT 0
COUNTBACK FROM PEAK START OR END 4
MAXIMUM HEIGHT OF NOISE PEAK 1.5 *BASELINE NOISE
SAMPLE TIME 250 uS
F.S.D. 40 mV
ASYMETRIC PEAK FACTOR 2

PEAK 1 AREA 217981 at time 267 (220 365) 166.3 mVs Negative Peak

HHE1114

BASELINE NOISE 200
FILTER CONSTANT 0
COUNTBACK FROM PEAK START OR END 2
MAXIMUM HEIGHT OF NOISE PEAK 1.5 *BASELINE NOISE
SAMPLE TIME 250 mS
F.S.D. 100 mV
ASYMETRIC PEAK FACTOR 1.7

PEAK 1 AREA 209206 at time 140 (119 296) 150.8 mVs Positive Peak

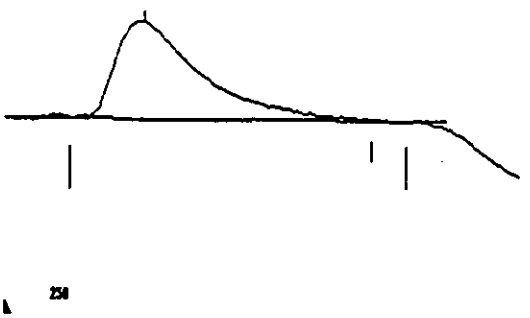

HHE1114

BASELINE NOISE 200
FILTER CONSTANT 0
COUNTBACK FROM PEAK START OR END 4
MAXIMUM HEIGHT OF NOISE PEAK 1.5 *BASELINE NOISE
SAMPLE TIME 250 mS
F.S.D. 40 mV
ASYMETRIC PEAK FACTOR 1.0

PEAK 1 AREA 201580 at time 255 (207 336) 153.8 mVs Negative Peak

HHE1115

BASELINE NOISE 400
FILTER CONSTANT 0
COUNTBACK FROM PEAK START OR END 1
MAXIMUM HEIGHT OF NOISE PEAK 1.5 *BASELINE NOISE
SAMPLE TIME 250 mS
F.S.D. 100 mV
ASYMETRIC PEAK FACTOR 2.8

PEAK 1 AREA 211495 at time 142 (125 207) 161.3 mVs Positive Peak

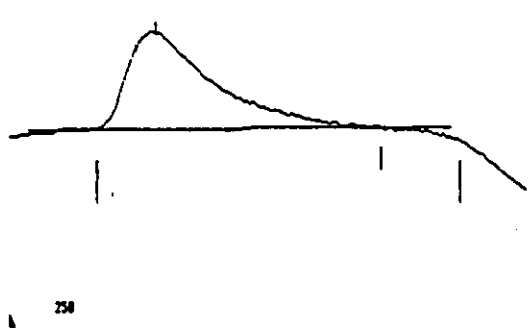

HHE1115

BASELINE NOISE 700
FILTER CONSTANT 0
COUNTBACK FROM PEAK START OR END 2
MAXIMUM HEIGHT OF NOISE PEAK 1.5 *BASELINE NOISE
SAMPLE TIME 250 mS
F.S.D. 40 mV
ASYMETRIC PEAK FACTOR 4

PEAK 1 AREA 243123 at time 257 (215 353) 185.5 mVs Negative Peak

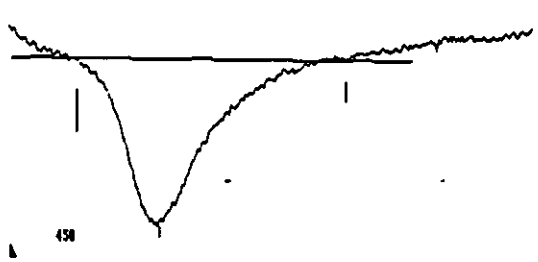

Appendix XV - Argon Peak Analyses

AHE311

BASELINE NOISE 100
FILTER CONSTANT 0
COUNTBACK FROM PEAK START OR END 1
MAXIMUM HEIGHT OF NOISE PEAK 1.5 *BASELINE NOISE
SAMPLE TIME 250 mS
F.S.D. 200 mV
ASYMETRIC PEAK FACTOR 1.5

PEAK 1 AREA 475965 at time 150 (131 254) 363.1 mVs Positive Peak

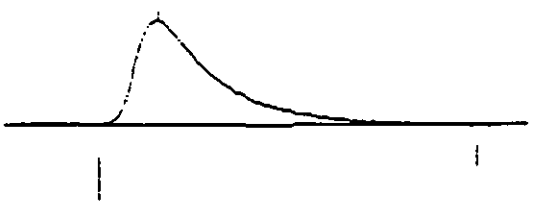

270

AHE312

BASELINE NOISE 100
FILTER CONSTANT 0
COUNTBACK FROM PEAK START OR END 1
MAXIMUM HEIGHT OF NOISE PEAK 1.5 *BASELINE NOISE
SAMPLE TIME 250 mS
F.S.D. 200 mV
ASYMETRIC PEAK FACTOR 1.5

PEAK 1 AREA 469709 at time 153 (134 234) 358.4 mVs Positive Peak

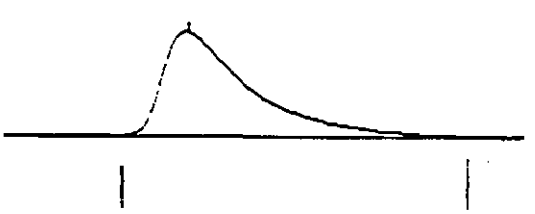

250

AHE313

BASELINE NOISE 600
FILTER CONSTANT 0
COUNTBACK FROM PEAK START OR END 10
MAXIMUM HEIGHT OF NOISE PEAK 1.5 *BASELINE NOISE
SAMPLE TIME 250 mS
F.S.D. 40 mV
ASYMETRIC PEAK FACTOR 1

PEAK 1 AREA 483595 at time 552 (440 675) 369 mVs Negative Peak

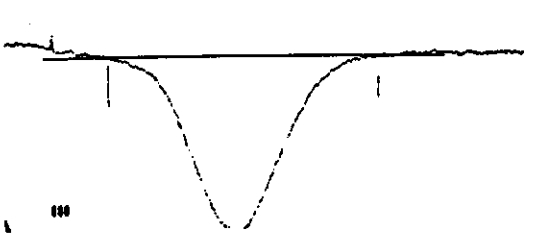

600

AHE311

BASELINE NOISE 600
FILTER CONSTANT 0
COUNTBACK FROM PEAK START OR END 10
MAXIMUM HEIGHT OF NOISE PEAK 1.5 *BASELINE NOISE
SAMPLE TIME 250 mS
F.S.D. 40 mV
ASYMETRIC PEAK FACTOR 2

PEAK 1 AREA 485002 at time 547 (451 735) 370 mVs Negative Peak

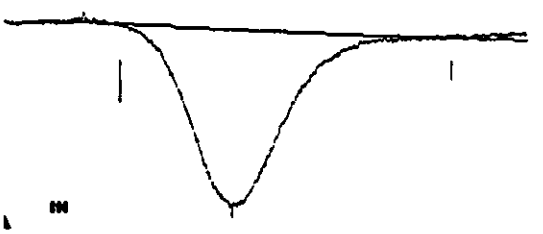

600

AHE312

BASELINE NOISE 600
FILTER CONSTANT 0
COUNTBACK FROM PEAK START OR END 12
MAXIMUM HEIGHT OF NOISE PEAK 1.5 *BASELINE NOISE
SAMPLE TIME 250 mS
F.S.D. 40 mV
ASYMETRIC PEAK FACTOR 1.2

PEAK 1 AREA 459611 at time 543 (442 687) 350.7 mVs Negative Peak

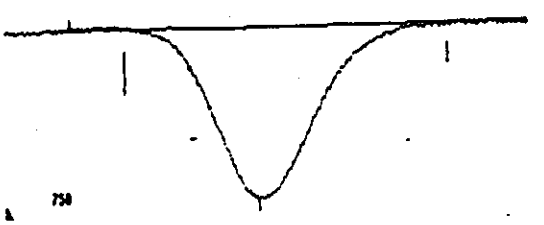

750

AHE313

BASELINE NOISE 200
FILTER CONSTANT 0
COUNTBACK FROM PEAK START OR END 1
MAXIMUM HEIGHT OF NOISE PEAK 1.5 *BASELINE NOISE
SAMPLE TIME 250 mS
F.S.D. 200 mV
ASYMETRIC PEAK FACTOR 1.5

PEAK 1 AREA 477876 at time 168 (141 255) 364.6 mVs Positive Peak

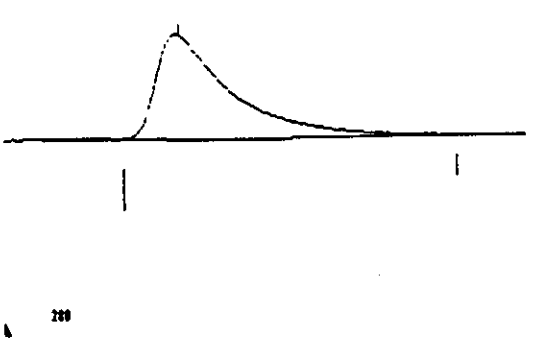

200

AMES10

BASELINE NOISE 200
FILTER CONSTANT 0
COUNTBACK FROM PEAK START OR END 1
MAXIMUM HEIGHT OF NOISE PEAK 1.5 *BASELINE NOISE
SAMPLE TIME 250 mS
F.S.D. 200 mV
ASYMETRIC PEAK FACTOR 1.5

PEAK 1 AREA 466307 at time 175 (156 260) 353.8 mVs Positive Peak

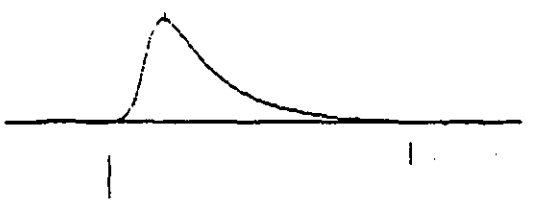

300

AMES12

BASELINE NOISE 100
FILTER CONSTANT 0
COUNTBACK FROM PEAK START OR END 1
MAXIMUM HEIGHT OF NOISE PEAK 1.5 *BASELINE NOISE
SAMPLE TIME 250 mS
F.S.D. 200 mV
ASYMETRIC PEAK FACTOR 0.5

PEAK 1 AREA 479892 at time 170 (150 263) 365.5 mVs Positive Peak

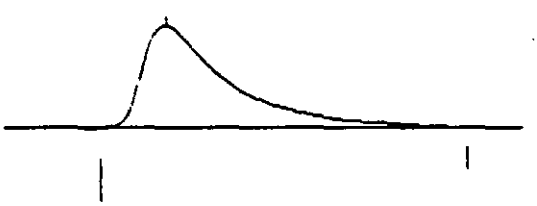

200

AMES13

BASELINE NOISE 200
FILTER CONSTANT 0
COUNTBACK FROM PEAK START OR END 1
MAXIMUM HEIGHT OF NOISE PEAK 1.5 *BASELINE NOISE
SAMPLE TIME 250 mS
F.S.D. 200 mV
ASYMETRIC PEAK FACTOR 1.5

PEAK 1 AREA 588870 at time 171 (153 295) 449.3 mVs Positive Peak

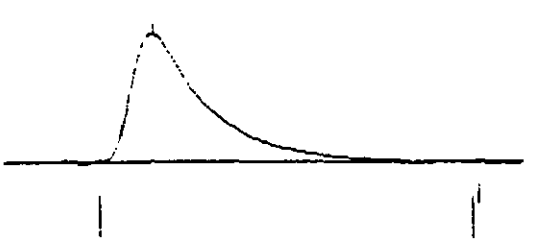

300

AMES11

BASELINE NOISE 250
FILTER CONSTANT 0
COUNTBACK FROM PEAK START OR END 11
MAXIMUM HEIGHT OF NOISE PEAK 1.5 *BASELINE NOISE
SAMPLE TIME 250 mS
F.S.D. 40 mV
ASYMETRIC PEAK FACTOR 0

PEAK 1 AREA 446632 at time 562 (447 686) 340.0 mVs Negative Peak

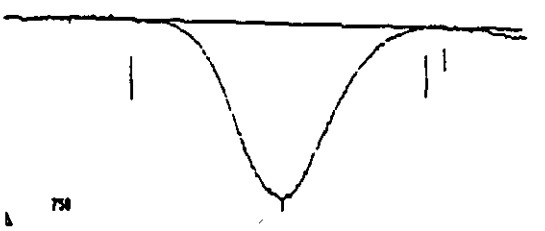

750

AMES12

BASELINE NOISE 240
FILTER CONSTANT 0
COUNTBACK FROM PEAK START OR END 2
MAXIMUM HEIGHT OF NOISE PEAK 1.5 *BASELINE NOISE
SAMPLE TIME 250 mS
F.S.D. 40 mV
ASYMETRIC PEAK FACTOR 0.8

PEAK 1 AREA 482388 at time 554 (454 680) 368 mVs Negative Peak
PEAK 2 IGNORED

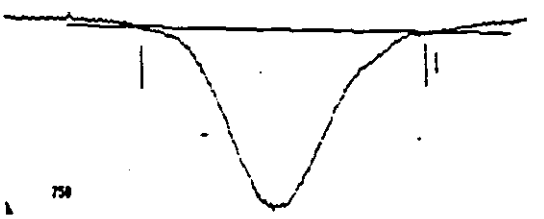

750

AMES13

BASELINE NOISE 450
FILTER CONSTANT 0
COUNTBACK FROM PEAK START OR END 11
MAXIMUM HEIGHT OF NOISE PEAK 1.5 *BASELINE NOISE
SAMPLE TIME 250 mS
F.S.D. 40 mV
ASYMETRIC PEAK FACTOR 0.5

PEAK 1 AREA 591217 at time 557 (450 786) 451.1 mVs Negative Peak

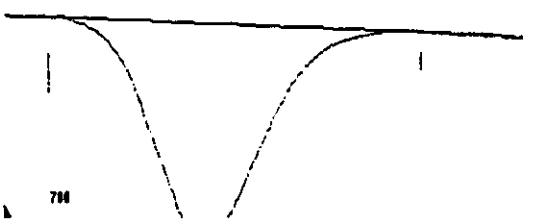

700

AMES14

BASELINE NOISE 300
FILTER CONSTANT 0
COUNTBACK FROM PEAK START OR END 1
MAXIMUM HEIGHT OF NOISE PEAK 1.5 *BASELINE NOISE
SAMPLE TIME 250 mS
F.S.D. 200 mV
ASYMETRIC PEAK FACTOR 1.5

PEAK 1 AREA 583894 at time 191 (173 211) 445.5 mVs Positive Peak

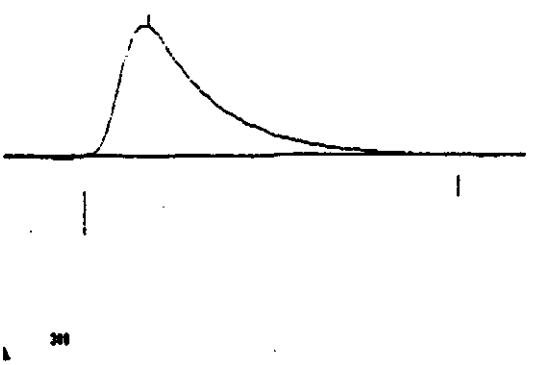

300

AMES14

BASELINE NOISE 400
FILTER CONSTANT 0
COUNTBACK FROM PEAK START OR END 10
MAXIMUM HEIGHT OF NOISE PEAK 1.5 *BASELINE NOISE
SAMPLE TIME 250 mS
F.S.D. 40 mV
ASYMETRIC PEAK FACTOR 1.5

PEAK 1 AREA 591453 at time 576 (475 747) 451.2 mVs Negative Peak

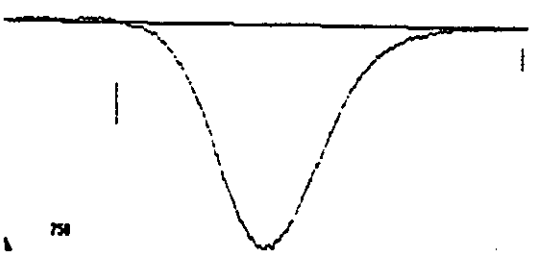

750

Appendix XVI - Hydrogen and Argon Mixture Analyses

NAME1011

BASELINE NOISE 300
FILTER CONSTANT 0
COUNTBACK FROM PEAK START OR END 1
MAXIMUM HEIGHT OF NOISE PEAK 1.5 *BASELINE NOISE
SAMPLE TIME 250 mS
F.S.D. 133.3 mV
ASYMETRIC PEAK FACTOR 1.0

PEAK 1 AREA 386417 at time 150 (133 216) 294.8 mVs Positive Peak

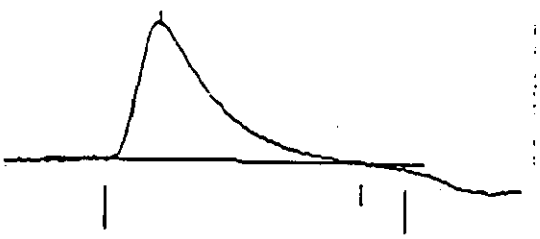

270

NAME1012

BASELINE NOISE 400
FILTER CONSTANT 0
COUNTBACK FROM PEAK START OR END 1
MAXIMUM HEIGHT OF NOISE PEAK 1.5 *BASELINE NOISE
SAMPLE TIME 250 mS
F.S.D. 100 mV
ASYMETRIC PEAK FACTOR 1.0

PEAK 1 AREA 375913 at time 156 (136 221) 286.8 mVs Positive Peak

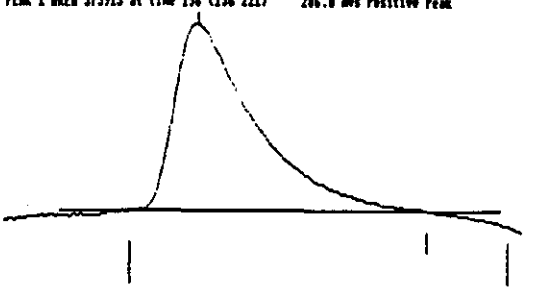

250

NAME1011

BASELINE NOISE 1000
FILTER CONSTANT 0
COUNTBACK FROM PEAK START OR END 8
MAXIMUM HEIGHT OF NOISE PEAK 1.5 *BASELINE NOISE
SAMPLE TIME 250 mS
F.S.D. 25 mV
ASYMETRIC PEAK FACTOR 0.0

PEAK 1 AREA 94963 at time 259 (221 320) 72.5 mVs Negative Peak

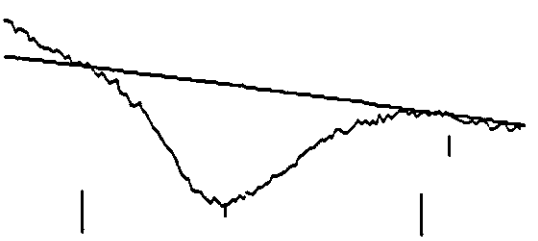

340

NAME1012

BASELINE NOISE 1000
FILTER CONSTANT 0
COUNTBACK FROM PEAK START OR END 2
MAXIMUM HEIGHT OF NOISE PEAK 1.5 *BASELINE NOISE
SAMPLE TIME 250 mS
F.S.D. 40 mV
ASYMETRIC PEAK FACTOR 5

PEAK 1 AREA 95367 at time 268 (236 339) 72.8 mVs Negative Peak

370

NAME1011

BASELINE NOISE 400
FILTER CONSTANT 0
COUNTBACK FROM PEAK START OR END 8
MAXIMUM HEIGHT OF NOISE PEAK 1.5 *BASELINE NOISE
SAMPLE TIME 250 mS
F.S.D. 25 mV
ASYMETRIC PEAK FACTOR 0.0

PEAK 1 AREA 291700 at time 426 (347 554) 222.5 mVs Negative Peak

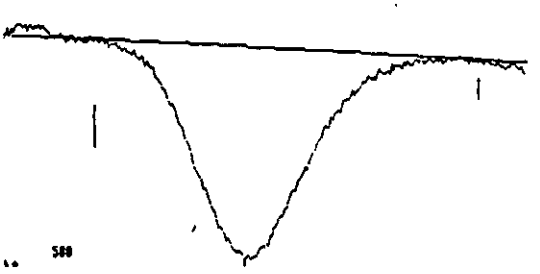

500

NAME1012

BASELINE NOISE 300
FILTER CONSTANT 0
COUNTBACK FROM PEAK START OR END 8
MAXIMUM HEIGHT OF NOISE PEAK 1.5 *BASELINE NOISE
SAMPLE TIME 250 mS
F.S.D. 40 mV
ASYMETRIC PEAK FACTOR 1.4

PEAK 1 AREA 285303 at time 431 (356 545) 217.7 mVs Negative Peak

500

NAME1013

BASELINE NOISE 300
FILTER CONSTANT 0
COUNTBACK FROM PEAK START OR END 1
MAXIMUM HEIGHT OF NOISE PEAK 1.5 *BASELINE NOISE
SAMPLE TIME 250 mS
F.S.D. 100 mV
ASYMETRIC PEAK FACTOR 0

PEAK 1 AREA 396619 at time 145 (127 218) 382.6 mVs Positive Peak

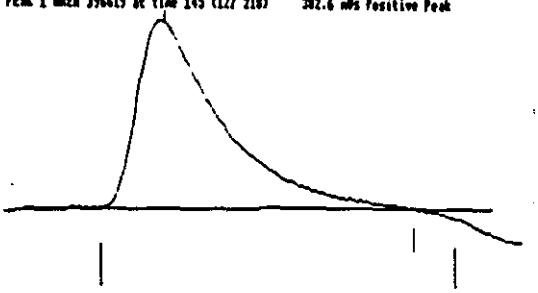

250

NAME1014

BASELINE NOISE 1100
FILTER CONSTANT 0
COUNTBACK FROM PEAK START OR END 5
MAXIMUM HEIGHT OF NOISE PEAK 1.5 *BASELINE NOISE
SAMPLE TIME 250 mS
F.S.D. 40 mV
ASYMETRIC PEAK FACTOR 2

PEAK 1 AREA 121422 at time 268 (228 340) 92.6 mVs Negative Peak

350

NAME1013

BASELINE NOISE 300
FILTER CONSTANT 0
COUNTBACK FROM PEAK START OR END 7
MAXIMUM HEIGHT OF NOISE PEAK 1.5 *BASELINE NOISE
SAMPLE TIME 250 mS
F.S.D. 40 mV
ASYMETRIC PEAK FACTOR 1

PEAK 1 AREA 291150 at time 424 (358 531) 222.1 mVs Negative Peak

500

NAME1014

BASELINE NOISE 300
FILTER CONSTANT 0
COUNTBACK FROM PEAK START OR END 7
MAXIMUM HEIGHT OF NOISE PEAK 1.5 *BASELINE NOISE
SAMPLE TIME 250 mS
F.S.D. 40 mV
ASYMETRIC PEAK FACTOR 1

PEAK 1 AREA 235228 at time 441 (369 525) 179.5 mVs Negative Peak

600

NAME1015

BASELINE NOISE 400
FILTER CONSTANT 0
COUNTBACK FROM PEAK START OR END 2
MAXIMUM HEIGHT OF NOISE PEAK 1.5 *BASELINE NOISE
SAMPLE TIME 250 mS
F.S.D. 100 mV
ASYMETRIC PEAK FACTOR 0

PEAK 1 AREA 363692 at time 148 (126 219) 277.5 mVs Positive Peak

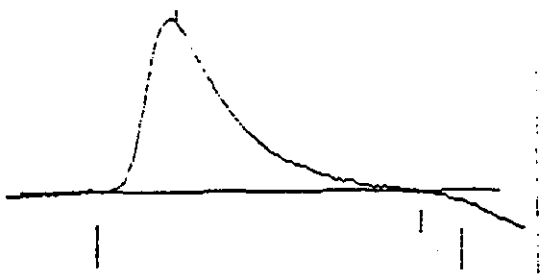

250

NAME1016

BASELINE NOISE 300
FILTER CONSTANT 0
COUNTBACK FROM PEAK START OR END 2
MAXIMUM HEIGHT OF NOISE PEAK 1.5 *BASELINE NOISE
SAMPLE TIME 250 mS
F.S.D. 100 mV
ASYMETRIC PEAK FACTOR 1.6

PEAK 1 AREA 363612 at time 150 (127 225) 277.4 mVs Positive Peak

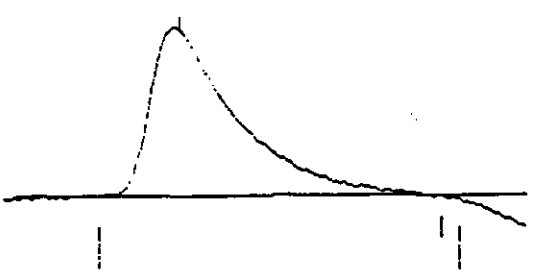

250

NAME1015

BASELINE NOISE 1000
FILTER CONSTANT 0
COUNTBACK FROM PEAK START OR END 4.5
MAXIMUM HEIGHT OF NOISE PEAK 1.5 *BASELINE NOISE
SAMPLE TIME 250 mS
F.S.D. 40 mV
ASYMETRIC PEAK FACTOR 3

PEAK 1 AREA 122838 at time 253 (222 345) 93.1 mVs Negative Peak

370

NAME1016

BASELINE NOISE 1000
FILTER CONSTANT 0
COUNTBACK FROM PEAK START OR END 6
MAXIMUM HEIGHT OF NOISE PEAK 1.5 *BASELINE NOISE
SAMPLE TIME 250 mS
F.S.D. 40 mV
ASYMETRIC PEAK FACTOR 1.6

PEAK 1 AREA 122215 at time 258 (221 328) 93.2 mVs Negative Peak

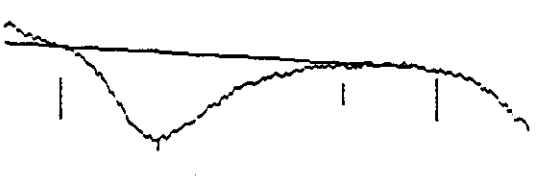

400

NAME1015

BASELINE NOISE 300
FILTER CONSTANT 0
COUNTBACK FROM PEAK START OR END 7
MAXIMUM HEIGHT OF NOISE PEAK 1.5 *BASELINE NOISE
SAMPLE TIME 250 mS
F.S.D. 40 mV
ASYMETRIC PEAK FACTOR 1.8

PEAK 1 AREA 238167 at time 426 (353 531) 181.7 mVs Negative Peak

580

NAME1016

BASELINE NOISE 300
FILTER CONSTANT 0
COUNTBACK FROM PEAK START OR END 10
MAXIMUM HEIGHT OF NOISE PEAK 1.5 *BASELINE NOISE
SAMPLE TIME 250 mS
F.S.D. 40 mV
ASYMETRIC PEAK FACTOR 1

PEAK 1 AREA 243249 at time 428 (348 520) 185.6 mVs Negative Peak

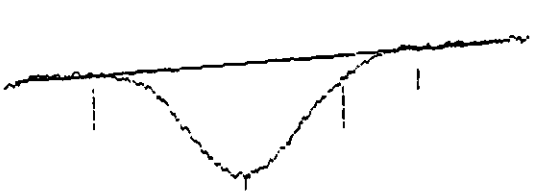

580

NAME1017

BASELINE NOISE 900
FILTER CONSTANT 0
COUNTBACK FROM PEAK START OR END 1
MAXIMUM HEIGHT OF NOISE PEAK 1.5 *BASELINE NOISE
SAMPLE TIME 250 mS
F.S.D. 100 uV
ASYMETRIC PEAK FACTOR 3

PEAK 1 AREA 334350 at time 162 (142 231) 255.1 mVs Positive Peak

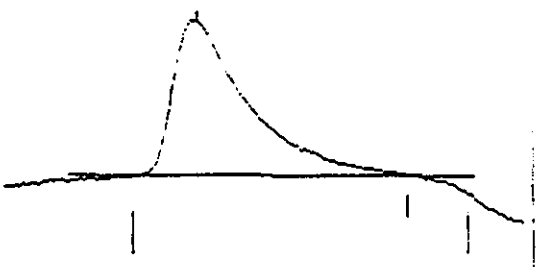

270

NAME1017

BASELINE NOISE 1100
FILTER CONSTANT 0
COUNTBACK FROM PEAK START OR END 3
MAXIMUM HEIGHT OF NOISE PEAK 1.5 *BASELINE NOISE
SAMPLE TIME 250 mS
F.S.D. 40 uV
ASYMETRIC PEAK FACTOR 4

PEAK 1 AREA 159597 at time 278 (233 361) 121.8 mVs Negative Peak

400

NAME1017

BASELINE NOISE 200
FILTER CONSTANT 0
COUNTBACK FROM PEAK START OR END 9
MAXIMUM HEIGHT OF NOISE PEAK 1.5 *BASELINE NOISE
SAMPLE TIME 250 mS
F.S.D. 40 uV
ASYMETRIC PEAK FACTOR 1.6

PEAK 1 AREA 179387 at time 442 (364 557) 136.8 mVs Negative Peak

500

NAME1018

BASELINE NOISE 400
FILTER CONSTANT 0
COUNTBACK FROM PEAK START OR END 1.5
MAXIMUM HEIGHT OF NOISE PEAK 1.5 *BASELINE NOISE
SAMPLE TIME 250 mS
F.S.D. 100 uV
ASYMETRIC PEAK FACTOR 1.7

PEAK 1 AREA 315493 at time 156 (135 223) 240.7 mVs Positive Peak

250

NAME1018

BASELINE NOISE 1000
FILTER CONSTANT 0
COUNTBACK FROM PEAK START OR END 3.5
MAXIMUM HEIGHT OF NOISE PEAK 1.5 *BASELINE NOISE
SAMPLE TIME 250 mS
F.S.D. 40 uV
ASYMETRIC PEAK FACTOR 3

PEAK 1 AREA 118191 at time 267 (233 339) 90.2 mVs Negative Peak

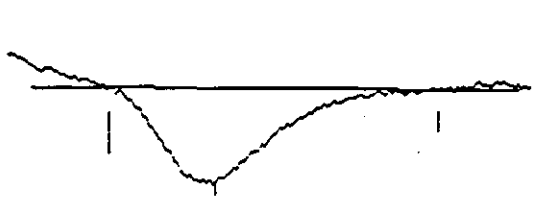

370

NAME1018

BASELINE NOISE 300
FILTER CONSTANT 0
COUNTBACK FROM PEAK START OR END 8
MAXIMUM HEIGHT OF NOISE PEAK 1.5 *BASELINE NOISE
SAMPLE TIME 250 mS
F.S.D. 40 uV
ASYMETRIC PEAK FACTOR 1.7

PEAK 1 AREA 197489 at time 434 (365 550) 150.6 mVs Negative Peak
PEAK 2 IGNORED

500

Appendix XVII - Retention Time Analyses

MEN34A

BASELINE NOISE 500
FILTER CONSTANT 0
COUNTBACK FROM PEAK START OR END 1
MAXIMUM HEIGHT OF NOISE PEAK 1.5 *BASELINE NOISE
SAMPLE TIME 250 mS
F.S.D. 500 mV
ASYMETRIC PEAK FACTOR 0

PEAK 1 AREA 388452 at time 179 (161 225) 1437.8 mVs Negative Peak
PEAK 2 AREA 138382 at time 247 (228 300) 1055.2 mVs Positive Peak

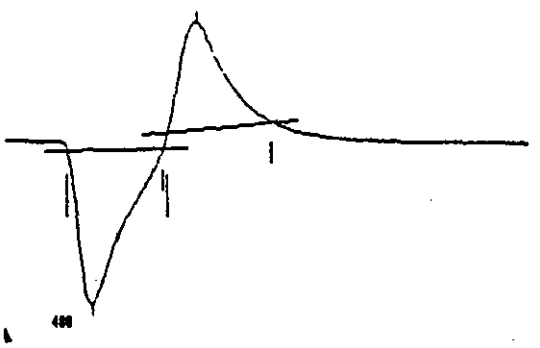

MEN34B

BASELINE NOISE 500
FILTER CONSTANT 0
COUNTBACK FROM PEAK START OR END 1
MAXIMUM HEIGHT OF NOISE PEAK 1.5 *BASELINE NOISE
SAMPLE TIME 250 mS
F.S.D. 500 mV
ASYMETRIC PEAK FACTOR 0

PEAK 1 AREA 387173 at time 171 (153 217) 1428 mVs Negative Peak
PEAK 2 AREA 141685 at time 239 (220 294) 1051 mVs Positive Peak

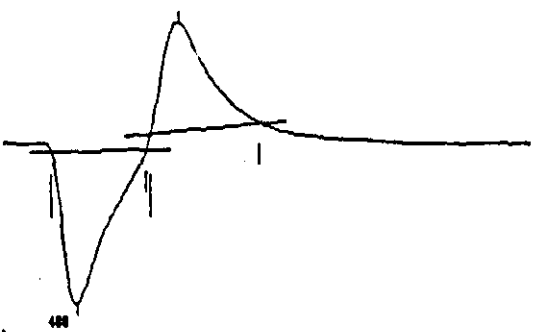

H2N34A

BASELINE NOISE 500
FILTER CONSTANT 0
COUNTBACK FROM PEAK START OR END 1
MAXIMUM HEIGHT OF NOISE PEAK 1.5 *BASELINE NOISE
SAMPLE TIME 250 mS
F.S.D. 500 mV
ASYMETRIC PEAK FACTOR 0

PEAK 1 AREA 114710 at time 172 (155 219) 875.2 mVs Negative Peak
PEAK 2 AREA 80242 at time 261 (240 303) 612.2 mVs Positive Peak

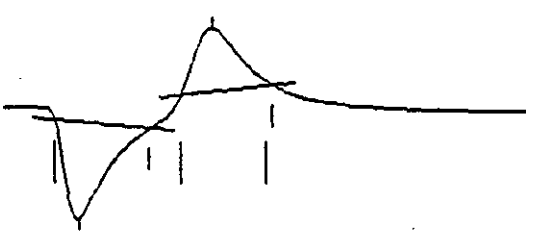

H2N34B

BASELINE NOISE 500
FILTER CONSTANT 0
COUNTBACK FROM PEAK START OR END 1
MAXIMUM HEIGHT OF NOISE PEAK 1.5 *BASELINE NOISE
SAMPLE TIME 250 mS
F.S.D. 500 mV
ASYMETRIC PEAK FACTOR 0

PEAK 1 AREA 114664 at time 179 (162 227) 874.8 mVs Negative Peak
PEAK 2 AREA 74149 at time 268 (248 306) 565.7 mVs Positive Peak
PEAK 3 IGNORED

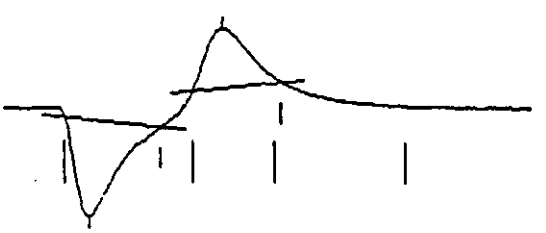

AN34A

BASELINE NOISE 500
FILTER CONSTANT 0
COUNTBACK FROM PEAK START OR END 1
MAXIMUM HEIGHT OF NOISE PEAK 1.5 *BASELINE NOISE
SAMPLE TIME 250 mS
F.S.D. 200 mV
ASYMETRIC PEAK FACTOR 0

PEAK 1 AREA 699812 at time 173 (154 250) 533.2 mVs Negative Peak
PEAK 2 IGNORED
PEAK 3 AREA 502994 at time 390 (344 468) 383.0 mVs Positive Peak

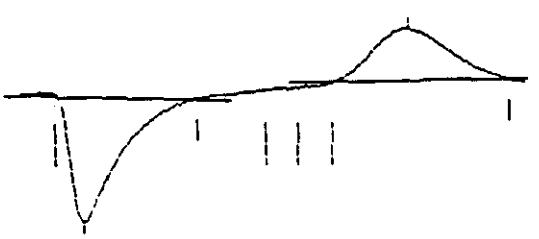

AN34B

BASELINE NOISE 500
FILTER CONSTANT 0
COUNTBACK FROM PEAK START OR END 1
MAXIMUM HEIGHT OF NOISE PEAK 1.5 *BASELINE NOISE
SAMPLE TIME 250 mS
F.S.D. 200 mV
ASYMETRIC PEAK FACTOR 0

PEAK 1 AREA 729143 at time 169 (150 239) 555.5 mVs Negative Peak
PEAK 2 IGNORED
PEAK 3 IGNORED
PEAK 4 AREA 584243 at time 392 (330 472) 445.7 mVs Positive Peak

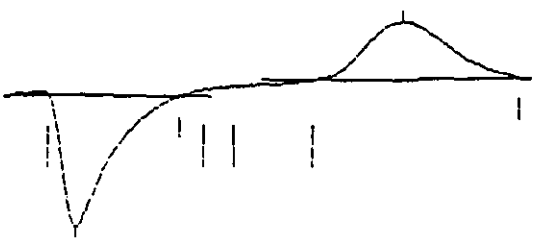

Appendix XVIII - Column Packing Procedure and Conditioning

1. The empty column (plus one end fitting and a glass wool plug) is weighed.

2. A water ejector pump is attached to the column end fitting. A water ejector pump produces a vacuum when mains tap water is passed through it. A suitable funnel is attached to the upstream end.

3. Previously graded, washed and dried column packing is poured into the funnel and drawn along the column by the action of the pump and gentle tapping of the column.

4. Once the column contains what is judged to be a sufficient amount of packing, the pump is disconnected. A glass wool plug is inserted and pushed up against the packing.

5. The column is weighed again to determine the mass of packing used. If a high degree of accuracy is required, the column should be weighed before insertion of the glass wool plug (taking care not to spill any packing.

6. The remaining column end union is fitted and a gas supply attached to this end. Gas is then blown through the column, usually at around 4 bar, whilst the column is tapped to encourage the adsorbent to pack as tightly as possible. This is repeated as often as is deemed necessary. After each blow-through, the glass wool plug is pushed up against the packing to keep it in place.

7. This procedure (steps 1 to 6) is repeated for a second column, if required, but using the same mass of packing as contained in the first column. The aim is to have two identical columns as far as possible.

8. The columns are now packed and can be installed in the chromatographic oven. Before any adsorption can take place the columns must be conditioned (activated, 'baked out'), that is, any substance which is already adsorbed must be removed from the adsorbent so that chromatographic separations can be accomplished. A supply of clean, dry gas is passed through each column. To avoid unnecessary problems the downstream end of each column must remain disconnected otherwise water vapour may be condensed in the detector(s) or elsewhere. The columns are heated up to 200-250°C and held there for around six hours. At all times the columns must be purged with clean, dry gas to carry away desorbing material.

9. Once the columns have cooled it may be desirable to recompress the packing as in step 6. The gas used must be clean and dry now that the columns have been activated.

10. To prevent the columns becoming deactivated by the sorption of water vapour, gas flow must be maintained at all times.

Appendix XIX - British Standard Sieves - Wire Mesh Series B.S. 410:1969

Mesh Number	Nominal Aperture Size (mm)	Mesh Number	Nominal Aperture Size (μm)
3	5.60	18	850
3.5	4.75	22	710
4	4.00	25	600
5	3.35	30	500
6	2.80	36	425
7	2.36	44	355
8	2.00	52	300
10	1.70	60	250
12	1.40	72	212
14	1.18	85	180
16	1.00	100	150

Appendix XX - Identification of Leaks

Any inconsistency in the operation of the apparatus could signify a gas leak somewhere in the system (usually a pipe fitting). There are a number of ways in which leaks can be identified depending upon the size of the leak.

1. Large leaks can be found by applying soap solution upon a suspect fitting. If the fitting is leaking escaping gas will blow bubbles.

2. Smaller leaks can be identified in the same way by increasing the pressure in the system. This can be achieved by sealing off the gas exit port so that the whole system is eventually pressured up to the delivery pressure. This exaggerates the previously small leaks so that they can be discovered using soap solution. Some soap solutions do corrode brass if they are not wiped off after the test is concluded.

3. If a stop valve is placed upstream of the system and the gas exit port sealed off as before, the system can be pressured up and then sealed off from the supply. If the pressure is not maintained after the valve is shut then there is a leak. The leak can be tracked down by isolating different parts of the system in turn by moving the valve.

4. If the gas is supplied via a mass-flow regulator a flow balance can be performed. The MFR is disconnected form the system momentarily and the volumetric flow being delivered is measured at atmospheric conditions. The MFR is reconnected and the flows allowed to re-equilibrate. The measured flow should match the sum of all exit streams in the system very closely if there are no leaks. The outlet streams in sorption-effect chromatography are usually the two carrier flows through the columns and the flow-setting system back-pressure regulator vent stream.

There are three areas where leaks are more likely than others.

Column end fittings (especially when the columns are glass because chromatographers are reluctant to tighten these fittings).

Fittings incorporating metal ferrules (especially if the ferrules are incorrectly inserted). Use of PTFE ferrules means that the fittings can be finger-tight and not leak. Overtightening of fittings with PTFE ferrules can lead to the pipe becoming restricted. However, with metal ferrules, the fittings must be tightened to the correct torque in order to make a gas-tight seal. When a mix of PTFE and metal ferrules is used in a system, fittings containing metal ferrules can be left under tightened.

Sampling and switching valves can begin to leak after long service (or incorrect use) but leaks are usually very apparent because of the unpredictable behaviour of the chromatograph.